Event-triggered Consensus Frameworks for Multi-agent Systems

Amir Amini

A Thesis
In the Department
of
Electrical and Computer Engineering

Presented in Partial Fulfillment of the Requirements
For the Degree of
Doctor of Philosophy (Electrical and Computer Engineering) at
Concordia University
Montréal, Québec, Canada

November 2020

Concordia University
School of Graduate Studies

This is to certify that the thesis prepared

By: **Amir Amini**
Entitled: **Event-triggered Consensus Frameworks for Multi-agent Systems**

and submitted in partial fulfillment of the requirements for the degree of

Doctor of Philosophy (Electrical Engineering)

complies with the regulations of this University and meets the accepted standards with respect to originality and quality.

Signed by the final examining commitee:

Dr. Liangzhu (Leon) Wang _____ Chair

Dr. Tongwen Chen _____ External Examiner

Dr. Abdessamad Ben Hamza _____ External to Program

Dr. Amir G. Aghdam _____ Examiner

Dr. Hassan Rivaz _____ Examiner

Dr. Arash Mohammadi _____ Thesis Co-supervisor

Dr. Amir Asif _____ Thesis Supervisor

Approved _____
Dr. Wei-Ping Zhu, Graduate Program Director

November 10, 2020

Date of Defense

Dr. Mourad Debbabi, Dean, Engineering and Computer Science

Abstract

Event-triggered Consensus Frameworks for Multi-agent Systems

Amir Amini, Ph.D.
Concordia University, 2020

Recently, distributed multi-agent systems (MAS) have been widely studied for a variety of engineering applications, including cooperative vehicular systems, sensor networks, and electrical power grids. To solve the allocated tasks in MASs, each agent autonomously determines the appropriate actions using information available locally and received from its neighbours. Many cooperative behaviours in MAS are based on a consensus algorithm. Consensus, by definition, is to distributively agree on a parameter of interest between the agents. Depending on the application, consensus has different configurations such as leader-following, formation, synchronization in robotic arms, and state estimation in sensor networks. Consensus in MASs requires local measurements and information exchanges between the neighbouring agents. Due to the energy restriction, hardware limitation, and bandwidth constraint, strategies that reduce the amount of measurements and information exchanges between the agents are of paramount interest. Event-triggering transmission schemes are among the most recent strategies that efficiently reduce the number of transmissions. This dissertation proposes a number of event-triggered consensus (ETC) implementations which are applicable to MASs. Different performance objectives and physical constraints, such as a desired convergence rate, robustness to uncertainty in control realization, information quantization, sampled-data processing, and resilience to denial of service (DoS) attacks are included in realization of the proposed algorithms. A novel convex optimization is proposed which simultaneously designs the control and event-triggering parameters in a unified framework. The optimization governs the trade-off between the consensus convergence rate and intensity of transmissions. This co-design optimization is extended to an advanced class of event-triggered schemes, known as the *dynamic* event-triggering (DET), which is able to substantially reduce the amount of transmissions. In the presence of DoS attacks, the co-design optimization simultaneously computes the control and DET parameters so that the number of transmissions is reduced and a desired level of resilience to DoS is guaranteed. In addition to consensus, a formation-containment implementation is proposed, where the amount of transmissions are reduced using the DET schemes. The performance of the proposed implementations are evaluated through simulation over several MASs. The experimental results demonstrate the effectiveness of the proposed implementations and verify their design flexibility.

Acknowledgments

First and foremost, I would like to thank my exceptional adviser, Dr. Amir Asif, for his technical advice and excellent cooperation during my research. I thank you very much for all your guidance throughout my studies at Concordia University. I feel truly privileged to have worked with you. In addition, I am very thankful to my outstanding co-supervisor, Dr. Arash Mohammadi, for his thoughtful comments, encouragements, and cordial manner. Your advice was invaluable throughout the work.

I deeply express my gratitude to the committee members, Dr. Tongwen Chen, Dr. Abdessamad Ben Hamza, Dr. Amir Aghdam, and Dr. Hassan Rivaz, for evaluating this dissertation and their thoughtful feedback.

My sincere thanks goes to my lovely parents and my brother for their emotional support, although we were mostly away from each other.

Above all, I would like to thank my fiancee and my best friend, Mahnaz, for her love and unbelievable support that helped me get to this point. I owe you a lot.

Contents

List of Figures

List of Tables

List of Abbreviations

AE	Average number of events
AIET	Average inter-event time
ARE	Algebraic riccati equation
AUV	Autonomous underwater vehicle
CEASE	Collaborative event-triggered average consensus sampled-data
DEASE	Dynamic event-triggered average consensus sampled-data
DET	Dynamic event-triggered
DG	Distributed generator
DoS	Denial of service
ET	Event-triggered
ETC	Event-triggered consensus
FCC	Formation-containment control
FCC/DEME	Formation-containment control using dynamic event-triggering mechanism
FWM	Free weighting matrix
IFWM	Improved free weighting matrix
ISS	Input-to-state stability
LKF	Lyapunov-Krasovskii functional
LMI	Linear matrix inequality
LQR	Linear quadratic regulator
MAS	Multi-agent system
MIET	Minimum inter-event time
NCS	Networked control system
PEC	Performance guaranteed event-triggered consensus
PSEC	Performance guaranteed sampled-data event-triggered consensus

Q-CEASE	Quantized collaborative event-triggered average consensus sampled-data
Q-DEASE	Quantized dynamic event-triggered average consensus sampled-data
R-PSEC	Resilient performance guaranteed sampled-data event-triggered consensus
ROCCET	Resilient optimized consensus using dynamic event-triggering scheme
RQ-CEASE	Resilient quantized collaborative event-triggered average consensus sampled-data
SDP	Semi-definite programming
S-DET	Sampled-data dynamic event-triggered
UAV	Unmanned aerial vehicle
USV	Unmanned surface vehicle

List of Symbols

N	Number of nodes (agents) in multi-agent system
$\mathcal{V}$	The set of all nodes
$\mathcal{N}_i$	Neighbouring set for node i
$\mathcal{A}=\{a_{i,j}\}$	Weighted adjacency matrix
$\boldsymbol{L}=\{l_{i,j}\}$	Laplacian matrix
λ_2	The second smallest eigenvalue of the Laplacian matrix
λ_N	The largest eigenvalue of the Laplacian matrix
$\boldsymbol{A}$ and $\boldsymbol{B}$	System matrices for general linear agents
$\boldsymbol{u}_i(t)$	Control input for agent i at time t
$\boldsymbol{x}_i(t)$	State of agent i at time t
t_k^i	The time instant that the k-th event is triggered by node i
$\boldsymbol{x}_i(t_k^i)$	The state of agent i at its k-th event (for continuous-time schemes)
$\hat{\boldsymbol{x}}_i(t)$	Same as $\boldsymbol{x}_i(t_k^i)$
$\boldsymbol{e}_i(t)$	The state error for agent i at time t due to event-triggering
h	Sampling period used in attack-free circumstances
g	Sampling period used in the presence of DoS attack
$\boldsymbol{x}_i(nh)$	State of agent i at sample n with sampling period h
n_k^i	The sample at which the k-th event is triggered by node i
$\boldsymbol{x}_i(n_k^i h)$	The state of agent i at its k-th event
$\hat{\boldsymbol{x}}_i(nh)$	Same as $\boldsymbol{x}_i(n_k^i h)$
$\bar{x}(t)$	The average value for states of all agents at time t
$\boldsymbol{K}$	Control gain for state-feedback protocol

Chapter 1

Introduction

This chapter provides necessary background to study event-triggered (ET) strategies for cooperative behaviours in multi-agent systems (MAS). To provide context, networked control systems (NCS) and their features are first introduced in Section 1.1. Then, Section 1.2 provides preliminary concepts about multi-agent systems. The chapter follows by introducing different types of consensus and their engineering applications in Section 1.3. Discussion over different communication and sensing schemes used for consensus are included in Section 1.4.

1.1 Networked Control Systems

This section presents important concepts in the field of NCSs. In many control systems, such as industrial plants, moving vehicles, spacecrafts, under water vehicles, ete, communication networks are adapted to exchange measurements and control signals between geographically distributed system components, such as smart sensors, actuators, and computer units. An NCS is established when different units of the system work together (i.e., the system is closed-loop) by means of communication channels. The advantages of NCSs compared to traditionally analog systems are due to their low cost, reduced weight, reduced power consumption, simple installation, easier fault detection, and higher reliability. Using communication channels in NCSs, however, brings some challenging matters such as, communication bandwidth, digitalization of the signals, communication delay, and security of the channels, to name a few. NCSs can be regarded as the basis of multi-agent systems where multiple sub-systems (agents) collaborate and interact with each other to achieve certain cooperative objectives.

1.2 Multi-agent systems

In the past few decades, advances in NCSs and different engineering areas have led to the development of complex systems composed of a large number of devices that communicate and cooperate with each other to achieve a common objective. Referred to

as the multi-agent systems, they have received considerable attention in computer science, robotics, and electrical engineering as a powerful tool to perform complex tasks in large-scale systems. In MASs, the underlying task is divided between multiple entities, known as the agents. To solve the allocated task, each agent autonomously determines the appropriate actions using information available locally and from immediate neighbours. In general, agents in MASs have the following features [3]:

- **Sociability**: Agents can communicate to a subset of other agents (neighbouring agents) to exchange and request information needed to achieve their objectives.
- **Autonomy**: Agents are autonomous in taking independent actions, such as measurement, actuation, information transmission, and decision making.
- **Proactivity**: Agents can use both current and past localized and neighbouring information to predict necessary future actions. This ability also enables agents to take proper actions based on their environment.

Although an agent is autonomous and capable of taking individual actions, the complete benefit is achieved only when they are configured as a multi-agent system. The main features of MASs that enables them to solve complex tasks are as follows:

- **Efficiency**: In MASs, a complex task is divided into multiple smaller tasks, which are assigned to different agents. The division of tasks in MASs increases the overall efficiency of the system.
- **Low cost**: As compared to the centralized approach where the entire complex task is solved by a single powerful system the distributed approach used by MASs often results in lower cost.
- **Reliability**: Another benefit of MASs is resilience to failure of agents. In case that an agent is non-operational, the task can be assigned to other agents without a major impact. Increased reliability is an important feature of distributed MASs.

While MASs provide the aforementioned benefits, their design and operation is more complex as compared to NCSs where a solitary system is under study mainly due to their distributed nature and lack of a fusion center. Several challenges, therefore, arise in MASs in addition to the design complexities associated with other control systems. Some of these challenges are as follows:

- In NCSs, there usually exists one main plant to be controlled. In contrast, in MAS there are multiple agents interacting with each other. Incorporation of the network connectivity which describes the interaction between the agents (i.e., in-neighbour communication network) adds additional level of difficulty.
- The control objective in NCSs are mainly stabilization or tracking control. However, in MASs the objective is usually a cooperative behaviour which requires participation of all agents. How to translate these behaviour into the stability of the MASs is challenging. In other words, it is usually not straightforward to transform the original cooperative problem into an equivalent stability problem.

- As mentioned above, in MASs there is usually no fusion center to control the MAS based on global information. Therefore, preserving the distributed nature of the solution in both the design and implementation stages is another challenging task in MASs.

- In contrast to NCSs, in MASs the number of interacting agents can vary and may be large. In MASs, preserving scalability of the design approach with respect to the number of agents is important. Increased computational complexity would limit the applicability of the scheme for MASs if complexity of design is dependent on the network size.

In MASs, the agents are often required to reach an agreement (consensus) between themselves upon a parameter of interest (state) [4]. When consensus is achieved, this reference parameter has the same value within the network. The reference parameter is application-specific. For example, in vehicular MASs, the parameter of interest is the motion of the agents (positions and velocities). In estimation applications, the quantity of interest can be the average of a state parameter measured by agents placed at different locations.

The thesis is concerned with such distributed consensus problems in MASs.

1.3 Consensus-based coordination

This section introduces different types of consensus and their related engineering applications.

Average Consensus: In traditional centralized systems, the fusion center collects information from all devices, makes necessary calculations, and sends necessary commands. By omission of the fusion center, distributed algorithms (preferably with minimal computational intensity) are required to compute necessary quantities which depend on all information of local devices. In some distributed control and signal processing applications such as parameter estimation using distributed sensors, node counting in networks, sensor calibration, and Kalman filtering [5, Sec 3.3], knowing the average value of all local information is necessary for each node. In the absence of a fusion center, nodes are able to achieve the average value of their parameter of interest using average consensus algorithms [4]. These algorithms originated in the analysis of Markov chains and have been studied in computer science. Average consensus is also required in microgrids which are small-scale power systems consist of local generators, loads, and energy storages. In microgrids, an important objective is to efficiently dispatch power supply of distributed generators (DGs) to distributed loads, which is referred to as the power sharing. Each distributed generator can be regarded as a node of a large multi-agent system. At node i, the apparent power flow is represented by $S_i = P_i + jQ_i$, where P_i and Q_i are, respectively, the active and reactive power components. The reactive power distribution can be achieved by voltage control, which needs a consensus algorithm [6].

Leader-following Consensus: In leader-following consensus, there exits one leader (reference) in the network and the remaining agents follow the leader. Only a subset of the followers are connected to the leader. In vehicular systems such as Unmanned Aerial Vehicles (UAV) [7], Unmanned Surface Vehicles (USV) [8], and Autonomous Underwater Vehicles (AUV) [9], multi-agent system configuration is employed to fulfill complex cooperative tasks, where direct human intervention is not possible due to environmental hazards, complexity of the tasks, and other restrictions. In this application, there usually exists one agent as the leader of the group which steers other agents (followers) towards the desired path. Another application that requires a leader-following consensus algorithm is the secondary voltage control in microgrids. The voltage control in microgrids often follow a hierarchical structure with three levels namely, primary, secondary, and tertiary control loops. The primary control loop maintains the voltage and frequency of the DGs close to their nominal values as the power supply and demand change over time. However, even in the presence of the primary control loop, voltage and frequency may still deviate from their nominal values. To restore the voltage and frequency of the DGs to their nominal values, the secondary control is also required. Tertiary loop is the highest level of the hierarchy and performs high-level tasks such as the optimization of economic performance and managing the main grids [10]. The problem of secondary voltage control in microgrids can be viewed as a distributed tracking control problem, similar to the leader-following consensus [11]. The DGs are connected to each other based a communication topology and the objective is to control their output voltage value based on a reference value.

Containment: In the presence of multiple leaders, the leader-following consensus problem extends to the containment control, with the followers moving and staying within a convex hull formed by the leaders [12]. In applications where a team of robots move towards a target even if only a few of them (the leaders) are equipped with sensors to detect obstacles and identify a safe operational area, other robots (the followers) with limited accessories seek to enter that safe area spanned by the leaders. One related application is the mixed containment-sensing problem [13] where the objective is to have a group of mobile agents (followers) cover and sense a sequence of regions of interest. In this application, the leaders steer the followers to the operational region and coordinate the sensing task at a higher level. Containment requires a consensus-based control protocol in its implementation. It should be noted that extending a consensus algorithm to containment is not trivial in many cases.

1.4 Communication and Measurement Schemes

Due to the well-known disadvantages of centralized and hierarchical schemes and the large scale of practical networks, the state-of-the-art consensus implementations in MASs are distributed. In other words, only local and neighbouring information is accessible at each node. To communicate with other nodes and perform necessary

actions, an operating agent in MASs consists of different units, including: (i) A sensor (estimator) which measures (estimates) the agent's state; (ii) An actuator which implements necessary signals (also known as the control input signal); (iii) A receiver which receives neighbouring information; and (iv) A transmitter which transmits information to neighbouring nodes. The local units used in each agent are usually small and powered by limited batteries. One important issue in cooperative MASs is, therefore, to design suitable communication and sensing schemes which sustain the desired objective with a reasonable consumption of communication and computation resources. The local measurement scheme, which provides the agent with its state values, is required in reaching consensus.

Primary implementations in the context of distributed consensus are based on continuous-time (time-triggered) stat measurement and communication. In other words, at each node local processing, such as measurement and information exchanges, are performed in a continuous-time fashion [14–16]. In practice, the continuous-time schemes are unfavorable due to physical constraints including: (i) Communication bandwidth; (ii) Hardware processing limitations; and (iii) The limited on-board energy resources allocated to each node.

To cope with the aforementioned constraints, implementations which reduce the amount of measurements and information exchanges are of great interest. In this regard, periodic implementations are proposed in [17] and [18] for consensus. In such schemes, states are measured periodically and neighbouring transmissions are based on the same period. Clock synchronization of the agents and using a sampler for consensus reduce the processing burden at the expense of imposing additional design and stability challenges [19]. Strategies depending on a constant sampling period operate irrespective of the agent states, time, and other trajectories of the system. One disadvantage of these schemes is that the transmission load, for example, remains the same for both cases when the agents are far from consensus and when consensus is closely achieved. Therefore, the sampling-based schemes may still lead to excessive communication and computation consumption.

A more advanced strategy is event-triggered (ET) schemes where a *time-varying* condition (such as time or the disagreement between the agents) is involved to determine when the desired action should take place. As for in-neighbour transmissions, ET strategies allow transmissions occur only if a pre-designed time-varying condition is satisfied. The time-varying condition should be smart enough to react to dynamics of the agents. For example, the proposed ET condition should transmit fewer information when consensus is nearly achieved. The superiority of the ET strategies over the sampling-based counterparts is intuitive and also proved in [20]. Due to their additional flexibility, the application of ET transmission schemes for consensus have been studied in literature from different perspectives. Although saving communication resources is an important feature, ET strategies bring additional challenges in design and stability analysis. For example, it was previously known that under some circumstances (such as noise-free measurement and communication) consensus can be achieved asymptotically with zero disagreement error. However, the introduction

of an ET scheme may lead to bounded consensus (i.e., consensus is reached within a bounded error) [21]. On another note, the ET schemes are subject to a phenomena known as the Zeno-behaviour. The Zeno-behaviour occurs if an infinite number of events are detected within a finite interval. The Zeno-behaviour, if occurs, destabilizes the event-detector unit and makes the scheme nonoperational in real practice.

Most ET schemes are localized, i.e., each node is autonomous in triggering its events and the event sequences for two nodes may or may not be the same. In fact, the nodes are not aware of the time when updates are triggered by their neighbouring nodes. Therefore, although transmission is event-triggered, the receiver might be constantly on to receive potential updates. If nodes are synchronized by a periodic clock, no event is expected in inter-sampling period. Therefore, the receiver at each node can operate based on the synchronized clock and thus follows a periodic pattern. Clearly, the periodic scheme is more favorable than the continuous-time scheme from the receiver's perspective.

As for the transmission scheme, all implementations proposed in the thesis focus on ET strategies. The measurement and receiver schemes, however, are either periodic (sampled-data) or continuous-time in different implementations.

1.5 Organization of the Thesis

The remaining thesis is organized as follows. Chapter 2 presents the general problem of ET consensus in MASs. An overview of the existing implementations in this area is given in Chapter 2. Some research gaps are identified based on the literature review. Chapter 3 presents the proposed implementations for ET consensus in single-order MASs. The implementations proposed in Chapter 3 are applicable for average consensus. Chapter 4 extends the implementations to MASs with general linear dynamics. In Chapter 6, the application of ET consensus for formation-containment in vehicular MASs is studied. Numerical examples which quantify the theoretical results are included in Chapter 7. Chapter 8 summarizes the proposed implementations based on their features and provides some future direction worthy of further investigation. An implementation for event-triggered stabilization control in NCSs is provided in Appendix.

Chapter 2

Problem Statement and Literature Review

In this chapter, the problem of event-triggered consensus (ETC) in multi-agent systems (MAS) is studied. Section 2.1 and 2.2 introduce necessary notation and background used in the thesis. Then, different design objectives in the context of ETC are elaborated in Section 2.3. Two commonly used design approaches for ETC are discussed in Section 2.4. An overview of the recent state-of-the-art implementations is provided in section 2.5 based on which important research gaps in ETC are presented. The main contributions of the thesis are given in Section 2.6. Section 2.7 lists the publications that are published from this dissertation.

2.1 Notation

Throughout the thesis, alphabets in bold fonts are used to denote matrices or vectors. Scalars are denoted by alphabets in normal font. Notation $\mathbb{R}^{m\times n}$ refers to $(m\times n)$ real-valued matrices. Let $\boldsymbol{A}=\{a_{i,j}\}\in\mathbb{R}^{m\times n}$ denote a matrix with entries $a_{i,j}$, $(1\leq i\leq m)$, $(1\leq j\leq n)$. Notation $\|\boldsymbol{A}\|$ denotes the L_2 norm of $\boldsymbol{A}$. Superscript T in $\boldsymbol{A}^T$ stands for the transpose of matrix $\boldsymbol{A}$. If $\boldsymbol{A}>0$, then $\boldsymbol{A}$ is symmetric positive definite, i.e., $\boldsymbol{x}^T\boldsymbol{A}\boldsymbol{x}>0$, $\forall\,\boldsymbol{x}\in\mathbb{R}^n$, $\boldsymbol{x}\neq\boldsymbol{0}$. Notation $\boldsymbol{A}^\dagger$ refers to the pseudo-inverse of $\boldsymbol{A}$. Matrices $\boldsymbol{I}$ and $\boldsymbol{0}$, respectively, stand for the identity matrix and zero matrix of appropriate dimensions. Vector $\boldsymbol{1}_n$ represents a column vector of order n with unit entries. Notations $\otimes$ and $\circ$, respectively, denote the Kronecker and Hadamard products. For two vectors $\boldsymbol{u}=\{u_i\}\in\mathbb{R}^n$ and $\boldsymbol{v}=\{v_i\}\in\mathbb{R}^n$, the inequality $\boldsymbol{u}\leq\boldsymbol{v}$ refers to their element-wise inequality, i.e., $u_i\leq v_i$, $(1\leq i\leq n)$. The asterisk $*$ in the lower triangle of symmetric matrices represents the transpose of the corresponding block from the upper triangle.

Class $\mathcal{K}$ and $\mathcal{KL}$ functions: A scalar continuous function $f_2(r)$ defined in $r\in[0,a)$ belongs to class $\mathcal{K}$ if the function is strictly increasing with $f_2(0)=0$. In addition, $f_2(r)$ belongs to class $\mathcal{K}_\infty$ if it is defined for all $r\geq 0$ and $f_2(r)\to\infty$ corresponds to $r\to\infty$. A scalar continuous function $f_1(r,s)$ with arguments $r\in[0,a)$ and $s\in[0,\infty)$ belongs to class $\mathcal{KL}$ if: (i) for any arbitrary fixed s, $f_1(r,s)$ belongs to class $\mathcal{K}$, and (ii)

for any arbitrary fixed r, $f_1(r,s)$ is decreasing in s such that $f_1(r,s)\to 0$ as $s\to\infty$.

Graph theory: The communication network of a MAS consisting of N nodes is modeled using a graph $\mathcal{G}=(\mathcal{V},\mathcal{E},\mathcal{A})$, where $\mathcal{V}=\{1,2,...,N\}$ denotes the node set, i.e., the i-th vertex indicates the i-th node. The edge set $\mathcal{E}$ includes the pair (i,j), $(1\leq i,j\leq N)$, if and only if node j transmits its information to node i. If node j communicates its information to node i, then the pair (j,i) is an element of $\mathcal{E}$ denoted by $j\to i$ in graph representation. In a directed graph, $(j,i)\in\mathcal{E}$ is not equivalent to $(i,j)\in\mathcal{E}$. Matrix $\mathcal{A}=\{a_{i,j}\}\in\mathbb{R}^{N\times N}$ is the weighted adjacency matrix for graph $\mathcal{G}$, where $a_{i,i}=0$, $a_{i,j}\neq 0$ if $(i,j)\in\mathcal{E}$, and $a_{i,j}=0$ if $(i,j)\notin\mathcal{E}$. The neighbour set of node i is defined by $\mathcal{N}_i=\{j\in\mathcal{V}\,|\,(i,j)\in\mathcal{E}\}$. A directed graph contains a directed spanning tree if there exists at least one path that spans all nodes in the graph. The Laplacian matrix for $\mathcal{G}$ is defined by $\boldsymbol{L}=\{l_{i,j}\}=\mathcal{D}-\mathcal{A}$, where $\mathcal{D}=\text{diag}\,(\deg_1,...,\deg_N)$, with $\deg_i=\sum_{j=1}^{N}a_{i,j}$. The Laplacian matrix can be viewed as $l_{ii}=\sum_{j\in\mathcal{N}_i}a_{ij}$, and $l_{ij}=-a_{ij}$, $\forall i\neq j, 1\leq i,j\leq N$. The Laplacian matrix has exactly one eigenvalue of zero if and only if the directed network contains a directed spanning tree. Under this condition, all other eigenvalues of $\boldsymbol{L}$ have positive real components [22].

Illustrative Example: To illustrate the graph notation used in the thesis, an example of a MAS with with 6 nodes is given. The network topology for this MAS is shown in Fig. 2.1. Each labeled circle illustrates a node and the bidirectional arrows indicate bidirectional communication between the corresponding nodes. Based on Fig. 2.1, the neighbouring sets for node 6, for example, is: $\mathcal{N}_6=\{1,5\}$. Considering that all the weights associated to communication links are 1, the degree matrix $\mathcal{D}$, weighted adjacency matrix $\mathcal{A}$, and Laplacian matrix $\boldsymbol{L}$ for the network shown in Fig. 2.1 are given below

$$\mathcal{D}=\text{diag}\,(2,2,2,2,2,2),$$
$$\mathcal{A}=\begin{bmatrix}0&1&0&0&0&1\\1&0&1&0&0&0\\0&1&0&1&0&0\\0&0&1&0&1&0\\0&0&0&1&0&1\\1&0&0&0&1&0\end{bmatrix},\ \boldsymbol{L}=\begin{bmatrix}2&-1&0&0&0&-1\\-1&2&-1&0&0&0\\0&-1&2&-1&0&0\\0&0&-1&2&-1&0\\0&0&0&-1&2&-1\\-1&0&0&0&-1&2\end{bmatrix}. \tag{2.1}$$

2.2 Event-triggered consensus

In this section, an overview of the event-triggered consensus problem is given.

2.2.1 Preliminaries and problem statement

A MAS with N nodes is represented by the dynamics of each agent and the network connectivity between the nodes. The general dynamics of the agents can be viewed

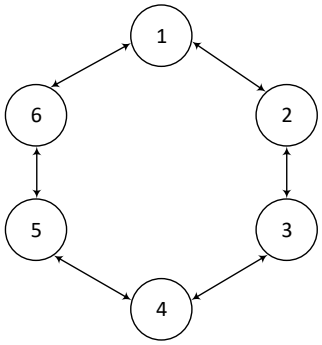

Figure 2.1: An illustrative communication network with 6 nodes. The 6 nodes are connected with a ring topology.

as

$$\dot{\boldsymbol{x}}_i(t) = f(\boldsymbol{x}_i(t), \boldsymbol{u}_i(t)), \quad (1 \leq i \leq N), \tag{2.2}$$

where $\boldsymbol{x}_i(t) \in \mathbb{R}^n$ is the state of agent i and $\boldsymbol{u}_i(t) \in \mathbb{R}^m$ is the control input for agent i. Function $f(\boldsymbol{x}_i(t), \boldsymbol{u}_i(t))$ describes the relationship between the state of agent i and its control input. A special case of (2.2) is the following general linear model

$$\dot{\boldsymbol{x}}_i(t) = \boldsymbol{A}\boldsymbol{x}_i(t) + \boldsymbol{B}\boldsymbol{u}_i(t), \quad (1 \leq i \leq N). \tag{2.3}$$

Matrices $\boldsymbol{A}$ and $\boldsymbol{B}$ with appropriate dimensions represent the system matrix and control input matrix, respectively. Model (2.3) is useful as it represents a wide range of MASs which are either: (i) Linear in nature; (ii) Feedback linearizable; (iii) Can be approximated using a linear model. The distributed ETC problem is stated as follows:

Design a distributed control protocol $\boldsymbol{u}_i(t)$ *and a distributed communication scheme, which transmits only under certain situations, such that the following condition is satisfied for all agents and any initial states* $\boldsymbol{x}_i(0) \in \mathbb{R}^n$, $1 \leq i \leq N$

$$\lim_{t\to\infty} \| \boldsymbol{x}_i(t) - \boldsymbol{x}_j(t) \| = 0, \qquad 1 \leq i, j \leq N. \tag{2.4}$$

Conceptually speaking, when consensus is reached the disagreement between the states of any two agents (regardless of being neighbours or not) approaches zero. It should be noted that in some situations the disagreement can only approach a bounded error [23], i.e.,

$$\lim_{t\to\infty} \| \boldsymbol{x}_i(t) - \boldsymbol{x}_j(t) \| \leq \delta, \qquad 1 \leq i, j \leq N, \tag{2.5}$$

where $\delta > 0$ is the consensus error. The case that δ is strictly positive is known as the 'bounded consensus'.

A special case of the consensus definition (2.4) is the average consensus where all

states converge to the average value of the initial states, i.e.,

$$\lim_{t\to\infty} \| \boldsymbol{x}_i(t) - \frac{1}{N}\sum_{j=1}^{N} \boldsymbol{x}_j(0) \| = 0, \quad (1 \le i \le N). \tag{2.6}$$

The average consensus problem is usually concerned with distributed averaging for a measured set of *scalars*. The following first-order integrator agent is often used for average consensus

$$\dot{x}_i(t) = u_i(t), \qquad (1 \le i \le N). \tag{2.7}$$

2.2.2 Basic configuration for event-triggered consensus

A basic configuration for an ETC implementation is shown in Fig. 2.2, where an event-detector and a controller block are incorporated with each agent [1]. The event-detector is responsible for monitoring a proposed distributed event-triggering (ET) condition to determine whether or not to transmit necessary information (usually the most recent state measurement) to its neighbours. If the ET condition is satisfied, new information is transmitted to the neighbouring nodes. A common terminology used in this regard is that 'an event is triggered.' Let $t_0^i, t_1^i, \ldots, t_k^i$ denote the time sequence at which events are triggered by node i, where $k = 0, 1, 2, \ldots$ defines the event index for node i [2]. Additionally, let t_k^i denote the most recent event instant for node i up to time t. Following this notation, $\boldsymbol{x}_i(t_k^i)$ is the state of agent i at the most recently triggered event. This state is known as the 'event state'. A *disagreement* index is usually used to specify the relative difference between the states of the neighbouring agents. A larger value for the disagreement implies a larger gap from consensus between the agents and vice versa. The disagreement is usually used for the following purposes:

- It is used in the controller block and to generate the control input as such a larger (smaller) value for disagreement leads to a larger (smaller) control input $\boldsymbol{u}_i(t)$.
- It is used in the event-detector to detect events (transmission instants) as such a larger disagreement be more likely to trigger a new event.

One example of a disagreement for node i is $\boldsymbol{q}_i(t) = \sum_{j\in\mathcal{N}_i}(\boldsymbol{x}_i(t_k^i) - \boldsymbol{x}_j(t_k^j))$. In fact, parameter $\boldsymbol{q}_i(t)$ computes a sum of relative differences between 'the most recent local event state' and 'the most recent neighbouring event states'. In 'state-feedback' control protocols, the controller also utilizes the disagreement $\boldsymbol{q}_i(t)$ and generates the control input $\boldsymbol{u}_i(t)$ based on $\boldsymbol{q}_i(t)$. In general, the state-feedback consensus protocol can be viewed as follows

$$\boldsymbol{u}_i(t) = \boldsymbol{K}\boldsymbol{q}_i(t), \tag{2.8}$$

[1] Each agent is accompanied by other units such as a sensor, a transmitter, and a receiver. For brevity these block units are omitted from the block diagram shown in Fig. 2.2.

[2] Note that the event-detectors in different nodes may operate asynchronously, implying that the sequence of events for nodes i and j, $(1 \le i, j \le N, j \ne i)$, may not be the same.

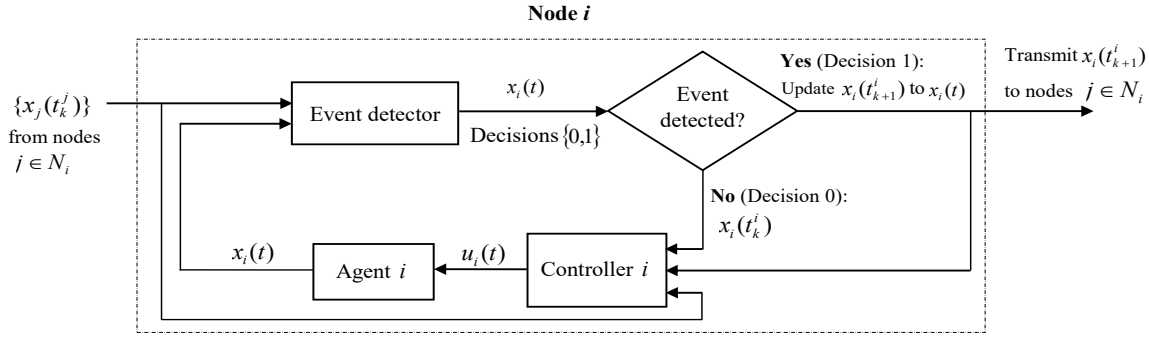

Figure 2.2: A general event-triggered consensus configuration in node i for $t \in [t_k^i, t_{k+1}^i)$.

where $\boldsymbol{K} \in \mathbb{R}^{m \times n}$ is a control gain to be designed. According to (2.8), the controller signal $\boldsymbol{u}_i(t)$ remains the same in the time interval between two events (either local or neighbouring events). In other words, the control protocol is also event-triggered [3].

In ET schemes, a parameter (known as the state error or measurement error) is often computed based on the difference between the 'real-time local state $\boldsymbol{x}_i(t)$' and 'the most recent local event state $\boldsymbol{x}_i(t_k^i)$'. One example of the state error is $\boldsymbol{e}_i(t) = \boldsymbol{x}_i(t_k^i) - \boldsymbol{x}_i(t)$, $t \in [\, t_k^i,\, t_{k+1}^i \,)$. The state error and disagreement value usually play an important role in the event-triggering condition. In one sort of the ET schemes, for example, the next event is detected as soon as the norm of the state error exceeds the norm of the disagreement (with a design parameter for scaling). Mathematically, this ET scheme can be viewed as

$$t_{k+1}^i = \inf\{t > t_k^i \mid \|\boldsymbol{e}_i(t)\| - \phi \|\boldsymbol{q}_i(t)\| \geq 0\}, \qquad t_0^i = 0, \qquad 1 \leq i \leq N, \tag{2.9}$$

where $\phi > 0$ is a design parameter. When t_{k+1}^i is detected, the event state $\boldsymbol{x}_i(t_{k+1}^i)$ is transmitted to both the local controller and the neighbouring nodes. The feedback loop in Fig. 2.2 is continued until a desired level of consensus is achieved.

Once the structures of the control protocol and ET scheme are determined, the next step is to design unknown control and ET parameters (in this case the control gain $\boldsymbol{K}$ and ET constant ϕ). The most common approach for tuning unknown parameters and guarantee event-triggered consensus is to convert the consensus problem into a stability problem. In other words, the stability conditions for the converted system is the sufficient conditions for consensus in the original system. A deep discussion for the design approaches in ETC is given in Section 2.4. Next, a phenomenon known as the Zeno-behaviour that may occur in ET schemes is discussed.

[3] It should be noted that in some ETC implementations, unlike Fig. 2.2, only the control input $\boldsymbol{u}_i(t)$ is event-triggered and transmission between the nodes is not event-triggered. In all implementations proposed in the thesis the transmission is event-triggered. The control protocol may or may not be event-triggered.

2.2.3 Zeno-behaviour

It should be noted that in any ET scheme, the time interval between two event instants must be strictly positive. Otherwise, the event-detector may detect an infinite number of events in a finite interval. This phenomenon, which may destabilize the ET scheme, is known as the Zeno-behaviour. It is, therefore, necessary to exclude the Zeno-behaviour in any proposed ET schemes. As it will be observed later, the Zeno-behaviour does not appear in the stability analysis of the MAS and its exclusion should be carried out as a separate step. The exclusion of the Zeno-behaviour is usually accomplished by obtaining a strictly positive lower-bound between two potential event instants. In other words, if one guarantees that the minimum possible interval between two event instants in a row is strictly positive, then the possibility of detecting infinite number of events in a finite period is ruled out. This implies that the possibility of the Zeno-behaviour is ruled out.

The implementation of an ETC scheme is influenced by the design objectives and operational constraints. In what follows, some important design objectives and constraints in the context of ETC are discussed.

2.3 Design objectives and constraints

The design of an ETC implementation requires assessment of different matters which arise from either the nature of the event-triggered cooperative MASs or the environmental constraints. In what follows, some of the important objectives and constraints for ETC are discussed.

- *Consensus guarantee*: The main design objective in an ETC implementation is to guarantee consensus among the agents. Otherwise, the main goal of the implementation, which is consensus, may not be achieved. As mentioned previously, the most common approach to guarantee ETC consensus is to convert the consensus problem into a stability problem. In other words, the stability conditions for the converted system is the sufficient condition for consensus in the original system.

- *Control protocol*: The consensus control protocol is the main component that evolves the agents through consensus. Even if consensus is guaranteed, a poorly designed control protocol may impact the MAS in the following ways: (i) It may generate large and fluctuating input values that are undesirable for the actuators; (ii) It may lead to a slow consensus convergence rate and consensus reaches after an excessive amount of time; and (iii) It may force the ET scheme to trigger events more frequently than required which wastes communication energy resources [4]. Therefore, designing an efficient control protocol is crucial. The most common control protocols used for consensus is the state-feedback [24], static

[4]It will be shown in Section 4.1 that the control gain directly impacts the minimum interval between two event instants.

output-feedback [25], dynamic output feedback [26], sliding mode [27], and model predictive protocols [28].

- *Event-triggering condition*: The event-detector (which is responsible to trigger events) is based on an ET condition with some unknown design thresholds. Even if consensus is guaranteed, an ET scheme may be conservative. Conservation in the context of the ET schemes usually refers to inefficiency in saving transmission packets. The structure of the ET condition and proper design of its unknown thresholds are two crucial matters for an efficient ET scheme.

- *Exclusion of the Zeno behaviour*: As mentioned previously, in any proposed ET scheme, there must be a finite number of event-triggerings within a finite time interval. It should be noted that the analytical approaches (such as the Lyapunov stability theorem) which guarantee stability (consensus) does not exclude the possibility of the Zeno behaviour. Therefore, the exclusion of the Zeno behaviour is accomplished as a separate step. Some physical constraints such as measurement noise and communication delay may lead to Zeno-behaviour in an ET scheme which does not exhibit the Zeno-behaviour in ideal circumstances. Therefore, it is important to equip the ET scheme with proper structure to operate in a non-Zeno situation.

- *Measurement and event monitoring schemes*: The ET scheme is capable of saving transmissions only from the *transmitter* side. It is still important to reduce processing from other departments such as the state measurement. Additionally, if an ET scheme is required to be monitored continuously to detect possible events, it wastes energy. One approach to reduce the amount of state-measurement and event monitoring is to incorporate a sampler with the agents [29]. Then, all processing can be performed periodically and no continuous-time processing is needed. Consensus (stability) guarantees for sampled-data implementations is often more challenging.

- *Steady-state Consensus Error*: Ideally, the ET scheme should not lead to a steady-state error in consensus. In some ETC schemes [30], however, consensus can be reached only within a steady-state bounded error. It is worth mentioning that the exclusion of the Zeno-behaviour in some implementations is only guaranteed for bounded consensus. In other words, an error from consensus is inevitable for exclusion of the Zeno behaviour.

- *Agent dynamical model*: ETC implementations are often designed for a certain class of agents. Depending on the application, the agents may be first-order integrators, second-order integrators, general linear, and nonlinear models. First-order integrators are usually used for average consensus. The other models may represent dynamics of mobile robots, spacecraft satellites, UAVs, AUVs, etc. The design complexity grows with the complexity of the agent dynamics. Homogeneity or heterogeneity in agent models is also an important matter in ETC. If the agents are

heterogeneous (i.e., agents have different dynamical models in a MAS), the ETC problem becomes more challenging. In case that the agents are not identical, the heterogeneity of the models should also be taken into consideration for consensus analysis.

- *Directed or Undirected Communication Topology*: Based on the bi-directional or uni-directional communication topology between the nodes, networks are classified into two categories of directed and undirected networks. The type of the operating network (directed or undirected) plays an important role in consensus analysis. Ideally, consensus implementation should be applicable to both types of the networks. In some schemes, however, bi-directional communication is used to facilitate stability and consensus analysis.

- *Physical Constraints*: In practice, operational MASs are subject to many physical and environmental constraints such as the channel noise, measurement errors, performance degradation due to the finite word length, packet dropouts, communication delays, uncertainties in modeling, round-off errors, malicious attacks, network connectivity changes, actuator faults, and actuator saturation. These constraints can vastly influence the performance of the proposed implementation. An ideal implementation should cope with the above constraints. In theory, however, the complexity of ETC analysis may significantly grow when the above physical and environmental constraints are considered in analysis. Similar to other control engineering problems, explicit analysis may be overwhelming (or in some cases not feasible) when too many constraints are considered for ETC.

- *Optimality of Design*: In many control applications, a cost or a performance index is included which optimizes the design parameters and the overall performance of the system with respect to the proposed objective function or cost. In the context of ETC, it is also desirable to include control optimization techniques (such as the H_∞ optimization, H_2 optimization, and guaranteed cost techniques) in analysis. Having a structured trade-off between the consensus convergence rate and the number of transmissions, for example, can only be reached using a sort of optimization.

- *Distributed Design Stage*: As stated previously, the consensus iterations are distributed and performed locally without requiring a fusion center. Recently, there has been a surge of interest to design unknown parameters for the ETC in a distributed fashion based only on neighbouring information. Tunning necessary parameters in a distributed manner increases flexibility of the scheme to unknown and unpredictable changes in the configuration.

- *Resilience to Cyber attacks*: A major objective in control of networked systems is resilience to Cyber-attacks directed to make the network non-operational. In general, these attacks can be classified into two categories, namely, deception [31] and denial of service (DoS) [32]. In deception attacks, the attacker manipulates the

actual measurements. The falsified information degrades the performance of the MAS. In DoS, on the other hand, the attacker attempts to block transmissions and measurements. It is important to study the resilience of MAS to malicious attacks and provide necessary defense actions, so that the MAS remains operational in the presence of attack.

2.4 Design approaches

Event-triggered consensus implementations require a procedure to design the control and ET parameters. In general, the design approaches can be classified into two categories: (i) Emulation-based, and (ii) Co-design.

2.4.1 Emulation-based

Typically, the emulation-based approaches [1, 33–35] are based on two steps. In the first step, the ET scheme is ignored, i.e., it is assumed that the transmission scheme between the neighbouring nodes is continuous-time. The control parameters are designed under this assumption and based on the stability of the system without the ET scheme [5]. Given these values for the control parameters, the second step designs the required ET parameters. The emulation-based design approach has the following advantages:

- It usually gives way to *explicit* stability solution for the MAS. In other words, using an emulation-based approach unknown design parameters can be obtained *analytically* and the feasible regions are clearly determined.
- The computational complexity of design does not grow with the number of participating agents in the MAS.

On the other hand, the emulation-based approaches have three main disadvantages:

- The initial choice of the control parameters limits the feasibility region of the ET parameters. Therefore, in these approaches the inter-event time (i.e., the time between two successive events) may be small leading to frequent transmissions [36] and conservativeness in the ET scheme.
- The emulation-based approaches often derive some feasible *regions* for the operating values of the ET parameters. However, selecting proper values from a continuous domain is still difficult and requires trial and error to fully observe the impact of each variable on the MAS performance.

[5] It is worth mentioning that the control gain in many ETC implementations for average consensus is assumed *a priori* and equals one. This technique, i.e., assuming a priori value for the control gain (which guarantees stability for the closed-loop system without the ET scheme) is also regarded as an emulation-based approach.

- Incorporating optimization and performance objectives within the emulation-based approaches is difficult. In other words, these approaches often guarantee only asymptotic (or exponential) stability (consensus) for the MAS with no further performance objectives.

2.4.2 Co-design

Another method for tuning unknown parameters in ETC is the Co-design approach [36–40]. In co-design approaches (which is also known as the unified approach) all unknown parameters are simultaneously designed in one step. Compared to emulation-based approaches, co-design provides the following benefits

- It is more convenient to include physical constraints (such as communication delay and uncertainties) in co-design approaches.
- The co-design approaches are able to include performance objectives such as the H_∞ optimization [39], guaranteed cost [41], L_2 optimization [38], and inter-event interval maximization [36]. Unlike the emulation-based approach, co-design usually computes the exact values of the unknown parameters based on the desired objective.

The co-design approach has the following disadvantages

- Many co-design implementations are dependent on a numerical solution. More importantly, the feasible regions for design parameters usually remain unknown in co-design techniques.
- In most cases, the computational complexity of the solution grows as the number of agents increases in the MAS.

With the advances in numerical computation, linear-matrix-inequality-based solutions have been extensively used in the literature within a co-design approach [42–45].

As discussed above, both design approaches offer some advantageous and have some disadvantageous. In the thesis, both the approaches are used in the proposed implementations.

2.5 Research gaps

The basics of many proposed implementations for ETC is mainly based on the configuration explained in Section 2.3. An in-depth overview of recent advances in ETC is provided in [6] (up to 2018) and [46] (up to 2019), where some insightful understanding is given on advantages and limitations of different ETC implementations. In what follows, some of the research gaps observed in the literature are discussed.

G1. Consensus convergence rate: An important topic in cooperative MASs is the *convergence rate* of the proposed implementation to the desired objective [47]. In this

regard, a *flexible rate* or a finite-time convergence is of great importance. Asymptotic rate of convergence does not provide any flexibility in terms of consensus convergence and may result in conservative performance, i.e., the agents may not converge to consensus in a timely manner. Alternatively, the control and ET parameters can be designed according to a flexible exponential rate of consensus. To preserve a satisfactory rate of convergence in an event-triggered fashion, an exponentially fast approach is developed in [48] which requires continuous-time measurement and monitoring of the ET conditions. An ET method is proposed in [49] that guarantees a finite-time consensus within only first-order agents. In more general cases where agents may be of high order dynamics and only sampled states of the agents are available, maintaining a minimum rate of consensus convergence is a challenging task.

G2. Inefficient parameter design for the ET scheme: As mentioned previously, a major disadvantage of emulation-based approaches is that the initial choice of the control parameters limits the feasibility region for the ET parameters. While the inter-event time (i.e., the time between two consecutive events) can be guaranteed to be strictly positive in emulation-based approaches, its value may be small, leading to a relatively high frequency of transmissions [36]. One solution to overcome this limitation and increase the inter-event time is to simultaneously design the control and ET parameters in a co-design approach and based on increasing the inter-event interval. Formulation of a co-design framework is usually more challenging. Non-existence of an efficient approach to co-design the control and ET parameters through a distributed optimization deserves further attention.

G3. Continuous-time states measurement and monitoring: In many ETC schemes [1, 32, 50–52] the ET condition is required to be monitored in a continuous-time manner for detection of potential events. These schemes are feasible only if continuous-time measurement of the states is possible. Along with the implementation difficulties of such approaches, constant measurement and monitoring of the ET conditions waste valuable energy resources allocated to nodes. To eliminate this limitation, sampled-data approaches which allow the ET condition to be monitored only at periodic samples of the systems are proposed in [53–58]. However, the applicability of these implementations to more complicated situations, such as the presence of malicious attacks, is still in its infancy.

G4. Resilience to Cyber Attacks: Resilience to DoS attacks has been studied in [1, 32, 37, 50–52, 59–69] for a variety of applications under different assumptions. Despite presenting several advantageous results, existing strategies that investigate resilience to DoS attacks face different shortcomings and are based on some unrealistic assumptions. For example, the ET schemes considered in [1, 50–52] are required to be monitored continuously. Additionally, transmission with precise values of the state is a common assumption is the context of consensus subject to DoS attacks. Quantized transmission leads to an additional term in the closed-loop system, which makes the design analysis challenging when DoS attacks are considered, as such have been overlooked. Assuming that the DoS follows a periodic behavior, the resilience of different NCSs under DoS is investigated in [37,63,66]. Due to the unknown nature of

the adversary, considering a periodic pattern for DoS may not be the case in practice.

G5. Infinite precision for the nominally designed parameters: It is a common assumption in ETC that the design parameters such as the control gains are implementable with infinite precision. However, it is widely known that the precise realization of the control gain, for example, is often subject to round-off error and uncertainties due to the physical restrictions from hardware aspects [70]. The uncertainties in realization of the control gains can cause considerable performance deterioration. In this regard, *non-fragile* control design techniques, which take into account the uncertainties of the controller realization, are considered in various control problems [70, 71]. It should be noted that since limited neighbouring information is used in ET schemes, the closed-loop system is more vulnerable to such uncertainties. A distributed implementation for non-fragile control design is of great interest for ETC.

G6. Infinite precision for state transmissions: Due to the limited storage and communication bandwidth in practical applications, information exchanges between the neighbouring agents is quantized (coded) prior to transmission [72,73]. Therefore, quantization is a necessary step for real implementations. In the context of ETC, it is often assumed that the information can be transmitted with infinite precision.

G7. Old-fashioned ET schemes: Many ET schemes are only based on the disagreement between the states and some set-valued thresholds. Developing more advanced ET schemes to further reduce the number of transmissions without introducing steady-state error in consensus is in great demand. As one of the most advanced ET schemes, *dynamic* event-triggered (DET) mechanisms have been utilized recently in MASs [74–76]. In such schemes, an internal dynamic variable is included which acts as an additional threshold in the ET condition. One interesting property of the DET schemes is that their inter-event time is larger than many old-fashioned schemes. At the same time, consensus can still be reached without any steady-state error when using DET schemes. This is in contrast to some other ET schemes [35] where the cooperative objective can be reached only within a bounded error. In DET schemes, the stability analysis of the closed-loop system is typically more difficult due to the introduction of an additional dynamic variable [46]. The applicability of the co-design optimization approach for DET consensus-based schemes has not yet been studied. Additionally, continuous-time measurement and event monitoring is required in [74–76] which is not desirable.

2.6 Main contributions of the Thesis

To address the research gaps discussed in Section 2.5, the following implementations have been proposed in the thesis. Based on the dynamic model considered for the agents, these implementations are categorized as 'single-order agents' and 'general linear agents'.

2.6.1 Single-order agents:

- **CEASE** [77]: is a distributed framework for collaborative, event-triggered, average consensus, sampled data (CEASE) algorithm for undirected networked multi-agent systems. CEASE focuses on research gaps G1, G2, and G3. This algorithm ensures a desired exponential consensus convergence rate and computes control and ET parameters based on an objective function for increasing the inter-event intervals and decreasing the steady-state consensus error. The ET threshold and control gain are designed simultaneously through a convex constrained optimization problem. Following some preliminary steps, the optimization can be performed locally. Additionally, the computational complexity of the proposed optimization does not grow proportionally with the number of nodes in the network.

- **Q-CEASE** [78]: is a distributed framework for quantized collaborative event-triggered average consensus sampled-data in MASs. Q-CEASE addresses gaps G3 and G6. Q-CEASE communicates quantized information with its neighbouring nodes only if a periodic ET condition is satisfied. Both design and implementation of Q-CEASE are distributed and do not require a fusion center. The design stage determines operating regions for the sampling period and ET thresholds for the constituent nodes using an emulation-based approach.

- **RQ-CEASE** [79]: is a resilient framework for quantized, collaborative, event-triggered, average consensus, sampled-data in multi-agent systems subject to denial of service (DoS) attacks. RQ-CEASE addresses gaps G3, G4, and G6. The DoS attacks attempt to block the measurement and communication channels in the network. Two different ET approaches are considered in RQ-CEASE based on whether the ET condition is dependent or independent of the state dynamics. For each approach, the operating conditions (bounds) for the sampling period and ET design parameter are derived analytically so as to guarantee the input-to-state (ISS) stability of the network under DoS attacks. In addition, upper bounds for duration and frequency of DoS attacks are derived within which the network remains operational. For each approach, the maximum possible error from the average consensus value is derived.

- **DEASE**: A distributed dynamic event-triggering average consensus algorithm with sampled-data (DEASE) is proposed with the focus to improve the efficiency of the ET scheme and avoid consensus error. DEASE addresses the gaps G2, G3, and G7. In contrast to CEASE, Q-CEASE, RQ-CEASE, where the ET scheme reduces the number of transmissions at the expense of a bounded error for consensus DEASE does not produce error and better saves unnecessary transmissions. The state measurement and event monitoring schemes in DEASE are periodic. Parameter design in DEASE is based on the co-design method and increases the minimum inter-event interval using convex optimization. However, unlike CEASE, the dimensions of the optimization grows with the network size.

2.6.2 General linear agents

- **PEC** [80]: is a performance guaranteed event-triggered consensus implementation for general linear multi-agent systems. PEC addresses gaps G1, G2, and G5. PEC guarantees a desired rate of convergence convergence, non-fragility to control gain uncertainties, and optimality of design parameters, namely, the control and ET parameters. Using an approximated linear scalarization method, the ET thresholds and control gain are designed simultaneously by solving a convex constrained optimization problem. Similar to CEASE, the optimization in PEC can be performed locally. In PEC continuous-time state measurement and event monitoring are required.

- **PSEC** [81]: is a performance guaranteed sampled-data event-triggered consensus algorithm for linear MASs. PSEC addresses gaps G1, G3, and G5. Communication between the nodes is based on the fulfillment of distributed state-dependent sampled-data ET conditions. PSEC ensures a guaranteed exponential convergence rate and is non-fragile to norm-bounded uncertainties in control gains resulting from implementation distortions. The Lyapunov-Krasovskii theorem is used to incorporate the performance objectives. Consensus design parameters in PSEC are simultaneously computed within a set of linear matrix inequalities.

- **R-PSEC**: R-PSEC (resilient-PSEC) extends PSEC to the situation where unknown DoS attacks attempts to prevent consensus. R-PSEC addresses the gaps G1, G3, G4, and G5. In R-PSEC, the desired level of resilience to DoS is included as a design input. The proposed R-PSEC demonstrates the trade-off between the DoS resilience level and consensus performance indices. R-PSEC is based on a co-design approach and simultaneously co-designs control and ET parameters based on desired values for the sampling period, consensus convergence rate, non-fragility level, and DoS resilience level.

- **ROCCET** [82]: is a resilient optimized consensus using dynamic event-triggered scheme for linear MASs configured as undirected networks. ROCCET addresses gaps G1, G2, G4, and G7. ROCCET is based on continuous-time state measurement and event monitoring. Similar to DEASE, the event-triggering scheme used in ROCCET is dynamic which further reduces the number of events. Similar to R-PSEC, in ROCCET a desired level of resilience to DoS is included as a design input. A co-design optimization technique is used to simultaneously compute all required control and dynamic event-triggering parameters. The optimization in ROCCET increases the inter-event interval based on a given consensus convergence rate and resilience to DoS attacks.

2.6.3 Extension to formation-containment

Cooperative behaviours in the form of leader-following consensus, formation, and containment have attracted considerable attention in a variety of vehicular MASs. Recently, the formation-containment control (FCC) framework, which can be regarded as the combined problem of formation and containment for MASs, has arisen in several engineering applications [83–94]. In FCC, the leaders converge to a desired geometric formation. Simultaneously, the followers merge within the convex hull spanned by the leaders. As compared to solitary containment [12, 95–98] and solitary formation [99–101], FCC is more complex and a topic of increasing interest in the control and signal processing community. A formation-containment control approach using a dynamic event-triggered mechanism (FCC/DEME [102]) that offers optimality for design parameters, namely the control gains and dynamic event-triggering parameters is proposed in Chapter 6. The main features of the proposed FCC/DEME [102] that differentiate it from existing implementations are listed below:

- As opposed to FCC implementations [83,84,86,88–93], where all transmissions are time-triggered (i.e., continuous-time), in FCC-DEME the follower-follower and leader-leader transmissions are event-triggered.
- FCC/DEME is the first implementation for formation-containment that utilizes the *dynamic* event-triggered mechanism. This leads to considerable energy and communication savings for formation-containment in MASs.
- Two different sets of control and dynamic event-triggering parameters are introduced for: (i) formation of the leaders, and; (ii) containment of the followers. FCC/DEME utilizes two convex optimizations for co-designing associated parameters based on enabling a trade-off between the rate of convergence for formation-containment and the frequency of transmission.

2.6.4 Stabilization control

In appendix, a co-design framework for stabilization control of a class of NCSs under unknown DoS attacks is proposed. To reduce the number of control inputs, a sampled-data dynamic event-triggering (S-DET) scheme is developed. Both the state measurements and monitoring of the S-DET are conducted periodically. The parameter design is based on the solution of linear matrix inequalities (LMI) obtained from a delay-dependent Lyapunov-Krasovskii functional using the improved free weighting matrix technique. The proposed co-design approach demonstrates the trade-off between the DoS resilience level and system performance indices.

2.7 Publications

The following articles have been published from this dissertation.

J6. A. Amini, A. Asif, A. Mohammadi, and A. Azarbahram, "Sampled-data Dynamic Event-triggering Control for Networked Systems Subject to DoS Attacks", *IEEE Transactions on Network Science and Engineering*, *second round of peer review*, 2020.

J5. A. Amini, A. Asif, and A. Mohammadi, "A Unified Optimization for Resilient Dynamic Event-triggering Consensus Under Denial ", *IEEE Transactions on Cybernetics*, In press, 2020.

J4. A. Amini, A. Asif, and A. Mohammadi, "Formation-Containment Control Using Dynamic Event-triggering Mechanism for Multi-agent Systems", *IEEE/CAA Journal of Automatica Sinica*, vol. 7, no. 5, pp. 1235 - 1248, 2020.

J3. A. Amini, A. Asif, and A. Mohammadi, "RQ-CEASE: A Resilient Quantized Collaborative Event-Triggered Average-Consensus Sampled-Data Framework Under Denial of Service Attack", *IEEE Transactions on Systems, Man, and Cybernetics: Systems*, Early access, 2020.

J2. A. Amini, A. Asif, and A. Mohammadi, "A performance guaranteed sampled-data event-triggered consensus approach for linear multi-agent systems", *Information Sciences*, vol. 484, pp.338-349, 2019.

J1. A. Amini, A. Asif, and A. Mohammadi, "CEASE: A collaborative event-triggered average-consensus sampled-data framework with performance guarantees for multi-agent systems," *IEEE Transactions on Signal Processing*, vol. 66, no. 23, pp.6096-6109, 2018.

C7. A. Amini, Z. Zeinaly, A. Mohammadi, and A. Asif, "Performance constrained distributed event-triggered consensus in multi-agent systems," in 2019 American Control Conference (ACC), pp. 1830-1835, 2019.

C6. A. Amini, A. Asif, and A. Mohammadi, "Quantized event-triggered sampled-data average consensus with guaranteed rate of convergence," *in ICASSP 2019-2019 IEEE International Conference on Acoustics, Speech and Signal Processing (ICASSP)*, pp. 4614-4618, 2019.

C5. A. Amini, A. Azarbahram, A. Mohammadi, and A. Asif, "Resilient Event-triggered Average Consensus Under Denial of Service Attack and Uncertain Network," *In 2019 6th International Conference on Control, Decision and Information Technologies (CoDIT)*, pp. 291-296. IEEE, 2019.

C4. A. Amini, A. Mohammadi, and A. Asif, "Resilient Event-Triggered Consensus with Exponential Convergence in Multi-agent Systems," *In 2018 Annual American Control Conference (ACC)*, pp. 2889-2896. IEEE, 2018.

C3. A. Amini, A. Asif, and A. Mohammadi, "A Robust Event-Triggered Consensus Strategy for Linear Multi-agent Systems with Uncertain Network Topology." *In 2018 IEEE International Conference on Acoustics, Speech and Signal Processing (ICASSP)*, pp. 3659-3663. IEEE, 2018.

C2. A. Amini, A. Asif, and A. Mohammadi, "An Event-Triggered Average Consensus Algorithm with Performance Guarantees for Distributed Sensor Networks." *In 2018 IEEE International Conference on Acoustics, Speech and Signal Processing (ICASSP)*, pp. 3409-3413. IEEE, 2018.

C1. A. Amini, A. Mohammadi, and A. Asif, "Event-based consensus for a class of heterogeneous multi-agent systems: An lmi approach," *In 2017 IEEE International Conference on Acoustics, Speech and Signal Processing (ICASSP)*, pp. 3306-3310. IEEE, 2017.

2.8 Summary

This chapter introduces necessary background for the event-triggered consensus (ETC) in multi-agent systems (MAS). The ETC problem is reviewed from a general point of view. Important design objectives and constraints for ETC are discussed based on an overview of the recent state-of-the-art literature. Based on the research gaps observed in existing ETC works, some consensus algorithms are proposed for both the first-order and general linear MASs, which will be presented in the next chapters. Additionally, two implementations for the event-triggered formation-containment problem and stabilization problem of networked control systems are proposed.

Chapter 3

Consensus in First-order Agents

This chapter focuses on event-triggered consensus in first-order agents, where three different implementations (namely, CEASE [77], Q-CEASE [78], and DEASE) are proposed in this regard[1]. Each implementation is presented in a separate section of this chapter (Sections 3.2 to 3.4). Section 3.5 provides a summary of the proposed implementations. Proofs of all the proposed theorems in this chapter are given in Section 3.6. Before presenting the proposed implementations, the nature of the schemes are reviewed for different processes required in consensus.

3.1 Measurement, communication, and control schemes

In this chapter, it is assumed that all nodes are clock synchronized, i.e., there exists a common clock which handles certain processing in all nodes. In all the proposed implementations in this chapter, the measurement, event-monitoring, communication, and control schemes are based on the following structures

- **State measurements scheme**: The state measurement scheme is periodic, i.e., a sampler is incorporated with each node to measure the state of the agent. The sampler operates based on the synchronized clock.
- **Event monitoring scheme**: The ET monitoring schemes considered in this chapter are periodic (sampled-data) which operate according to the synchronized clock.
- **Transmitter scheme**: The state transmission to the neighbouring nodes is sampled-data event-triggered. This implies that the transmission only occurs on *some* samples of the agents determined by the ET condition.

[1]Proposed implementations for ETC in MASs with general linear dynamics are given in Chapters 4 and 5.

- **Receiver scheme**: Since the ET scheme is localized, nodes are not aware of the time when updates are transmitted by their neighbouring nodes. However, due to the synchronized clock, no event is expected in inter-sampling period. Therefore, the receiver at each node operates based on the synchronized clock and thus follows a periodic pattern.

- **Control scheme**: The control protocol, which enforces the nodes to reach average consensus, is sampled-data event-triggered in this chapter.

3.2 CEASE

As mentioned in Chapter 2, several strategies [103–106] are proposed to reduce the number of information exchanges between the nodes and preserve energy resources. As a major drawback, the event detection process in many ET schemes are modeled in continuous-time and requires continuous measurements and threshold comparisons [107]. In an effort to overcome this limitation, a sampled-data ET mechanism has been proposed in [108], where the event condition is monitored periodically at certain instants.

In practice, it is often desirable to design average consensus algorithms that guarantee a certain level of performance or cost. As mentioned in [6, Section V], distributed optimization techniques, which aim at finding an optimal strategy subject to desired performance constraints, have not yet been investigated for sampled-data event-triggered consensus. Ensuring a finite time or a minimum rate of consensus convergence (as opposed to asymptotic convergence) is another important performance index [109]. In this regard, an exponentially fast ET consensus framework has been proposed in [48]. However, only control inputs are event-triggered and constant communications across the network is still a requirement. The literature review shows that there is a need to develop a distributed structured optimization framework for ETC which ensures some performance guarantees such as a flexible rate of convergence and optimization for design parameters. To this end, a distributed framework for collaborative, event-triggered, average consensus with sampled data (CEASE) is proposed. The main contributions of CEASE are as follows

- In CEASE, a co-design approach for computing the consensus design parameters, i.e., control gain and ET threshold, is used to incorporate the exponential convergence conditions. Using the Lyapunov stability theorem, the problem of finding optimal solutions for consensus parameters is transformed to a constrained convex optimization problem.

- The proposed objective function also reduces the steady-state error from consensus. Additionally, the computation complexity of the optimization stage does not grow with the network size.

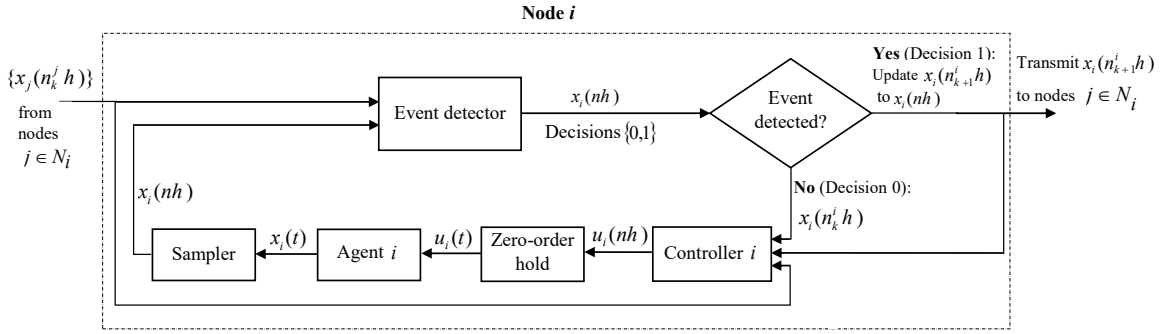

Figure 3.1: The CEASE block diagram for average consensus in node i.

3.2.1 Problem statement

Consider a multi-agent/sensor system with N nodes that require average consensus on parameter $x(t)$ associated with the system. Prior to the average consensus process, each node has a different estimate of $x(t)$, denoted by $x_i(0)$. The consensus time index is denoted by t. It is noted that the time scale for the main system may be different from the t considered for consensus steps. Similar to [4], the first-order MAS model given below is used to reach average consensus on $x_i(t)$

$$\dot{x}_i(t) = u_i(t), \quad (1 \leq i \leq N), \tag{3.1}$$

where $u_i(t) \in \mathbb{R}$ is a distributed consensus control protocol to be introduced later.

Assumption 1. MAS (3.1) is configured as an undirected (symmetric) connected network.

A proposed protocol for $u_i(t)$ is said to solve the average consensus problem, if and only if, the following condition is satisfied

$$\lim_{t\to\infty} |x_i(t) - \bar{x}(0)| = 0, \quad (1 \leq i \leq N), \tag{3.2}$$

where $\bar{x}(0) = \frac{1}{N}\sum_{i=1}^{N} x_i(0)$. To reach average consensus, each node shares its state values with its neighbouring nodes. In order to reduce the number of transmissions, a distributed event-detector is incorporated locally with each node. The event-detector allows the node to transmit its states to the neighbouring nodes only if an ET condition (to be introduced later) is fulfilled. The event-detector monitors a discretized samples of the states [108], i.e., $x_i(nh)$ with sampling period h and $n \in \mathbb{N}_0$. Upon receiving a new state from node j, $(j \in \mathcal{N}_i)$, node i updates its information regarding node j and stores this new state. The new state is being used in node i until the next event is triggered by node j. The CEASE configuration for node i $(1 \leq i \leq N)$ is shown in Fig 3.1.

Denote $\{n_0^i, n_1^i, \ldots n_k^i\}$ as the sample sequence until $t = nh$ at which events are detected (triggered) at node i and the corresponding states are transmitted to the

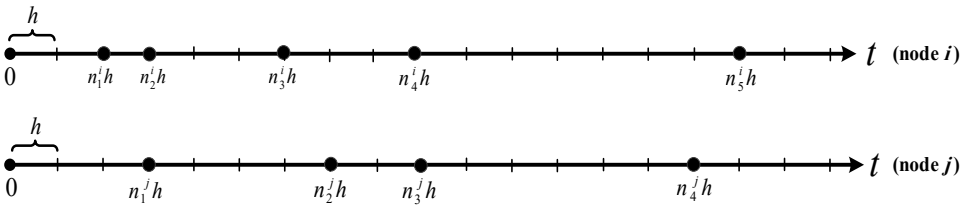

Figure 3.2: Illustrative sampled-data event-triggered (or periodic event-triggered) time diagram, with period h, for two arbitrary nodes in the network (nodes i and j). Black circles show the instants when events are detected. Since the event-triggering process is performed locally, events for node i and j does not necessarily occur at the same time instant.

neighbours. In n_k^i, the node itself is specified by superscript i [2]. Note that the event-detector is a localized unit for each node, implying that the $k-$th event for node i does not necessarily occur at the same time as the $k-$th event for node j. Fig. 3.2 shows an illustrative example of sampled-data event-triggering for two nodes (nodes i and j) in the MAS.

Define the most recently transmitted state of node i as $\hat{x}_i(nh) \triangleq x_i(n_k^i h)$ for $t \in [\, n_k^i h,\, n_{k+1}^i h\,)$. Relying on the last received/transmitted states, the following distributed control protocol is used for node i, $(1 \leq i \leq N)$, to reach distributed event-triggered average consensus in (3.1)

$$u_i(t) = \mathcal{K}\mathbb{X}_i(nh), \tag{3.3}$$

where scalar $\mathcal{K} \in \mathbb{R}$ is the control gain to be designed and

$$\mathbb{X}_i(nh) = \sum_{j \in \mathcal{N}_i} a_{ij}\Big(x_j(n_k^j h) - x_i(n_k^i h)\Big). \tag{3.4}$$

It is worth noting that the control protocol (3.3) is a more general protocol for achieving average consensus as compared to the one frequently used in existing literature where $\mathcal{K}$ is assumed *a priori* [110] and equals 1. Since the choice of $\mathcal{K}$ affects both the convergence rate of consensus and the number of transmissions, its design is important.

Given the sample instant $n_k^i h$, the next event for node i is triggered at instant $n_{k+1}^i h$, where n_{k+1}^i satisfies the following condition (monitored by the event-detector)

$$n_0^i = 0, \qquad n_{k+1}^i = \min_n \{n \mid n > n_k^i, \quad |e_i(nh)| \geq \phi_1 |\mathbb{X}_i(nh)| + \phi_2\}. \tag{3.5}$$

Positive scalars ϕ_1 and ϕ_2 are the ET constants to be designed and $e_i(nh) = x_i(nh) - x_i(n_k^i h)$ is the state error (also known as the measurement error). In fact, $e_i(nh)$ is the difference between the most recently transmitted state $x_i(n_k^i h)$ and the state value at sample n, i.e., $x(nh)$.

Remark 3.1 (Zeno behaviour)**.** It should be noted that in a *sampled-date* event-triggering mechanism (such as CEASE) any two consecutive events are lower-bounded

[2]With h as the sampling period, $n_3^2 h$, for example, denotes the instant when the 4^{th} event is triggered at node 2.

by at least one sampling period h. Therefore, Zeno-behaviour is avoided in such a scheme and no further analysis is needed in this regard. The exclusion of Zeno behaviour is not trivial if the event detection process needs continuous-time measurements and monitoring [111]. In chapter 4, necessary analysis for exclusion of the Zeno-behaviour for implementation of PEC will be given.

Consensus analysis in CEASE is mainly based on the input-to-state stability of a converted system. The definition of Input-to-State Stability is given below.

Definition 1 (*Input-to-State Stability* [107])**.** A dynamical system with state $x(t)$ and input $v(t)$ is input-to-state stable (ISS) if there exist a class $\mathcal{KL}$ function f_1 and a class $\mathcal{K}$ function f_2 such that $\|x(t)\| \leq f_1(\|x(0)\|, t) + f_2(\|v(t)\|_\infty)$, $\forall t \geq 0$, where $\|.\|_\infty$ denotes the $\mathcal{L}_\infty$ norm.

3.2.2 Design objectives

It is clear from (3.5) that extremely small values for ϕ_1 and ϕ_2 lead to detection of events on almost every samples. In this case, the ET scheme reduces to a mere sampled-data scheme. On the other hand, an extremely large value for ϕ_1 may endanger the closed-loop stability due to lack of sufficient state exchanges. Therefore, a proper value for ϕ_1 which efficiently reduces the number of event-triggerings is of great importance. From (3.5), it can be noticed that a larger value for parameter ϕ_2 increases the ET threshold. Hence, a fewer number of transmission is expected with a larger ϕ_2. In return, increasing the value of ϕ_2, as will be shown later, increases the consensus steady-state error. From a control point of view, the value of control gain $\mathcal{K}$ impacts the convergence rate. A large value for $\mathcal{K}$ accelerates the consensus convergence. However, it forces undesirable large control inputs. It can be shown that a higher value for $\mathcal{K}$ leads to a higher frequency of event-triggerings as well. The design objectives in CEASE are summarized as follows:

- Guarantee a predefined exponential rate for consensus convergence;
- Include an objective function in the parameter design optimization to reduce the number of event-triggerings, reduce the control input effort, and reduce the steady-state error from average consensus;
- Preserve the distributed nature of the MAS in the design stage. In other words, the optimization stage for computing unknown parameters should be performed in a distributed fashion.
- Computational complexity of the optimization is desired to be irrespective of the network size N.

3.2.3 Closed-loop multi-agent system

Define the following global vectors

$$\begin{aligned} \boldsymbol{x}(t) &= [x_1(t), \ldots, x_N(t)]^T, \qquad \hat{\boldsymbol{x}}(nh) = [\hat{x}_1(nh), \ldots, \hat{x}_N(nh)]^T, \\ \boldsymbol{u}(t) &= [u_1(t), \ldots, u_N(t)]^T, \qquad \boldsymbol{e}(nh) = [e_1(nh), \ldots, e_N(nh)]^T. \end{aligned} \tag{3.6}$$

Based on (3.6), it holds that $\boldsymbol{e}(nh) = \hat{\boldsymbol{x}}(nh) - \boldsymbol{x}(nh)$. Combining (3.3) with (3.1) leads to the following augmented MAS

$$\dot{\boldsymbol{x}}(t) = -\mathcal{K}\boldsymbol{L}\left(\boldsymbol{x}(nh) + \boldsymbol{e}(nh)\right), \quad nh \leq t < (n+1)h, \tag{3.7}$$

where $\boldsymbol{L}$ is the Laplacian matrix. The next section converts the consensus problem into an equivalent stability problem.

3.2.4 Consensus to stability conversion

A commonly used approach to guarantee consensus in (3.7) is to convert the consensus problem to an equivalent stability problem. To this end, the following vector [107] is defined

$$\boldsymbol{r}(t) = \boldsymbol{x}(t) - \bar{x}(t)\mathbf{1}_N. \tag{3.8}$$

Recall that $\bar{x}(t) = \frac{1}{N}\mathbf{1}_N^T\boldsymbol{x}(t)$. From Assumption 1 it holds that $\mathbf{1}_N^T\boldsymbol{L} = \mathbf{0}_N^T$. Additionally, for a connected symmetric network, one can verify that $\dot{\bar{x}}(t) = 0$. Since $\dot{\bar{x}}(t) = 0$, it is concluded that $\bar{x}(t) = \bar{x}(0)$. In other words, if $\|\boldsymbol{r}(t)\| \to 0$, then $\|\boldsymbol{x}(t) - \bar{x}(t)\mathbf{1}_N\| \to 0$ which leads to average consensus. Therefore, the average consensus for (3.7) is equivalent to the stability for the system expressed by $\boldsymbol{r}(t)$. Using transformation (3.8), system (3.7) is converted to the following system

$$\dot{\boldsymbol{r}}(t) = -\mathcal{K}\boldsymbol{L}(\boldsymbol{r}(nh) + \boldsymbol{e}(nh)), \qquad nh \leq t < (n+1)h. \tag{3.9}$$

Note that expression $\hat{\boldsymbol{r}}(nh) = \hat{\boldsymbol{x}}(nh) - \bar{x}(nh)\mathbf{1}_N$ holds for system (3.9). To enhance readability, in the remaining section subscript n is used to denote the argument (nh), e.g., $\boldsymbol{r}_n = \boldsymbol{r}(nh)$.

3.2.5 Parameter design

Given desired values for sampling period h and the set-valued ET constant ϕ_2, the following theorem gives sufficient conditions to compute the optimal values for control gain $\mathcal{K}$ and ET threshold ϕ_1 with respect to a proposed objective function. These values, collectively, guarantee a bounded ζ-exponential rate of consensus convergence for (3.7). The largest (λ_N) and the second smallest (λ_2) eigenvalues of the Laplacian matrix are required in the parameter optimization which can be computed distributively (with arbitrary accuracy) as follows.

Distributed computation of Laplacian eigenvalues

To compute λ_2 and λ_N (which is required in optimization (3.11)) in a distributed manner, the proposed approaches in [112–114] are suggested. Based on [112], all eigenvalues of the Laplacian matrix (including λ_2 and λ_N) can be computed locally. The maximum eigenvalue λ_N can be computed using [113, Section 4]. Additionally, the Fiedler value (λ_2) can be computed distributively from the algorithm summarized in [114, Table 1]. The proposed algorithms in [113] and [114] are scalable with respect to the network size N, i.e., the per-node computational complexity does not grow proportionally with an increase in the value of N. For ease of reference, Algorithm 3.4 (given in section 3.6.1) is provided to summarize the main steps for computing all eigenvalues and eigenvectors in a distributed fashion with arbitrary accuracy. Algorithm 3.4 is derived from on [112].

Theorem 3.1. Given desired values for exponential convergence rate ζ, sampling period h, and set-valued ET threshold ϕ_2, consensus parameters $\{\mathcal{K}, \phi_1\}$ are calculated from

$$\mathcal{K} = p^{-1}\mu, \qquad \phi_1 = \sqrt{\alpha^{-1}\gamma^{-1}}. \tag{3.10}$$

These values are conditioned on the existence of positive scalars p, α, ϵ_1, ϵ_2, μ, and γ satisfying the following convex minimization problem

$$\min_{p,\alpha,\epsilon_1,\epsilon_2,\mu,\gamma} \quad \mathcal{F} = \mu + \alpha + \gamma - p, \tag{3.11}$$

$$\textit{subject to}: \qquad \boldsymbol{\Xi} = \begin{bmatrix} \boldsymbol{\Xi}_{11} & \boldsymbol{\Xi}_{12} \\ * & \boldsymbol{\Xi}_{22} \end{bmatrix} < 0. \tag{3.12}$$

The undefined terms in (3.12) are listed below

$$\boldsymbol{\Xi}_{11} = \begin{bmatrix} -2\mu\lambda_2 + 2\zeta p & 0 & \sqrt{2}\lambda_N \\ * & -\alpha + (\epsilon_1+\epsilon_2)\lambda_N^2 & \sqrt{2}\lambda_N \\ * & * & -\gamma \end{bmatrix}, \quad \boldsymbol{\Xi}_{12} = \begin{bmatrix} h\mu\lambda_N & h\mu\lambda_N & \mu & 2h\zeta\mu \\ h\mu\lambda_N & h\mu\lambda_N & 0 & 0 \\ 0 & 0 & 0 & 0 \end{bmatrix},$$

$$\boldsymbol{\Xi}_{22} = \operatorname{diag}(-\frac{h}{2}p, -\frac{1}{2\zeta}p, -\epsilon_1, -\epsilon_2).$$

For any initial vector $\boldsymbol{r}(0)$, design parameters $\{\mathcal{K}, \phi_1\}$ computed from (3.10), stabilize system (3.9) at the given ζ-exponential rate satisfying the following ISS condition with respect to $\boldsymbol{r}(t)$

$$\|\boldsymbol{r}(t)\| < e^{-\zeta t}\|\boldsymbol{r}(0)\| + C, \tag{3.13}$$

where $C = \sqrt{\frac{\alpha}{\zeta}}\phi_2$ is the steady-state consensus error. The objective function $\mathcal{F}$ reduces the number of event-triggerings, the control effort, and the steady-state error.

Proof. Proof of Theorem 3.1 is given in Appendix, section 3.6.2. □

Remark 3.2 (Logic of the objective function (3.11))**.** As mentioned previously, an ideal objective function for CEASE would attempt to (i) Reduce the number of event-triggerings (transmissions); (ii) Reduce the steady-state error from consensus; and

Algorithm 3.1 CEASE

Input: Neighbouring connectivity information.

Output: Exponential rate of Convergence for Sampled-data Event-triggered Average-consensus.

Preliminary: Using a distributed algorithm such as Algorithm 3.4, each node computes λ_2 and λ_N. Using an average consensus the nodes agree on the value of the desired sampling period h and exponential rate of convergence ζ. Each node chooses the set-valued threshold ϕ_2.

Optimization and Parameter Design: (D1 – D2)

D1. Each node solves the minimization problem (3.11).

D2. Using the solution of (3.11), unknown parameters $\{\mathcal{K}, \phi_1\}$ are computed from (3.10).

Distributed Consensus Iterations: (C1 – C4)

C1. Each node transmits the initial state $x_i(0)$ to its neighbours.

C2. The state of agent i is excited by control law (3.3) using the $\mathcal{K}$ designed from D1.

C3. To determine the next triggering sample, condition (3.5) is locally monitored at $t = nh$ ($n \in \mathbb{N}$) using the designed ϕ_1 from step D1 and given ϕ_2.

C4. Steps C2 and C3 continue until average consensus is achieved among the nodes. MAS trajectories satisfy (3.13).

(iii) Reduce the control effort. For given sampling period h and set-valued threshold ϕ_2, the optimization should increase the value of ϕ_1 and decrease $\mathcal{K}$ to reduce the number of event-triggerings and control effort. Motivated by the proposed approaches in [115, Section 3] and [116, Section 2.2], a linear scalarization method is used to minimize the decision variables involved in obtaining $\mathcal{K}$ (i.e., p and μ) and ϕ_1 (i.e., α and γ). In fact, the proposed objective function $\mathcal{F}$ is a linear approximation of maximizing ϕ_1 (by minimizing α and γ) and minimizing $\mathcal{K}$ (by minimizing μ and $-p$). For given convergence rate ζ and set-valued threshold ϕ_2, the objective function also reduces the steady-state consensus error $C = \sqrt{\alpha/\zeta}\phi_2$ by including α in $\mathcal{F}$. The corresponding coefficients to μ, α, γ, and p are considered equal so that $\mathcal{K}$ and ϕ_1 contribute equally in $\mathcal{F}$. Alternatively, the objective function $\mathcal{F}$ can be modified as $\mathcal{F} = a_1\mu + a_2\alpha + a_3\gamma - a_4 p$, where a_c, $(1 \leq c \leq 4)$, is a desired positive weighting coefficient that differentiates the contribution of each variable in $\mathcal{F}$.

Remark 3.3 (Computational complexity)**.** The convex constrained optimization (3.11) can be solved using the interior-point algorithms which iteratively approach the optimal solution starting from the interior of the feasible set. Generally, the interior-point computational effort required to solve a semi-definite programming (SDP) problem, such as (3.11), depends on two factors: (i) The number of iterations required to approach the optimal point, and; (ii) The order of arithmetic operations required for each iteration. Let d_m denote 'the highest dimension of the LMIs associated with an SDP problem', e.g., d_m for (3.11) is the dimension of matrix $\boldsymbol{\Xi}$ and thus $d_m = 7$. Additionally, denote n_v as the 'total number of decision variables' involved in an SDP problem, e.g., $n_v = 6$ for (3.11). According to [117, 118], in the worst-case complexity the number of iterations required to solve an SDP problem grows at the $O(\sqrt{N_p}\,|\log \epsilon_g|)$ with the problem size $N_p = \max\{d_m, n_v\}$ and the duality gap denoted by ϵ_g [3]. For optimization (3.11), the problem size N_p is not dependent on

[3]The duality gap ϵ_g is the difference between the values of optimal solution for the primal and

the network size N. Therefore, the number of interior-point iterations required for solving (3.11) grows only with the desired accuracy. As for the order of arithmetic operations required in each iteration, the structure of the matrix inequalities plays a significant role. Ignoring special matrix structures (such as sparsity), each iteration in solving an SPD problem requires on the order of $\max\{d_m^3, d_m^2 n_v, C_d\}$ operations, where C_d is the cost of evaluating the first and second derivatives of the objective and constraint functions [120, Section 1.3]. That being said, the complexity of total arithmetic operations required to solve (3.11) is also irrespective of N.

Remark 3.4 (Other forms of threshold ϕ_2)**.** It should be noted that any function f that satisfies $f \leq \phi_2$, $\forall t \geq 0$, can be utilized instead of the constant threshold ϕ_2. One interesting candidate for f is a decaying exponential term in the form of $f_0 = \phi_2 e^{-ct}$, where c is a desired decaying rate. There exists a trade-off between f_0 and ϕ_2 in terms of transmission savings and consensus error. Since $\phi_2 \geq f$, $\forall t \geq 0$, the constant threshold ϕ_2 is more efficient in reducing the number of transmissions that f_0. However, f_0 is a vanishing term and does not lead to consensus error.

The next section considers state quantization within the framework of CEASE.

3.3 Q-CEASE

In the context of ETC it is often assumed that the information can be transmitted with infinite precision. In practice, however, the information is quantized to a finite number of levels [73]. It is, therefore, necessary to consider quantization of the states before transmission. This section proposes a quantized implementation for collaborative, event-triggered, average consensus with sampled data (Q-CEASE).

Different from CEASE, in Q-CEASE (as shown in Fig. 3.3) an additional block is included for quantization of the events before transmission. The parameter design approach in Q-CEASE is based on analytic upper-bounds of the Lyapunov function. Therefore, no parameter optimization is developed for Q-CEASE.

3.3.1 Problem statement

A uniform quantizer $q(\cdot) : \mathbb{R} \to \delta\mathbb{Z}$ with a quantization level $\delta > 0$ is defined by $q(x) = \lfloor x\delta^{-1} + 0.5 \rfloor \delta$, where the operation $\lfloor \cdot \rfloor$ is the greatest integer less than or equal to the argument. For a uniform quantizer with quantization level δ, it holds that $|\, q(x) - x \,| \leq 0.5\, \delta$, [121].

A uniform quantizer (with quantization level δ) is incorporated at each node to quantize the state value before being transmitted. Using the quantized values of the most recent events, the following control signal is generated to enable consensus at

dual SDP problems. This parameter is usually used as an indication of accuracy in solving SDP problems. See [119] for more details.

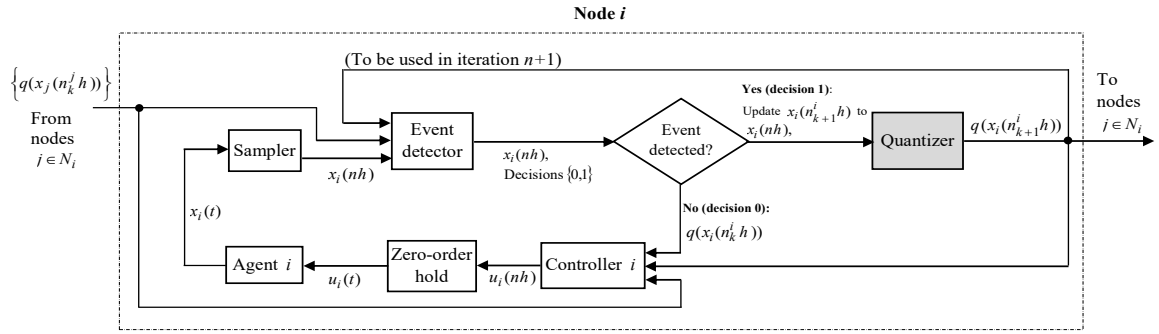

Figure 3.3: Proposed Q-CEASE for node i, iteration n, and the previously quantized event $q(x_i(n_k^i h))$. Compared to CEASE, the shaded quantization block adds an additional level of complexity.

node i

$$u_i(t) = -\mathbb{X}_i^q(nh), \;\; (1 \leq i \leq N), \tag{3.14}$$

where $\mathbb{X}_i^q(nh) = \sum_{j\in\mathcal{N}_i} a_{ij}(\, q(\hat{x}_i(nh)) - q(\hat{x}_j(nh))\,)$ is the *quantized* disagreement value for node i. Based on the definition of the uniform quantizer, it holds that $q\,(\,\hat{x}_i(nh)\,) = \hat{x}_i(nh) + \tilde{\delta}_i(nh)$, where $|\,\tilde{\delta}_i(nh)\,| \leq 0.5\,\delta$. The disagreement value $\mathbb{X}_i^q(nh)$ is also used by the event detector. For a given event instant $t = n_k^i h$, the next event for agent i is triggered at $t = n_{k+1}^i h$, with n_{k+1}^i satisfying the following ET condition

$$n_{k+1}^i = \min_n \{\, n \,|\quad n > n_k^i, \quad |e_i(nh)| \geq \phi\,|\mathbb{X}_i^q(nh)|\}, \tag{3.15}$$

where $e_i(nh) = \hat{x}_i(nh) - x_i(nh)$ is the state error for node i. Scalar $\phi > 0$ is the ET thresholds to be designed.

Consider the global vectors in (3.6). Additionally, let $\tilde{\boldsymbol{\delta}}(t) = [\,\tilde{\delta}_1(t), \ldots, \tilde{\delta}_N(t)\,]^T$. Combining (3.1) with (3.14) leads to the following closed-loop system

$$\dot{\boldsymbol{x}}(t) = -\boldsymbol{L}\, q\,(\,\hat{\boldsymbol{x}}(nh)\,), \tag{3.16}$$

where $\boldsymbol{L}$ is the Laplacian matrix. Using transformation (3.8), system (3.16) is converted to $\dot{\boldsymbol{r}}(t) = \dot{\boldsymbol{x}}(t) = -\boldsymbol{L}\, q\,(\,\hat{\boldsymbol{x}}(nh)\,)$. It then follows that

$$\begin{aligned}\dot{\boldsymbol{r}}(t) =& -\boldsymbol{L} q\,(\boldsymbol{x}(nh) + \boldsymbol{e}(nh)) = -\boldsymbol{L}\left(\boldsymbol{x}(nh) + \boldsymbol{e}(nh) + \tilde{\boldsymbol{\delta}}(nh)\right) \\ =& -\boldsymbol{L}\,(\,\boldsymbol{r}(nh) + \bar{x}(0)\mathbf{1}_N + \boldsymbol{e}(nh) + \tilde{\boldsymbol{\delta}}(nh)\,).\end{aligned} \tag{3.17}$$

Since $\bar{x}(0)\boldsymbol{L}\mathbf{1}_N = \mathbf{0}$, the following expression holds from (3.17)

$$\dot{\boldsymbol{r}}(t) = -\boldsymbol{L}\,(\,\boldsymbol{r}(nh) + \boldsymbol{e}(nh) + \tilde{\boldsymbol{\delta}}(nh)\,). \tag{3.18}$$

Next, the operating regions for h, ϕ, and δ that collectively guarantee an exponential rate for bounded consensus are computed. Moreover, the worst-case error from the average consensus value is calculated.

Theorem 3.2. Given a desired convergence rate ζ, if the selected values for the

sampling period h and ET threshold ϕ satisfy $h < h_{\max}$ and $\phi < \phi_{\max}$, where

$$h_{\max} = \frac{\lambda_2 - \zeta}{\lambda_N^2}, \qquad \phi_{\max} = \frac{c_1 - \sqrt{c_2}}{2\lambda_N c_3}, \tag{3.19}$$

with

$$\begin{aligned} &c_1 = 2\lambda_2 + \lambda_N + 2\zeta h\lambda_N - 2\zeta, \qquad c_2 = 8h^2\zeta\lambda_N^3 + 4h^2\zeta^2\lambda_N^2 + 4h\lambda_N^3 + 4h\lambda_2\lambda_N^2 + \lambda_N^2, \\ &c_3 = \lambda_2 + \lambda_N - \zeta + 2h\zeta\lambda_N \end{aligned} \tag{3.20}$$

then, the states of the agents converge to the following set

$$\{\boldsymbol{x}(t) \mid \|\boldsymbol{x}(nh) - \bar{x}(0)\mathbf{1}_N\| \leq M\}, \tag{3.21}$$

with a least convergence rate ζ, where $\bar{x}(0) = 1/N \sum_{i=1}^{N} x_i(0)$ and M is the maximum quantization error given below

$$M = \frac{0.5\sqrt{N}(1 - \phi\|\boldsymbol{L}\|)\lambda_N}{c_3\phi^2\|\boldsymbol{L}\|^2 - c_1\phi\|\boldsymbol{L}\| + (\lambda_2 - \zeta - h\lambda_N^2)}\delta. \tag{3.22}$$

Proof. Proof of Theorem 3.2 is given in Section 3.6.3. □

Remark 3.5 (Design trade-offs in Q-CEASE)**.** The following features of Q-CEASE are worth mentioning:

- If $h \to h_{\max}$, then $\phi_{\max} \to 0$ and $M \to \infty$. On the other hand, for a given h, if $\phi \to \phi_{\max}$, then $M \to \infty$. Therefore, there is a trade-off between the selected values for h and ϕ, and the maximum quantization error M. In general, parameter M in the selected region shown in Fig. 3.4 is a monotonically increasing function with respect to all parameters h, ϕ, ζ and δ.

- If $h \to 0$ and $\zeta \to 0$, the proposed Q-CEASE algorithm reduces to [121] where an asymptotic convergence without sampling is studied. In this case, i.e., $\{h, \zeta\} \to 0$, the operating region for ϕ would be $\phi < \frac{\lambda_2}{\lambda_N(\lambda_2 + \lambda_N)}$.

- The desired consensus convergence rate must satisfy $\zeta < \lambda_2$. Otherwise, h would be negative (see (3.19)). This is consistent with the widely known fact that the consensus convergence rate is higher than or equal to λ_2, [4].

- For a finite combination of networks with fixed N, the Q-CEASE algorithm can be operated based on a switching network topologies. In this case, λ_2 should be chosen less than or equal to the minimum of the second smallest eigenvalues, and λ_N greater than or equal to the maximum of maximum eigenvalues. The design parameters need not to be recomputed for networks with switching topologies.

Algorithm 3.2 Q-CEASE

Input: Neighbouring connectivity information.

Output: Sampled-data Event-triggered Average-consensus with Quantized transmission and guaranteed convergence.

Preliminary: Using a distributed algorithm such as Algorithm 3.4, each node computes λ_2 and λ_N.

Parameter Design Select the quantization level δ. Select the sampling period h and ET threshold ϕ such that the conditions given in (3.19) are guaranteed.

Distributed Consensus Iterations: (C1 – C4)

C1. Each node transmits the initial state $q(x_i(0))$ to its neighbours.

C2. The state of agent i is excited by control law (3.14).

C3. To determine the next triggering sample, condition (3.15) is locally monitored at $t = nh$ ($n \in \mathbb{N}$) using the designed values for ϕ.

C4. Steps C2 and C3 continue until average consensus is achieved among the nodes. MAS trajectories satisfy (3.21).

3.4 DEASE

One important area that still needs improvement is the efficiency of the ET scheme in reducing the number of transmissions. On the other hand, CEASE and Q-CEASE produce steady-state error in consensus, which is not desirable. As one of the most advanced ET schemes, *dynamic* event-triggering (DET) has recently been proposed in [74–76]. In DET, an internal dynamic variable is included as an additional threshold to the state-dependent ET threshold. As shown in Remark 3.7, a wide range of ET schemes considered in literature are special cases of the DET scheme. One interesting feature of the DETs is that their inter-event interval can be longer than the so-called static ET schemes. At the same time, consensus can still be reached using DET without introducing steady-state errors. It should be noted that continuous-time measurement and event monitoring is required in DET schemes [74–76] which is not desirable. Additionally, no optimization approach has been studied for sampled-data dynamic event-triggered consensus.

Following the previous implementations, a distributed dynamic event-triggering average consensus algorithm with sampled-data (DEASE) is proposed in this section. DEASE is expected to save more transmissions as compared to CEASE and Q-CEASE with no consensus error. In other words, the consensus error is DEASE asymptotically approaches zero.

3.4.1 Problem statement

Consider the first-order MAS given in (3.1). The MAS (3.1) is configured as an undirected (symmetric) connected network.

Similar to previous implementations, notation $n_0^i h, n_1^i h, \ldots$ denotes the time sequence at which events are detected and transmitted by node i. The following control protocol is used at node i to reach average consensus

$$u_i(t) = -\,\mathbb{X}_i(nh), \quad nh \leq t < (n+1)h, \tag{3.23}$$

where $\mathbb{X}_i(nh) = \sum_{j\in\mathcal{N}_i} a_{i,j}\,(x_j(n_k^j h) - x_i(n_k^i h))$. Let $e_i(nh) = x_i(n_k^i h) - x_i(nh)$ be the state error for node i. Given the most recent event instant $n_k^i h$, the next event for node i is triggered at $n_{k+1}^i h$, with n_{k+1}^i satisfying the following DET condition

$$n_{k+1}^i = \min_{n\in\mathbb{N}} \{ \quad n > n_k^i \quad | \quad \phi_1 e_i^2(nh) \geq \phi_2 \mathbb{X}_i^2(nh) + \eta_i^2(nh) \}, \tag{3.24}$$

where $\phi_1 > 0$ and $\phi_2 > 0$ are design parameters. Parameter $\eta_i(t)$, $\forall i \in \mathcal{V}$, satisfies the following equation

$$\dot{\eta}_i(t) = -\ \eta_i(t) + \phi_3 |\mathbb{X}_i(nh)|, \tag{3.25}$$

where $\eta_i(0) > 0$, and scalar $\phi_3 > 0$ is another design parameter.

Remark 3.6 (On the nature of $\eta_i(t)$)**.** Based on (3.25) parameter $\eta_i(t)$ is time-varying and its dynamic updating protocol is related to the disagreement vector $\mathbb{X}_i(nh)$ and a negative self-feedback. Intuitively, $\eta_i(t)$ can be regarded as a linear first-order filtered value of $|\mathbb{X}_i(nh)|$. Compared to the so-called static ET strategies (such as $e_i^2(nh) \geq \phi_1 \mathbb{X}_i^2(nh)$, [122]), the introduction of $\eta_i(t)$ is a key element to regulate threshold (3.24) dynamically and in better connection with the agents disagreements. As shown in [123, Prop. 2.3], including parameter $\eta_i(t)$ in (3.24) reduces the number of transmissions compared to the static ET schemes. As a final note, since $\eta_i(t)$ follows a dynamic equation, it acts as an auxiliary *state* along with state $x_i(t)$. Thus, as observed later in Theorem 3.3, $\eta_i(t)$ impacts the consensus convergence rate.

Remark 3.7 (Special cases of DET (3.24))**.** Many existing ET schemes that are widely used in the literature are special cases of DET (3.24). For example,

S1 If $\phi_3 = 0$, the dynamic threshold $\eta_i(t)$ would simply be a decreasing exponential term $\eta_i(t) = \eta_i(0)\exp(-t)$ which is irrespective of the system dynamics. In this case, DET condition (3.24) reduces to $\phi_1 e_i^2(nh) \geq \phi_2 \mathbb{X}_i^2(nh) + \eta_i^2(0)\exp(-2t)$ which is similar to the ET scheme considered in [124].

S2 If $\phi_2 = \phi_3 = 0$, the disagreement term $\mathbb{X}_i(nh)$ is disregarded. DET condition (3.24) reduces to $\phi_1 e_i^2(nh) \geq \eta_i^2(0)\exp(-2t)$ which is similar to [111].

S3 If $\eta_i(t) = 0$, $(\forall t \geq 0)$, then the DET condition is simplified to $\phi_1 e_i^2(nh) \geq \phi_2 \mathbb{X}_i^2(nh)$, which is analogous to [122].

S4 As another special case, if the dynamic threshold equals a constant (i.e., $\eta_i(t) = c$, $\forall t \geq 0$), the DET condition (3.24) reduces to $\phi_1 e_i^2(nh) \geq \phi_2 \mathbb{X}_i^2(nh) + c^2$, which is similar to CEASE and [35].

In many ET schemes such as CEASE [77] and [35], event-triggered consensus is only reached within a bounded error However, the DET scheme (3.24) do not cause any steady-state error.

Remark 3.8 (Benefits of co-design optimization)**.** The DET scheme (3.24) is based on multiple unknown gains (scalars ϕ_1, ϕ_2, and ϕ_3). A generic approach to design

these parameters is of great interest. The emulation-based approaches [75, 76, 125] derive some bounded regions for unknown DET gains. Even when the feasible regions for design parameters are obtained, selecting proper operating values that efficiently save transmissions is still difficult and requires trial and error. It will be observed in Theorem 3.3 that the proposed co-design optimization simultaneously computes the *exact* values for unknown DET gains based on an objective function which increases the minimum inter-event time.

Impact of design parameters on expected number of transmissions

The values of ϕ_1, ϕ_2, and ϕ_3 impact the inter-event-time and hence the intensity of transmissions. From (3.24), it is clear that small values for ϕ_1 and a large value for ϕ_2 help in reducing the number of events. The value of ϕ_3 play an important role in the trajectory of $\eta_i(t)$. With a higher value for ϕ_3, disagreement $|\mathbb{X}_i(nh)|$ is more involved in (3.25) and parameter $\eta_i(t)$ tends to vanish more slowly. Therefore, parameter $\eta_i(t)$ can contribute longer to (3.24) with a higher value for ϕ_3. In summary, the average inter-event-time is increased (i.e., the expected number of transmissions is reduced) with properly small values for ϕ_1 and large values for ϕ_2 and ϕ_3.

Design objectives

The following design objectives are considered in DEASE:

- Compute unknown parameters ϕ_1, ϕ_2, and ϕ_3 in a co-design setup.
- Incorporate an objective function to increase the inter-event time and improve efficiency of DET (3.24).

3.4.2 Closed-loop system

Define the following global vectors

$$\begin{aligned}
&\boldsymbol{x}(t)=[x_1^T(t),\ldots,x_N^T(t)]^T,\ \hat{\boldsymbol{x}}(t)=[\hat{x}_1^T(t),\ldots,\hat{x}_N^T(t)]^T,\quad \boldsymbol{e}(t)=[e_1^T(t),\ldots,e_N^T(t)]^T,\\
&\boldsymbol{\eta}(t)=[\eta_1(t),\ldots,\eta_N(t)]^T,\ \mathbb{X}(t)=[\mathbb{X}_1^T(t),\ldots,\mathbb{X}_N^T(t)]^T,\ \bar{\mathbb{X}}(t)=[\,|\mathbb{X}_1(t)|,\ldots,|\mathbb{X}_N(t)|\,]^T,\\
&\bar{\boldsymbol{e}}(t)=[\,|e_1(t)|,\ldots,|e_N(t)|\,]^T.
\end{aligned} \tag{3.26}$$

The closed-loop MAS from (3.1) and (3.23) is given below

$$\dot{\boldsymbol{x}}(t)=-\boldsymbol{L}(\boldsymbol{x}(nh)+\boldsymbol{e}(nh)),\quad t\in[nh,(n+1)h). \tag{3.27}$$

Let $d(t)\triangleq t-nh$ represent an artificial time-varying time-delay that satisfies $0\leq d(t)<h$. Using $d(t)$, system (3.27) is given below for the interval $nh\leq t<(n+1)h$.

$$\dot{\boldsymbol{x}}(t)=-\boldsymbol{L}\left(\boldsymbol{x}(t-d(t))+\boldsymbol{e}(t-d(t))\right), \tag{3.28}$$

with $\boldsymbol{x}(t)=\boldsymbol{x}(0)$ for $-h\leq t\leq 0$. One approach to guarantee consensus in (3.28) is to convert it to an equivalent system by eigenvalue and eigenvector decomposition

of $\boldsymbol{L}$. There exists an orthogonal matrix $\boldsymbol{V}=[v_{i,j}]\in\mathbb{R}^{N\times N}$ such that $\boldsymbol{V}\boldsymbol{J}\boldsymbol{V}^{-1}=\boldsymbol{L}$, where $\boldsymbol{J}=\text{diag}(0,\lambda_2,\ldots,\lambda_N)$. Let $\boldsymbol{V}^{-1}=[\tilde{v}_{i,j}]$. From $\boldsymbol{V}^{-1}$, denote the $(N-1)\times N$ dimensional matrix $\tilde{\boldsymbol{V}}=[\tilde{v}_{i,j}]$, $2\leq i\leq N$, $1\leq j\leq N$. In words, $\tilde{\boldsymbol{V}}$ includes rows 2 to N of matrix $\boldsymbol{V}^{-1}$. Now, the following transformation is considered

$$\boldsymbol{r}(t)=\tilde{\boldsymbol{V}}\,\boldsymbol{x}(t). \tag{3.29}$$

It is proved in [100, Theorem 1] that consensus is achieved in (3.28) if $\lim_{t\to\infty}\boldsymbol{r}(t)=0$. Using (3.29), system (3.28) is converted to

$$\dot{\boldsymbol{r}}(t)=-\tilde{\boldsymbol{J}}\,\boldsymbol{r}(t-d(t))-\tilde{\boldsymbol{J}}\tilde{\boldsymbol{V}}\,\boldsymbol{e}(t-d(t), \tag{3.30}$$

where $\tilde{\boldsymbol{J}}=\text{diag}(\lambda_2,\ldots,\lambda_N)$. In summary, the parameter design for DET (3.24) is based on stabilization of (3.30).

3.4.3 Parameter design

This section develops an LMI optimization that simultaneously computes all unknown DET parameters. The optimization requires all the eigenvalues and eigenvectors of the Laplacian matrix $\boldsymbol{L}$, which can be computed in a distributed fashion using Algorithm 3.4.

Theorem 3.3. Given a desired sampling period h, DET parameters ϕ_1, ϕ_2, and ϕ_3 are computed from the following LMI constrained optimization

$$\min \quad \mathbb{F}=\theta_1+\theta_2+\theta_3, \tag{3.31}$$

subject to:

$$\boldsymbol{\Pi}=\begin{bmatrix}\boldsymbol{\pi}_{11} & \boldsymbol{\pi}_{12} & -\boldsymbol{F}_1 & \boldsymbol{P}_1-\boldsymbol{H}_1 & -\boldsymbol{H}_1\tilde{\boldsymbol{J}}\tilde{\boldsymbol{V}}\\ * & \boldsymbol{\pi}_{22} & -\boldsymbol{F}_2 & -\boldsymbol{H}_2\tilde{\boldsymbol{J}}-\boldsymbol{H}_3 & \boldsymbol{\pi}_{25}\\ * & * & -\boldsymbol{Q}_1 & \boldsymbol{0} & \boldsymbol{0}\\ * & * & * & \boldsymbol{\pi}_{44} & -\boldsymbol{H}_2\tilde{\boldsymbol{J}}\tilde{\boldsymbol{V}}\\ * & * & * & * & \boldsymbol{\pi}_{55}\end{bmatrix}<0, \tag{3.32}$$

$$\boldsymbol{\Psi}=\begin{bmatrix}\boldsymbol{\psi}_{11} & \boldsymbol{\psi}_{12} & -\boldsymbol{W}_1 & \boldsymbol{P}_2-2\boldsymbol{I}\\ * & \boldsymbol{\psi}_{22} & -\boldsymbol{W}_2 & \boldsymbol{0}\\ * & * & -\boldsymbol{Q}_2 & \boldsymbol{0}\\ * & * & * & \boldsymbol{\psi}_{44}\end{bmatrix}<0, \tag{3.33}$$

$$\boldsymbol{C}_1=\begin{bmatrix}\boldsymbol{Y} & \boldsymbol{F}\\ * & \boldsymbol{Z}_1\end{bmatrix}\geq 0,\quad \boldsymbol{C}_2=\begin{bmatrix}\boldsymbol{Y} & \boldsymbol{G}\\ * & \boldsymbol{Z}_1\end{bmatrix}\geq 0,\quad \boldsymbol{C}_3=\begin{bmatrix}\boldsymbol{U} & \boldsymbol{W}\\ * & \boldsymbol{Z}_2\end{bmatrix}\geq 0,\quad \boldsymbol{C}_4=\begin{bmatrix}\boldsymbol{U} & \boldsymbol{E}\\ * & \boldsymbol{Z}_2\end{bmatrix}\geq 0,$$
$$\boldsymbol{C}_5=\begin{bmatrix}-\theta_1 & \phi_1\\ * & -1\end{bmatrix}<0,\quad \boldsymbol{C}_6=\begin{bmatrix}\theta_2 & 1\\ * & \phi_2\end{bmatrix}>0,\quad \boldsymbol{C}_7=\begin{bmatrix}\theta_3 & 1\\ * & \phi_3\end{bmatrix}>0, \tag{3.34}$$

with the following decision variables

- Positive scalars ϕ_1, ϕ_2, ϕ_3, θ_1, θ_2, θ_3;
- $(N-1)\times(N-1)$ dimensional matrices $\boldsymbol{P}_1>0$, $\boldsymbol{Q}_1>0$, $\boldsymbol{Z}_1>0$, and $(N\times N)$ dimensional matrices $\boldsymbol{P}_2>0$, $\boldsymbol{Q}_2>0$, $\boldsymbol{Z}_2>0$;

- $(N-1)\times(N-1)$ dimensional matrices $\boldsymbol{H}_1$, $\boldsymbol{H}_2$, $\boldsymbol{H}_3$, $\boldsymbol{Y}_{11}$, $\boldsymbol{Y}_{12}$, $\boldsymbol{Y}_{22}$, $\boldsymbol{F}_1$, $\boldsymbol{F}_2$, $\boldsymbol{G}_1$, $\boldsymbol{G}_2$, and $N\times N$ dimensional matrices $\boldsymbol{U}_{11}$, $\boldsymbol{U}_{12}$, $\boldsymbol{U}_{22}$, $\boldsymbol{W}_1$, $\boldsymbol{W}_2$, $\boldsymbol{E}_1$, $\boldsymbol{E}_2$.

Unknown block matrices in (3.32)-(3.34) are defined below

$$\begin{aligned}
&\boldsymbol{\pi}_{11}=\boldsymbol{Q}_1+\boldsymbol{G}_1+\boldsymbol{G}_1^T+h\boldsymbol{Y}_{11}, \qquad \boldsymbol{\pi}_{12}=\boldsymbol{F}_1-\boldsymbol{G}_1+\boldsymbol{G}_2^T+h\boldsymbol{Y}_{12}-\boldsymbol{H}_1\tilde{\boldsymbol{J}},\\
&\boldsymbol{\pi}_{22}=\boldsymbol{F}_2+\boldsymbol{F}_2^T-\boldsymbol{G}_2-\boldsymbol{G}_2^T+h\boldsymbol{Y}_{22}-\tilde{\boldsymbol{J}}\boldsymbol{H}_3-\boldsymbol{H}_3^T\tilde{\boldsymbol{J}}+\tilde{\boldsymbol{J}}^2(\phi_2+2\phi_3),\\
&\boldsymbol{\pi}_{25}=-\boldsymbol{H}_3\tilde{\boldsymbol{J}}\tilde{\boldsymbol{V}}+(\phi_2+2\phi_3)\tilde{\boldsymbol{J}}^2\tilde{\boldsymbol{V}}, \qquad \boldsymbol{\pi}_{44}=h\boldsymbol{Z}_1-\boldsymbol{H}_2-\boldsymbol{H}_2^T,\\
&\boldsymbol{\pi}_{55}=-\phi_1\boldsymbol{I}+2\lambda_N^2\phi_3\boldsymbol{I}+\lambda_N^2\phi_2\boldsymbol{I}, \qquad \boldsymbol{\psi}_{11}=\boldsymbol{Q}_2+\boldsymbol{E}_1+\boldsymbol{E}_1^T+h\boldsymbol{U}_{11}-2\boldsymbol{I}+\phi_3\boldsymbol{I},\\
&\boldsymbol{\psi}_{12}=\boldsymbol{W}_1-\boldsymbol{E}_1+\boldsymbol{E}_2^T+h\boldsymbol{U}_{12}, \qquad \boldsymbol{\psi}_{22}=\boldsymbol{W}_2+\boldsymbol{W}_2^T-\boldsymbol{E}_2-\boldsymbol{E}_2^T+h\boldsymbol{U}_{22}+\boldsymbol{I},\\
&\boldsymbol{\psi}_{44}=h\boldsymbol{Z}_2-2\boldsymbol{I}+\phi_3\boldsymbol{I},\\
&\boldsymbol{Y}=\begin{bmatrix}\boldsymbol{Y}_{11} & \boldsymbol{Y}_{12}\\ * & \boldsymbol{Y}_{22}\end{bmatrix}, \quad \boldsymbol{U}=\begin{bmatrix}\boldsymbol{U}_{11} & \boldsymbol{U}_{12}\\ * & \boldsymbol{U}_{22}\end{bmatrix}, \quad \boldsymbol{F}=[\boldsymbol{F}_1^T\ \boldsymbol{F}_2^T]^T,\\
&\boldsymbol{G}=[\boldsymbol{G}_1^T\ \boldsymbol{G}_2^T]^T, \quad \boldsymbol{W}=[\boldsymbol{W}_1^T\ \boldsymbol{W}_2^T]^T, \quad \boldsymbol{E}=[\boldsymbol{E}_1^T\ \boldsymbol{E}_2^T]^T.
\end{aligned}$$

The objective function $\mathbb{F}$ decreases the value of ϕ_1 and increases the values of ϕ_2 and ϕ_3 which together reduce the number of transmissions. In particular, the following bounds are guaranteed

$$\phi_1\leq\sqrt{\theta_1}, \quad \phi_2\geq\frac{1}{\theta_2}, \quad \phi_3\geq\frac{1}{\theta_3}. \tag{3.35}$$

Proof. Proof of Theorem 3.3 is given in Appendix, Section 3.6.4. □

Remark 3.9 (On weighting coefficients for the objective function)**.** In objective function (3.31), the weights for decision variables θ_c, $(1\leq c\leq 3)$, are all set at 1. In other words, all DET parameters are treated equally in increasing the inter-event time. Similar to CEASE, one can revise (3.31) to $\mathbb{F}=w_1\theta_1+w_2\theta_2+w_3\theta_3$ with positive weighting coefficients w_i, $(1\leq i\leq 3)$, satisfying $\sum_{i=1}^{3}w_i=1$. These weights can differentiate the contribution of each design variable in the optimization and impact the events density and convergence rate.

Remark 3.10 (Conservation in CEASE and DEASE)**.** The co-design framework in Theorem 3.3 is based on a delay-dependent Lyapunov-Krasovskii functional (LKF) with improved free weighting matrices (IFWM). It is generally known that the IFWM technique (compared to other techniques such as FWM) preserves useful terms in the derivative of the LKF and incorporates the relationships among the time-varying delay $d(t)$, its upper bound h, and their difference, which result in less conservative parameters. For further information refer to [126, Chapter 3]. The same observation is made in Chapter 7, as Theorem 3.3 computes efficient values for unknown parameters of DET (3.24) with large given sampling periods h. It should be noted that the Lyapunov function used to develop CEASE is delay-independent. Additionally, the time-varying delay $d(t)$ is approximated by its upper bound h. Therefore, CEASE is more conservatives than DEASE in terms of transmission savings.

Algorithm 3.3 DEASE

Input: Neighbouring connectivity information.

Output: Dynamic event-triggered Average-consensus with Sampled-data

Preliminary: Using a distributed algorithm such as Algorithm 3.4, each node computes all eigenvalues and eigenvectors of the Laplacian matrix. Using an average consensus the nodes agree on the value of the desired sampling period h.

Optimization and Parameter Design: (D1 – D2)

D1. Each node solves the minimization problem (3.31).

D2. Using the solution of (3.31), unknown parameters for DET (3.24) (i.e., ϕ_i, $1 \leq i \leq 3$) are computed.

Distributed Consensus Iterations: (C1 – C4)

C1. Each node transmits the initial state $x_i(0)$ to its neighbours. Each node selects an initial value $\eta_i(0)$ for the dynamic threshold (3.24).

C2. The state of agent i is excited by control law (3.23).

C3. To determine the next triggering sample, condition (3.24) is locally monitored at $t = nh$ ($n \in \mathbb{N}$) using the designed values for ϕ_i, ($1 \leq i \leq 3$), from step D1.

C4. Steps C2 and C3 continue until average consensus is achieved among the nodes.

Remark 3.11 (Comparison between CEASE and DEASE)**.** Unlike CEASE, where the computational complexity of the proposed optimization does not grow with the network size N, dimensions of some LMIs in DEASE grow as N is increased. Therefore the computational intensity of solving (3.31) increases with N. As mentioned in Remark 3.3, the highest number of iterations required to solve (3.31) grows at the $O(\sqrt{N_p}\,|\log \epsilon_g|)$ with the problem size $N_p = \max\{d_m, n_v\}$ and the duality gap denoted by ϵ_g. Note that d_m is 'the highest dimension of the LMIs associated with the optimization problem' and n_v is the 'total number of decision variables' involved. Both parameters are dependent to the network size N. The order of arithmetic operations required in each iteration is $\max\{d_m^3, d_m^2 n_v, C_d\}$) with C_d the cost of evaluating the first and second derivatives of the objective and constraint functions. Therefore, the complexity of total arithmetic operations required to solve (3.11) grows at the $O(N^3)$. In return, the performance of DEASE in terms of transmission savings is expected to be higher than CEASE. Additionally, DEASE (unlike CEASE) does not produce any steady-state error in consensus.

The proposed DEASE algorithm is summarized in Algorithm 3.3.

3.5 Summary

Based on the research gaps observed in existing ETC literature, this chapter proposes some ETC implementations, namely, (CEASE [77], Q-CEASE [78], and DEASE) for multi-agent systems (MAS) with first-order dynamics. The objective of all implementations is to achieve average consensus based on only sampled measurements and reducing the information exchanges by means of ET schemes.

CEASE uses the theory of convex optimization and linear matrix inequalities (LMIs) to develop a sampled-data event-triggering average consensus with optimal

Table 3.1: Comparison of different proposed ETC implementations.

Characteristics	**CEASE** [77]	**Q-CEASE** [78]	**DEASE**
Transmitter scheme	Sampled-data Event-triggered	Sampled-data Event-triggered	Sampled-data Event-triggered
Receiver scheme	Periodic	Periodic	Periodic
Measurement scheme	Periodic	Periodic	Periodic
Control scheme	Sampled-data Event-triggered	Sampled-data Event-triggered	Sampled-data Event-triggered
Event monitoring	Periodic	Periodic	Periodic
Optimization for Design Parameters	Yes	No	Yes
Steady-state error	Yes	Yes	No
State Quantization	No	Yes	No
Control gain Design	Yes	No	No
Computation Complexity of Parameter Design	Medium	Low	High
Relative expected number of transmissions	Medium	Medium	Low
Network Topology	Undirected	Undirected	Undirected

consensus parameters (i.e., a control gain and a transmission threshold). The optimization stage in CEASE can be performed in a distributed manner. Additionally, the computational complexity of CEASE does not grow with the network size. In CEASE, no quantization is considered in the implementation and precise values of the states are used for transmission. Q-CEASE considers a more realistic scenario where information exchanges between the neighbouring nodes are quantized. The parameter design approach in Q-CEASE is based on analytical manipulation of the Lyapunov functional. Thus, no LMI optimization is considered in Q-CEASE. Required parameters in Q-CEASE can be chosen within an operational range of values.

DEASE incorporates a dynamic event-triggering (DET) scheme which is more general and more efficient that the one used in other implementations. Parameter design in DEASE in based on a convex optimization. In DEASE, a delay-dependent Lyapunov-krasovskii functional (LKF) is used which results in less conservative parameters compared to CEASE. Additionally, DEASE does not produce steady-state error for consensus.

Table 3.1 lists the proposed ETC implementations and compares them in terms of their different characteristics. According to Table 3.1, each implementation offers some advantages and has some shortcomings. Based on the desired application, one can choose the suitable implementation.

3.6 Appendix

Proofs of the Theorems developed in this chapter are given in this appendix.

Algorithm 3.4 [112]. Distributed computation of Laplacian eigenvalues and eigenvectors.

Input: Neighbouring set $\mathcal{N}_i$ and network size N.
Output: Local computation of Laplacian eigenvalues and eigenvectors.

I. Initialization: (I1 − I4)

I1. Node i, $(\forall i \in \mathcal{V})$, denotes row vector $\boldsymbol{e}_i \in \mathbb{R}^{1\times N}$, where entry i in $\boldsymbol{e}_i$ equals 1 and all other entries are zero.

I2. Node i, $(\forall i \in \mathcal{V})$, sets $\boldsymbol{b}_i = \boldsymbol{L}_i + N\,\boldsymbol{e}_i$, where $\boldsymbol{L}_i$ is row i of the Laplacian matrix $\boldsymbol{L}$ and N is the network size.

I3. Matrix $\boldsymbol{Z}_i(0)$ is initialized by node i, $(\forall i \in \mathcal{V})$, such that $\boldsymbol{b}_i\boldsymbol{Z}_i(0) = \boldsymbol{e}_i$.

I4. Node i, $(\forall i \in \mathcal{V})$, sets matrix $\mathbb{P}_i = \boldsymbol{I}_N - \frac{1}{\boldsymbol{b}_i\boldsymbol{b}_i^T}\boldsymbol{b}_i^T\boldsymbol{b}_i$.

II. Update: (U1 − U2)

U1. Node i, $(\forall i \in \mathcal{V})$, updates $\boldsymbol{Z}_i(k)$, $(k \in \mathbb{N})$, from

$$\boldsymbol{Z}_i(k+1) = \boldsymbol{Z}_i(k) - \frac{1}{|\mathcal{N}_i|}\mathbb{P}_i\left(|\mathcal{N}_i|\boldsymbol{Z}_i(k) - \sum_{j\in\mathcal{N}_i}\boldsymbol{Z}_j(k)\right).$$

U2. Node i, $(\forall i \in \mathcal{V})$, updates matrix $\boldsymbol{Z}_i(k)$ based on Step U1 until $\|\boldsymbol{Z}_i(k+1) - \boldsymbol{Z}_i(k)\| \le \epsilon_i$, where ϵ_i is the desired local computation accuracy.

III. Computation: (C1-C3)

C1. After Step U2, node i, $(\forall i \in \mathcal{V})$, computes all eigenvalues of $\boldsymbol{Z}_i(k+1)$, denoted by $\lambda_c(Z_i)$, $(1 \le c \le N)$.

C2. Node i, $(\forall i \in \mathcal{V})$, computes $\tilde{\lambda}_c^{[i]} = \frac{1}{\lambda_c(Z_i)} - N$ for $(1 \le c \le N)$. It holds that the set $\{\tilde{\lambda}_c^{[i]} \,|\, 1 \le c \le N\}$ is an estimate of the Laplacian eigenvalues at node i.

C3. Node i, $(\forall i \in \mathcal{V})$, computes the eigenvectors of $\boldsymbol{Z}_i(k+1)$, which are estimated values of Laplacian eigenvectors.

3.6.1 Distributed computation of Laplacian eigenvalues and eigenvectors

First, Algorithm 3.4 is presented which computes the eigenvalues and eigenvectors of the Laplacian matrix in a distributed manner. Note that the network size N which is required in Algorithm 3.4 can be determined in a distributed manner from [127].

Before proceeding with the proof of Theorems, the following Lemmas which will be used in the proofs are presented.

Lemma 1. *Schur Complement* [128].
Consider matrices $\boldsymbol{X}$, $\boldsymbol{Y}$, and $\boldsymbol{Z}$ with appropriate dimensions. The following two statements are equivalent

$$\boldsymbol{X} > 0, \quad \boldsymbol{Y} - \boldsymbol{Z}\boldsymbol{X}^{-1}\boldsymbol{Z}^T > 0 \quad \Leftrightarrow \quad \begin{bmatrix} \boldsymbol{Y} & \boldsymbol{Z} \\ * & \boldsymbol{X} \end{bmatrix} > 0.$$

Lemma 2. *Young Inequality* [129].
Given properly dimensioned matrices $\boldsymbol{Z} = \boldsymbol{Z}^T$, $\boldsymbol{M}$, and $\boldsymbol{N}$, the inequality $\boldsymbol{Z} + \boldsymbol{M}^T\boldsymbol{N} +$

$\boldsymbol{N}^T\boldsymbol{M}<0$ is satisfied, if and only if there exists a scalar $\epsilon>0$ such that $\boldsymbol{Z}+\epsilon\boldsymbol{M}^T\boldsymbol{M}+\epsilon^{-1}\boldsymbol{N}^T\boldsymbol{N}<0$ holds.

3.6.2 Proof of Theorem 3.1

Proof of Theorem 3.1 is given below.

Proof. Consider the following Lyapunov candidate

$$V(t)=p\ \boldsymbol{r}^T(t)\,\boldsymbol{r}(t). \tag{3.36}$$

In what follows, the time evolution of $\boldsymbol{r}(t)$ in the interval $nh\leq t<(n+1)h$ is considered which is generated from (3.9)

$$\dot{\boldsymbol{r}}(t)=-(t-nh)\mathcal{K}\,\boldsymbol{L}\,(\boldsymbol{r}_n+\boldsymbol{e}_n)+\boldsymbol{r}_n. \tag{3.37}$$

From (3.36) and (3.37), parameter $\dot{V}(t)=\mathcal{Z}+\mathcal{Z}^T$ is expanded, where

$$\mathcal{Z}=((t-nh)\mathcal{K}^2p\,(\boldsymbol{r}_n+\boldsymbol{e}_n))^T\boldsymbol{L}^T\boldsymbol{L}(\boldsymbol{r}_n+\boldsymbol{e}_n)-\boldsymbol{r}_n^T\,\mathcal{K}p\,\boldsymbol{L}(\boldsymbol{r}_n+\boldsymbol{e}_n). \tag{3.38}$$

Expression $\mathcal{Z}$ is upper-bounded by the following term

$$\mathcal{Z}\leq h\mathcal{K}^2\,p\,\lambda_N^2\Big(\boldsymbol{r}_n+\boldsymbol{e}_n\Big)^T\Big(\boldsymbol{r}_n+\boldsymbol{e}_n\Big)-\mathcal{K}p\,\lambda_2\boldsymbol{r}_n^T\,\boldsymbol{r}_n-\mathcal{K}p\,\boldsymbol{r}_n^T\ \boldsymbol{L}\,\boldsymbol{e}_n. \tag{3.39}$$

From (3.36) and (3.37), the term $2\zeta V(t)$ is expanded as follows.

$$\begin{aligned}2\zeta V(t)=&\,2\zeta\,p\,\boldsymbol{r}_n^T\boldsymbol{r}_n\ +2(t-nh)^2\zeta\mathcal{K}^2p\Big(\boldsymbol{r}_n+\boldsymbol{e}_n\Big)^T\boldsymbol{L}^T\boldsymbol{L}\Big(\boldsymbol{r}_n+\boldsymbol{e}_n\Big)\\&-2(t-nh)\zeta\,\mathcal{K}p\,\Big(\boldsymbol{r}_n+\boldsymbol{e}_n\Big)^T\boldsymbol{L}^T\boldsymbol{r}_n-2(t-nh)\zeta\,\mathcal{K}p\,\boldsymbol{r}_n^T\boldsymbol{L}\Big(\boldsymbol{r}_n+\boldsymbol{e}_n\Big).\end{aligned} \tag{3.40}$$

Using the largest eigenvalue of $\boldsymbol{L}$, the term $2\zeta V(t)$ is upper-bounded by

$$\begin{aligned}2\zeta V(t)\leq&\,2\,\zeta\,p\,\boldsymbol{r}_n^T\,\boldsymbol{r}_n+2\zeta h^2\lambda_N^2\mathcal{K}^2p\Big(\boldsymbol{r}_n+\boldsymbol{e}_n\Big)^T\Big(\boldsymbol{r}_n+\boldsymbol{e}_n\Big)\\&-2(t-nh)\zeta\mathcal{K}p\,\boldsymbol{e}_n^T\,\boldsymbol{L}^T\boldsymbol{r}_n-2(t-nh)\zeta\mathcal{K}p\,\boldsymbol{r}_n^T\,\boldsymbol{L}\boldsymbol{e}_n.\end{aligned} \tag{3.41}$$

From (3.39) and (3.41), the following inequality is derived

$$\dot{V}(t)+2\,\zeta\,V(t)\leq\boldsymbol{\tau}^T\bar{\boldsymbol{\Xi}}_1\boldsymbol{\tau}, \tag{3.42}$$

where $\boldsymbol{\tau}=[\,\boldsymbol{r}_n^T,\,\boldsymbol{e}_n^T\,]^T$ and

$$\bar{\boldsymbol{\Xi}}_1=\begin{bmatrix}(2\zeta p-2\mathcal{K}p\lambda_2+\xi_1+\xi_2)\boldsymbol{I} & (\xi_1+\xi_2)\boldsymbol{I}+\boldsymbol{\xi}_3+\boldsymbol{\xi}_4\\ * & (\xi_1+\xi_2)\boldsymbol{I}\end{bmatrix}, \tag{3.43}$$

with $\xi_1=2h\mathcal{K}^2p\lambda_N^2,\ \xi_2=2\zeta h^2\mathcal{K}^2p\lambda_N^2,\ \boldsymbol{\xi}_3=-\,\mathcal{K}p\boldsymbol{L},$ and $\boldsymbol{\xi}_4=-2\,(t-nh)\,\zeta\mathcal{K}p\boldsymbol{L}$. At this stage, the ET constraint (3.5) should be included with $\bar{\boldsymbol{\Xi}}_1$. The quadratic form of (3.5) can be viewed as follows

$$\boldsymbol{e}_n^T\,\boldsymbol{e}_n\leq(\,\boldsymbol{e}_n+\boldsymbol{r}_n\,)^T2\phi_1^2\,\lambda_N^2(\,\boldsymbol{e}_n+\boldsymbol{r}_n\,)+2\phi_2^2, \tag{3.44}$$

The ET constraint (3.44) is re-arranged to $\alpha(\boldsymbol{\tau}^T\,\bar{\boldsymbol{\Xi}}_2\,\boldsymbol{\tau}+2\phi_2^2)\geq 0$, where $\alpha>0$ and

$$\bar{\boldsymbol{\Xi}}_2=\begin{bmatrix}2\phi_1^2\lambda_N^2\boldsymbol{I} & 2\phi_1^2\lambda_N^2\boldsymbol{I}\\ * & -\boldsymbol{I}+2\phi_1^2\lambda_N^2\boldsymbol{I}\end{bmatrix}.$$

By including $\alpha(\boldsymbol{\tau}^T\,\bar{\boldsymbol{\Xi}}_2\,\boldsymbol{\tau}+2\phi_2^2)\geq 0$ in (3.43), inequality (3.42) is revised to

$$\dot{V}(t)+2\,\zeta\,V(t)\leq \boldsymbol{\tau}^T\bar{\boldsymbol{\Xi}}_3\boldsymbol{\tau}+2\alpha\phi_2^2, \tag{3.45}$$

where

$$\bar{\boldsymbol{\Xi}}_3=\begin{bmatrix}(2\zeta p-2\mathcal{K}p\lambda_2+\xi_1+\xi_2)\boldsymbol{I}+2\alpha\phi_1^2\lambda_N^2\boldsymbol{I} & (\xi_1+\xi_2)\boldsymbol{I}+\boldsymbol{\xi}_3+\boldsymbol{\xi}_4+2\alpha\phi_1^2\lambda_N^2\boldsymbol{I}\\ * & (\xi_1+\xi_2)\boldsymbol{I}-\alpha\boldsymbol{I}+2\alpha\phi_1^2\lambda_N^2\boldsymbol{I}\end{bmatrix}.$$

Based on (3.45), if $\bar{\boldsymbol{\Xi}}_3<0$ then the ISS stability for $\boldsymbol{r}(t)$ given in (3.13) is guaranteed. To guarantee $\bar{\boldsymbol{\Xi}}_3<0$, the following matrix inequality is developed by applying multiple times Schur complement (Lemma 1) on $\bar{\boldsymbol{\Xi}}_3<0$

$$\bar{\boldsymbol{\Xi}}_4=\begin{bmatrix}(2\zeta p-2\mathcal{K}p\lambda_2)\boldsymbol{I} & \boldsymbol{\xi}_3+\boldsymbol{\xi}_4 & \sqrt{2}\alpha\phi_1\lambda_N\boldsymbol{I} & h\mathcal{K}p\lambda_N\boldsymbol{I} & h\mathcal{K}p\lambda_N\boldsymbol{I}\\ * & -\alpha\boldsymbol{I} & \sqrt{2}\alpha\phi_1\lambda_N\boldsymbol{I} & h\mathcal{K}p\lambda_N\boldsymbol{I} & h\mathcal{K}p\lambda_N\boldsymbol{I}\\ * & * & -\alpha\boldsymbol{I} & \boldsymbol{0} & \boldsymbol{0}\\ * & * & * & -\frac{h}{2}p\boldsymbol{I} & \boldsymbol{0}\\ * & * & * & * & -\frac{1}{2\zeta}p\boldsymbol{I}\end{bmatrix}<0.$$

Matrix $\bar{\boldsymbol{\Xi}}_4$ is then pre- and post-multiplied by $\boldsymbol{B}=\mathrm{diag}\,(\boldsymbol{I},\boldsymbol{I},\alpha^{-1}\phi_1^{-1}\boldsymbol{I},\boldsymbol{I},\boldsymbol{I})$. The block matrices $\boldsymbol{\xi}_3$ and $\boldsymbol{\xi}_4$ include matrix $\boldsymbol{L}$ which requires full knowledge of the Laplacian matrix. Since $\boldsymbol{\xi}_3$ and $\boldsymbol{\xi}_4$ are located in an off-diagonal block entry, no upper bounds can be used to replace these terms. In order to relocate $\boldsymbol{\xi}_3$ and $\boldsymbol{\xi}_4$ to diagonal block entries, $\bar{\boldsymbol{\Xi}}_4$ is re-organized in the following format

$$\bar{\boldsymbol{\Xi}}_4=\bar{\boldsymbol{\Xi}}_5+\boldsymbol{\mathcal{M}}_1^T\boldsymbol{\mathcal{N}}+\boldsymbol{\mathcal{N}}^T\boldsymbol{\mathcal{M}}_1+\boldsymbol{\mathcal{M}}_2^T\boldsymbol{\mathcal{N}}+\boldsymbol{\mathcal{N}}^T\boldsymbol{\mathcal{M}}_2<0, \tag{3.46}$$

where

$$\bar{\boldsymbol{\Xi}}_5=\begin{bmatrix}(2\zeta p-2\mathcal{K}p\lambda_2)\boldsymbol{I} & \boldsymbol{0} & \sqrt{2}\lambda_N\boldsymbol{I} & h\mathcal{K}p\lambda_N\boldsymbol{I} & h\mathcal{K}p\lambda_N\boldsymbol{I}\\ * & -\alpha\boldsymbol{I} & \sqrt{2}\lambda_N\boldsymbol{I} & h\mathcal{K}p\lambda_N\boldsymbol{I} & h\mathcal{K}p\lambda_N\boldsymbol{I}\\ * & * & -\alpha^{-1}\phi_1^{-2}\boldsymbol{I} & \boldsymbol{0} & \boldsymbol{0}\\ * & * & * & -\frac{h}{2}p\boldsymbol{I} & \boldsymbol{0}\\ * & * & * & * & -\frac{1}{2\zeta}p\boldsymbol{I}\end{bmatrix},$$

$\boldsymbol{\mathcal{M}}_1=[\,-\mathcal{K}p\boldsymbol{I},\boldsymbol{0},\boldsymbol{0},\boldsymbol{0},\boldsymbol{0}\,]$, $\boldsymbol{\mathcal{N}}=[\,\boldsymbol{0},\boldsymbol{L},\boldsymbol{0},\boldsymbol{0},\boldsymbol{0}\,]$, and $\boldsymbol{\mathcal{M}}_2=[\,-2\,(t-nh)\,\zeta\,\mathcal{K}p\boldsymbol{I},\boldsymbol{0},\boldsymbol{0},\boldsymbol{0},\boldsymbol{0}\,]$. Twice using Lemma 2, inequality $\bar{\boldsymbol{\Xi}}_4<0$ holds if and only if there exist positive scalars ϵ_1 and ϵ_2 such that

$$\bar{\boldsymbol{\Xi}}_5+\epsilon_1^{-1}\boldsymbol{\mathcal{M}}_1^T\boldsymbol{\mathcal{M}}_1+\epsilon_2^{-1}\boldsymbol{\mathcal{M}}_2^T\boldsymbol{\mathcal{M}}_2+(\epsilon_1+\epsilon_2)\,\boldsymbol{\mathcal{N}}^T\boldsymbol{\mathcal{N}}<0. \tag{3.47}$$

Since non-zero entries of $\boldsymbol{\mathcal{M}}_1^T\boldsymbol{\mathcal{M}}_1$, $\boldsymbol{\mathcal{M}}_2^T\boldsymbol{\mathcal{M}}_2$, and $\boldsymbol{\mathcal{N}}^T\boldsymbol{\mathcal{N}}$ are now located in diagonal block entries, proper upper bounds are used to develop the following inequality

from (3.47)

$$\bar{\boldsymbol{\Xi}}_5 + \epsilon_1^{-1}\boldsymbol{\mathcal{M}}_1^T\boldsymbol{\mathcal{M}}_1 + \epsilon_2^{-1}\bar{\boldsymbol{\mathcal{M}}}_2^T\bar{\boldsymbol{\mathcal{M}}}_2 + (\epsilon_1+\epsilon_2)\,\bar{\boldsymbol{\mathcal{N}}}^T\bar{\boldsymbol{\mathcal{N}}} < 0. \tag{3.48}$$

where $\bar{\boldsymbol{\mathcal{M}}}_2$=$[\,2h\zeta\mathcal{K}p\boldsymbol{I}, \mathbf{0}, \mathbf{0}, \mathbf{0}, \mathbf{0}\,]$ and $\bar{\boldsymbol{\mathcal{N}}}$=$[\mathbf{0}, \lambda_N\boldsymbol{I}, \mathbf{0}, \mathbf{0}, \mathbf{0}\,]$. For better illustration, expressions (3.48) is expanded in what follows

$$\begin{bmatrix} \boldsymbol{\xi}_5 & \mathbf{0} & \lambda_N\boldsymbol{I} & h\mathcal{K}p\lambda_N\boldsymbol{I} & h\mathcal{K}p\lambda_N\boldsymbol{I} \\ * & -\alpha\boldsymbol{I} + (\epsilon_1+\epsilon_2)\lambda_N^2\boldsymbol{I} & \lambda_N\boldsymbol{I} & h\mathcal{K}p\lambda_N\boldsymbol{I} & h\mathcal{K}p\lambda_N\boldsymbol{I} \\ * & * & -\alpha^{-1}\phi_1^{-2}\boldsymbol{I} & \mathbf{0} & \mathbf{0} \\ * & * & * & -\frac{h}{2}p\boldsymbol{I} & \mathbf{0} \\ * & * & * & * & -\frac{1}{2\zeta}p\boldsymbol{I} \end{bmatrix} < 0, \tag{3.49}$$

where $\boldsymbol{\xi}_5 = (2\zeta p - 2\mathcal{K}p\lambda_2)\boldsymbol{I} + (\mathcal{K}p)\,\epsilon_1^{-1}(\mathcal{K}p)\boldsymbol{I} + (2h\zeta\mathcal{K}p)\,\epsilon_2^{-1}(2h\zeta\mathcal{K}p)\boldsymbol{I}$. To linearize the two terms $(\mathcal{K}p)\,\epsilon_1^{-1}(\mathcal{K}p)\boldsymbol{I}$ and $(2h\zeta\mathcal{K}p)\,\epsilon_2^{-1}(2h\zeta\mathcal{K}p)\boldsymbol{I}$, Lemma 1 is used twice for (3.49), which leads to

$$\begin{bmatrix} (2\zeta p-2\mathcal{K}p\lambda_2)\boldsymbol{I} & \mathbf{0} & \sqrt{2}\lambda_N\boldsymbol{I} & h\mathcal{K}p\lambda_N\boldsymbol{I} & h\mathcal{K}p\lambda_N\boldsymbol{I} & \mathcal{K}p\boldsymbol{I} & 2h\zeta\mathcal{K}p\boldsymbol{I} \\ * & -\alpha\boldsymbol{I}+(\epsilon_1+\epsilon_2)\lambda_N^2\boldsymbol{I} & \sqrt{2}\lambda_N\boldsymbol{I} & h\mathcal{K}p\lambda_N\boldsymbol{I} & h\mathcal{K}p\lambda_N\boldsymbol{I} & \mathbf{0} & \mathbf{0} \\ * & * & -\alpha^{-1}\phi_1^{-2}\boldsymbol{I} & \mathbf{0} & \mathbf{0} & \mathbf{0} & \mathbf{0} \\ * & * & * & -\frac{T}{2}p\boldsymbol{I} & \mathbf{0} & \mathbf{0} & \mathbf{0} \\ * & * & * & * & -\frac{1}{2\zeta}p\boldsymbol{I} & \mathbf{0} & \mathbf{0} \\ * & * & * & * & * & -\epsilon_1\boldsymbol{I} & \mathbf{0} \\ * & * & * & * & * & \mathbf{0} & -\epsilon_2\boldsymbol{I} \end{bmatrix} < 0. \tag{3.50}$$

The matrix inequality $\boldsymbol{\Xi} < 0$ in (3.12) is then obtained from (3.50) by using alternative variables $\gamma = \alpha^{-1}\phi_1^{-2}$ and $\mu = \mathcal{K}p$, and removing identity block matrices from all rows and columns.

Motivated by [115], a linear objective function which optimizes the decision variables involved in obtaining $\mathcal{K}$ and ϕ_1, i.e., p, μ, α, and γ, is incorporated with $\boldsymbol{\Xi} < 0$. Based on the proposed change of variables, the values of γ and α should be restricted to enlarge ϕ_1. On the other hand, one should restrict μ and enlarge p to restrict $\mathcal{K}$. Therefore, the proposed objective function $\mathcal{F}$ considers minimizing γ, α, and μ, and maximizing p in a summation. Once the optimization problem with feasible outputs is solved, optimal consensus parameters with respect to the objective function (3.11) are obtained from (3.10) and that completes the proof. □

3.6.3 Proof of Theorem 3.2

Proof. To develop the ζ-exponential stability conditions for system (3.18), the following inequality is considered

$$\dot{V}(t) + 2\zeta V(t) < 0, \tag{3.51}$$

where $V(t) = 0.5\,\boldsymbol{r}^T(t)\,\boldsymbol{r}(t)$ is a Lyapunov candidate. If (3.51) is guaranteed, then it holds that

$$0.5\,\|\boldsymbol{r}(t)\|^2 \leq V(t) < V(0)\,e^{-2\zeta t} \leq 0.5\,e^{-2\zeta t}\|\boldsymbol{r}(0)\|^2. \tag{3.52}$$

Thus, $\|\boldsymbol{r}(t)\| \leq e^{-\zeta t}\|\boldsymbol{r}(0)\|$ is guaranteed if inequality (3.51) holds. The time evolution of $\boldsymbol{r}(t)$ in the interval $nh \leq t < (n+1)h$ is considered which is generated from (3.18)

$$\boldsymbol{r}(t) = -(t-nh)\boldsymbol{L}\left(\boldsymbol{r}(nh) + \boldsymbol{e}(nh) + \tilde{\boldsymbol{\delta}}(nh)\right) + \boldsymbol{r}(nh). \tag{3.53}$$

From (3.53), expression $\dot{V}(t)$ is expanded in what follows

$$\begin{aligned}\dot{V}(t) = \boldsymbol{r}^T(t)\dot{\boldsymbol{r}}(t) = &-\boldsymbol{r}^T(nh)\boldsymbol{L}\left(\boldsymbol{r}(nh) + \boldsymbol{e}(nh) + \tilde{\boldsymbol{\delta}}(nh)\right) \\ &+(t-nh)\left(\boldsymbol{r}(nh)+\boldsymbol{e}(nh)+\tilde{\boldsymbol{\delta}}(nh)\right)^T \boldsymbol{L}^T\boldsymbol{L}\left(\boldsymbol{r}(nh)+\boldsymbol{e}(nh)+\tilde{\boldsymbol{\delta}}(nh)\right) \\ &\leq h\lambda_N^2\left(\|\boldsymbol{r}(nh)\| + \|\boldsymbol{e}(nh)\| + \|\tilde{\boldsymbol{\delta}}(nh)\|\right)^2 - \lambda_2\|\boldsymbol{r}(nh)\|^2 \\ &+ \lambda_N\|\boldsymbol{r}(nh)\|\,\|\boldsymbol{e}(nh)\| + \lambda_N\|\boldsymbol{r}(nh)\|\,\|\tilde{\boldsymbol{\delta}}(nh)\|. \end{aligned} \tag{3.54}$$

For the uniform quantizers, it holds that

$$\|\tilde{\boldsymbol{\delta}}(nh)\| \leq 0.5\sqrt{N}\delta. \tag{3.55}$$

Between two consecutive events, one can obtain $|e_i(nh)| \leq \phi\,|\mathbb{X}_i^q(nh)|$. This inequality can be further revised in the global sense as $\|\boldsymbol{e}(nh)\| \leq \phi\,\|\boldsymbol{L}\boldsymbol{q}(\hat{\boldsymbol{x}}(nh))\|$, or equivalently $\|\boldsymbol{e}(nh)\| \leq \phi\,\left\|\boldsymbol{L}\boldsymbol{r}(nh) + \boldsymbol{L}\boldsymbol{e}(nh) + \boldsymbol{L}\tilde{\boldsymbol{\delta}}(nh)\right\|$. Under $\phi \leq \frac{1}{\|\boldsymbol{L}\|}$, the former condition on $\boldsymbol{e}(nh)$ leads to the following inequality

$$\|\boldsymbol{e}(nh)\| \leq \alpha\,\|\boldsymbol{r}(nh)\| + 0.5\,\alpha\,\sqrt{N}\,\delta, \tag{3.56}$$

where $\alpha = \frac{\phi\|\boldsymbol{L}\|}{1-\phi\|\boldsymbol{L}\|}$. Using (3.55), (3.56), and ignoring negligible terms that include h^2, δ^2, $h\delta$, and their higher order terms, expression (3.54) is upper bounded by the following terms

$$\begin{aligned}\dot{V}(t) \leq &\left(h\lambda_N^2 + 2\alpha h\lambda_N^2 + \alpha^2 h\lambda_N^2 - \lambda_2 + \alpha\lambda_N\right)\|\boldsymbol{r}(nh)\|^2 \\ &+ 0.5\sqrt{N}\,(\alpha+1)\,\lambda_N\delta\,\|\boldsymbol{r}(nh)\|. \end{aligned} \tag{3.57}$$

Likewise, $2\zeta V(t)$ is expanded and upper-bounded as below

$$2\zeta V(t) = \zeta\,\boldsymbol{r}^T(t)\,\boldsymbol{r}(t) \leq (2\alpha\zeta h\lambda_N + \zeta)\,\|\boldsymbol{r}(nh)\|^2. \tag{3.58}$$

From (3.57) and (3.58), the following inequality holds for $\boldsymbol{r}(nh) \neq 0$

$$\begin{aligned}\dot{V}(t) + 2\zeta V(t) \leq &\,0.5\sqrt{N}\,(\alpha+1)\,\lambda_N\delta \\ &+ \left(\alpha^2 h\lambda_N^2 + \alpha(2h\lambda_N^2 + \lambda_N + 2\zeta h\lambda_N) + \zeta + h\lambda_N^2 - \lambda_2\right)\|\boldsymbol{r}(nh)\|. \end{aligned} \tag{3.59}$$

Next, parameter α is replaced in (3.59). Inequality (3.51) is guaranteed if condition $\|\boldsymbol{r}(nh)\| < M$ is guaranteed, where M is given in (3.22). It is clear that M must be a positive scalar. With respect to ϕ, M has one zero at $\phi = \frac{1}{\|\boldsymbol{L}\|}$ and tow poles at $\phi = \frac{c_1 \pm \sqrt{c_2}}{2c_3\|\boldsymbol{L}\|}$. Since $c_2 > 0$, both poles are real values. It can be verified that if $h < (\lambda_2 - \zeta)\lambda_N^{-2}$, then $c_1 > \sqrt{c2}$ and the poles of M remain positive. Assuming $h < (\lambda_2 - \zeta)\lambda_N^{-2}$, in Fig. 3.4 the sign of M is shown with respect to different ranges of ϕ.

Sign of $M>0$	+	$+\infty$	$-\infty$	-	0^-	0^+	+	$+\infty$	$-\infty$	-	

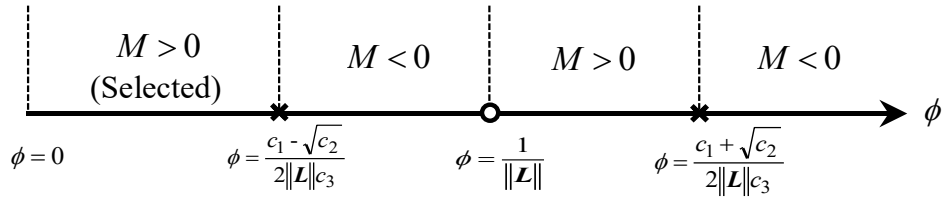

Figure 3.4: Operational range for ϕ for guaranteed convergence. '$\times$' and '$\circ$', respectively, denote the poles and zeros of M .

According to Fig. 3.4, if $0 \leq \phi < \frac{c_1-\sqrt{c_2}}{2c_3\|\boldsymbol{L}\|}$ and $h < (\lambda_2 - \zeta)\lambda_N^{-2}$, then M is guaranteed to remain positive for all $t > 0$. Since, the upper-bound for ϕ, i.e., $\frac{c_1-\sqrt{c_2}}{2c_3\|\boldsymbol{L}\|}$, depends on the global information $\|\boldsymbol{L}\|$, the largest eigenvalue (λ_N) should be used instead, and that completes the proof. □

3.6.4 Proof of Theorem 3.3

Proof of Theorem 3.3 is given below.

Proof. Necessary global parameters used in the proof are previously given in (3.26). Consider the Lyapunov-Krasovskii functional $V = V_1 + V_2$, where

$$V_1 = \boldsymbol{r}^T(t)\boldsymbol{P}_1\,\boldsymbol{r}(t) + \int_{t-h}^{t} \boldsymbol{r}^T(s)\boldsymbol{Q}_1\,\boldsymbol{r}(s)ds + \int_{t-h}^{t}\int_{s}^{t} \dot{\boldsymbol{r}}^T(v)\boldsymbol{Z}_1\dot{\boldsymbol{r}}(v)dvds, \tag{3.60}$$

$$V_2 = \boldsymbol{\eta}^T(t)\boldsymbol{P}_2\,\boldsymbol{\eta}(t) + \int_{t-h}^{t} \boldsymbol{\eta}^T(s)\boldsymbol{Q}_2\,\boldsymbol{\eta}(s)ds + \int_{t-h}^{t}\int_{s}^{t} \dot{\boldsymbol{\eta}}^T(v)\boldsymbol{Z}_2\dot{\boldsymbol{\eta}}(v)dvds. \tag{3.61}$$

Step I. (**Time derivative of** V): The time derivative of V is obtained as follows

$$\begin{aligned}\dot{V}_1 =& 2\dot{\boldsymbol{r}}^T(t)\boldsymbol{P}_1\boldsymbol{r}(t) + \boldsymbol{r}^T(t)\boldsymbol{Q}_1\boldsymbol{r}(t) - \boldsymbol{r}^T(t-h)\boldsymbol{Q}_1\boldsymbol{r}(t-h),\\ &+ h\dot{\boldsymbol{r}}^T(t)\boldsymbol{Z}_1\dot{\boldsymbol{r}}(t) - \left(\int_{t-h}^{t-d(t)} \dot{\boldsymbol{r}}^T(v)\boldsymbol{Z}_1\dot{\boldsymbol{r}}(v)dv + \int_{t-d(t)}^{t} \dot{\boldsymbol{r}}^T(v)\boldsymbol{Z}_1\dot{\boldsymbol{r}}(v)dv\right),\end{aligned} \tag{3.62}$$

$$\begin{aligned}\dot{V}_2 =& 2\dot{\boldsymbol{\eta}}^T(t)\boldsymbol{P}_2\boldsymbol{\eta}(t) + \boldsymbol{\eta}^T(t)\boldsymbol{Q}_2\boldsymbol{\eta}(t) - \boldsymbol{\eta}^T(t-h)\boldsymbol{Q}_2\boldsymbol{\eta}(t-h),\\ &+ h\dot{\boldsymbol{\eta}}^T(t)\boldsymbol{Z}_2\dot{\boldsymbol{\eta}}(t) - \left(\int_{t-h}^{t-d(t)} \dot{\boldsymbol{\eta}}^T(v)\boldsymbol{Z}_2\dot{\boldsymbol{\eta}}(v)dv + \int_{t-d(t)}^{t} \dot{\boldsymbol{\eta}}^T(v)\boldsymbol{Z}_2\dot{\boldsymbol{\eta}}(v)dv\right).\end{aligned} \tag{3.63}$$

Step II. (**Incorporation of DET** (3.24)): The global form of DET (3.24) is given below [4]

$$-\phi_1\boldsymbol{e}^T\boldsymbol{e} + \phi_2\,\mathbb{X}^T\mathbb{X} + \boldsymbol{\eta}^T\,\boldsymbol{\eta} \geq 0. \tag{3.64}$$

Next, the term $\mathbb{X}^T\mathbb{X}$ is expanded. By definition, it holds that $\mathbb{X} = \boldsymbol{L}\hat{\boldsymbol{x}}$. Considering that $\boldsymbol{e} = \hat{\boldsymbol{x}} - \boldsymbol{x}$ and $\boldsymbol{L} = \tilde{\boldsymbol{V}}^\dagger\tilde{\boldsymbol{J}}\tilde{\boldsymbol{V}}$, one obtains $\mathbb{X} = \boldsymbol{L}\boldsymbol{e} + \tilde{\boldsymbol{V}}^\dagger\tilde{\boldsymbol{J}}\tilde{\boldsymbol{V}}\boldsymbol{x}$. Using transformation (3.29), this equality can be further revised as $\mathbb{X} = \tilde{\boldsymbol{V}}^\dagger\tilde{\boldsymbol{J}}\tilde{\boldsymbol{V}}\boldsymbol{e} + \tilde{\boldsymbol{V}}^\dagger\tilde{\boldsymbol{J}}\boldsymbol{r}$. The

[4] To improve readability, time arguments are omitted in expressions (3.64) and (3.65). All time arguments in (3.64) and (3.65) are $(t-d(t))$, i.e., $\boldsymbol{r} \triangleq \boldsymbol{r}(t-d(t))$, $\boldsymbol{e} \triangleq \boldsymbol{e}(t-d(t))$, $\boldsymbol{\eta} \triangleq \boldsymbol{\eta}(t-d(t))$.

term $\mathbb{X}^T\mathbb{X}$ is expanded as follows

$$\mathbb{X}^T\mathbb{X} \leq \boldsymbol{r}^T\tilde{\boldsymbol{J}}^2\boldsymbol{r} + \lambda_N^2\boldsymbol{e}^T\boldsymbol{e} + \boldsymbol{e}^T(\tilde{\boldsymbol{V}}^T\tilde{\boldsymbol{J}}^2)\boldsymbol{r} + \boldsymbol{r}^T(\tilde{\boldsymbol{J}}^2\tilde{\boldsymbol{V}})\boldsymbol{e}. \tag{3.65}$$

Let $\boldsymbol{\nu}_1 = [\boldsymbol{r}^T(t-d(t)), \boldsymbol{e}^T(t-d(t)), \boldsymbol{\eta}^T(t-d(t))]^T$. Using (3.65) in (3.64) results in the following condition

$$\boldsymbol{\nu}_1^T \begin{bmatrix} \phi_2\tilde{\boldsymbol{J}}^2 & \phi_2\tilde{\boldsymbol{J}}^2\tilde{\boldsymbol{V}} & \boldsymbol{0} \\ * & (\phi_2\lambda_N^2 - \phi_1)\boldsymbol{I} & \boldsymbol{0} \\ * & * & \boldsymbol{I} \end{bmatrix} \boldsymbol{\nu}_1 \geq 0. \tag{3.66}$$

Step III. (**Null expressions**): Let $\boldsymbol{\nu}_2 = [\,\boldsymbol{r}^T(t), \boldsymbol{r}^T(t-d(t))]^T$, $\boldsymbol{\nu}_3 = [\,\boldsymbol{\eta}^T(t), \boldsymbol{\eta}^T(t-d(t))]^T$. The following null equalities hold for any matrices $\boldsymbol{F}$, $\boldsymbol{G}$, $\boldsymbol{W}$, $\boldsymbol{E}$, $\boldsymbol{Y}$, and $\boldsymbol{U}$ with appropriate dimensions

$$2\boldsymbol{\nu}_2^T\boldsymbol{F}\Big[\boldsymbol{r}(t-d(t)) - \boldsymbol{r}(t-h) - \int_{t-h}^{t-d(t)} \dot{\boldsymbol{r}}(s)ds\Big] = 0, \tag{3.67}$$

$$2\boldsymbol{\nu}_2^T\boldsymbol{G}\Big[\boldsymbol{r}(t) - \boldsymbol{r}(t-d(t)) - \int_{t-d(t)}^{t} \dot{\boldsymbol{r}}(s)ds\Big] = 0, \tag{3.68}$$

$$2\boldsymbol{\nu}_3^T\boldsymbol{W}\Big[\boldsymbol{\eta}(t-d(t)) - \boldsymbol{\eta}(t-h) - \int_{t-h}^{t-d(t)} \dot{\boldsymbol{\eta}}(s)ds\Big] = 0, \tag{3.69}$$

$$2\boldsymbol{\nu}_3^T\boldsymbol{E}\Big[\boldsymbol{\eta}(t) - \boldsymbol{\eta}(t-d(t)) - \int_{t-d(t)}^{t} \dot{\boldsymbol{\eta}}(s)ds\Big] = 0, \tag{3.70}$$

$$\int_{t-h}^{t-d(t)} \boldsymbol{\nu}_2^T\boldsymbol{Y}\boldsymbol{\nu}_2 ds + \int_{t-d(t)}^{t} \boldsymbol{\nu}_2^T\boldsymbol{Y}\boldsymbol{\nu}_2 ds = h\boldsymbol{\nu}_2^T\boldsymbol{Y}\boldsymbol{\nu}_2, \tag{3.71}$$

$$\int_{t-h}^{t-d(t)} \boldsymbol{\nu}_3^T\boldsymbol{U}\boldsymbol{\nu}_3 ds + \int_{t-d(t)}^{t} \boldsymbol{\nu}_3^T\boldsymbol{U}\boldsymbol{\nu}_3 ds = h\boldsymbol{\nu}_3^T\boldsymbol{U}\boldsymbol{\nu}_3. \tag{3.72}$$

From (3.30), it holds that

$$2\Big(\boldsymbol{r}^T(t)\boldsymbol{H}_1 + \dot{\boldsymbol{r}}^T(t)\boldsymbol{H}_2 + \boldsymbol{r}^T(t-d(t))\boldsymbol{H}_3\Big)\Big(- \tilde{\boldsymbol{J}}\,\boldsymbol{r}(t-d(t)) - \tilde{\boldsymbol{J}}\tilde{\boldsymbol{V}}\,\boldsymbol{e}(t-d(t)) - \dot{\boldsymbol{r}}(t)\Big) = 0. \tag{3.73}$$

Likewise, from (3.25) one obtains that

$$2\Big(\boldsymbol{\eta}^T(t) + \dot{\boldsymbol{\eta}}^T(t)\Big)\Big(-\dot{\boldsymbol{\eta}}(t) - \boldsymbol{\eta}(t) + \phi_3\bar{\mathbb{X}}(t-d(t))\Big) = 0, \tag{3.74}$$

where $\bar{\mathbb{X}}(t) = [\,|\mathbb{X}_1(t)|, \ldots, |\mathbb{X}_N(t)|\,]^T$. By using the Young inequality, the following expression is obtained from (3.74)

$$\begin{aligned} &2\Big(\boldsymbol{\eta}^T(t) + \dot{\boldsymbol{\eta}}^T(t)\Big)\Big(-\dot{\boldsymbol{\eta}}(t) - \boldsymbol{\eta}(t)\Big) + \phi_3\boldsymbol{\eta}^T(t)\boldsymbol{\eta}(t) \\ &\quad + \phi_3\dot{\boldsymbol{\eta}}^T(t)\dot{\boldsymbol{\eta}}(t) + 2\phi_3\mathbb{X}^T(t-d(t))\mathbb{X}(t-d(t)) \geq 0. \end{aligned} \tag{3.75}$$

The term $\mathbb{X}^T(t-d(t))\mathbb{X}(t-d(t))$ in condition (3.75) is further expanded by considering (3.65).

Step IV. (**Stability Conditions**): Let $\boldsymbol{\nu}_4 = [\boldsymbol{\nu}_2^T,\ \dot{\boldsymbol{r}}^T(s)\,]^T$, $\boldsymbol{\nu}_5 = [\boldsymbol{\nu}_3^T,\ \dot{\boldsymbol{\eta}}^T(s)\,]^T$, and $\boldsymbol{\nu}_6 = [\boldsymbol{\nu}_7^T,\ \boldsymbol{\nu}_8^T]^T$, where $\boldsymbol{\nu}_7 = [\boldsymbol{r}^T(t),\, \boldsymbol{r}^T(t-d(t)),\, \boldsymbol{r}^T(t-h),\, \dot{\boldsymbol{r}}^T(t),\, \boldsymbol{e}^T(t-d(t))]^T$, and $\boldsymbol{\nu}_8 =$

$[\boldsymbol{\eta}^T(t),\, \boldsymbol{\eta}^T(t-d(t)),\, \boldsymbol{\eta}^T(t-h),\, \dot{\boldsymbol{\eta}}^T(t)]^T$. Considering all expressions from (3.66) to (3.75), the following upper bound holds for $\dot{V}$

$$\dot{V} \leq \boldsymbol{\nu}_6^T \begin{bmatrix} \boldsymbol{\Pi} & \mathbf{0} \\ * & \boldsymbol{\Psi} \end{bmatrix} \boldsymbol{\nu}_6 - \int_{t-h}^{t-d(t)} \boldsymbol{\nu}_4^T \boldsymbol{C}_1 \boldsymbol{\nu}_4 ds - \int_{t-d(t)}^{t} \boldsymbol{\nu}_4^T \boldsymbol{C}_2 \boldsymbol{\nu}_4 ds$$
$$- \int_{t-h}^{t-d(t)} \boldsymbol{\nu}_5^T \boldsymbol{C}_3 \boldsymbol{\nu}_5 ds - \int_{t-d(t)}^{t} \boldsymbol{\nu}_5^T \boldsymbol{C}_4 \boldsymbol{\nu}_5 ds. \tag{3.76}$$

Based on (3.76), if $\boldsymbol{\Pi} < 0$, $\boldsymbol{\Psi} < 0$, and $\boldsymbol{C}_i \geq 0$, $(1 \leq i \leq 4)$, then it holds that $\dot{V} < 0$.

Step V. (**Objective Function**): Consider the following constraints for design parameters ϕ_c, $(1 \leq c \leq 3)$,

$$\phi_1^2 < \theta_1, \qquad \phi_2^{-1} < \theta_2, \quad \phi_3^{-1} < \theta_3, \tag{3.77}$$

where $\theta_c > 0$, $(1 \leq c \leq 3)$, are decision variables. By minimizing $\mathbb{F} = \theta_1 + \theta_2 + \theta_3$, the optimization attempts to decrease the values of θ_1, θ_2, and θ_3. In return, parameter ϕ_1 is decreased and parameters $\{\phi_2, \phi_3\}$ are increased according to (3.77). As mentioned previously, lower values for ϕ_1 and higher values for $\{\phi_2, \phi_3\}$ increase the inter-event-time. Then LMIs given in (3.34) are obtained from (3.77). This completes the proof □

Chapter 4

Consensus in general linear agents

Proposed implementations in Chapter 3 are limited to first-order agents and their application is mainly for average consensus. This chapter studies a more general consensus problem where the agents can be of any order. Two implementations (namely, PEC [80] and PSEC [81]) are proposed in this regard. Section 4.1 presents implementation PEC, where event-triggered consensus for general linear MASs is studied in the presence of control gain uncertainties. Only the transmission scheme is event-triggered in PEC and other processing (measurement and control update) is continuous-time. Section 4.2 proposes the PSEC implementation, which is an extended case for PEC where a sampled-data scheme is incorporated for measurements.

4.1 PEC

Refereed to as the PEC, a distributed performance guaranteed event triggered consensus algorithm for general linear MASs is presented in this section. The performance guarantees include a desired rate of consensus convergence, a certain level of non-fragility to control gain uncertainties, and pareto optimality of the design parameters (the control and ET gains). Using an approximated linear scalarization method similar to CEASE (Section 3.2) and DEASE (Section 3.4), the ET parameters and control gain are co-designed by solving a convex constrained optimization problem. Followed by some preliminary steps, the optimization can be performed locally. However, the optimization complexity is dependent on N. The communication network in PEC is undirected. The PEC block diagram is exactly similar to Fig 2.2. As shown in Fig 2.2, the consensus process is based on continuous-time state measurement. Additionally, the event-detection in PEC is performed in a continuous-time fashion.

It is widely known that the control parameters are often subject to uncertainties due to physical constraints, round-off error, and digitization [70]. The uncertainties in realization of the control gains can cause considerable performance deterioration. PEC offers a level of non-fragility in control designs.

4.1.1 Problem statement

Consider a linear time-invariant MAS described by the following dynamics

$$\dot{\boldsymbol{x}}_i(t) = \boldsymbol{A}\boldsymbol{x}_i(t) + \boldsymbol{B}\boldsymbol{u}_i(t), \quad (1 \leq i \leq N), \tag{4.1}$$

where $\boldsymbol{x}_i(t) \in \mathbb{R}^n$ and $\boldsymbol{u}_i(t) \in \mathbb{R}^m$. It is assumed that the pair $(\boldsymbol{A}, \boldsymbol{B})$ is controllable. In PEC, the disagreement for agent i, $(1 \leq i \leq N)$, is defined as follows

$$\mathbb{X}_i(t) = \sum_{j \in \mathcal{N}_i} a_{i,j} \left(\boldsymbol{\Lambda}_i(t)\boldsymbol{x}_i(t_k^i) - \boldsymbol{\Lambda}_j(t)\boldsymbol{x}_j(t_k^j) \right), \tag{4.2}$$

where $\boldsymbol{\Lambda}_i(t) = e^{\boldsymbol{A}(t-t_k^i)}$. Note that $\boldsymbol{\Lambda}_i(t)\boldsymbol{x}_i(t_k^i)$ is an open-loop estimate of $\boldsymbol{x}_i(t)$ in $t \in [\, t_k^i,\, t_{k+1}^i \,)$ [111, 130], which will be further explained in Remark 4.1. Note that the control protocol (4.2) is *not* event-triggered due to continuous-time updates used in $\boldsymbol{\Lambda}_i(t) = e^{\boldsymbol{A}(t-t_k^i)}$.

Similar to previous implementations in Chapter 3, in PEC all nodes transmit their initial state values $\boldsymbol{x}_i(0)$ to their neighbours, i.e., $t_0^i = 0$, $(1 \leq i \leq N)$. Given t_k^i, the next event for agent i, $(1 \leq i \leq N)$, is triggered based on the following ET condition

$$t_{k+1}^i = \inf\{ \quad t > t_k^i \quad | \quad \|\boldsymbol{\Phi}\boldsymbol{e}_i(t)\| \geq \alpha \|\mathbb{X}_i(t)\| \quad \}, \tag{4.3}$$

Matrix $\boldsymbol{\Phi}$ and scalar $\alpha > 0$ are the ET parameters to be designed. Vector $\boldsymbol{e}_i(t) = \boldsymbol{\Lambda}_i(t)\boldsymbol{x}_i(t_k^i) - \boldsymbol{x}_i(t)$, $(1 \leq i \leq N)$, is the state error. Note that $\boldsymbol{e}_i(t)$ is based on the difference between the estimated value of the state, i.e., $\boldsymbol{\Lambda}_i(t)\boldsymbol{x}_i(t_k^i)$, and the real-time state value, i.e., $\boldsymbol{x}_i(t)$. The following control protocol is proposed for (4.1)

$$\boldsymbol{u}_i(t) = \boldsymbol{K}\, \mathbb{X}_i(t), \quad (1 \leq i \leq N), \tag{4.4}$$

where matrix $\boldsymbol{K} \in \mathbb{R}^{m \times n}$ is the nominal control gain to be designed. However, in realization the control signal is often perturbed with actuator faults, aging, system modeling uncertainties, and digitalization errors [70]. One approach to model these physical constraints is to consider an additive uncertainty in the control gain as follows

$$\boldsymbol{u}_i(t) = (\boldsymbol{K} + \boldsymbol{\Delta}_K)\, \mathbb{X}_i(t), \quad (1 \leq i \leq N). \tag{4.5}$$

The time-varying matrix $\boldsymbol{\Delta}_K$ represents the uncertainties in the control gain.

Assumption 2. The uncertainty $\boldsymbol{\Delta}_K$ satisfies $\|\boldsymbol{\Delta}_K\| \leq \delta$ for $t > 0$, where δ is a predetermined desired non-fragility level for $\boldsymbol{K}$.

Remark 4.1 (Open-loop estimation)**.** According to the agent dynamics (4.1), the expression $e^{\boldsymbol{A}(t-t_k^i)}\boldsymbol{x}_i(t_k^i) \triangleq \boldsymbol{\Lambda}_i(t)\boldsymbol{x}_i(t_k^i)$, $t \in [t_k^i, t_{k+1}^i)$, is the zero input response ($\boldsymbol{u}_i = \boldsymbol{0}$) of agent i with initial condition $\boldsymbol{x}_i(t_k^i)$. In literature [1, 111, 131, 132], the expression $\boldsymbol{\Lambda}_i(t)\boldsymbol{x}_i(t_k^i)$ is known as the open-loop estimate of $\boldsymbol{x}_i(t)$ for inter-event interval $t \in [t_k^i, t_{k+1}^i)$. The phrase 'open-loop' is used since $\boldsymbol{u}_i(t)$ is ignored in the estimation, which makes $\boldsymbol{\Lambda}_i(t)\boldsymbol{x}_i(t_k^i)$ an estimate of $\boldsymbol{x}_i(t)$ 'to a certain extent'. Compared to [33, 76] where no estimation is used (i.e., $\boldsymbol{\Lambda}_i = \boldsymbol{I}_n$), the control protocol (4.5) and ET scheme (4.3) benefits from the open-loop estimation in two ways: (i) Compared

to $\boldsymbol{e}_i(t) = \boldsymbol{x}_i(t_k^i) - \boldsymbol{x}_i(t)$, the rate of changes in $\boldsymbol{e}_i(t) = e^{\boldsymbol{A}(t-t_k^i)}\boldsymbol{x}_i(t_k^i) - \boldsymbol{x}_i(t)$ is lower, which results in a reduction in the number of events triggered by (4.3), [131, 132]. (ii) Due to the estimate of the neighbouring states considered in disagreement (4.2), control protocol (4.5) is more suitable for dynamic consensus problems, where the final consensus states are time-varying [111, 131]. One disadvantage of using such an estimation approach is that the control protocol is not event-triggered and should be updated continuously. A closed-loop estimation technique is proposed in [133], where neighbours exchange their control update values as well as their states. Each agent estimates the state of its neighbours based on the last state and control value received from the neighbour. In this scheme, the control update remains event-triggered. As indicated in [6, Sec. III. B], the control value is regarded as private information. This precludes the closed-loop estimation approach from practical MASs.

Remark 4.2 (Special cased on MAS (4.1))**.** It should be noted that the general linear model considered in (4.1) can be reduced to first-order agents if $\boldsymbol{A} = 0$ and $\boldsymbol{B} = 1$. Additionally, the second-order integrator agents, which is widely considered in the literature [134], is a special case of (4.1), where $\boldsymbol{A} = [0, 1; 0, 0]$ and $\boldsymbol{B} = [0, 1]^T$.

Before proceeding to the problem formulation and developing the main results, the following discussion is provided for the Zeno-behaviour exclusion. The observations made in excluding the Zeno-behaviour are also important for the design objectives considered in PEC.

4.1.2 Zeno behaviour

If the ET scheme is based on periodic samples of the system (such as all implementations given in Chapter 3), the Zeno behaviour is inherently excluded. The reason is that any two event instants are guaranteed to be at least one sampling period apart. In continuous-time event detection such as PEC, however, it is essential to analytically exclude the possibility of the Zeno-behaviour. The following theorem provides a lower-bound on the interval between any two event instants. This interval is also known as the minimum inter-event interval.

Theorem 4.1. Consider MAS (4.1) with control protocol (4.5) and ET scheme (4.3). The minimum inter-event interval for agent i is strictly positive and lower bounded by the following term

$$t_{k+1}^i - t_k^i \geq \frac{1}{2\left\|\boldsymbol{A}\right\|} \ln\left(1 + \frac{2\alpha\left\|\boldsymbol{A}\right\|}{\left\|\boldsymbol{B}\bar{\boldsymbol{K}}\right\|\left\|\boldsymbol{\Phi}\right\|}\right), \tag{4.6}$$

where $\bar{\boldsymbol{K}} = \boldsymbol{K} + \boldsymbol{\Delta}_K$.

Proof. Proof of Theorem 4.1 is included in Appendix, Section 4.4.1. □

Apart from the fact that (4.6) provides a lower-bound for exclusion of the Zeno-behaviour, it shows how design parameters $\boldsymbol{K}$, $\boldsymbol{\Phi}$, and α influence the minimum

inter-event interval. According to (4.6), the events are more sparse for larger values of α, and smaller values of $\|\boldsymbol{K}\|$ and $\|\boldsymbol{\Phi}\|$. This observation can be used to construct the objective function for designing unknown parameters so that the minimum inter-event time is increased.

Design Objectives: The design objectives considered in PEC are as follows:

- Control the rate of consensus convergence by an exponentially decreasing term;
- Guarantee non-fragility to some level of uncertainty in the control gain;
- Optimize consensus parameters, i.e., the ET parameters $\{\boldsymbol{\Phi}, \alpha\}$ and control gain $\boldsymbol{K}$, using a convex constrained optimization. To increase the inter-event interval, an objective function is proposed which limits the norm of $\boldsymbol{K}$ and $\boldsymbol{\Phi}$, and enlarges α based on a weighted-sum approach.

4.1.3 Problem formulation

Define the following global vectors

$$\begin{aligned}
&\boldsymbol{x} = [\boldsymbol{x}_1^T(t), \ldots, \boldsymbol{x}_N^T(t)]^T,\ \hat{\boldsymbol{x}} = [\hat{\boldsymbol{x}}_1^T(t), \ldots, \hat{\boldsymbol{x}}_N^T(t)]^T, \boldsymbol{e} = [\boldsymbol{e}_1^T(t), \ldots, \boldsymbol{e}_N^T(t)]^T,\\
&\mathbb{X} = [\mathbb{X}_1^T(t), \ldots, \mathbb{X}_N^T(t)]^T, \boldsymbol{\Lambda} = \operatorname{diag}(\boldsymbol{\Lambda}_1(t), \ldots, \boldsymbol{\Lambda}_N(t)),\ \bar{\mathbb{X}} = [\, \|\mathbb{X}_1(t)\|, \ldots, \|\mathbb{X}_N(t)\| \,]^T,\\
&\bar{\boldsymbol{e}} = [\, \|\boldsymbol{e}_1(t)\|, \ldots, \|\boldsymbol{e}_N(t)\| \,]^T. \qquad (4.7)
\end{aligned}$$

It holds that $\boldsymbol{e} = \boldsymbol{\Lambda}(t)\hat{\boldsymbol{x}}(t) - \boldsymbol{x}(t)$. The closed-loop system from (4.1) and (4.5) is given below

$$\dot{\boldsymbol{x}} = (\boldsymbol{I}_N \otimes \boldsymbol{A} + \boldsymbol{L} \otimes \boldsymbol{B}(\boldsymbol{K} + \boldsymbol{\Delta}_K))\, \boldsymbol{x} + \boldsymbol{L} \otimes \boldsymbol{B}(\boldsymbol{K} + \boldsymbol{\Delta}_K)\, \boldsymbol{e}. \qquad (4.8)$$

Next, the consensus problem for the original closed-loop MAS (4.8) is converted into the stability problem of a transformed system. Let $0 < \lambda_2 \leq \ldots \leq \lambda_N$ denote the eigenvalues of $\boldsymbol{L}$ in the ascending order. Let matrix $\boldsymbol{W} = [w_{i,j}] \in \mathbb{R}^{N \times N}$ include the normalized eigenvectors of $\boldsymbol{L}$ such that

$$\boldsymbol{W}\boldsymbol{J}\boldsymbol{W}^{-1} = \boldsymbol{L}, \qquad \|\boldsymbol{W}\| = 1, \qquad (4.9)$$

where $\boldsymbol{J} = \operatorname{diag}(0, \lambda_2, \ldots, \lambda_N)$. Let $\boldsymbol{W}^{-1} = [\tilde{w}_{i,j}]$. From $\boldsymbol{W}^{-1}$, the $(N-1) \times N$ dimensional matrix $\tilde{\boldsymbol{W}} = [\tilde{w}_{i,j}]$, for $2 \leq i \leq N$ and $1 \leq j \leq N$ is constructed. More precisely, $\tilde{\boldsymbol{W}}$ includes rows 2 to N of matrix $\boldsymbol{W}^{-1}$. Now, consider the following transformation

$$\boldsymbol{\psi} = \tilde{\boldsymbol{W}} \otimes \boldsymbol{I}_n \boldsymbol{x}. \qquad (4.10)$$

Using (4.10), system (4.8) is transformed to

$$\dot{\boldsymbol{\psi}} = (\boldsymbol{I}_{N-1} \otimes \boldsymbol{A} + \tilde{\boldsymbol{J}} \otimes \boldsymbol{B}(\boldsymbol{K} + \boldsymbol{\Delta}_k))\, \boldsymbol{\psi} + \tilde{\boldsymbol{J}}\tilde{\boldsymbol{W}} \otimes \boldsymbol{B}(\boldsymbol{K} + \boldsymbol{\Delta}_k)\, \boldsymbol{e}, \qquad (4.11)$$

where $\tilde{\boldsymbol{J}} = \operatorname{diag}(\lambda_2, \ldots, \lambda_N)$. It is proved in [100, Theorem 1] that consensus is achieved in (4.8) if and only if $\lim_{t \to \infty} \boldsymbol{\psi} = 0$. Therefore, consensus in MAS (4.8) is converted to stability of system (4.11).

Remark 4.3 (Final state values for consensus)**.** Although the final state values of the agents in verification of consensus is irrelevant, it is interesting to find the steady-state values of the agents. Let $\boldsymbol{y}(t)=\tilde{\boldsymbol{w}}_1\otimes\boldsymbol{I}_n\boldsymbol{x}(t)$, where $\tilde{\boldsymbol{w}}_1$ is the first row of matrix $\boldsymbol{W}^{-1}$ defined in (4.9). In [100, Theorem 1], it is shown that the steady state values in terms of $\boldsymbol{y}(t)$ satisfies

$$\lim_{t\to\infty}[\boldsymbol{y}(t)-e^{\boldsymbol{A}t}\boldsymbol{y}(0)]=\boldsymbol{0}. \tag{4.12}$$

4.1.4 Parameter design

This section develops a linear matrix inequality (LMI) optimization that simultaneously computes all unknown parameters required in PEC. The optimization requires all the eigenvalues and eigenvectors of the Laplacian matrix $\boldsymbol{L}$, which can be computed using Algorithm 3.4.

Theorem 4.2. Given desired values for exponential rate of consensus convergence ζ and non-fragility level δ, if there exist matrices $\boldsymbol{P}\in\mathbb{R}^{n\times n}>0$, $\tilde{\boldsymbol{\Phi}}\in\mathbb{R}^{n\times n}>0$, $\boldsymbol{\Omega}\in\mathbb{R}^{m\times n}$, positive scalars $\tilde{\alpha}$, τ_1, τ_2, ϵ_1, ϵ_2, and θ_c, $(1\le c\le 4)$, satisfying the following convex constrained optimization

$$\min \qquad \mathbb{F}=\sum_{c=1}^{4}\theta_c, \tag{4.13}$$

subject to:

$$\boldsymbol{\Xi}=\begin{bmatrix}\boldsymbol{\Xi}_{11} & \tilde{\boldsymbol{J}}\tilde{\boldsymbol{W}}\otimes\boldsymbol{B}\boldsymbol{\Omega} & \tilde{\boldsymbol{J}}\otimes\boldsymbol{P} & \boldsymbol{0} & \boldsymbol{I}_{N-1}\otimes\boldsymbol{P} & \boldsymbol{0}\\ * & -\boldsymbol{I}_N\otimes\tilde{\boldsymbol{\Phi}} & \boldsymbol{0} & \boldsymbol{I}_N\otimes\boldsymbol{P} & \boldsymbol{0} & \boldsymbol{I}_N\otimes\boldsymbol{P}\\ * & * & -\tau_1\boldsymbol{I} & \boldsymbol{0} & \boldsymbol{0} & \boldsymbol{0}\\ * & * & * & -\tau_2\boldsymbol{I} & \boldsymbol{0} & \boldsymbol{0}\\ * & * & * & * & -\epsilon_1\boldsymbol{I} & \boldsymbol{0}\\ * & * & * & * & * & -\epsilon_2\boldsymbol{I}\end{bmatrix}<0,$$

$$\pi_1=2\tilde{\alpha}+(-2+\tau_1)<0, \qquad \boldsymbol{\pi}_2=2\tilde{\alpha}\tilde{\boldsymbol{J}}^2+(-2+\tau_2)\boldsymbol{I}_{N-1}<0,$$

$$\boldsymbol{C}_1=\begin{bmatrix}\theta_1\boldsymbol{I} & \boldsymbol{I}\\ * & \boldsymbol{P}\end{bmatrix}>0,\ \boldsymbol{C}_2=\begin{bmatrix}-\theta_2\boldsymbol{I} & \tilde{\boldsymbol{\Phi}}\\ * & -\boldsymbol{I}\end{bmatrix}<0,\ \boldsymbol{C}_3=\begin{bmatrix}\theta_3 & 1\\ * & \tilde{\alpha}\end{bmatrix}>0,$$

$$\boldsymbol{C}_4=\begin{bmatrix}-\theta_4\boldsymbol{I} & \boldsymbol{\Omega}\\ * & -\boldsymbol{I}\end{bmatrix}<0, \tag{4.14}$$

where

$$\begin{aligned}\boldsymbol{\Xi}_{11}=&\boldsymbol{I}_{N-1}\otimes(\boldsymbol{P}\boldsymbol{A}^T+\boldsymbol{A}\boldsymbol{P})+\tilde{\boldsymbol{J}}\otimes\boldsymbol{B}\boldsymbol{\Omega}+(\tilde{\boldsymbol{J}}\otimes\boldsymbol{B}\boldsymbol{\Omega})^T+2\zeta\boldsymbol{I}_{N-1}\otimes\boldsymbol{P}\\ &+\epsilon_1\delta^2(\tilde{\boldsymbol{J}}\otimes\boldsymbol{B})(\boldsymbol{B}^T\otimes\tilde{\boldsymbol{J}}^T)+\epsilon_2\delta^2(\tilde{\boldsymbol{J}}\tilde{\boldsymbol{W}}\otimes\boldsymbol{B})(\boldsymbol{B}^T\otimes\tilde{\boldsymbol{W}}^T\tilde{\boldsymbol{J}}^T),\end{aligned}$$

then consensus design parameters are computed as

$$\boldsymbol{K}=\boldsymbol{\Omega}\boldsymbol{P}^{-1}, \qquad \boldsymbol{\Phi}=(\boldsymbol{P}^{-1}\tilde{\boldsymbol{\Phi}}\boldsymbol{P}^{-1})^{1/2}, \qquad \alpha=\sqrt{\tilde{\alpha}}. \tag{4.15}$$

Algorithm 4.5 . The PEC algorithm

Input: Neighbouring information, System matrices $\boldsymbol{A}$ and $\boldsymbol{B}$.

Output: Performance guaranteed event-triggered consensus in general linear MASs.

Preliminary: Using a distributed algorithm such as Algorithm 3.4, each node computes all eigenvalues and eigenvectors of the Laplacian matrix. Using an average consensus the nodes agree on the value of the desired convergence rate ζ and non-fragility level δ.

I. Parameter Design: (D1 -D2)

D1. *Optimization*: Using a semi-definite programming solver, solve (4.13) for given ζ and δ.

D2. *Parameter design*: Compute consensus design parameters $\boldsymbol{K}$, $\boldsymbol{\Phi}$, and α from (4.15).

Distributed Consensus Iterations: (C1 – C2)

C1. *Initialization*: Node i transmits $\boldsymbol{x}_i(0)$ to its neighbours, $(1 \leq i \leq N)$.

C2. *Consensus process*: Using designed $\boldsymbol{K}$ for (4.5) and $\{\boldsymbol{\Phi}, \alpha\}$ for (4.3) the states of the agents approach a consensus with a decaying rate satisfying (4.16).

Using design parameters (4.15), consensus trajectories converge at a rate which satisfies the following inequality

$$\boldsymbol{\psi}^T(t)\,\boldsymbol{\psi}(t) \leq \frac{\lambda_{\max}(\boldsymbol{P}^{-1})}{\lambda_{\min}(\boldsymbol{P}^{-1})}\, e^{-2\zeta t}\, \boldsymbol{\psi}^T(0)\,\boldsymbol{\psi}(0). \tag{4.16}$$

Additionally, the following bounds are guaranteed by minimizing $\mathbb{F}$

$$\|\boldsymbol{K}\| \leq \theta_1\sqrt{\theta_4}, \qquad \|\boldsymbol{\Phi}\| \leq \theta_1\theta_2^{1/4}, \qquad \alpha \geq \frac{1}{\sqrt{\theta_3}}. \tag{4.17}$$

Proof. The proof is provided in Section 4.4. □

The PEC algorithm is summarized in Algorithm 4.5.

Remark 4.4 (Logic behind the proposed objective function and design trade-offs)**.** The logic behind the proposed objective function in (4.13) is similar to CEASE and DEASE. In short, the objective function in (4.13) minimizes a weighted sum of the alternative variables involved in computing $\boldsymbol{K}$, $\boldsymbol{\Phi}$, and α so that the minimum inter-event interval (4.6) is increased. The trade-offs involved for parameter design in PEC are related to the physical interpretation of the given parameters ζ and δ. Parameter ζ is related to the consensus convergence rate of PEC. Therefore, a larger value for ζ (faster consensus) leads to larger norms for the control gain $\boldsymbol{K}$ at the expense of more frequent transmissions and vice versa. As for δ which shows the desired level of non-fragility to control gain uncertainty, large values for δ result in higher values for $\boldsymbol{K}$ to compensate the impact of uncertainty. In return, it is expected that larger values for δ adversely impact the efficiency of the ET scheme and more transmissions be allowed.

Remark 4.5 (The objective function as a comparison index)**.** Since the objective function (4.13) is formulated based on increasing the inter-event interval, its value can be used as an index to compare the expected average inter-event interval between different MASs. Consider two different MASs, namely MAS 1 and 2. Consensus parameters are computed from Theorem 4.2 for these two MASs which leads to two

different values for the objective function, namely $\mathbb{F}_1$ and $\mathbb{F}_2$. If $\mathbb{F}_1 \leq \mathbb{F}_2$, it is concluded that the expected average inter-event interval for MAS 1 is larger than MAS 2 (and vice versa). That is MAS 1 is more likely to save more transmissions. Refer to Section 7.4.1 for experimental comparison in this regard.

Remark 4.6 (PEC in the presence of measurement noise)**.** It should be reminded that PEC is based on continuous-time state measurement and continuous-time monitoring of the ET condition. Apart from the above shortcommings, as shown in [135], the continuous-time ET scheme (4.3) may lead to Zeno-behaviour in the presence of arbitrary small disturbance or measurement noise. One approach to exclude the Zeno-behaviour in the presence of external disturbance is to include a constant threshold (such as ϕ_2 in CEASE). The constant threshold guarantees that the inter-event interval is at least equal to the constant value which is strictly positive. However, including a constant value in th ET condition results in steady-state error in consensus. Another approach to exclude the Zeno-behaviour in the presence of external disturbance is to incorporate a sampler with the ET scheme so that the inter-event interval remains inherently positive.

The next section proposes PSEC by incorporating a sampler in PEC.

4.2 PSEC

PSEC is a performance guaranteed sampled-data event-triggered consensus approach for linear MASs. The performance guarantees include a desired exponential convergence rate for consensus and non-fragility to some level of control gain uncertainties. Different from PEC, a sampler is incorporated in the implementation of PSEC so that measurements and event-triggerings are based on sampled states not the real-time states. This reduces the amount of measurements and computations. The PSEC configuration is similar to the block diagram shown in Fig. 3.1 for CEASE.

The introduction of a sampler in the implementation of PSEC produces an artificial time-varying time-delay in the closed-loop system. Thus, the consensus (stability) analysis in PSEC is more complicated compared to PEC. Similar to DEASE in Chapter 3, the parameter design in PSEC is based on a co-design framework. The co-design in PSEC simultaneously computes all control and ET parameters from some delay-dependent Lyapunov-Krasovskii functionals.

4.2.1 Problem statement

Consider the linear time-invariant MAS in (4.1). In PSEC, the disagreement for agent i, $(1 \leq i \leq N)$, is defined as follows

$$\mathbb{X}_i(t) = \sum_{j \in \mathcal{N}_i} a_{i,j} \left(\mathbf{\Lambda}_i(nh)\hat{\boldsymbol{x}}_i(nh) - \mathbf{\Lambda}_j(nh)\hat{\boldsymbol{x}}_j(nh) \right), \quad t \in [nh, (n+1)h), \tag{4.18}$$

where $\hat{\boldsymbol{x}}_i(nh) = \boldsymbol{x}_i(n_k^i h)$ and $\boldsymbol{\Lambda}_i(nh) = e^{\boldsymbol{A}(nh - n_k^i h)}$, $(n \in \mathbb{N}_0)$. Unlike PEC, in PSEC the control updates are also sampled-data event-triggered. Given n_k^i, the next event for agent i, $(1 \leq i \leq N)$, is triggered based on the following ET condition

$$n_{k+1}^i = \min_{n \in \mathbb{N}} \{n > n_k^i \mid \|\boldsymbol{\Phi}_1^{1/2} \boldsymbol{e}_i(nh)\| \geq \|\boldsymbol{\Phi}_2^{-1/2} \mathbb{X}_i(nh)\|\}, \qquad n_0^i = 0. \tag{4.19}$$

Matrices $\boldsymbol{\Phi}_1$ and $\boldsymbol{\Phi}_2$ are the sampled-data ET parameters to be designed. Vector $\boldsymbol{e}_i(nh) = \hat{\boldsymbol{x}}_i(nh) - \boldsymbol{x}_i(nh)$, $(1 \leq i \leq N)$, is the state error. The following control protocol is considered in PSEC

$$\boldsymbol{u}_i(t) = \boldsymbol{K}\, \mathbb{X}_i(nh), \quad (1 \leq i \leq N), \quad t \in [nh, (n+1)h), \tag{4.20}$$

where matrix $\boldsymbol{K} \in \mathbb{R}^{m \times n}$ is the nominal control gain to be designed. Similar to PEC, the physical constraints in control realization (actuator faults, aging, system modeling, and digitalization errors [70]) are taken into account which are modeled by

$$\boldsymbol{u}_i(t) = (\boldsymbol{K} + \boldsymbol{\Delta}_K)\, \mathbb{X}_i(t), \quad (1 \leq i \leq N). \tag{4.21}$$

The time-varying uncertainty $\boldsymbol{\Delta}_K$ satisfies Assumption 2.

Design Objectives: The design objectives considered in PSEC are as follows:

- A co-design framework is proposed which simultaneously computes unknown parameters, i.e., the control gain $\boldsymbol{K}$ and ET parameters $\boldsymbol{\Phi}_1$ and $\boldsymbol{\Phi}_2$.
- A desired exponential rate of consensus convergence and a desired level of non-fragility to control gain uncertainty are included in the co-design framework. The sampling period h is also predetermined.

4.2.2 Problem formulation

Denote global parameters as $\boldsymbol{x}(t) = [\boldsymbol{x}_1^T(t), \ldots, \boldsymbol{x}_N^T(t)]^T$, $\hat{\boldsymbol{x}}(t) = [\hat{\boldsymbol{x}}_1^T(t), \ldots, \hat{\boldsymbol{x}}_N^T(t)]^T$, $\boldsymbol{\Lambda}(nh) = \text{diag}(\boldsymbol{\Lambda}_1(nh), \ldots, \boldsymbol{\Lambda}_N(nh))$, and $\boldsymbol{e}(t) = [\boldsymbol{e}_1^T(t), \ldots, \boldsymbol{e}_N^T(t)]^T$. It holds that $\boldsymbol{e}(nh) = \boldsymbol{\Lambda}(nh)\hat{\boldsymbol{x}}(nh) - \boldsymbol{x}(nh)$. The closed-loop system from (4.1) and (4.21) is

$$\dot{\boldsymbol{x}}(t) = (\boldsymbol{I}_N \otimes \boldsymbol{A})\boldsymbol{x}(t) + \boldsymbol{L} \otimes \boldsymbol{B}(\boldsymbol{K} + \boldsymbol{\Delta}_K))\, \boldsymbol{x}(nh) + \boldsymbol{L} \otimes \boldsymbol{B}(\boldsymbol{K} + \boldsymbol{\Delta}_K)\, \boldsymbol{e}(nh). \tag{4.22}$$

A similar transformation used in PEC is considered for PSEC to convert the consensus problem for MAS (4.22) into stability problem. Using (4.9) and (4.10), closed-loop system (4.22) is transformed to

$$\begin{aligned} \dot{\boldsymbol{\psi}}(t) = {} & (\boldsymbol{I}_{N-1} \otimes \boldsymbol{A})\boldsymbol{\psi}(t) + (\tilde{\boldsymbol{J}} \otimes \boldsymbol{B}(\boldsymbol{K} + \boldsymbol{\Delta}_k))\, \boldsymbol{\psi}(nh) \\ & + (\tilde{\boldsymbol{J}}\tilde{\boldsymbol{W}} \otimes \boldsymbol{B}(\boldsymbol{K} + \boldsymbol{\Delta}_k))\, \boldsymbol{e}(nh), \quad t \in [nh, (n+1)h). \end{aligned} \tag{4.23}$$

Consensus is achieved in (4.22) if and only if $\lim_{t \to \infty} \boldsymbol{\psi}(t) = 0$ [100, Theorem 1]. It should be noted that the final state values in PSEC also satisfies expression (4.12).

4.2.3 Parameter design

An LMI constrained framework is developed in this section that simultaneously computes all unknown parameters required in PSEC, i.e., $\boldsymbol{K}$, $\boldsymbol{\Phi}_1$, and $\boldsymbol{\Phi}_2$. PSEC requires all the eigenvalues and eigenvectors of the Laplacian matrix $\boldsymbol{L}$ which can be computed in a distributed fashion using Algorithm 3.4.

Theorem 4.3. Given desired values for sampling period h, convergence rate ζ, and control gain non-fragility level δ, if there exist the following parameters

- $m\times n$ dimensional matrix $\boldsymbol{V}$, $n\times n$ dimensional matrices $\boldsymbol{H}$, $\boldsymbol{Y}_{11}$, $\boldsymbol{Y}_{12}$, $\boldsymbol{Y}_{22}$, $\boldsymbol{F}_1$, $\boldsymbol{F}_2$, $\boldsymbol{G}_1$, $\boldsymbol{G}_2$;
- $n\times n$ dimensional positive definite matrices $\boldsymbol{P}$, $\boldsymbol{Q}$, $\boldsymbol{Z}$, $\boldsymbol{M}_1$, $\boldsymbol{M}_2$;
- positive scalars ϵ_1, ϵ_2 ϵ_3;

satisfying the following LMIs

$$\boldsymbol{C}_1=\begin{bmatrix}\boldsymbol{\Pi} & \boldsymbol{\Theta}\\ * & \boldsymbol{\Omega}\end{bmatrix}<0,\quad \boldsymbol{C}_2=\begin{bmatrix}\boldsymbol{Y} & \boldsymbol{F}\\ * & he^{-2\zeta h}\boldsymbol{Z}\end{bmatrix}\geq 0,\quad \boldsymbol{C}_3=\begin{bmatrix}\boldsymbol{Y} & \boldsymbol{G}\\ * & he^{-2\zeta h}\boldsymbol{Z}\end{bmatrix}\geq 0, \tag{4.24}$$

then, the control gain $\boldsymbol{K}$ and ET parameters $\boldsymbol{\Phi}_1$ and $\boldsymbol{\Phi}_2$ are computed from the following expressions

$$\boldsymbol{K}=\boldsymbol{V}(\boldsymbol{H}^{-1})^T,\qquad \boldsymbol{\Phi}_1=\boldsymbol{H}^{-1}\boldsymbol{M}_1(\boldsymbol{H}^{-1})^T,\qquad \boldsymbol{\Phi}_2=\boldsymbol{M}_2, \tag{4.25}$$

and the closed-loop MAS (4.23) satisfies the following exponential convergence rate

$$\|\boldsymbol{\psi}(t)\|^2\leq\frac{\lambda_2}{\lambda_1}e^{-2\zeta t}\|\boldsymbol{\psi}(0)\|^2, \tag{4.26}$$

where $\lambda_1=\lambda_{\min}(\bar{\boldsymbol{P}})$, $\lambda_2=\lambda_{\max}(\bar{\boldsymbol{P}})+h\lambda_{\max}(\bar{\boldsymbol{Q}})$, with $\bar{\boldsymbol{P}}=\boldsymbol{H}^{-1}\boldsymbol{P}(\boldsymbol{H}^{-1})^T$, $\bar{\boldsymbol{Q}}=\boldsymbol{H}^{-1}\boldsymbol{Q}(\boldsymbol{H}^{-1})^T$, and $\bar{\boldsymbol{Z}}=\boldsymbol{H}^{-1}\boldsymbol{Z}(\boldsymbol{H}^{-1})^T$. Unknown block matrices in (4.24) are defined below

$$\boldsymbol{\Pi}=\begin{bmatrix}\boldsymbol{\pi}_{11} & \boldsymbol{\pi}_{12} & -\boldsymbol{I}_{N-1}\otimes\boldsymbol{F}_1 & \boldsymbol{\pi}_{14} & \tilde{\boldsymbol{J}}\tilde{\boldsymbol{W}}\otimes\boldsymbol{B}\boldsymbol{V} & \boldsymbol{0}\\ * & \boldsymbol{\pi}_{22} & -\boldsymbol{I}_{N-1}\otimes\boldsymbol{F}_2 & \boldsymbol{\pi}_{24} & \tilde{\boldsymbol{J}}\tilde{\boldsymbol{W}}\otimes\boldsymbol{B}\boldsymbol{V} & \tilde{\boldsymbol{J}}\tilde{\boldsymbol{W}}^{\dagger^T}\otimes\boldsymbol{H}\\ * & * & -e^{-2\zeta h}\boldsymbol{I}_{N-1}\otimes\boldsymbol{Q} & \boldsymbol{0} & \boldsymbol{0} & \boldsymbol{0}\\ * & * & * & \boldsymbol{\pi}_{44} & \tilde{\boldsymbol{J}}\tilde{\boldsymbol{W}}\otimes\boldsymbol{B}\boldsymbol{V} & \boldsymbol{0}\\ * & * & * & * & -\boldsymbol{I}_N\otimes\boldsymbol{M}_1 & \tilde{\boldsymbol{W}}^{\dagger}\tilde{\boldsymbol{J}}\tilde{\boldsymbol{W}}\otimes\boldsymbol{H}\\ * & * & * & * & * & -\boldsymbol{I}_N\otimes\boldsymbol{M}_2\end{bmatrix}, \tag{4.27}$$

$$\boldsymbol{\Theta}=\begin{bmatrix}\boldsymbol{0} & \boldsymbol{I}_{N-1}\otimes\boldsymbol{H}^T & \boldsymbol{0} & \boldsymbol{0} & \boldsymbol{0} & \boldsymbol{0}\\ \boldsymbol{0} & \boldsymbol{I}_{N-1}\otimes\boldsymbol{H} & \boldsymbol{0} & \boldsymbol{0} & \boldsymbol{0} & \boldsymbol{0}\\ \boldsymbol{0} & \boldsymbol{0} & \boldsymbol{0} & \boldsymbol{0} & \boldsymbol{I}_N\otimes\boldsymbol{H}^T & \boldsymbol{0}\end{bmatrix}^T, \tag{4.28}$$

$$\boldsymbol{\Omega}=\mathrm{diag}(-\epsilon_1\boldsymbol{I}_{n\times(N-1)},\ -\epsilon_2\boldsymbol{I}_{n\times(N-1)},\ -\epsilon_3\boldsymbol{I}_{n\times N}), \tag{4.29}$$

$$\boldsymbol{\pi}_{11}=\boldsymbol{I}_{N-1}\otimes\Big(\boldsymbol{Q}+\boldsymbol{G}_1+\boldsymbol{G}_1^T+\boldsymbol{A}\boldsymbol{H}+\boldsymbol{H}^T\boldsymbol{A}^T+h\boldsymbol{Y}_{11}+2\zeta\boldsymbol{P}\Big)+\delta^2(\epsilon_1\boldsymbol{\Xi}_1+\epsilon_3\boldsymbol{\Xi}_2),$$
$$\boldsymbol{\pi}_{12}=\boldsymbol{I}_{N-1}\otimes\Big(\boldsymbol{F}_1-\boldsymbol{G}_1+\boldsymbol{G}_2^T+h\boldsymbol{Y}_{12}+\boldsymbol{H}\boldsymbol{A}^T\Big)+\tilde{\boldsymbol{J}}\otimes\boldsymbol{B}\boldsymbol{V}+\delta^2(\epsilon_1\boldsymbol{\Xi}_1+\epsilon_3\boldsymbol{\Xi}_2),$$

Algorithm 4.6 . The PSEC algorithm

Input: Neighbouring information, System matrices $\boldsymbol{A}$ and $\boldsymbol{B}$.

Output: Performance guaranteed sampled-data event-triggered consensus in general linear MASs.

Preliminary: Using a distributed algorithm such as Algorithm 3.4, each node computes all eigenvalues and eigenvectors of the Laplacian matrix. Using an average consensus the nodes agree on the value of the desired sampling period h, convergence rate ζ, and non-fragility level δ.

I. Parameter Design: (D1 -D2)

D1. Compute consensus design parameters $\boldsymbol{K}$, $\boldsymbol{\Phi}_1$, and $\boldsymbol{\Phi}_2$ from (4.25).

Distributed Consensus Iterations: (C1 – C2)

C1. *Initialization*: Node i transmits $\boldsymbol{x}_i(0)$ to its neighbours, $(1 \leq i \leq N)$.

C2. *Consensus process*: Using the designed $\boldsymbol{K}$ for (4.21) and $\boldsymbol{\Phi}_1$ and $\boldsymbol{\Phi}_2$ for (4.19) the states of the agents approach sampled-data consensus with a decaying rate satisfying (4.26).

$$
\begin{aligned}
\boldsymbol{\pi}_{14} &= \boldsymbol{I}_{N-1} \otimes (\boldsymbol{P} - \boldsymbol{H}^T + \boldsymbol{H}\boldsymbol{A}^T) + \delta^2 \epsilon_3 \boldsymbol{\Xi}_2, \\
\boldsymbol{\pi}_{22} &= \boldsymbol{I}_{N-1} \otimes (\boldsymbol{F}_2 + \boldsymbol{F}_2^T - \boldsymbol{G}_2 - \boldsymbol{G}_2^T + h\boldsymbol{Y}_{22}) + \tilde{\boldsymbol{J}} \otimes \boldsymbol{B}\boldsymbol{V} + (\tilde{\boldsymbol{J}} \otimes \boldsymbol{B}\boldsymbol{V})^T \\
&\quad + \delta^2(\epsilon_1 \boldsymbol{\Xi}_1 + \epsilon_3 \boldsymbol{\Xi}_2), \\
\boldsymbol{\pi}_{24} &= -\boldsymbol{I}_{N-1} \otimes \boldsymbol{H}^T + (\tilde{\boldsymbol{J}} \otimes \boldsymbol{B}\boldsymbol{V})^T + \delta^2(\epsilon_2 \boldsymbol{\Xi}_1 + \epsilon_3 \boldsymbol{\Xi}_2), \\
\boldsymbol{\pi}_{44} &= \boldsymbol{I}_{N-1} \otimes (h^2 \boldsymbol{Z} - \boldsymbol{H} - \boldsymbol{H}^T) + \epsilon_3 \delta^2 \boldsymbol{\Xi}_2,
\end{aligned} \tag{4.30}
$$

and

$$
\begin{aligned}
&\boldsymbol{Y} = \begin{bmatrix} \boldsymbol{Y}_{11} & \boldsymbol{Y}_{12} \\ * & \boldsymbol{Y}_{22} \end{bmatrix}, \quad \boldsymbol{F} = \begin{bmatrix} \boldsymbol{F}_1^T & \boldsymbol{F}_2^T \end{bmatrix}^T, \quad \boldsymbol{G} = \begin{bmatrix} \boldsymbol{G}_1^T & \boldsymbol{G}_2^T \end{bmatrix}^T, \\
&\boldsymbol{\Xi}_1 = (\tilde{\boldsymbol{J}} \otimes \boldsymbol{B})(\tilde{\boldsymbol{J}} \otimes \boldsymbol{B})^T, \qquad \boldsymbol{\Xi}_2 = (\tilde{\boldsymbol{J}}\tilde{\boldsymbol{W}} \otimes \boldsymbol{B})(\tilde{\boldsymbol{J}}\tilde{\boldsymbol{W}} \otimes \boldsymbol{B})^T.
\end{aligned} \tag{4.31}
$$

Proof. Proof of Theorem 4.3 is provided in Appendix, Section 4.4.3. □

The PSEC implementation is summarized in Algorithm 4.6.

Remark 4.7 (Trade-offs in PSEC)**.** Similar to PEC, some performance trade-offs are expected in PSEC based on the selected values for sampling period h, non-fragility level δ, and convergence rate ζ. A larger value for ζ (faster consensus) leads to larger norms for the control gain $\boldsymbol{K}$ at the expense of more frequent transmissions and vice versa. Larger values for δ are expected to result in higher values for $\boldsymbol{K}$ to compensate the impact of uncertainty. In return, larger values for δ would lead to more transmissions between the nodes. Higher values for the sampling period h may help in saving more transmissions. However, the control gain obtained with a higher value for h may be conservative.

Remark 4.8 (Extension of PSEC to H_∞ disturbance rejection)**.** In case that the measurement noise, denoted by $\boldsymbol{\omega}_i(t)$, is not negligible the agent model is usually represented by $\dot{\boldsymbol{x}}_i(t) = \boldsymbol{A}\boldsymbol{x}(t) + \boldsymbol{B}\boldsymbol{u}_i(t) + \boldsymbol{D}\boldsymbol{\omega}_i(t)$. The H_∞ optimization technique can be included in Theorem 4.3 to take into account the impact of external disturbance. In the H_∞ disturbance rejection the following objectives are usually considered:

- The closed-loop system remains stable when $\boldsymbol{\omega}(t) = \boldsymbol{0}$. In the case of converted system (4.23), this condition implies that $\lim_{t\to\infty} \boldsymbol{\psi}(t) = \boldsymbol{0}$ if $\boldsymbol{\omega}(t) = \boldsymbol{0}$.

Table 4.1: Comparison of PEC and PSEC.

Characteristics	**PEC** [80]	**PSEC** [81]
Transmitter scheme	Event-triggered	Sampled-data Event-triggered
Receiver scheme	Continuous-time	Periodic
State Measurement scheme	Continuous-time	Periodic
Control scheme	Continuous-time	Periodic
Event monitoring	Continuous-time	Periodic
Optimization for Design Parameters	Yes	No
Steady-state error	No	No
State Quantization	No	No
Control gain Design	Yes	Yes
Relative expected number of transmissions	Low	Low
Network Topology	Undirected	Undirected

- Under zero initial condition $\boldsymbol{\psi}(0)=\mathbf{0}$, it holds that $\|\boldsymbol{\psi}(t)\|_2 \leq \gamma^2 \|\boldsymbol{\omega}(t)\|_2$, where γ is a prescribed level of noise attenuation.

It can be shown that if $\dot{V}(t)+2\zeta V(t)+\boldsymbol{\psi}^T(t)\boldsymbol{\psi}(t)-\gamma^2\boldsymbol{\omega}^T(t)\boldsymbol{\omega}(t)<0$, then the H_∞ disturbance rejection for system (4.23) is guaranteed [136].

Remark 4.9 (Considering communication delay in PSEC)**.** The stability analysis in PSEC in based on an artificial time-varying time-delay and Lyapunov-Krasovskii functionals. More precisely, the alternative variable $d(t) \triangleq t-nh$ is used to relate the real-time t and sample instants nh (refer to proof of Theorem 4.3 for more details). Then, it holds that $0 \leq d(t) \leq h$. The time-varying time-delay approach also allows including the communication time delays that usually occur in networked communication. One necessary condition is that *the communication delay should be equal or less than the sampling period*. Let τ_{ij} denote the communication delay from node j to node i, where node j is in the neighbouring set of node i. It is assumed that $\tau_{ij} \leq h$, $(1 \leq i,j \leq N)$. Considering the impact of the communication time delay, parameter $d(t)$ is revised as $d(t) \triangleq t-nh+h$ and $h \leq d(t) \leq 2h$. This implies that the closed-loop MAS is exposed to a time-varying time-delay with both lower and upper-bounds. In this case, the stability analysis in PSEC can be performed using the same LKF proposed in [137].

Remark 4.10 (PSEC has no objective function in its parameter design)**.** Comparing Theorem 4.2 (parameter design for PEC) and Theorem 4.3 (parameter design for PSEC), it is observed that the LMI conditions derived for PSEC depend on a larger set of decision variables than that of PEC. This prevents including an objective function for increasing the inter-event interval in PSEC.

4.3 Summary

This chapter proposes two implementations for event-triggered (ET) consensus in general linear multi-agent systems (MAS). In particular, PEC proposes an event-triggered consensus approach that guarantees a desired exponential rate of consensus convergence and some level of non-fragility to control gain perturbations. The parameter design in PEC is based on a co-design LMI optimization approach that increases the inter-event interval so as to save transmission resources. The optimization can be performed distributively following some preliminary steps. State measurement and monitoring of the ET condition in PEC is continuous-time.

PSEC adds the flexibility of measuring only samples of the system. Hence, the ET condition is monitored periodically using local samplers. The trade-off for incorporating a sampler in PSEC is that the stability analysis becomes more complicated and no parameter optimization is considered in PSEC.

Table 4.1 summarizes the main features of PEC and PSEC.

4.4 Appendix

In this section, the proofs of the theorems proposed in Chapter 4 are provided.

4.4.1 Proof of Theorem 4.1

Proof. Consider t_k^i and t_{k+1}^i as two consecutive event instants for node i. From (4.3), it holds that $\|\boldsymbol{e}_i(t_k^i)\|= 0$. For $t \geq t_k^i$, the state error $\boldsymbol{e}_i(t)$ evolves from zero until the next event is triggered at $t = t_{k+1}^i$ which fulfills (4.3). From $\boldsymbol{e}_i(t) = \boldsymbol{\Lambda}_i(t)\hat{\boldsymbol{x}}_i(t)-\boldsymbol{x}_i(t)$, it follows that $\dot{\boldsymbol{e}}_i(t) = \boldsymbol{A}\boldsymbol{\Lambda}_i(t)\hat{\boldsymbol{x}}_i(t)-\dot{\boldsymbol{x}}_i(t)$. From (4.5) and (4.1), one obtains that $\dot{\boldsymbol{x}}_i(t) = \boldsymbol{A}\boldsymbol{x}_i(t) + \boldsymbol{B}\bar{\boldsymbol{K}}\,\mathbb{X}_i(t)$. Some manipulation leads to $\dot{\boldsymbol{e}}_i(t) = \boldsymbol{A}\boldsymbol{e}_i(t) - \boldsymbol{B}\bar{\boldsymbol{K}}\,\mathbb{X}_i(t)$, or

$$\|\dot{\boldsymbol{e}}_i(t)\| \leq \|\boldsymbol{A}\|\,\|\boldsymbol{e}_i(t)\| + \|\boldsymbol{B}\bar{\boldsymbol{K}}\|\|\mathbb{X}_i(t)\|\,, \quad t \in [t_k^i, t_{k+1}^i). \tag{4.32}$$

Let $r_i(t) = \frac{\|\boldsymbol{e}_i(t)\|}{\|\mathbb{X}_i(t)\|}$. It follows that

$$\|\dot{r}_i(t)\| \leq \frac{\|\dot{\boldsymbol{e}}_i(t)\|}{\|\mathbb{X}_i(t)\|} + r_i(t)\frac{\|\dot{\mathbb{X}}_i(t)\|}{\|\mathbb{X}_i(t)\|}, \quad t \in [t_k^i,\, t_{k+1}^i). \tag{4.33}$$

Dividing (4.32) by $\|\mathbb{X}_i(t)\|$ and applying (4.33) lead to $\dot{r}_i(t) \leq 2\,\|\boldsymbol{A}\|\,r_i(t) + \|\boldsymbol{B}\bar{\boldsymbol{K}}\|$, or equivalently

$$r_i(t) \leq c\left(e^{2\|\boldsymbol{A}\|(t-t_k^i)} - 1\right), \quad t \in [t_k^i,\, t_{k+1}^i), \tag{4.34}$$

where $c = \frac{\|\boldsymbol{B}\bar{\boldsymbol{K}}\|}{2\|\boldsymbol{A}\|}$. The next event is triggered by (4.3) at $t = t^i_{k+1}$ when $\|\boldsymbol{\Phi} \boldsymbol{e}_i(t^i_{k+1})\| = \alpha \|\mathbb{X}_i(t^i_{k+1})\|$. From (4.34), one obtains that

$$\frac{\|\boldsymbol{\Phi} \boldsymbol{e}_i(t^i_{k+1})\|}{\|\mathbb{X}_i(t^i_{k+1})\|} = \alpha \leq c\|\boldsymbol{\Phi}\| \left(e^{2\|\boldsymbol{A}\|(t^i_{k+1} - t^i_k)} - 1 \right) , \tag{4.35}$$

From (4.35), it holds that $t^i_{k+1} - t^i_k \geq \frac{1}{2\|\boldsymbol{A}\|} \ln \left(1 + \frac{\alpha}{c\|\boldsymbol{\Phi}\|} \right)$ which is equivalent to (4.6). The right hand side of (4.6) is strictly positive. Therefore, the minimum time between two events is strictly positive, i.e., ET scheme (4.3) does not exhibit the Zeno behaviour. □

4.4.2 Proof of Theorem 4.2

Proof. Consider the following inequality

$$\dot{V} + 2\,\zeta\, V < 0, \tag{4.36}$$

where

$$V = \boldsymbol{\psi}^T (\boldsymbol{I}_{N-1} \otimes \boldsymbol{P}^{-1})\, \boldsymbol{\psi}. \tag{4.37}$$

Condition (4.36) leads to the exponential convergence rate specified in (4.16). The time derivative of V is obtained below

$$\dot{V} = \boldsymbol{\psi}^T\, \bar{\boldsymbol{\Xi}}_{11}\, \boldsymbol{\psi} + 2\boldsymbol{\psi}^T\, \bar{\boldsymbol{\Xi}}_{12}\, \boldsymbol{e}, \tag{4.38}$$

where

$$\begin{aligned} \bar{\boldsymbol{\Xi}}_{11} &= \boldsymbol{I}_{N-1} \otimes (\boldsymbol{A}^T \boldsymbol{P}^{-1} + \boldsymbol{P}^{-1} \boldsymbol{A}) + 2\tilde{\boldsymbol{J}} \otimes \boldsymbol{P}^{-1} \boldsymbol{B} (\boldsymbol{K} + \boldsymbol{\Delta}_K), \\ \bar{\boldsymbol{\Xi}}_{12} &= \tilde{\boldsymbol{J}} \tilde{\boldsymbol{W}} \otimes \boldsymbol{P}^{-1} \boldsymbol{B} (\boldsymbol{K} + \boldsymbol{\Delta}_K). \end{aligned}$$

The global form of (4.2) can be viewed as follows

$$\mathbb{X} = \boldsymbol{L} \otimes \boldsymbol{I}_n \boldsymbol{\Lambda} \hat{\boldsymbol{x}}(t). \tag{4.39}$$

Reminding that $\boldsymbol{e} = \boldsymbol{\Lambda}\hat{\boldsymbol{x}} - \boldsymbol{x}$ and $\boldsymbol{L} = \tilde{\boldsymbol{W}}^\dagger \tilde{\boldsymbol{J}} \tilde{\boldsymbol{W}}$, The following expression is developed from (4.10) and (4.39)

$$\mathbb{X} = (\tilde{\boldsymbol{W}}^\dagger \tilde{\boldsymbol{J}}) \otimes \boldsymbol{I}_n \boldsymbol{\psi} + (\tilde{\boldsymbol{W}}^\dagger \tilde{\boldsymbol{J}} \tilde{\boldsymbol{W}}) \otimes \boldsymbol{I}_n \boldsymbol{e}. \tag{4.40}$$

Considering that $\tilde{\boldsymbol{W}}^{\dagger^T} \tilde{\boldsymbol{W}}^\dagger = \boldsymbol{I}$, expression $\mathbb{X}^T \mathbb{X}$ is expanded

$$\mathbb{X}^T \mathbb{X} \leq 2\boldsymbol{\sigma}_1^T \boldsymbol{\sigma}_1 + 2\boldsymbol{\sigma}_2^T (\tilde{\boldsymbol{J}}^2 \otimes \boldsymbol{I}_n) \boldsymbol{\sigma}_2, \tag{4.41}$$

where $\boldsymbol{\sigma}_1 = (\tilde{\boldsymbol{W}}^\dagger \tilde{\boldsymbol{J}}) \otimes \boldsymbol{I}_n \boldsymbol{\psi}$ and $\boldsymbol{\sigma}_2 = \tilde{\boldsymbol{W}} \otimes \boldsymbol{I}_n \boldsymbol{e}$. The following equalities hold by definition

$$\tau_1^{-1} \left(\boldsymbol{\psi}^T (\tilde{\boldsymbol{J}}^2 \otimes \boldsymbol{I}_n) \boldsymbol{\psi} - \boldsymbol{\sigma}_1^T \boldsymbol{\sigma}_1 \right) = 0, \tag{4.42}$$

$$\tau_2^{-1} (\boldsymbol{e}^T \boldsymbol{e} - \boldsymbol{\sigma}_2^T \boldsymbol{\sigma}_2) \geq 0, \tag{4.43}$$

where $\tau_1>0$ and $\tau_2>0$ are decision variables. Based on (4.3), it holds that $\|\boldsymbol{\Phi e}_i(t)\| \leq \alpha\|\mathbb{X}_i(t)\|$. Let $\boldsymbol{a}_1 = [\,\|\boldsymbol{\Phi e}_1(t)\|, \ldots, \|\boldsymbol{\Phi e}_N(t)\|\,]^T$. In a collective fashion, it holds that $\boldsymbol{a}_1 \leq \alpha\bar{\mathbb{X}}$, which is equivalent to

$$\boldsymbol{a}_1^T\boldsymbol{a}_1 = \boldsymbol{e}^T(\boldsymbol{I}_N\otimes\boldsymbol{\Phi}^2)\boldsymbol{e} \leq \alpha^2\bar{\mathbb{X}}^T\bar{\mathbb{X}}. \tag{4.44}$$

Using (4.41), the following expression holds from (4.44)

$$\boldsymbol{e}^T(\boldsymbol{I}_N\otimes\boldsymbol{\Phi}^2)\boldsymbol{e} \leq 2\alpha^2\boldsymbol{\sigma}_1^T\boldsymbol{\sigma}_1 + 2\alpha^2\boldsymbol{\sigma}_2^T(\tilde{\boldsymbol{J}}^2\otimes\boldsymbol{I}_n)\boldsymbol{\sigma}_2. \tag{4.45}$$

Let $\boldsymbol{\nu} = [\,\boldsymbol{\psi}^T, \boldsymbol{e}^T, \boldsymbol{\sigma}_1^T, \boldsymbol{\sigma}_2^T\,]^T$. Based on (4.38), (4.42), (4.43), and (4.45), we re-arrange (4.36) as follows

$$\boldsymbol{\nu}^T\begin{bmatrix}\tilde{\boldsymbol{\Xi}} & \boldsymbol{0}\\ * & \tilde{\boldsymbol{\Pi}}\end{bmatrix}\boldsymbol{\nu} < 0, \tag{4.46}$$

where $\tilde{\boldsymbol{\Xi}} = \begin{bmatrix}\tilde{\boldsymbol{\Xi}}_{11} & \bar{\boldsymbol{\Xi}}_{12}\\ * & \bar{\boldsymbol{\Xi}}_{22}\end{bmatrix}$, $\tilde{\boldsymbol{\Pi}} = \mathrm{diag}(\tilde{\boldsymbol{\pi}}_1, \tilde{\boldsymbol{\pi}}_2)$, and

$$\begin{aligned}
&\tilde{\boldsymbol{\Xi}}_{11} = \bar{\boldsymbol{\Xi}}_{11} + \tau_1^{-1}\tilde{\boldsymbol{J}}^2\otimes\boldsymbol{I}_n + 2\zeta\boldsymbol{I}_{N-1}\otimes\boldsymbol{P}^{-1}, \qquad \tilde{\boldsymbol{\Xi}}_{22} = -\boldsymbol{I}_N\otimes\boldsymbol{\Phi}^2 + \tau_2^{-1}\boldsymbol{I},\\
&\tilde{\boldsymbol{\pi}}_1 = (-\tau_1^{-1} + 2\alpha^2)\boldsymbol{I}_{Nn}, \qquad \tilde{\boldsymbol{\pi}}_2 = -\tau_2^{-1}\boldsymbol{I} + 2\alpha^2(\tilde{\boldsymbol{J}}^2\otimes\boldsymbol{I}_n).
\end{aligned} \tag{4.47}$$

From (4.46), inequality (4.36) is guaranteed if $\tilde{\boldsymbol{\Xi}}<0$ and $\tilde{\boldsymbol{\Pi}}<0$. Inequality $\tilde{\boldsymbol{\Xi}}$ is pre- and post multiplied by $\boldsymbol{T} = \mathrm{diag}(\boldsymbol{I}_{N-1}\otimes\boldsymbol{P}, \boldsymbol{I}_N\otimes\boldsymbol{P})$ which results in

$$\begin{bmatrix}\hat{\boldsymbol{\Xi}}_{11} & \hat{\boldsymbol{\Xi}}_{12}\\ * & \hat{\boldsymbol{\Xi}}_{22}\end{bmatrix} + \boldsymbol{\mathcal{S}}_1\boldsymbol{\mathcal{R}}_1^T + \boldsymbol{\mathcal{R}}_1\boldsymbol{\mathcal{S}}_1^T + \boldsymbol{\mathcal{S}}_2\boldsymbol{\mathcal{R}}_2^T + \boldsymbol{\mathcal{R}}_2\boldsymbol{\mathcal{S}}_2^T < 0, \tag{4.48}$$

$$\begin{aligned}
&\hat{\boldsymbol{\Xi}}_{11} = \boldsymbol{I}_{N-1}\otimes(\boldsymbol{PA}^T + \boldsymbol{AP}) + 2\tilde{\boldsymbol{J}}\otimes\boldsymbol{BKP} + \tau_1^{-1}(\tilde{\boldsymbol{J}}\otimes\boldsymbol{P})^2 + 2\zeta\boldsymbol{I}_{N-1}\otimes\boldsymbol{P},\\
&\hat{\boldsymbol{\Xi}}_{12} = \tilde{\boldsymbol{J}}\tilde{\boldsymbol{W}}\otimes\boldsymbol{BKP}, \qquad \hat{\boldsymbol{\Xi}}_{22} = -\boldsymbol{I}_N\otimes(\boldsymbol{P}\boldsymbol{\Phi}^2\boldsymbol{P}) + \tau_2^{-1}\boldsymbol{I}_N\otimes\boldsymbol{P}^2,\\
&\boldsymbol{\mathcal{S}}_1 = \begin{bmatrix}\tilde{\boldsymbol{J}}\otimes\boldsymbol{B}\boldsymbol{\Delta}_K\\ \boldsymbol{0}\end{bmatrix}, \quad \boldsymbol{\mathcal{R}}_1 = \begin{bmatrix}\boldsymbol{P}\\ \boldsymbol{0}\end{bmatrix}, \quad \boldsymbol{\mathcal{S}}_2 = \begin{bmatrix}\tilde{\boldsymbol{J}}\tilde{\boldsymbol{W}}\otimes\boldsymbol{B}\boldsymbol{\Delta}_K\\ \boldsymbol{0}\end{bmatrix}, \quad \boldsymbol{\mathcal{R}}_2 = \begin{bmatrix}\boldsymbol{0}\\ \boldsymbol{P}\end{bmatrix}.
\end{aligned} \tag{4.49}$$

Inequality (4.48) holds if and only if there exist scalars $\epsilon_1 > 0$ and $\epsilon_2 > 0$ such that

$$\begin{bmatrix}\hat{\boldsymbol{\Xi}}_{11} & \hat{\boldsymbol{\Xi}}_{12}\\ * & \hat{\boldsymbol{\Xi}}_{22}\end{bmatrix} + \epsilon_1\boldsymbol{\mathcal{S}}_1\boldsymbol{\mathcal{S}}_1^T + \epsilon_1^{-1}\boldsymbol{\mathcal{R}}_1\boldsymbol{\mathcal{R}}_1^T + \epsilon_2\boldsymbol{\mathcal{S}}_2\boldsymbol{\mathcal{S}}_2^T + \epsilon_2^{-1}\boldsymbol{\mathcal{R}}_2\boldsymbol{\mathcal{R}}_2^T < 0. \tag{4.50}$$

The following inequalities hold based on Assumption 2

$$(\tilde{\boldsymbol{J}}\otimes\boldsymbol{B}\boldsymbol{\Delta}_K)(\boldsymbol{\Delta}_K^T\boldsymbol{B}^T\otimes\tilde{\boldsymbol{J}}^T) \leq \delta^2(\tilde{\boldsymbol{J}}\otimes\boldsymbol{B})(\boldsymbol{B}^T\otimes\tilde{\boldsymbol{J}}^T), \tag{4.51}$$

$$(\tilde{\boldsymbol{J}}\tilde{\boldsymbol{W}}\otimes\boldsymbol{B}\boldsymbol{\Delta}_K)(\boldsymbol{\Delta}_K^T\boldsymbol{B}^T\otimes\tilde{\boldsymbol{W}}^T\tilde{\boldsymbol{J}}^T) \leq \delta^2(\tilde{\boldsymbol{J}}\tilde{\boldsymbol{W}}\otimes\boldsymbol{B})(\boldsymbol{B}^T\otimes\tilde{\boldsymbol{W}}^T\tilde{\boldsymbol{J}}^T). \tag{4.52}$$

Denote $\boldsymbol{\Omega} = \boldsymbol{KP}$ and $\tilde{\boldsymbol{\Phi}} = \boldsymbol{P}\boldsymbol{\Phi}^2\boldsymbol{P}$ as alternative variables. Considering (4.51), (4.52), and applying the *Schur complement* Lemma [138] on (4.50) results in $\boldsymbol{\Xi}<0$ given in the statement of the theorem. Denote the alternative variable $\tilde{\alpha} = \alpha_1^2$. The following

inequality is also considered

$$-\tau_i^{-1} \leq -2 + \tau_i, \qquad i \in \{1, 2\}. \tag{4.53}$$

Using $\tilde{\alpha}$ and considering (4.53), inequalities $\pi_1 < 0$ and $\boldsymbol{\pi}_2 < 0$ given in the statement of the theorem are obtained. The relations between design parameters and decision variables are given in (4.15).

Motivated by [116, Sec. 2.2], a linear scalarization method is used to decrease/increase the decision variables used in $\boldsymbol{K}$, $\boldsymbol{\Phi}$, α (see (4.15)). To this end, consider the following constraints

$$\boldsymbol{P}^{-1} < \theta_1 \boldsymbol{I}, \qquad \tilde{\boldsymbol{\Phi}}^T \tilde{\boldsymbol{\Phi}} < \theta_2 \boldsymbol{I}, \qquad \tilde{\alpha}^{-1} < \theta_3, \qquad \boldsymbol{\Omega}^T \boldsymbol{\Omega} < \theta_4 \boldsymbol{I}, \tag{4.54}$$

where $\theta_c > 0$, $(1 \leq c \leq 4)$, are decision variables. Based on inequalities (4.54), if one decreases θ_c, $(1 \leq c \leq 4)$, parameters $\{\|\tilde{\boldsymbol{\Phi}}\|, \|\boldsymbol{\Omega}\|\}$ are decreased and parameters $\{\|\boldsymbol{P}\|, \tilde{\alpha}\}$ are increased. Therefore, design parameters $\{\|\boldsymbol{K}\|, \|\boldsymbol{\Phi}\|\}$ are decreased and α is increased based on (4.15). These together increase the right hand side of (4.6). Inequalities (4.17) are obtained from (4.54). The objective function $\mathbb{F}$ in (4.13) minimizes a weighted sum of the decision variables θ_c with all weights equal to 1. The LMIs given in (4.14) that include θ_c, $(1 \leq c \leq 4)$, are equivalent to (4.54) using Schur complement. Once (4.13) is solved, design parameters are computed from (4.15) and that completes the proof. □

4.4.3 Proof of Theorem 4.3

Proof. Let $d(t) \triangleq t - nh$ represent an artificial time-varying time-delay that satisfies $0 \leq d(t) < h$. Using $d(t)$, system (4.23) is given below for the interval $nh \leq t < (n+1)h$.

$$\begin{aligned} \dot{\boldsymbol{\psi}}(t) = (\boldsymbol{I}_{N-1} \otimes \boldsymbol{A}) \boldsymbol{\psi}(t) + (\tilde{\boldsymbol{J}} \otimes \boldsymbol{B}(\boldsymbol{K} + \boldsymbol{\Delta}_k))\, \boldsymbol{\psi}(t - d(t)) \\ + (\tilde{\boldsymbol{J}} \tilde{\boldsymbol{W}} \otimes \boldsymbol{B}(\boldsymbol{K} + \boldsymbol{\Delta}_k))\, \boldsymbol{e}(t - d(t)). \end{aligned} \tag{4.55}$$

Consider the LKF $V = \sum_{i=1}^{3} V_i$ for stabilization of system (4.55), where

$$\begin{aligned} V_1 &= \boldsymbol{\psi}^T(t)(\boldsymbol{I}_{N-1} \otimes \bar{\boldsymbol{P}})\, \boldsymbol{\psi}(t), \qquad V_2 = \int_{t-h}^{t} e^{2\zeta(s-t)} \boldsymbol{\psi}^T(s)(\boldsymbol{I}_{N-1} \otimes \bar{\boldsymbol{Q}})\, \boldsymbol{\psi}(s) ds, \\ V_3 &= h \int_{-h}^{0} \int_{t+s}^{t} e^{2\zeta(v-t)} \dot{\boldsymbol{\psi}}^T(v)(\boldsymbol{I}_{N-1} \otimes \bar{\boldsymbol{Z}}) \dot{\boldsymbol{\psi}}(v) dv ds, \end{aligned} \tag{4.56}$$

with positive definite matrices $\bar{\boldsymbol{P}}$, $\bar{\boldsymbol{Q}}$, $\bar{\boldsymbol{Z}}$. The time derivative of V is derived as follows

$$\begin{aligned} \dot{V}_1 &= 2\dot{\boldsymbol{\psi}}^T(t)(\boldsymbol{I}_{N-1} \otimes \bar{\boldsymbol{P}}) \boldsymbol{\psi}(t), \\ \dot{V}_2 &= \boldsymbol{\psi}^T(t)(\boldsymbol{I}_{N-1} \otimes \bar{\boldsymbol{Q}}) \boldsymbol{\psi}(t) - e^{-2\zeta h} \boldsymbol{\psi}^T(t-h)(\boldsymbol{I}_{N-1} \otimes \bar{\boldsymbol{Q}}) \boldsymbol{\psi}(t-h) - 2\zeta V_2, \\ \dot{V}_3 &= h^2 \dot{\boldsymbol{\psi}}^T(t)(\boldsymbol{I}_{N-1} \otimes \bar{\boldsymbol{Z}}) \dot{\boldsymbol{\psi}}(t) - h \int_{t-h}^{t} e^{2\zeta(v-t)} \dot{\boldsymbol{\psi}}^T(v)(\boldsymbol{I}_{N-1} \otimes \bar{\boldsymbol{Z}}) \dot{\boldsymbol{\psi}}(v) dv - 2\zeta V_3 \\ &\leq h^2 \dot{\boldsymbol{\psi}}^T(t)(\boldsymbol{I}_{N-1} \otimes \bar{\boldsymbol{Z}}) \dot{\boldsymbol{\psi}}(t) - h e^{-2\zeta h} \int_{t-h}^{t} \dot{\boldsymbol{\psi}}^T(v)(\boldsymbol{I}_{N-1} \otimes \bar{\boldsymbol{Z}}) \dot{\boldsymbol{\psi}}(v) dv - 2\zeta V_3. \end{aligned} \tag{4.57}$$

Considering $[t-h,t]=[t-h,t-d(t)]\cup[t-d(t),t]$, the following expression is obtained

$$\int_{t-h}^{t} f(v)dv = \int_{t-h}^{t-d(t)} f(v)dv + \int_{t-d(t)}^{t} f(v)dv. \tag{4.58}$$

where $f(v)=\dot{\boldsymbol{\psi}}^T(v)(\boldsymbol{I}_{N-1}\otimes\bar{\boldsymbol{Z}})\dot{\boldsymbol{\psi}}(v)$. Let $\boldsymbol{a}_1=[\boldsymbol{\psi}^T(t),\boldsymbol{\psi}^T(t-d(t))]^T$. For any matrices $\bar{\boldsymbol{F}}=\begin{bmatrix}\bar{\boldsymbol{F}}_1^T & \bar{\boldsymbol{F}}_2^T\end{bmatrix}^T$ and $\bar{\boldsymbol{G}}=\begin{bmatrix}\bar{\boldsymbol{G}}_1^T & \bar{\boldsymbol{G}}_2^T\end{bmatrix}^T$, the following null expressions hold

$$2\boldsymbol{a}_1^T(\boldsymbol{I}_{N-1}\otimes\bar{\boldsymbol{F}})\Big[\boldsymbol{\psi}(t-d(t))-\boldsymbol{\psi}(t-h)-\int_{t-h}^{t-d(t)}\dot{\boldsymbol{\psi}}(s)ds\Big]=0, \tag{4.59}$$

$$2\boldsymbol{a}_1^T(\boldsymbol{I}_{N-1}\otimes\bar{\boldsymbol{G}})\Big[\boldsymbol{\psi}(t)-\boldsymbol{\psi}(t-d(t))-\int_{t-d(t)}^{t}\dot{\boldsymbol{\psi}}(s)ds\Big]=0. \tag{4.60}$$

Additionally, one can obtain the following expression for any matrix $\bar{\boldsymbol{Y}}=\begin{bmatrix}\bar{\boldsymbol{Y}}_{11} & \bar{\boldsymbol{Y}}_{12}\\ * & \bar{\boldsymbol{Y}}_{22}\end{bmatrix}$

$$\int_{t-h}^{t-d(t)}\boldsymbol{a}_1^T(\bar{\boldsymbol{Y}}\otimes\boldsymbol{I}_{N-1})\boldsymbol{a}_1ds+\int_{t-d(t)}^{t}\boldsymbol{a}_1^T(\bar{\boldsymbol{Y}}\otimes\boldsymbol{I}_{N-1})\boldsymbol{a}_1ds=h\boldsymbol{a}_1^T(\bar{\boldsymbol{Y}}\otimes\boldsymbol{I}_{N-1})\boldsymbol{a}_1. \tag{4.61}$$

The following null equality holds from (4.55)

$$\begin{aligned}&2\Big(\boldsymbol{\psi}^T(t)+\dot{\boldsymbol{\psi}}^T(t)+\boldsymbol{\psi}^T(t-d(t))\Big)(\boldsymbol{I}_{N-1}\otimes\boldsymbol{H}^{-1})\\ &\times\Bigg((\boldsymbol{I}_{N-1}\otimes\boldsymbol{A})\boldsymbol{\psi}(t)+(\tilde{\boldsymbol{J}}\otimes\boldsymbol{B}(\boldsymbol{K}+\boldsymbol{\Delta}_k))\,\boldsymbol{\psi}(t-d(t))\\ &\qquad+(\tilde{\boldsymbol{J}}\tilde{\boldsymbol{W}}\otimes\boldsymbol{B}(\boldsymbol{K}+\boldsymbol{\Delta}_k))\,\boldsymbol{e}(t-d(t))-\dot{\boldsymbol{\psi}}(t)\Bigg)=0.\end{aligned} \tag{4.62}$$

The event-triggering condition (4.19) ensures that

$$\boldsymbol{e}^T(t-d(t))(\boldsymbol{I}_N\otimes\boldsymbol{\Phi}_1)\boldsymbol{e}(t-d(t))\le\hat{\boldsymbol{x}}^T(t-d(t))(\boldsymbol{L}^T\boldsymbol{L}\otimes\boldsymbol{\Phi}_2^{-1})\hat{\boldsymbol{x}}(t-d(t)). \tag{4.63}$$

Considering $\boldsymbol{L}=\tilde{\boldsymbol{W}}^\dagger\tilde{\boldsymbol{J}}\tilde{\boldsymbol{W}}$, $\hat{\boldsymbol{x}}=\boldsymbol{x}+\boldsymbol{e}$, and $\boldsymbol{\psi}=\tilde{\boldsymbol{W}}\otimes\boldsymbol{I}_n\boldsymbol{x}$ the following condition is obtained from (4.63)

$$\begin{bmatrix}\boldsymbol{\psi}(t-d(t))\\ \boldsymbol{e}(t-d(t))\end{bmatrix}^T\begin{bmatrix}\boldsymbol{S}_{11} & \boldsymbol{S}_{12}\\ * & \boldsymbol{S}_{22}\end{bmatrix}\begin{bmatrix}\boldsymbol{\psi}(t-d(t))\\ \boldsymbol{e}(t-d(t))\end{bmatrix}\ge 0, \tag{4.64}$$

where

$$\begin{aligned}\boldsymbol{S}_{11}&=(\tilde{\boldsymbol{W}}^\dagger\tilde{\boldsymbol{J}})^T\tilde{\boldsymbol{W}}^\dagger\tilde{\boldsymbol{J}}\otimes\boldsymbol{\Phi}_2^{-1},\\ \boldsymbol{S}_{12}&=(\tilde{\boldsymbol{W}}^\dagger\tilde{\boldsymbol{J}})^T\tilde{\boldsymbol{W}}^\dagger\tilde{\boldsymbol{J}}\tilde{\boldsymbol{W}}\otimes\boldsymbol{\Phi}_2^{-1},\\ \boldsymbol{S}_{22}&=(\tilde{\boldsymbol{W}}^\dagger\tilde{\boldsymbol{J}}\tilde{\boldsymbol{W}})^T\tilde{\boldsymbol{W}}^\dagger\tilde{\boldsymbol{J}}\tilde{\boldsymbol{W}}\otimes\boldsymbol{\Phi}_2^{-1}-\boldsymbol{I}_N\otimes\boldsymbol{\Phi}_1.\end{aligned} \tag{4.65}$$

Let $\boldsymbol{a}_2=[\boldsymbol{a}_1^T,\ \dot{\boldsymbol{\psi}}^T(s)\,]^T$ and $\boldsymbol{\nu}=[\boldsymbol{\psi}^T(t),\,\boldsymbol{\psi}^T(t-d(t)),\,\boldsymbol{\psi}^T(t-h),\,\dot{\boldsymbol{\psi}}^T(t),\,\boldsymbol{e}^T(t-d(t))]^T$. Considering all expressions from (4.57) to (4.63), the following upper bound holds

$$\dot{V}+2\zeta V\le\boldsymbol{\nu}^T\bar{\boldsymbol{\Pi}}\boldsymbol{\nu}-\int_{t-h}^{t-d(t)}\boldsymbol{a}_2^T(\bar{\boldsymbol{C}}_2\otimes\boldsymbol{I}_{N-1})\boldsymbol{a}_2ds-\int_{t-d(t)}^{t}\boldsymbol{a}_2^T(\bar{\boldsymbol{C}}_3\otimes\boldsymbol{I}_{N-1})\boldsymbol{a}_2ds, \tag{4.66}$$

where

$$\bar{\boldsymbol{\Pi}} = \begin{bmatrix} \bar{\boldsymbol{\pi}}_{11} & \bar{\boldsymbol{\pi}}_{12} & -\boldsymbol{I}_{N-1} \otimes \bar{\boldsymbol{F}}_1 & \bar{\boldsymbol{\pi}}_{14} & \tilde{\boldsymbol{J}}\tilde{\boldsymbol{W}} \otimes \boldsymbol{H}^{-1}\boldsymbol{B}(\boldsymbol{K}+\boldsymbol{\Delta}_K) \\ * & \bar{\boldsymbol{\pi}}_{22} & -\boldsymbol{I}_{N-1} \otimes \bar{\boldsymbol{F}}_2 & \bar{\boldsymbol{\pi}}_{24} & \tilde{\boldsymbol{J}}\tilde{\boldsymbol{W}} \otimes \boldsymbol{H}^{-1}\boldsymbol{B}(\boldsymbol{K}+\boldsymbol{\Delta}_K) + \boldsymbol{S}_{12} \\ * & * & -e^{-2\zeta h}\boldsymbol{I}_{N-1} \otimes \bar{\boldsymbol{Q}} & \boldsymbol{0} & \boldsymbol{0} \\ * & * & * & \bar{\boldsymbol{\pi}}_{44} & \tilde{\boldsymbol{J}}\tilde{\boldsymbol{W}} \otimes \boldsymbol{H}^{-1}\boldsymbol{B}(\boldsymbol{K}+\boldsymbol{\Delta}_K) \\ * & * & * & * & \boldsymbol{S}_{22} \end{bmatrix},$$

$$\bar{\boldsymbol{C}}_2 = \begin{bmatrix} \bar{\boldsymbol{Y}} & \bar{\boldsymbol{F}} \\ * & he^{-2\zeta h}\bar{\boldsymbol{Z}} \end{bmatrix}, \quad \bar{\boldsymbol{C}}_3 = \begin{bmatrix} \bar{\boldsymbol{Y}} & \bar{\boldsymbol{G}} \\ * & he^{-2\zeta h}\bar{\boldsymbol{Z}} \end{bmatrix}, \tag{4.67}$$

$$\begin{aligned}
\bar{\boldsymbol{\pi}}_{11} &= \boldsymbol{I}_{N-1} \otimes \left(\bar{\boldsymbol{Q}} + \bar{\boldsymbol{G}}_1 + \bar{\boldsymbol{G}}_1^T + \boldsymbol{H}^{-1}\boldsymbol{A} + (\boldsymbol{H}^{-1}\boldsymbol{A})^T + h\bar{\boldsymbol{Y}}_{11} + 2\zeta\bar{\boldsymbol{P}}\right), \\
\bar{\boldsymbol{\pi}}_{12} &= \boldsymbol{I}_{N-1} \otimes \left(\bar{\boldsymbol{F}}_1 - \bar{\boldsymbol{G}}_1 + \bar{\boldsymbol{G}}_2^T + h\bar{\boldsymbol{Y}}_{12} + (\boldsymbol{H}^{-1}\boldsymbol{A})^T\right) + \tilde{\boldsymbol{J}} \otimes \boldsymbol{H}^{-1}\boldsymbol{B}(\boldsymbol{K}+\boldsymbol{\Delta}_K), \\
\bar{\boldsymbol{\pi}}_{14} &= \boldsymbol{I}_{N-1} \otimes \left(\bar{\boldsymbol{P}} - \boldsymbol{H}^{-1} + (\boldsymbol{H}^{-1}\boldsymbol{A})^T\right), \\
\bar{\boldsymbol{\pi}}_{22} &= \boldsymbol{I}_{N-1} \otimes \left(\bar{\boldsymbol{F}}_2 + \bar{\boldsymbol{F}}_2^T - \bar{\boldsymbol{G}}_2 - \bar{\boldsymbol{G}}_2^T + h\bar{\boldsymbol{Y}}_{22}\right) + \boldsymbol{S}_{11} + \tilde{\boldsymbol{J}} \otimes \boldsymbol{H}^{-1}\boldsymbol{B}(\boldsymbol{K}+\boldsymbol{\Delta}_K) \\
&\quad + (\tilde{\boldsymbol{J}} \otimes \boldsymbol{H}^{-1}\boldsymbol{B}(\boldsymbol{K}+\boldsymbol{\Delta}_K))^T, \\
\bar{\boldsymbol{\pi}}_{24} &= (\tilde{\boldsymbol{J}} \otimes \boldsymbol{H}^{-1}\boldsymbol{B}(\boldsymbol{K}+\boldsymbol{\Delta}_K))^T - \boldsymbol{I}_{N-1} \otimes \boldsymbol{H}^{-1}, \\
\bar{\boldsymbol{\pi}}_{44} &= \boldsymbol{I}_{N-1} \otimes \left(h^2\bar{\boldsymbol{Z}} - \boldsymbol{H}^{-1} - (\boldsymbol{H}^{-1})^T\right).
\end{aligned} \tag{4.68}$$

Based on (4.66), if $\bar{\boldsymbol{\Pi}}_1 < 0$, $\bar{\boldsymbol{C}}_1 \geq 0$, and $\bar{\boldsymbol{C}}_2 \geq 0$ then it holds that $\dot{V} + 2\zeta V < 0$. Now, consider $\boldsymbol{D}_1 = \text{diag}(\boldsymbol{I}_{N-1}\otimes\boldsymbol{H}, \boldsymbol{I}_{N-1}\otimes\boldsymbol{H}, \boldsymbol{I}_{N-1}\otimes\boldsymbol{H}, \boldsymbol{I}_{N-1}\otimes\boldsymbol{H}, \boldsymbol{I}_N\otimes\boldsymbol{H})$. Matrix $\bar{\boldsymbol{\Pi}}$ is pre- and post multiplied by $\boldsymbol{D}_1$ and $\boldsymbol{D}_1^T$. In a similar fashion, block matrices $\bar{\boldsymbol{C}}_1$ and $\bar{\boldsymbol{C}}_2$ are pre- and post multiplied by $\boldsymbol{D}_2$ and $\boldsymbol{D}_2^T$, where $\boldsymbol{D}_2 = \text{diag}(\boldsymbol{H}, \boldsymbol{H}, \boldsymbol{H})$. The following alternative variables are considered $\boldsymbol{P} = \boldsymbol{H}\bar{\boldsymbol{P}}\boldsymbol{H}^T$, $\boldsymbol{Q} = \boldsymbol{H}\bar{\boldsymbol{Q}}\boldsymbol{H}^T$, $\boldsymbol{Z} = \boldsymbol{H}\bar{\boldsymbol{Z}}\boldsymbol{H}^T$, $\boldsymbol{F} = \boldsymbol{H}\bar{\boldsymbol{F}}\boldsymbol{H}^T$, $\boldsymbol{G} = \boldsymbol{H}\bar{\boldsymbol{G}}\boldsymbol{H}^T$, $\boldsymbol{Y}_{ij} = \boldsymbol{H}\bar{\boldsymbol{Y}}_{ij}\boldsymbol{H}^T$, $(i, j \in \{1, 2\})$, $\boldsymbol{M}_1 = \boldsymbol{H}\bar{\boldsymbol{\Phi}}_1\boldsymbol{H}^T$. Additionally, let $\boldsymbol{V} = \boldsymbol{K}\boldsymbol{H}^T$. The terms including control gain uncertainty $\boldsymbol{\Delta}_K$ are treated in a similar way used in PEC for expressions (4.48), (4.50), (4.51), and (4.52). Using the alternative variables above and Schur complement, the LMIs given in (4.24) are obtained. Design parameters $\boldsymbol{K}$, $\boldsymbol{\Phi}_1$, and $\boldsymbol{\Phi}_2$ are computed from (4.25) and that completes the proof. □

Chapter 5

Consensus against denial of service attack

Chapters 3 and 4 study the event-triggered consensus (ETC), respectively, in first-order and general linear MASs. One common assumption considered in Chapters 3 and 4 is that the MAS operates in an ideal situation where Cyber-attacks never occur. The topic of Cyber-security has received wide attention due to the recent incidents of malicious attacks directed to make the networked systems non-operational. There exist different types of attacks such as false data injection and denial-of-service (DoS) [1, 37, 60]. In DoS, the adversary blocks the communication channels. It is important to develop resilient strategies that are able to tolerate and bounce back after DoS attacks and maintain the closed-loop stability.

This chapter proposes three implementations (namely, RQ-CEASE [79], R-PSEC, and ROCCET [82]) for ETC in the presence of DoS attacks. RQ-CEASE studies the impact of DoS attack on average consensus and explains the trade-offs between the amount of tolerable DoS attack and communication savings. The design procedure in RQ-CEASE is similar to Q-CEASE. The R-PSEC implementation in Section 5.2 extends PSEC for the case where the MAS is subject to DoS attacks. R-PSEC includes a desired level of resilience to DoS, and the unknown parameters for control and event-triggering are computed based on the desired level of resilience. Section 5.3 proposes ROCCET, where a dynamic event-triggering scheme is used to further reduce the amount of transmissions in the presence of DoS attacks. ROCCET deals with unknown DoS attacks in a similar fashion to R-PSEC. However, ROCCET incorporates a dynamic-event triggering scheme to further reduce the number of transmissions and computes required control and ET parameters from an optimization. A summary of the three proposed implementations are given in Section 5.4.

5.1 RQ-CEASE

Resilience to DoS attacks has been studied for both a single system [32, 62–65, 68, 69] and a network of cooperative systems [1, 37, 50–52, 60, 61, 139–142]. Existing

implementations against DoS attacks [1, 37, 50–52, 60, 61, 139–142] face at least one of the following shortcomings:

- *Inefficient Transmission Scheme*: Considering a continuous time transmission scheme, the impact of DoS attack in connected smart vehicle systems is studied in [139]. In [140], a distributed consensus approach is proposed, which depends on continuous transmission between the agents, which is not desirable. To relax the real-time transmission, sampling-based schemes are proposed in [60,61] for consensus under DoS attacks. Sampled-data schemes, however, transmit information periodically and irrespective of any system trajectories.

- *Continuous Measurement*: Although ET schemes are widely used in the context of DoS attacks for NCSs and MASs [1, 37, 50–52], the ET conditions in [1, 50–52, 141] are required to be monitored continuously. Considering a single plant, reference [37] couples a sampler with the ET scheme to relax real-time measurements. In [142], a resilient sampled-data event-triggered scheme is proposed for load frequency control in multi-area power systems. However, all power areas are assumed to be connected to each other. In other words, the implementation is not distributed.

- *Infinite precision for information exchange*: As previously mentioned, quantization is a necessary step for real network implementations. In the context of DoS, existing implementations are based on infinite precision for information exchanged between the nodes. In [66], quantization is considered for some inner loops to control one single plant. The quantization in [67] is limited to the local control input and is not utilized for state transmission between the agents. The quantized control input leads to an uncertain control gain [143, Section II], which can be handled by non-fragile design techniques. On the other hand, quantized transmission in a network of agents leads to an additional term in the closed-loop system, which makes the design analysis challenging when DoS attacks are considered, as such have been overlooked.

- *Restricted models for DoS*: The DoS attacks considered in a number of works such as [144] and [37] are assumed to follow a periodic pattern. Considering a periodic or stochastic pattern for DoS may not fully represent the unknown and malicious nature of the adversary. A more general model for DoS is considered in [32, 52, 64], where DoS is assumed to occur with an unknown pattern. Such DoS models with unknown patterns can be characterized only by the energy constraints of the adversary. In [32], for example, only the total duration and frequency of attacks are considered for formulating DoS. The amount of resilience to DoS in [32] is derived as a joint condition based on the duration and frequency of attacks.

Referred to as the RQ-CEASE [79], in this section a resilient framework for quantized collaborative event-triggered, average consensus, sampled-data, for first-order multi-agent systems subject to denial of service (DoS) attacks is proposed.

In RQ-CEASE, the applicability of CEASE is investigated considering two additional constraints as follow (i): DoS attacks, and (ii): quantized information. In RQ-CEASE, the state values are being quantized before transmission and before generating control inputs. Two different ET approaches are considered in RQ-CEASE based on whether the ET threshold is dependent or independent of the state dynamics. For each approach, the operating conditions (bounds) for the sampling period and ET design parameter that guarantee the input-to-state (ISS) stability of the network under DoS attacks are analytically derived. In addition, upper bounds for duration and frequency of DoS attacks are derived within which the network remains operational. The maximum possible error from the average consensus value is derived. Due to the additional difficulties imposed by the DoS attacks and quantization, in RQ-CEASE the control gain is fixed at 1 and the other parameters are computed based on only the stability of the closed-loop system, i.e., no optimization is concerned.

5.1.1 Ideal control protocol and event-triggering scheme

In RQ-CEASE, the agent dynamics are similar to (3.1). The proposed RQ-CEASE implementations are shown in Figs. 5.1 and 5.2. The ET scheme used in the first RQ-CEASE implementation (shown in Fig. 5.1) is based on the state disagreement. Therefore, the event detector requires the most recent local and neighbouring quantized events to determine the next event (the lines in blue color). However, the ET threshold used in the second implementation (shown in Fig. 5.2) is constant and does not require the quantized values of the most recent events.

By considering the *ideal* scenario, where DoS never occurs, this section introduces the ideal control protocol and ET scheme. In the *ideal* scenario, the following control protocol is used at node i to reach average consensus

$$u_i^{[idl]}(t) = -\ \mathbb{X}_i^{[idl]}(nh), \quad nh \leq t < (n+1)h, \tag{5.1}$$

where $\mathbb{X}_i^{[idl]}(nh) = \sum_{j\in\mathcal{N}_i} a_{i,j}\,(q(x_j(n_k^j h)) - q(x_i(n_k^i h)))$. Let $e_i(nh) = x_i(n_k^i h) - x_i(nh)$ be the state error. Given $n_0^i = 0$, the next event is triggered at $n_{k+1}^i h$, with n_{k+1}^i satisfying the following ET condition

$$n_{k+1}^i = \min_{n\in\mathbb{N}} \{\, n \mid n > n_k^i,\ |e_i(nh)| - \mathbb{T}_i(nh) \geq 0\}, \tag{5.2}$$

where $\mathbb{T}_i(nh)$ is the proposed threshold which is chosen from the following options:

State-dependent ET threshold: In this approach, $\mathbb{T}_i(nh) = \phi|\mathbb{X}_i^{[idl]}(nh)|$ for $(1 \leq i \leq N)$ with scalar $\phi > 0$ as the ET parameter to be designed. In words, the ET threshold is based on the disagreement value for node i scaled by a design coefficient ϕ. RQ-CEASE with state-dependent event-triggering is shown in Fig. 5.1.

State-independent ET threshold: In the second approach, $\mathbb{T}_i(nh) = \phi,\ \forall i \in \mathcal{V}$, $\forall n \in \mathbb{N}_0$. Hence, the state error $e_i(nh)$ is compared with constant coefficient ϕ for all samples. The configuration of RQ-CEASE with state-independent event-triggering is shown in Fig. 5.2.

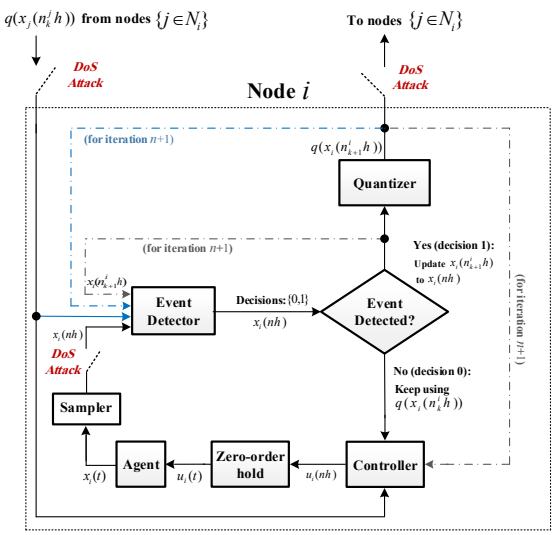

Figure 5.1: RQ-CEASE with *state-dependent* ET threshold for node i, iteration n, and the previously quantized events $q(x_i(n^i_k h))$ and $q(x_j(n^j_k h))$.

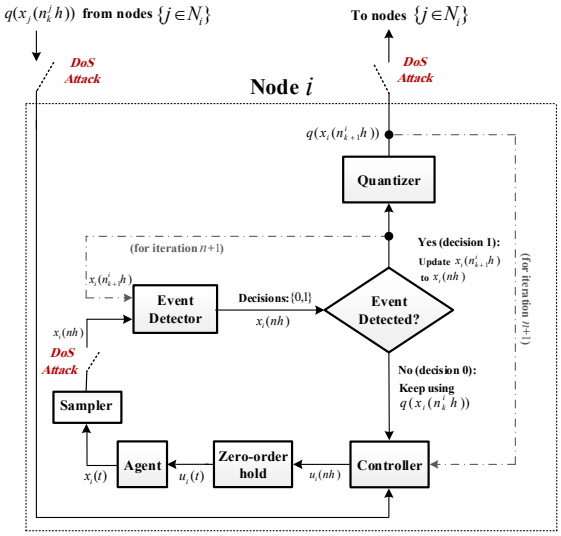

Figure 5.2: RQ-CEASE with *state-independent* ET threshold for node i, iteration n, and the previously quantized events $q(x_i(n^i_k h))$ and $q(x_j(n^j_k h))$.

In the ideal scenario, the following inequality holds true for both ET schemes

$$|e_i(nh)| \leq \mathbb{T}_i(nh), \quad \forall i \in \mathcal{V}. \tag{5.3}$$

Remark 5.1 (Combined ET thresholds)**.** Similar to CEASE and Q-CEASE, in RQ-CEASE the ET condition can be a combination of both state-dependent and state-dependent thresholds, i.e., the state error $|e_i(nh)|$ is compared with $\phi_1|\mathbb{X}_i(nh)|+\phi_2$ at each sample ($i \in \mathcal{V}$). In order not to overshadow the main results with exhaustive derivations due to DoS analysis, RQ-CEASE considers two separate ET thresholds as discussed above.

5.1.2 Denial of Service Attack

As shown in Figs. 5.1 and 5.2 in the presence of DoS attacks both the MAS network and local nodes are impacted in the following ways:

(i) **Impact on the network**: The DoS attack blocks all communication channels between the nodes. Therefore, information exchange is denied across the nodes.

(ii) **Impact on the nodes**: Inside the nodes, the adversary blocks the communication channels. Therefore, the measurements cannot be transmitted to the event-detector block. Thus, the agents evolve in a local open-loop based on the last measurement prior to the DoS attack.

Similar to [60] and [1], this chapter considers that simultaneous DoS attack intervals for all nodes in the MAS.

Assumption 3. The DoS attacks occur over disconnected time intervals. Let d_c denote the time instant at which the c^{th} DoS attack interval begins ($c \in \mathbb{N}_0$). This interval ends at time instant $d_c + \tau_c$, with $\tau_c > 0$. Accordingly, the c^{th} DoS interval is given by the following expression

$$D_c = [\, d_c, d_c + \tau_c \,), \quad c \in \mathbb{N}_0. \tag{5.4}$$

Assumption 4. It is assumed that the duration of each DoS interval is at least h, i.e., $\tau_c \geq h$, $\forall c \in \mathbb{N}_0$.

DoS intervals (5.4) are the same for all nodes. Assumption 3 is based on energy constraints from the attackers perspective. After an active period, the attacker goes to the sleep mode to save on energy [65]. Based on Assumption 4, it is assumed that each DoS interval denies at least one measurement samples. This assumption facilitates the formulation of DoS given in Section 5.1.3. It should be noted that this assumption is relaxed in R-PSEC and ROCCET.

The union of DoS intervals for $t \in [t_1, t_2)$ is denoted by

$$\mathcal{D}(t_1, t_2) = \Big\{ \bigcup_{c \in \mathbb{N}_0} D_c \Big\} \bigcap [\, t_1, t_2 \,). \tag{5.5}$$

The *healthy* intervals where DoS is off are denoted by

$$\mathcal{H}(t_1, t_2) = [\, t_1, t_2 \,) \setminus \mathcal{D}(t_1, t_2). \tag{5.6}$$

Let $|\mathcal{D}(t_1, t_2)|$ denote the total length of all attack intervals for $t \in [\, t_1, t_2 \,)$. Likewise, $|\mathcal{H}(t_1, t_2)|$ denotes the total length of healthy intervals for $t \in [t_1, t_2 \,)$. Let $\mathcal{c}(t_1, t_2)$ define the total number of DoS off-to-on transitions in the interval $[t_1, t_2)$. The following assumption is considered for the duration and frequency of the DoS attacks.

Assumption 5. There exist positive constants T_0, T_1, F_0, and F_1 such that the following upper-bounds hold [65],

$$|\, \mathcal{D}(t_1, t_2) \,| \leq T_0 + \frac{t_2 - t_1}{T_1}, \quad \forall\, t_1, t_2 \in \mathbb{R}_{\geq 0},\ t_1 \leq t_2, \tag{5.7}$$

$$\mathcal{c}\,(t_1, t_2) \leq F_0 + \frac{t_2 - t_1}{F_1}, \quad \forall\, t_1, t_2 \in \mathbb{R}_{\geq 0},\ t_1 \leq t_2. \tag{5.8}$$

Based on Assumption 5, the pattern of DoS attack considered in this chapter is not limited to any form (such as periodic or any stochastic distribution). The only assumption for the DoS attacks is the boundedness of the duration and frequency of occurrence specified by (5.7) and (5.8).

Remark 5.2 (The nature of DoS attacks)**.** Assumption 5, which is widely used for formulation of unknown DoS attacks [1, 32], constrains DoS in terms of its *average* duration and frequency of occurrence. Based on (5.7) and (5.8), the strength of the DoS attacks (in terms of duration and frequency of occurrence) is scalable with time t using some coefficients. Inequality (5.7) expresses the property that the DoS intervals satisfy a slow-on-the-average type condition as indicated by [32]. It implies that the

total duration for DoS, on average, should not exceed a certain fraction of time, which is scaled by $1/T_1$. Parameter T_0 is included to allow for consideration of DoS at the start time, i.e. when $d_0 = 0$. Inequality (5.8) expresses a similar rationale with respect to the frequency of DoS. In fact, F_1 can be defined as the average dwell-time between consecutive DoS intervals, while F_0, like the constant T_0 plays the role of regularization.

Remark 5.3 (Difference of DoS and packet loss)**.** While sensor/control packet losses have been previously considered in [145,146], dealing with DoS phenomena induced by adversary requires a different problem formulation. As mentioned in [65], in contrast to genuine packet dropouts, which conceivably can be modeled as a random process, assuming a stochastic behaviour for the DoS attacks fails to fully model the malicious and intelligent nature of the adversary.

Design objectives: The following questions should be addressed as the main design objectives:

Q1. What are the operating regions for the sampling period h and ET threshold ϕ to guarantee resilient average consensus in the presence of DoS?

Q2. What are the upper bounds for DoS duration and frequency of occurrence so that consensus is preserved?

Q3. How is the rate of consensus convergence affected by design parameters h and ϕ, and the DoS strength?

Q4. What is the maximum possible consensus error under quantization and DoS?

Q5. What are the differences between the two implementations in terms of resilience to attacks, steady-state consensus error, and transmission savings?

5.1.3 DoS formulation

Unlike the ideal (attack free) scenario, the DoS attack, during its intervals, denies transmission of local state measurement to the event-detector. Additionally, the state exchanges between the nodes are denied. Fig. 5.3 is provided to visualize different time notation used to model DoS, sampling, and ET transmissions. As a result of DoS, the control protocol (5.1) cannot be updated in coordination with (5.2). After a measurement failure due to occurrence of DoS, no acknowledgment is received by the event-detector and a DoS interval is detected. Once DoS is detected, the measurement scheme attempts periodically (with the same period h) to update the next block (i.e., event-detector) with the earliest available measurement after the DoS interval is over. Therefore, it takes at the most h seconds to update the system with a new state after the DoS interval ends. Let $\underline{n}_c h$ with $\underline{n}_c = \min_{n\in\mathbb{N}_0} \{n \,|\, nh > d_c\}$ denote 'the first instant after d_c where transmission of the measurement is denied by D_c'. Since the system

has no inter-sampling measurement, the impact of D_c on the system takes effect at $t = \underline{n}_c h$. Additionally, $\bar{n}_c h$ with $\bar{n}_c = \max_{n \in \mathbb{N}_0} \{n \,|\, nh \leq d_c + \tau_c\}$ specifies the largest sampled instant before the c^{th} on-to-off DoS transition. With $\sigma_c = (\bar{n}_c - \underline{n}_c)h$, define $\bar{D}_c = [\, \underline{n}_c h,\, \sigma_c + h\,)$ as the c^{th} *effective* DoS interval during which (5.3) may not hold.

Note that with such definition two consecutive intervals for $\bar{D}_c$ have one sample in common if they are not at least h seconds apart (as in the case for $\bar{D}_1$ and $\bar{D}_2$ in Fig. 5.3). To precisely determine the effective DoS intervals without overlap, the following parameter is defined

$$\bar{\mathcal{D}}(t_1, t_2) = \bigcup_{m \in \mathbb{N}_0} Z_m \cap [t_1, t_2], \tag{5.9}$$

with $Z_m = [\, \xi_m, \xi_m + \nu_m)$. Parameter ξ_m is defined by $\xi_0 = \underline{n}_0\, h$ and

$$\xi_{m+1} = \min\{\underline{n}_c h \,|\, \underline{n}_c h > \xi_m,\, d_c - d_{c-1} > h\}.$$

Additionally, ν_m is as follows

$$\nu_m = \sum_{\substack{c \in \mathbb{N}_0, \\ \xi_m \leq d_c < \xi_{m+1}}} |\bar{D}_c \backslash \bar{D}_{c+1}|. \tag{5.10}$$

In other words, parameter ν_m determines the first possible sample instant after a DoS interval is over. If two or more attack intervals are less than h seconds apart, i.e., $d_{c+1} - (d_c + \tau_c) < h$ for some $c \in \mathbb{N}_0$, then ν_m excludes the overlaps between $\bar{D}_c$ and $\bar{D}_{c+1}$ and sums up the intervals to determine the next possible sample instant. For visualization, refer to Fig. 5.3 where D_1 and D_2 are shown. On the other hand, parameter

$$\bar{\mathcal{H}}(t_1, t_2) = \bigcup_{m \in \mathbb{N}_0} W_{m-1} \cap [\, t_1, t_2\,], \tag{5.11}$$

with $W_{-1} = [\, 0, \xi_0\,)$ and $W_m = [\, \xi_m + \nu_m, \xi_{m+1})$, is the union of *healthy* intervals with no overlap where (5.3) holds. Fig. 5.3 is provided to visually illustrate different time notation used to formulate the problem.

Note that $|\bar{\mathcal{D}}(t_1, t_2)|$ and $|\bar{\mathcal{H}}(t_1, t_2)|$, respectively, denote the total length of corresponding intervals for $t \in [t_1, t_2)$. Since $\bar{\mathcal{H}}(t_1, t_2)$ and $\bar{\mathcal{D}}(t_1, t_2)$ are complements of each other, the following expression holds true $\forall t_1, t_2 \in \mathbb{R}_{\geq 0},\, t_1 \leq t_2$

$$|\bar{\mathcal{H}}(t_1, t_2)| = t_2 - t_1 - |\bar{\mathcal{D}}(t_1, t_2)|. \tag{5.12}$$

Since the MAS has no inter-sampling measurement, one can assume that d_c is arbitrarily close to $\underline{n}_c h$. Then, inequality $|\bar{D}_c| \leq |D_c| + h$, $c \in \mathbb{N}_0$, holds true by construction and can be verified from Fig. 5.3. The latter inequality gives way to the following relation between $|\bar{\mathcal{D}}(t_1, t_2)|$, $|\mathcal{D}(t_1, t_2)|$, and $c(t_1, t_2)$

$$|\bar{\mathcal{D}}(t_1, t_2)| \leq |\mathcal{D}(t_1, t_2)| + c(t_1, t_2)h, \quad (t_1 \leq t_2). \tag{5.13}$$

Table 5.1 lists important parameters used to model DoS.

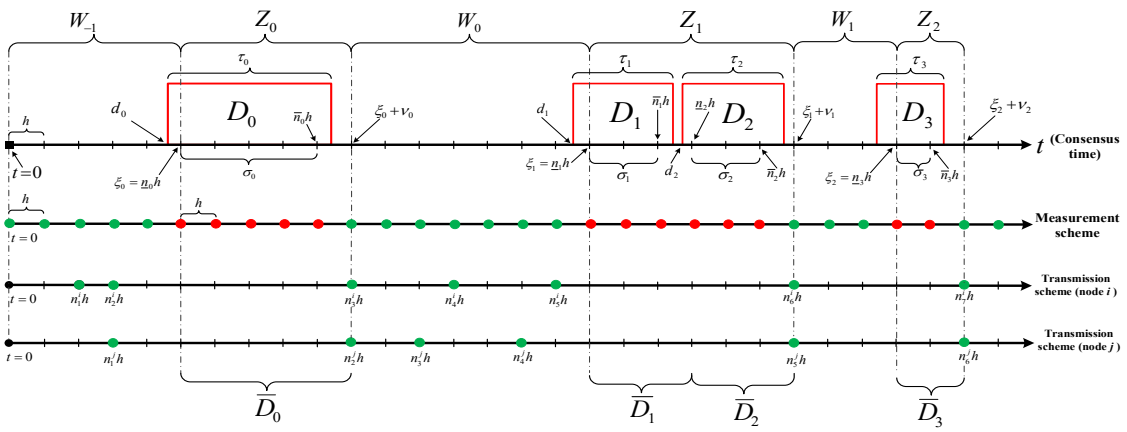

Figure 5.3: Schematic time diagram for an illustrative DoS attack, measurement, and transmission instants for nodes i and j. Successfully transmitted measurements to local event-detectors are labeled with green circles in the 'measurement scheme' diagram. Red circles show measurements that are denied by DoS from transmission to local event-detectors. Intervals W_{-1}, W_0, and W_1 are healthy and (5.3) is satisfied. Intervals Z_0, Z_1, and Z_2 are the effective DoS intervals where (5.3) does not necessarily hold for all nodes. Note that $d_2-(d_1+\tau_1)<h$ leading to a common instant between $\bar{D}_1$ and $\bar{D}_2$. This instant is excluded by (5.10). Therefore, Z_1 is the unique interval where transmission is blocked and (5.3) does not necessarily hold.

5.1.4 Actual control protocol and transmission scheme

Let $n^i_{s_i(t)}h$ be the most recent *successful* update instant for node i, $(i\in\mathcal{V})$, until time t. Mathematically, one can view $s_i(t)$ as follows

$$s_i(t)=\sup\{k\in\mathbb{N}_0 \mid n^i_k h\le t,\ n^i_k h\notin \bigcup_{c\in\mathbb{N}_0}\bar{D}_c\}. \tag{5.14}$$

Based on (5.14), the disagreement value in healthy intervals, i.e., $t\in W_m$ and $nh\le t<(n+1)h$, is modified to $\mathbb{X}_i(nh)=\sum_{j\in\mathcal{N}_i}a_{i,j}\Big(q(\hat{x}_j(nh))-q(\hat{x}_i(nh))\Big)$, where $\hat{x}_i(nh)=x_i(n^i_{s_i(t)}h)$. In words, $\hat{x}_i(nh)$ is the last successfully transmitted state of agent i. The difference between $\mathbb{X}_i(nh)$ and $\mathbb{X}^{[idl]}_i(nh)$ is that $\mathbb{X}_i(nh)$ is based on the last *successfully* transmitted states denoted by index $s_i(t)$ defined by (5.14). However, in the ideal scenario there exists no DoS attack and event instants do need to be labeled by t. Now, according to the ET logic (5.2) and including the periodic update attempts, the general transmission rule is as follows ($\forall i\in\mathcal{V}$ and $m\in\mathbb{N}_0$)

$$n^i_{k+1}=\begin{cases}\min\limits_n\Big\{n\mid n>n^i_{s_i(t)},\ |e_i(nh)|-\mathbb{T}_i(nh)\ge 0\Big\}, & \text{if } t\in W_m,\\ n^i_k+1, & \text{if } t\in Z_m,\end{cases} \tag{5.15}$$

where $e_i(nh)=\hat{x}_i(nh)-x_i(nh)$ for $nh\le t<(n+1)h$.

For the ET scheme with state-dependent threshold, the actual state-disagreement with coefficient ϕ is used, i.e.,

$$\mathbb{T}_i(nh)=\phi|\mathbb{X}_i(nh)|,\quad (\forall i\in\mathcal{V}). \tag{5.16}$$

Table 5.1: List of parameters used to model DoS attacks.

Parameter	Definition	Parameter	Definition
d_c	Start time of the c^{th} DoS interval	τ_c	Duration of the c^{th} DoS interval
$\mathcal{D}(t_1,t_2)$	Union of DoS attacks in $[t_1,t_2)$	$\mathcal{H}(t_1,t_2)$	Union of healthy intervals in $[t_1,t_2)$
$\lvert\mathcal{D}(t_1,t_2)\rvert$	Total attack duration in $[t_1,t_2)$	$\lvert\mathcal{H}(t_1,t_2)\rvert$	Total healthy duration in $[t_1,t_2)$
$c(t_1,t_2)$	Total number of off-to-on DoS transitions in $[t_1,t_2)$	T_0, T_1	Upper-bounds for DoS duration
F_0, F_1	Upper-bounds for DoS frequency	$\bar{D}_c$	c^{th} effective DoS interval
Z	Effective DoS intervals with no overlap	W	Complement of Z
ξ_m	Start time for Z_m	$\xi_m+\nu_m$	End time for Z_m (also the start time for W_m)
$\bar{\mathcal{D}}(t_1,t_2)$	Union of intervals Z in $[t_1,t_2)$	$\bar{\mathcal{H}}(t_1,t_2)$	Union of intervals W in $[t_1,t_2)$
$\lvert\bar{\mathcal{D}}(t_1,t_2)\rvert$	Total duration of Z intervals in $[t_1,t_2)$	$\lvert\bar{\mathcal{H}}(t_1,t_2)\rvert$	Total duration of W intervals in $[t_1,t_2)$

For the state-independent ET scheme it holds that

$$\mathbb{T}_i(nh)=\phi, \quad (\forall i\in\mathcal{V},\forall n\in\mathbb{N}_0). \tag{5.17}$$

The control input in the presence of DoS is as follows

$$u_i(t)=\begin{cases}-\mathbb{X}_i(nh), & \text{if} \quad t\in W_m,\\ -\mathbb{X}_i(\xi_m), & \text{if} \quad t\in Z_m,\end{cases} \tag{5.18}$$

where $\mathbb{X}_i(\xi_m)=\sum_{j\in\mathcal{N}_i}a_{i,j}\Big(\,q(\hat{x}_j(\xi_m))-q\left(\hat{x}_i(\xi_m)\right)\Big)$, with $\hat{x}_i(\xi_m)=x_i(n^i_{s_i(\xi_m)}h)$. In words, $\mathbb{X}_i(\xi_m)$ is the disagreement based on the last successful event updates before ξ_m.

5.1.5 Closed-loop system

Consider global vectors (3.6). Additionally, $\hat{\boldsymbol{\delta}}(nh)=[\hat{\delta}_1(nh),\dots,\hat{\delta}_N(nh)]^T$, where $\hat{\delta}_i(nh)=q(\hat{x}_i(nh))-\hat{x}_i(nh)$. To enhance readability, subscript n is used to denote the argument (nh), e.g., $\boldsymbol{r}_n=\boldsymbol{r}(nh)$. From (3.1), (5.15), and (5.18) the closed-loop system is given below

$$\boldsymbol{\Sigma}:\begin{cases}\dot{\boldsymbol{x}}(t)=-\boldsymbol{L}(\boldsymbol{x}_n+\boldsymbol{e}_n+\hat{\boldsymbol{\delta}}_n), & \text{if } t\in W_m,\\ \dot{\boldsymbol{x}}(t)=-\boldsymbol{L}\left(\hat{\boldsymbol{x}}(\xi_m)+\hat{\boldsymbol{\delta}}(\xi_m)\right), & \text{if } t\in Z_m.\end{cases} \tag{5.19}$$

Using the same system transformation given in (3.8), system (5.19) is converted to

$$\boldsymbol{\Sigma}^{[c]}:\begin{cases}\dot{\boldsymbol{r}}(t)=-\boldsymbol{L}(\boldsymbol{r}_n+\boldsymbol{e}_n+\hat{\boldsymbol{\delta}}_n), & \text{if } t\in W_m,\\ \dot{\boldsymbol{r}}(t)=-\boldsymbol{L}\left(\hat{\boldsymbol{r}}(\xi_m)+\hat{\boldsymbol{\delta}}(\xi_m)\right), & \text{if } t\in Z_m,\end{cases} \tag{5.20}$$

where $\hat{\boldsymbol{r}}(nh)=\hat{\boldsymbol{x}}(nh)-\bar{x}(nh)\mathbf{1}_N$.

5.1.6 Stability analysis

This section answers questions Q1 to Q4 specified in section 5.1.2 by analyzing the ISS conditions for system (5.20) for the two proposed ET approaches. For the state-dependent ET approach (5.16), the following theorem derives: (i) Operating regions for design parameters h and ϕ, (ii) Tolerable DoS strength, (iii) Rate of consensus, and (iv) Maximum possible steady-state consensus error.

Theorem 5.1. For a given uniform quantization level $\bar{\delta}$, if the following conditions are satisfied for h, ϕ, T_1, and F_1

$$h < h_M, \qquad \phi < \phi_M, \qquad \frac{1}{T_1} + \frac{h}{F_1} < \Omega_1, \tag{5.21}$$

then, system (5.20) is guaranteed to be ISS (i.e., $\|\boldsymbol{r}(t)\| \leq f_1(\|\boldsymbol{r}(0)\|, t) + f_2(\bar{\delta})$, $\forall t \geq 0$) with the following functions

$$f_1 = \sqrt{\eta_1}\, e^{-\frac{\zeta_1}{2}t} \|\boldsymbol{r}(0)\|, \quad f_2 = \sqrt{C + 2C\eta_1 \frac{e^{\zeta_1 F_0 F_1}}{1 - e^{-\zeta_1 F_1}}}, \tag{5.22}$$

where

$$\begin{aligned}
&h_M = \frac{2\lambda_2 - \delta_\star}{2\lambda_N^2(1+\delta_\star)}, \quad \phi_M = \frac{\sqrt{a_1^2 + 4a_2a_0} - a_1}{\lambda_N(2a_2 + \sqrt{a_1^2 + 4a_2a_0} - a_1)}, \quad \omega_1 = -a_2\theta_1^2 - a_1\theta_1 + a_0,\\
&\omega_2 = \lambda_N\theta_2\,(1 + 0.5\delta_\star), \quad \Omega_1 = \frac{\omega_1}{\omega_1 + \omega_2}, \qquad \eta_1 = e^{(T_0 + hF_0)(\omega_1 + \omega_2)},\\
&\zeta_1 = \omega_1 - (\omega_1 + \omega_2)\left(\frac{1}{T_1} + \frac{h}{F_1}\right),\\
&C = \frac{\delta_\star\lambda_N\,(\theta_1^2 h\lambda_N + \theta_1 h\lambda_N + h\lambda_N + \theta_1/2 + 1/2)}{\omega_1(1 - \omega_1 h)},
\end{aligned} \tag{5.23}$$

with $\delta_\star = 0.5\bar{\delta}\sqrt{N}$, $a_0 = \lambda_2 - h\lambda_N^2 - \delta_\star h\lambda_N^2 - 0.5\delta_\star\lambda_N$, $a_1 = 2h\lambda_N^2 + \lambda_N + \delta_\star h\lambda_N^2 + 0.5\delta_\star\lambda_N$, $a_2 = h\lambda_N^2(1 + \delta_\star)$, $\theta_1 = \frac{\phi\lambda_N}{1 - \phi\lambda_N}$, and $\theta_2 = \frac{1}{1 - \phi\lambda_N}$.

Proof. Proof of Theorem 5.1 is given in Appendix, section 5.5.1 □

In summary, the inequalities given in (5.21) determine the operating regions (Q1) and tolerable DoS strength (Q2) for the state-dependent ET approach. Furthermore, function f_1 computes the least rate for consensus (Q3) and f_2 is the maximum possible consensus error.

Remark 5.4 (Parameter design based on Theorem 5.1)**.** For a given quantization level, the maximum value for sampling period h, i.e., h_M, depends only on λ_2, λ_N and N. Therefore, the first design step is to select the proper value for h which satisfies $h < h_M$. Then, as the second step and based on the selected value for h, the maximum value for the ET parameter, i.e., ϕ_M, is determined. The operating ϕ is designed such that $\phi < \phi_M$. With selected values for h and ϕ, the value for Ω_1 is

Algorithm 5.7 RQ-CEASE with State-dependent ET Threshold.

Preliminary Step: (P1-P2)

P1. Using distributed estimation algorithm such as Algorithm 3.4, each node computes λ_2, λ_N, and N.

P2. Select the quantization level $\bar{\delta}$.

Parameter Design: (D1 – D3)

D1. A sampling period h is selected such that $h < h_M$.

D2. Using the selected value for h, each node selects the ET parameter ϕ within $\phi < \phi_M$.

D3. Based on the selected values for h and ϕ, consensus is resilient to DoS attacks satisfying $\frac{1}{T_1}+\frac{h}{F_1} < \Omega_1$.

Distributed Consensus Iterations: (C1 – C5)

C1. At $t=0$, node i transmits $q(x_i(0))$ to its neighbour.

C2. The state of agent i is excited by (5.18).

C3. Using the designed values for h and ϕ from the parameter design step, condition (5.15) with the state-dependent threshold (5.16) is locally monitored at $t=nh$ $(n\in\mathbb{N}_0)$ to determine the next triggering event.

C4. Events are uniformly quantized before transmission.

C5. Steps C2 to C4 continue until a predefined level of consensus is achieved. Average consensus is guaranteed under DoS attacks satisfying (5.22). The maximum possible steady-state consensus error is C defined in (5.23).

computed. Hence, F_1 and T_1 can be jointly determined such that $\frac{1}{T_1} + \frac{h}{F_1} < \Omega_1$. In fact Ω_1 is an upper-bound for DoS parameters F_1 and T_1. In case that F_1 and T_1 are estimated beforehand (or they satisfy some known upper-bounds), the design procedure does not change since both h_M and ϕ_M do not depend on either T_1 or F_1. Algorithm 5.7 is provided to show necessary steps in RQ-CEASE with *state-dependent* ET threshold.

Remark 5.5 (Design trade-offs)**.** According to Theorem 5.1, if $h \to h_M$, then $\phi_M \to 0$, $C \to \infty$, $\omega_1 \to 0$, and no amount of DoS is theoretically tolerable. Additionally, for a given h, if $\phi \to \phi_M$, then $C \to \infty$, $\omega_1 \to 0$ and no amount of DoS is tolerable. Therefore, there exits a trade-off between the selected values for h and ϕ, the maximum steady-state error f_2, and maximum tolerable DoS. Larger (smaller) values for h and ϕ reduce (increase) the measurements and events intensity. However, they result in a higher (lower) consensus error and less (more) resilience to DoS. Based on (5.22), the upper-bound for the consensus error f_2 is proportional to C given in (5.23). Parameter C itself is proportional to $\theta_1 = \frac{\phi\lambda_N}{1-\phi\lambda_N}$. Since the derivative of θ_1 with respect to the ET threshold ϕ is always positive, a higher value for ϕ increases the upper-bound for the consensus error f_2.

The next theorem derives ISS conditions for system (5.20) under the *state-independent* ET threshold (5.17).

Theorem 5.2. For a given uniform quantization level $\bar{\delta}$, and DoS parameters F_1 and T_1, if the selected values for h and ϕ satisfy the following conditions

$$\omega_3 > 0, \qquad \frac{1}{T_1} + \frac{h}{F_1} < \Omega_2, \tag{5.24}$$

Algorithm 5.8 RQ-CEASE with State-independent ET threshold.

Preliminaries: Follow Steps P1 and P2 in Algorithm 5.7.

Parameter Design: (D1)

D1. Select the sampling period h and ET parameter ϕ such that $\omega_3 > 0$ and $\frac{1}{T_1} + \frac{h}{F_1} < \Omega_2$.

Distributed Consensus Iterations: (C1 – C5)

C1-C2. Follow Steps C1 and C2 in Algorithm 5.7.

C3. Using the designed values for h and ϕ, condition (5.15) with the state-independent threshold (5.17) is monitored at $t = nh$ ($n \in \mathbb{N}_0$) to determine the next events.

C4. Events are uniformly quantized before transmission.

C5. Steps C2 to C4 continue until a predefined level of consensus is achieved. Average consensus is guaranteed under DoS attacks satisfying (5.25). The maximum possible steady-state consensus error is R defined in (5.26).

then, system (5.20) is guaranteed to be ISS (i.e., $\|\boldsymbol{r}(t)\| \leq f_3(\|\boldsymbol{r}(0)\|, t) + f_4$, $\forall t \geq 0$) with the following functions

$$f_3 = \sqrt{\eta_2}\, e^{-\frac{\zeta_2}{2}t}\, \|\boldsymbol{r}(0)\|, \quad f_4 = \sqrt{R + 2R\eta_2 \frac{e^{\zeta_2 F_0 F_1}}{1 - e^{-\zeta_2 F_1}}}. \tag{5.25}$$

The undefined variables are as follow

$$\begin{aligned}
&\omega_3 = \lambda_2 - h\lambda_N^2(1 + \delta_\star/2 + \phi_\star/2) - \lambda_N(\delta_\star/2 + \phi_\star/2),\\
&\omega_4 = \lambda_N\,(1 + \delta_\star/2 + \phi_\star/2)\,, \quad \Omega_2 = \frac{\omega_3}{\omega_3 + \omega_4},\\
&\eta_2 = e^{(T_0 + hF_0)(\omega_3 + \omega_4)}, \quad \zeta_2 = \omega_3 - (\omega_3 + \omega_4)\left(\frac{1}{T_1} + \frac{h}{F_1}\right),\\
&R = \frac{h\lambda_N^2(\delta_\star + \phi_\star)^2 + \lambda_N(h\lambda_N + 1)(\delta_\star + \phi_\star)}{\omega_3(1 - \omega_3 h)},
\end{aligned} \tag{5.26}$$

with $\delta_\star = 0.5\bar{\delta}\sqrt{N}$, $\phi_\star = \sqrt{N}\phi$.

Proof. Proof of Theorem 5.2 is given in Appendix, section 5.5.2. □

In summary, the inequalities given in (5.24) determine the operating regions (Q1) and tolerable DoS strength (Q2) for the state-independent ET approach. Furthermore, function f_3 computes the least rate for consensus (Q3) and f_4 is the maximum possible consensus error.

Remark 5.6 (Parameter design based on Theorem 5.2)**.** Unlike Theorem 5.1, in Theorem 5.2 the sampling period h and ET parameter ϕ are jointly designed such that both conditions given in (5.24) are satisfied. Algorithm 5.8 is provided to list necessary steps in implementing the RQ-CEASE with *state-independent* ET threshold.

Remark 5.7 (Sampling period in healthy and attack intervals)**.** As observed earlier, in RQ-CEASE the sampling period h remains the same for both the healthy and attack intervals. From a design point of view, however, having a constant sampling period is not a suitable strategy when DoS is considered. The reason lies within the

fact that the sampling period during the healthy intervals is desired to be properly large so as to reduce the burden of measurements and event-triggered transmissions. On the other hand, the sampling period during the attack intervals is desired to be properly small so that the MAS returns to normal operation almost as soon as DoS is over. The R-PSEC implementation, which is proposed in the next section, is based on two different sampling periods for healthy and attack intervals.

5.1.7 Comparison between Algorithms 5.7 and 5.8

This section answers Q5 by comparing Algorithms 5.7 and 5.8 from three perspectives: (i) Resilience to DoS attacks, (ii) Steady state consensus error, and (iii) Transmission savings.

- *Resilience to DoS attacks*: Parameters Ω_1 and Ω_2, respectively, determine resilience upper-bounds for Algorithms 5.7 and 5.8. One can verify the following expression for given parameters N, λ_N, λ_2, h, ϕ and $\bar{\delta}$

$$\Omega_2 - \Omega_1 = b_5^{-1}(b_1 + b_2 + b_3 + b_4), \tag{5.27}$$

where

$$\begin{aligned}
b_1 &= 8\phi\,(\lambda_2 + \lambda_N)\,(1 - \phi\lambda_N)(2\lambda_N - \sqrt{N} + \sqrt{N}\phi\lambda_N),\\
b_2 &= \sqrt{N}\bar{\delta}\lambda_N(1-\phi\lambda_N)\left(4\phi(\lambda_2+\lambda_N) + \sqrt{N}h\lambda_N(\bar{\delta}+2\phi)\right),\\
b_3 &= 2h\bar{\delta}\phi^2\lambda_N^4(N\bar{\delta} + 4\sqrt{N} + 2N\phi),\\
b_4 &= 2h\lambda_N^2(8\phi\lambda_N + 2\sqrt{N}\bar{\delta} + 4\sqrt{N}\phi^2\lambda_N),\\
b_5 &= \lambda_N(1 - \phi\lambda_N)(\sqrt{N}\bar{\delta} + 4)(\sqrt{N}\bar{\delta} + 2\sqrt{N}\phi + 4)
\end{aligned} \tag{5.28}$$

Since $\phi_M < \frac{1}{\lambda_N}$, it holds that $1-\phi\lambda_N > 0$. Therefore, b_2, b_3, b_4, and b_5 are all positive scalars. Based on (5.27), a sufficient condition for $\Omega_2 > \Omega_1$ is $\lambda_N > \frac{\sqrt{N}}{2+\sqrt{N}\phi}$. In words, under the same design and network parameters, Algorithm 5.8 is guaranteed to tolerate stronger DoS attacks than Algorithm 5.7, if $\lambda_N > \frac{\sqrt{N}}{2+\sqrt{N}\phi}$. This condition can be simplified to $\lambda_N > \frac{\sqrt{N}}{2}$ which is often the case in connected networks. In cases where $\lambda_N \leq \frac{\sqrt{N}}{2+\sqrt{N}\phi}$, parameter Ω_2 may still be larger than Ω_1, depending on the values of b_2, b_3, and b_4.

- *Steady state consensus error*: The maximum steady state error from average consensus is denoted by f_2 and f_4 for the two algorithms. To see the difference between Algorithms 5.7 and 5.8 in terms of the consensus error, note that f_2 is proportional to the quantization level $\bar{\delta}$ implying that the consensus error using Algorithm 5.7 can be limited through selection of the appropriate value of $\bar{\delta}$, which is independent of the all design, network, and DoS parameters. Unlike Algorithm 5.7, parameter f_4 in Algorithm 5.8 is not limited solely by $\bar{\delta}$ as f_4 is proportional to $\phi_\star + \delta_\star$. This implies that reducing the consensus error using Algorithm 5.8 requires decreasing the value of the ET parameter ϕ as well as the quantization level $\bar{\delta}$. Since

decreasing ϕ results in detection of more events, Algorithm 5.7 is more capable of limiting the consensus error without other side effects.

- *Transmission savings*: It should be reminded that the ET threshold in Algorithm 5.7 is $\phi|\mathbb{X}_i(nh)|$. For Algorithm 5.8, this threshold is independent of disagreement $|\mathbb{X}_i(nh)|$ and only depends on the coefficient ϕ. Therefore, the transmission difference between Algorithms 5.7 and 5.8 depends on the value of $|\mathbb{X}_i(nh)|$. If for all nodes $|\mathbb{X}_i(0)|< 1$, Algorithm 5.8 detects a fewer number of events than Algorithm 5.7. In case that $|\mathbb{X}_i(0)| \geq 1$ for any node i, Algorithm 5.8 triggers more events than Algorithm 5.7 until $|\mathbb{X}_i(nh)| \geq 1$. As the disagreement $|\mathbb{X}_i(nh)|$ becomes smaller than 1, then Algorithm 5.8 outperforms Algorithm 5.7 by detecting fewer events.

5.2 R-PSEC

Existing DoS resilient ET implementations [1,37,79,141,144,147] have some practical shortcomings. For example, implementation [147] (similar to RQ-CEASE) is limited to first-order MASs and is not easily generalizable to MASs with higher-order dynamics. The DoS attacks considered in [144] and [37] are assumed to follow a periodic pattern, which may not be the case in practice. Another shortcoming observed in the existing DoS resilient works is that the theoretic upper-bounds obtained for the tolerable strength of DoS are conservative. The main reason is that the DoS resilience analysis (and the obtained upped-bounds for tolerable DoS) is often based on the extremum eigenvalues of the associated matrices in the Lyapunov candidate [1, 141]. How to obtain *more realistic* upper-bounds for tolerable amount of *unknown* DoS for *general linear* MASs is still an open problem, which is being covered in R-PSEC (and also in ROCCET presented in the next section).

R-PSEC (resilient PSEC) extends the PSEC implementation proposed in Section 4.2 to the situation where DoS attacks can degrade the consensus performance. In the presence of DoS with unknown patterns, R-PSEC includes a desired level of resilience to DoS as a design input. R-PSEC demonstrates the trade-off between the DoS resilience level and consensus performance indices in terms of convergence rate and the number of transmissions. It should be noted that Assumption 4 is not needed for R-PSEC (and ROCCET), and the DoS duration can be of any value.

5.2.1 Problem statement

In R-PSEC, the same linear time-invariant MAS (4.1) is considered. The DoS attack considered in R-PSEC is similar to the one in RQ-CEASE. The assumptions regarding DoS are given in Sections 5.1.2 and 5.1.3. DoS related notation is summarized in Table 5.1. For ease of reference, important expressions from the formulation of DoS in Sections 5.1.2 and 5.1.3 are reproduced here. There exist positive constants F_0,

F_1, T_0, and T_1 such that the following upper-bounds hold [65]

$$|\,\mathcal{D}(t_1,t_2)\,| \leq T_0 + \frac{t_2-t_1}{T_1}, \quad \forall\, t_1,t_2 \in \mathbb{R}_{\geq 0},\ t_1 \leq t_2, \tag{5.29}$$

$$c\,(t_1,t_2) \leq F_0 + \frac{t_2-t_1}{F_1}, \quad \forall\, t_1,t_2 \in \mathbb{R}_{\geq 0},\ t_1 \leq t_2. \tag{5.30}$$

5.2.2 Distinct sampling periods for healthy and attack intervals

In RQ-CEASE, the sampling period h remains the same during healthy and attack intervals. As mention in Remark 5.7, having a constant sampling period is not a suitable strategy in the presence of DoS. In R-PSEC, two different sampling periods for measurement are considered. Parameter h is the sampling period used for healthy intervals, while g is the sampling period used once DoS is detected.

Assumption 6. Sampling period g is selected such that $\frac{h}{g} \in \mathbb{N}$.

The introduction of the sampling period g is a defense strategy to decrease the worst upper-bound for the effective DoS intervals. It should be noted that introducing two different sampling periods h and g adds an additional degree of freedom to operate according to healthy/attack intervals. The sampling period h is desired to be appropriately large so as to reduce the burden of measurements and ET transmissions. On the other hand, the sampling period g is desired to be appropriately small so that the MAS returns to normal operation almost as soon as DoS is over.

5.2.3 Control protocol and event-triggering scheme

Due to the complexity caused by the multiple sampling periods, the notation used in R-PSEC is slightly different from other implementations. Sampled states of agent i is denoted by $\boldsymbol{x}_i(t_k)$, where $k \in \mathbb{N}_0$. In the ideal case where DoS does not occur the sampling period for measurement is h, i.e., $t_{k+1}-t_k = h$. Let $t^\star_{i,0}, t^\star_{i,1}, \ldots, t^\star_{i,k}$ denote the time sequence at which events for agent i are detected and in-neighbour transmissions are made until time t. In R-PSEC, the disagreement for agent i is defined as follows

$$\mathbb{X}_i(t) = \sum_{j\in\mathcal{N}_i} a_{i,j}\left(\boldsymbol{\Lambda}_i(t)\boldsymbol{x}_i(t^\star_{i,k}) - \boldsymbol{\Lambda}_j(t)\boldsymbol{x}_j(t^\star_{j,k})\right), \quad t \in [t_k, t_{k+1}), \tag{5.31}$$

where $\boldsymbol{\Lambda}_i(t) = e^{\boldsymbol{A}(t_k - t^\star_{i,k})}$. Starting from $t^\star_{i,0} = 0$, the next event for agent i is triggered at $t^\star_{i,k+1}$ which satisfies the following ET condition

$$t^\star_{i,k+1} = \min_{k\in\mathbb{N}} \{t_k > t^\star_{i,k} \mid \|\boldsymbol{\Phi}_1^{1/2}\boldsymbol{e}_i(t)\| \geq \|\boldsymbol{\Phi}_2^{-1/2}\mathbb{X}_i(t)\|\}, \tag{5.32}$$

Matrices $\boldsymbol{\Phi}_1$ and $\boldsymbol{\Phi}_2$ are the sampled-data ET parameters to be designed. Vector $\boldsymbol{e}_i(t) = \boldsymbol{x}_i(t^\star_{i,k}) - \boldsymbol{x}_i(t_k)$, $(1 \leq i \leq N)$, is the state error. The following control protocol is considered in R-PSEC

$$\boldsymbol{u}_i(t) = \boldsymbol{K}\,\mathbb{X}_i(t), \quad (1 \leq i \leq N), \quad t \in [t_k, t_{k+1}), \tag{5.33}$$

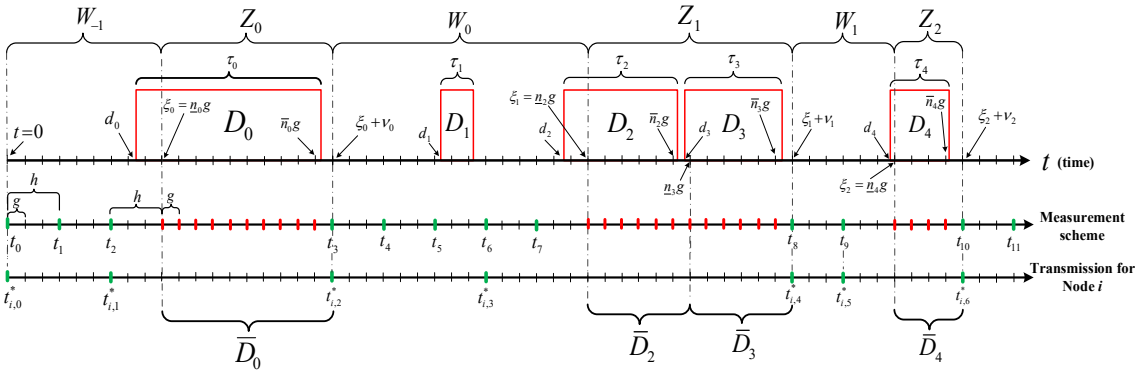

Figure 5.4: An illustrative time diagram showing the periodic measurement scheme and event-triggered transmissions under five DoS attack intervals. Successfully transmitted measurements are shown in green. The measurements denied from transmission are shown in red.

where matrix $\boldsymbol{K} \in \mathbb{R}^{m\times n}$ is the nominal control gain to be designed. Similar to PEC and PSEC, the uncertainty in control realization is taken into account as follows

$$\boldsymbol{u}_i(t) = (\boldsymbol{K} + \boldsymbol{\Delta}_K)\,\mathbb{X}_i(t), \quad (1 \le i \le N). \tag{5.34}$$

The time-varying uncertainty $\boldsymbol{\Delta}_K$ satisfies Assumption 2.

Design objectives: The design objectives considered in R-PSEC are as follows:

- The performance objectives considered in R-PSEC (i.e., exponential consensus convergence rate and non-fragility to control uncertainty) should be preserved.
- In the presence of DoS, a *desired* level of tolerance to unknown DoS attacks is included within the co-design framework. The proposed co-design approach demonstrates the trade-off between the DoS resilience level and consensus performance indices.

5.2.4 Problem formulation

As mentioned previously, the sampling period h is used for DoS-free intervals (i.e., when DoS is off). After a measurement failure due to the occurrence of DoS, no acknowledgment is received from the event-detector and a DoS interval is detected. When DoS is detected, the measurement scheme turns into another sampling period, denoted by g. The event-detector unit is not able to receive these measurements taken every g seconds, unless the DoS interval is over. Once a measurement is successfully received by the event-detector after DoS, the measurement scheme returns to period h. Based on the two sampling periods, possible time of occurrence for DoS intervals, and their duration, the actual impact of D_c may not start at $t = d_c$ and may not end at $t = d_c + \tau_c$. Motivated by [32, 50], in what follows we formulate the *effective* DoS intervals. As denoted previously, t_k is the instant where 'the most recent successfully transmitted measurement until time t is made'. Let $\underline{n}_c g$ be 'the first instant where transmission of the measurement is denied by D_c'. For $n \in \mathbb{N}_0$, let

$$\underline{n}_c = \begin{cases} \frac{t_k+h}{g} & \text{if } d_c - t_k \le h \ \wedge \ t_k + h \in D_c, \\ \min\{n \,|\, ng \ge d_c,\ ng \in D_c\} & \text{if } d_c - t_k > h, \\ \text{does not exist} & \text{otherwise,} \end{cases}$$

with $\underline{n}_0 = 0$ if $d_0 = 0$. Intuitively speaking, condition $d_c - t_k \le h$ implies that the sampler is using the period h as the agent enters interval D_c. Therefore, $\underline{n}_c g = t_k + h$ will be the first instant where transmission of the measurement is denied (for visualization, refer to D_0, D_2, and D_4 in Fig. 5.4). If two DoS intervals are located closely to each other, condition $d_c - t_k > h$ may occur for a DoS interval (such as for D_3 in Fig. 5.4). In this case, there were other DoS attacks before d_c and the sampler is using the period g as the agent approaches D_c. Hence, the first instant where transmission of the measurement is denied by D_c is ng for the smallest possible n satisfying $ng \ge d_c$. Note that if the duration of D_c is short, none of the above conditions may apply (such as for D_1 in Fig. 5.4). In this scenario, $\underline{n}_c$ does not exist. Additionally, for $n \in \mathbb{N}_0$ we define

$$\bar{n}_c = \begin{cases} \max\{n \,|\, ng \le d_c + \tau_c,\ ng \in D_c\} & \text{if } \underline{n}_c \text{ exists,} \\ \text{does not exist} & \text{otherwise.} \end{cases}$$

Conceptually speaking, parameter $\bar{n}_c g$ is the 'instant where the last measurement before $d_c + \tau_c$ is denied from transmission by D_c'. By using the sampling period g during DoS, at most g seconds after $\bar{n}_c g$ the system can 'potentially' recover from DoS. Therefore, if $\underline{n}_c$ and $\bar{n}_c$ exist we define the c^{th} *effective* DoS interval as

$$\bar{D}_c = [\underline{n}_c g,\ (\bar{n}_c + 1)g]. \tag{5.35}$$

Note that not all DoS attacks have a corresponding effective interval. For example, since $\underline{n}_1$ does not exist for D_1 in Fig. 5.4, $\bar{D}_1$ does not exist either, which implies that D_1 has no effect on the system. As shown in Fig. 5.4, if two DoS intervals are closely located to each other, their corresponding effective DoS intervals have one sample in common (as in the case for $\bar{D}_2$ and $\bar{D}_3$ in Fig. 5.4). To precisely determine the effective DoS intervals *without intersection*, we define [32]

$$\bar{\mathcal{D}}(t_1, t_2) = \bigcup_{m \in \mathbb{N}_0} Z_m \cap [t_1, t_2], \tag{5.36}$$

with $Z_m = [\,\xi_m, \xi_m + \nu_m)$. Parameter ξ_m is defined by

$$\xi_0 = \underline{n}_0\, g, \qquad \xi_{m+1} = \min\{\underline{n}_c g \,|\, \underline{n}_c g > \xi_m,\ d_c - t_k \le h\}.$$

Additionally, ν_m is the same as (5.10). Intuitively speaking, parameter $\nu_m + \xi_m$ specifies the earliest sample instant located in healthy intervals after DoS is over. If $d_c - t_k > h$ for $\bar{D}_c$, then ν_m excludes the in-common samples between $\bar{D}_c$ for some $c \in \mathbb{N}_0$ and sums up the intervals until the earliest measurement after attack which can be successfully transmitted. That sample is located at $t = \nu_m + \xi_m$. On the other hand,

parameter

$$\bar{\mathcal{H}}(t_1,t_2)=\bigcup_{m\in\mathbb{N}_0} W_{m-1}\cap[\,t_1,t_2\,], \tag{5.37}$$

with $W_{-1}=[\,0,\xi_0\,)$ and $W_m=[\,\xi_m+\nu_m,\,\xi_{m+1})$, is the union of healthy intervals. Parameters $|\bar{\mathcal{D}}(t_1,t_2)|$ and $|\bar{\mathcal{H}}(t_1,t_2)|$, respectively, denote the total length of corresponding intervals for $t\in[t_1,t_2)$. Note that $\bar{\mathcal{H}}(t_1,t_2)$ and $\bar{\mathcal{D}}(t_1,t_2)$ are complements of each other and the following expression holds true

$$|\bar{\mathcal{H}}(t_1,t_2)|=t_2-t_1-|\bar{\mathcal{D}}(t_1,t_2)|,\ \forall t_1,t_2\geq 0,\ t_2>t_1. \tag{5.38}$$

In addition, it holds that

$$|\bar{\mathcal{D}}(t_1,t_2)|\leq|\mathcal{D}(t_1,t_2)|+c(t_1,t_2)g,\quad (t_1\leq t_2). \tag{5.39}$$

5.2.5 Closed-loop MAS

In the absence of DoS ($t\in W_m$), the control protocol in R-PSEC is given by (5.34). In the presence of DoS ($t\in Z_m$), however, the control protocol is set as zero, i.e., $\boldsymbol{u}_i(t)=\mathbf{0}$. Considering both healthy and DoS intervals, the switched converted MAS (using the transformation (4.10)) is given below.

$$\dot{\boldsymbol{\psi}}(t)=\begin{cases}(\boldsymbol{I}_{N-1}\otimes\boldsymbol{A})\boldsymbol{\psi}(t)+(\tilde{\boldsymbol{J}}\otimes\boldsymbol{B}(\boldsymbol{K}+\boldsymbol{\Delta}_k))\,\boldsymbol{\psi}(t_k)\\ +(\tilde{\boldsymbol{J}}\tilde{\boldsymbol{W}}\otimes\boldsymbol{B}(\boldsymbol{K}+\boldsymbol{\Delta}_k))\,\boldsymbol{e}(t_k),\quad t\in[t_k,t_{k+1}),\quad & t\in W_m,\\ \\ (\boldsymbol{I}_{N-1}\otimes\boldsymbol{A})\boldsymbol{\psi}(t), & t\in Z_m.\end{cases} \tag{5.40}$$

Remark 5.8 (Switching between the two modes of $\boldsymbol{u}_i$)**.** Note that switching between the two modes of the control protocol (i.e., expression (5.33) and $\boldsymbol{u}_i(t)=\mathbf{0}$) requires the knowledge of intervals W_m and Z_m. As observed earlier, the beginning of Z_m is the instant when DoS is detected by the system. Additionally, the end of Z_m is the first instant after DoS when a measurement is successfully transmitted. It is reminded that the event-detector sends an acknowledgment (to the sampler) when it successfully receives a new measurement. Thanks to these acknowledgments and the definition of Z_m, interval Z_m and its complement W_m are fully detectable in practice.

5.2.6 Parameter design

The proposed framework in the next theorem co-designs the required parameters in R-PSEC (i.e., the control gain $\boldsymbol{K}$ and ET parameters $\boldsymbol{\Phi}_1$ and $\boldsymbol{\Phi}_2$) based on desired values for sampling period h, non-fragility level δ, and desired level of resilience to DoS γ. Similar to PSEC, the framework requires all the eigenvalues and eigenvectors of the Laplacian matrix which can be computed distributively using Algorithm 3.4.

Theorem 5.3. Select desired values for sampling periods h and g, ideal stabilization rate ζ, non-fragility level δ, and DoS resilience level $\gamma < 1$. Denote $\beta = \frac{\zeta(1-\gamma)}{\gamma}$. If there exist the following parameters

- $m \times n$ dimensional matrix $\boldsymbol{V}$, $n \times n$ dimensional matrices $\boldsymbol{H}$, $\boldsymbol{Y}_{11}$, $\boldsymbol{Y}_{12}$, $\boldsymbol{Y}_{22}$, $\boldsymbol{F}_1$, $\boldsymbol{F}_2$, $\boldsymbol{G}_1$, $\boldsymbol{G}_2$;
- $n \times n$ dimensional positive definite matrices $\boldsymbol{P}$, $\boldsymbol{Q}$, $\boldsymbol{Z}$, $\boldsymbol{M}_1$, $\boldsymbol{M}_2$;
- positive scalars ϵ_1, ϵ_2 ϵ_3;

satisfying the following LMIs

$$\boldsymbol{C}_1 = \begin{bmatrix} \boldsymbol{\Pi} & \boldsymbol{\Theta} \\ * & \boldsymbol{\Omega} \end{bmatrix} < 0, \quad \boldsymbol{C}_2 = \begin{bmatrix} \boldsymbol{Y} & \boldsymbol{F} \\ * & he^{-\zeta h}\boldsymbol{Z} \end{bmatrix} \geq 0, \quad \boldsymbol{C}_3 = \begin{bmatrix} \boldsymbol{Y} & \boldsymbol{G} \\ * & he^{-\zeta h}\boldsymbol{Z} \end{bmatrix} \geq 0, \tag{5.41}$$

$$\boldsymbol{C}_4 = \begin{bmatrix} \boldsymbol{A}\boldsymbol{H}^T + \boldsymbol{H}\boldsymbol{A}^T - \beta\boldsymbol{P} + \boldsymbol{Q} & \boldsymbol{P} - \boldsymbol{H}^T + \boldsymbol{H}\boldsymbol{A}^T \\ * & h^2\boldsymbol{Z} - \boldsymbol{H} - \boldsymbol{H}^T \end{bmatrix} < 0, \tag{5.42}$$

then, the control gain $\boldsymbol{K}$ and ET parameters $\boldsymbol{\Phi}_1$ and $\boldsymbol{\Phi}_2$ are computed from the following expressions

$$\boldsymbol{K} = \boldsymbol{V}(\boldsymbol{H}^{-1})^T, \qquad \boldsymbol{\Phi}_1 = \boldsymbol{H}^{-1}\boldsymbol{M}_1(\boldsymbol{H}^{-1})^T, \qquad \boldsymbol{\Phi}_2 = \boldsymbol{M}_2, \tag{5.43}$$

These parameters make system (5.40) resilient to DoS attacks satisfying

$$\frac{1}{T_1} + \frac{g}{F_1} < \gamma. \tag{5.44}$$

Additionally, trajectories of (5.40) satisfy

$$\lambda_1 \left\| \boldsymbol{\psi}(t) \right\|^2 \leq \rho\lambda_2 e^{-\bar{\zeta}t} \left\| \boldsymbol{\psi}(0) \right\|^2, \tag{5.45}$$

where

$$\rho = e^{(\zeta+\beta)(T_0+gF_0)}, \qquad \bar{\zeta} = \zeta - (\zeta+\beta)\left(\frac{1}{T_1} + \frac{g}{F_1}\right), \tag{5.46}$$

with $\lambda_1 = \lambda_{\min}(\bar{\boldsymbol{P}})$, $\lambda_2 = \lambda_{\max}(\bar{\boldsymbol{P}}) + h\lambda_{\max}(\bar{\boldsymbol{Q}}$, with $\bar{\boldsymbol{P}} = \boldsymbol{H}^{-1}\boldsymbol{P}(\boldsymbol{H}^{-1})^T$, $\bar{\boldsymbol{Q}} = \boldsymbol{H}^{-1}\boldsymbol{Q}(\boldsymbol{H}^{-1})^T$, and $\bar{\boldsymbol{Z}} = \boldsymbol{H}^{-1}\boldsymbol{Z}(\boldsymbol{H}^{-1})^T$. Unknown block matrices in (5.41) are the same as those defined in PSEC, i.e., expressions (4.27), (4.28), (4.29), (4.30), (4.31).

Proof. Proof of Theorem 5.3 is provided in Appendix, Section 5.5.3. □

Remark 5.9 (Less conservative DoS bounds)**.** As observed in Theorem 5.3, the guaranteed (theoretical) level of resilience to DoS (i.e., parameter γ) can be chosen *a priori* based on the design requirements. In many implementations such as [1, 141], the resilience level depends on many other parameters, which makes its precise regulation difficult. Additionally, the guaranteed resilience level to DoS in [1,32,141] is obtained based on the norm or extremum eigenvalues of some associated matrices (such as system matrix $\boldsymbol{A}$ and Lyapunov matrix $\boldsymbol{P}$). This approach often results in conservative

Algorithm 5.9 . The R-PSEC algorithm

Input: Neighbouring information, System matrices $\boldsymbol{A}$ and $\boldsymbol{B}$.

Output: Resilient Performance guaranteed sampled-data event-triggered consensus in general linear MASs.

Preliminary: Using a distributed algorithm such as Algorithm 3.4, each node computes all eigenvalues and eigenvectors of the Laplacian matrix. Select desired values for sampling periods h and g, convergence rate ζ, non-fragility level δ, and DoS resilience γ.

I. Parameter Design: (D1 -D2)

D1. Compute consensus design parameters $\boldsymbol{K}$, $\boldsymbol{\Phi}_1$, and $\boldsymbol{\Phi}_2$ from (5.43).

Distributed Consensus Iterations: (C1 – C2)

C1. *Initialization*: Node i transmits $\boldsymbol{x}_i(0)$ to its neighbours, $(1 \leq i \leq N)$.

C2. *Consensus process*: Using the designed $\boldsymbol{K}$ for (4.21) and $\boldsymbol{\Phi}_1$ and $\boldsymbol{\Phi}_2$ for (4.19) the states of the agents approach sampled-data consensus with a decaying rate satisfying (5.45). Consensus is resilient to DoS attacks satisfying $\frac{1}{T_1} + \frac{g}{F_1} < \gamma$.

bounds for the tolerable amount of DoS. This sort of conservation is reported in [32] and the authors express that the practical bounds to DoS are larger. Thanks to the LMI formulation which excludes the use of matrix norms and extremum eigenvalues, R-PSEC is less conservative in this regard compared to [1, 32, 141].

Remark 5.10 (Finding the maximum amount of resilience to DoS)**.** From Theorem 5.3 it is possible to obtain the maximum DoS resilience level, denoted by γ_m, for given values of h, δ, and ζ. To this end, one can select desired values for h, δ, and ζ and investigate the feasibility of Theorem 5.3 by incrementally increasing the value of γ until the LMIs become infeasible. The largest value of γ which leads to a feasible solution is the maximum resilience level to DoS (γ_m) guaranteed by Theorem 5.3.

5.3 ROCCET

ROCCET [82] is a resilient optimized consensus using dynamic event-triggered scheme for linear MASs configured as undirected networks. Similar to PEC, the state measurement, event monitoring, and control updates in ROCCET is performed continuously. Similar to DEASE, the ET scheme used in ROCCET is dynamic which further reduces the number of events. Similar to R-PSEC, in ROCCET a desired level of resilience to DoS is included as a design input. A co-design optimization technique is used to simultaneously design all required control and dynamic event-triggering (DET) parameters. The optimization in ROCCET increases the inter-event interval based on a given consensus convergence rate and resilience to DoS attacks. The upper-bound for guaranteed resilience associated with the proposed co-design approach in ROCCET is less conservative (larger) as compared to those obtained from analytical solutions. The main features of the proposed ROCCET are listed below:

- ROCCET is the first instance that studies the impact of unknown DoS attacks for general linear MASs with a DET transmission scheme.

- Unlike existing DET implementations [76], the design procedure in ROCCET is based on co-design optimization that simultaneously computes all required control and DET parameters. The optimization enables a structured trade-off between the consensus convergence rate, frequency of transmissions, and level of resilience to DoS. The theoretic upper-bound for guaranteed resilience to DoS is less conservative (larger).

5.3.1 Problem statement

To reduce data exchanges between the agents, in ROCCET a distributed DET scheme (to be introduced later) is incorporated for each agent. Denote the following disagreement vector for agent i

$$\mathbb{X}_i(t) = \sum_{j\in\mathcal{N}_i} a_{i,j}\Big(\boldsymbol{\Lambda}_i(t)\boldsymbol{x}_i(t_k^i) - \boldsymbol{\Lambda}_j(t)\boldsymbol{x}_j(t_k^j)\Big), \quad \forall i\in\mathcal{V}, \tag{5.47}$$

where $\boldsymbol{\Lambda}_i(t) = e^{\boldsymbol{A}(t-t_k^i)}$. The following control protocol is used for agent i

$$\boldsymbol{u}_i(t) = \boldsymbol{K}\,\mathbb{X}_i(t), \qquad \forall i\in\mathcal{V}, \tag{5.48}$$

where $\boldsymbol{K}\in\mathbb{R}^{m\times n}$ is the control gain to be designed. Let $\boldsymbol{e}_i(t) = \boldsymbol{\Lambda}_i(t)\boldsymbol{x}_i(t_k^i) - \boldsymbol{x}_i(t)$, $\forall i\in\mathcal{V}$, denote the state error. Initialized by $t_0^i = 0$, $\forall i\in\mathcal{V}$, the next event instant is triggered by the following DET condition

$$t_{k+1}^i = \inf\{\, t > t_k^i \mid \|\boldsymbol{\Phi}_1\boldsymbol{e}_i(t)\| \geq \phi_2\|\mathbb{X}_i(t)\| + \phi_3\eta_i(t)\,\}, \tag{5.49}$$

where symmetric matrix $\boldsymbol{\Phi}_1 \geq 0$ and scalars $\phi_2 \geq 0$ and $\phi_3 \geq 0$ are to be designed. Parameter $\eta_i(t)$ satisfies

$$\dot{\eta}_i(t) = -\,\phi_4\,\eta_i(t) + \phi_5\,\|\mathbb{X}_i(t)\|\,, \quad \forall i\in\mathcal{V}, \tag{5.50}$$

where $\eta_i(0) > 0$. Scalars $\phi_4 \geq 0$ and $\phi_5 \geq 0$ are to be designed.

In what follows, we observe that parameter $\eta_i(t)$ remains positive over time.

Lemma 3. It holds that $\eta_i(t) > \eta_i(0)\,e^{-(\phi_4+\phi_3\frac{\phi_5}{\phi_2})t}$, $\forall t\geq 0$, $\forall i \in \mathcal{V}$. Hence, $\eta_i(t)$ remains positive over time.

Proof. Based on (5.49), it holds that $\|\boldsymbol{\Phi}_1\boldsymbol{e}_i(t)\| - \phi_3\eta_i(t) \leq \phi_2\|\mathbb{X}_i(t)\|$ for $t\in[t_k^i, t_{k+1}^i)$. This condition is multiplied by $\frac{\phi_5}{\phi_2}$ which leads to $\frac{\phi_5}{\phi_2}\|\boldsymbol{\Phi}_1\boldsymbol{e}_i(t)\| - \phi_3\frac{\phi_5}{\phi_2}\eta_i(t) \leq \phi_5\|\mathbb{X}_i(t)\|$. Incorporating this inequality in (5.50), results in $\dot{\eta}_i(t) \geq -(\phi_4+\phi_3\frac{\phi_5}{\phi_2})\eta_i(t) + \frac{\phi_5}{\phi_2}\|\boldsymbol{\Phi}_1\boldsymbol{e}_i(t)\|$. Since $\frac{\phi_5}{\phi_2}\|\boldsymbol{\Phi}_1\boldsymbol{e}_i(t)\|$ is non-negative, one obtains $\dot{\eta}_i(t) \geq -(\phi_4+\phi_3\frac{\phi_5}{\phi_2})\eta_i(t)$ for $t\in[t_k^i, t_{k+1}^i)$. Thus, $\eta_i(t) \geq \eta_i(t_k^i)\,e^{-(\phi_4+\phi_3\frac{\phi_5}{\phi_2})(t-t_k^i)}$. Now, we move back to interval $t\in[t_{k-1}^i, t_k^i)$. Following the same steps above, one can show that $\eta_i(t_k^i) \geq \eta_i(t_{k-1}^i)\,e^{-(\phi_4+\phi_3\frac{\phi_5}{\phi_2})(t_k^i-t_{k-1}^i)}$. Comparing the former and latter expressions leads to $\eta_i(t) \geq \eta_i(t_{k-1}^i)\,e^{-(\phi_4+\phi_3\frac{\phi_5}{\phi_2})(t-t_{k-1}^i)}$ for $t\in[t_{k-1}^i, t_{k+1}^i)$. By induction and moving back through all events t_{k-2}^i, …, $t_0^i = 0$, one obtains $\eta_i(t) > \eta_i(0)\,e^{-(\phi_4+\phi_3\frac{\phi_5}{\phi_2})t}$ referring to its positive value over time. □

Remark 5.11 (Importance of the co-design approach for DET schemes)**.** Similar to DEASE, the DET scheme (5.49) depends on multiple unknown gains (matrix $\boldsymbol{\Phi}_1$ and scalars ϕ_2 to ϕ_5). A generic approach to design these parameters is of great interest. The emulation-based approaches [75, 76, 125] derive some bounded regions for unknown DET gains. It should be noted that even when the feasible regions for design parameters are obtained, selecting proper operating values that efficiently save transmissions is still difficult and is based on the trial and error approach. In [1], a resilient implementation for consensus under DoS attack is proposed, where another emulation-based approach is used to design the required parameters. The authors in [1, Remark 3 and Remark 6] suggest that an optimization to govern the trade-off between the consensus convergence rate and frequency of transmissions is essential for improved performance. As it will be observed in Theorems 5.4 and 5.5, the proposed co-design optimization in ROCCET simultaneously computes the *exact* values for unknown DET and control gains using a similar objective function considered in PEC.

The following Lemma excludes the possibility of the Zeno behaviour in ROCCET.

Lemma 4. The minimum inter-event time (MIET) for agent i, $(\forall i \in \mathcal{V})$, is strictly positive and lower-bounded by

$$t^i_{k_i+1} - t^i_{k_i} \geq \frac{1}{\|\boldsymbol{A}\|} \ln\Big(1 + \|\boldsymbol{A}\| \, (\kappa_{1i} + \kappa_{2i})\Big), \quad (i \in \mathcal{V}), \tag{5.51}$$

where

$$\begin{aligned} &\kappa_{1i} = \frac{\phi_2}{\|\boldsymbol{\Phi}_1\| \, \|\boldsymbol{BK}\|}, \quad \kappa_{2i} = \frac{\phi_3}{\kappa_{3i}} \, \eta_i(0) \, e^{-(\phi_4 + \phi_3 \frac{\phi_5}{\phi_2}) t^i_{k_i+1}}, \\ &\kappa_{3i} = \|\boldsymbol{\Phi}_1\| \, \|\boldsymbol{BK}\| \, \|\mathbb{X}_i(t^i_{k_i+1})\|. \end{aligned} \tag{5.52}$$

Proof. Consider t^i_k and t^i_{k+1} as two consecutive events for agent i. From (5.49), it holds that $\|\boldsymbol{e}_i(t^i_k)\| = 0$. For $t \geq t^i_k$, the state error $\boldsymbol{e}_i(t)$ evolves from zero until the next event is triggered at $t = t^i_{k+1}$ which fulfills (5.49). From $\boldsymbol{e}_i(t) = \boldsymbol{\Lambda}_i(t)\boldsymbol{x}_i(t^i_k) - \boldsymbol{x}_i(t)$, it follows that $\dot{\boldsymbol{e}}_i(t) = \boldsymbol{A\Lambda}_i(t)\boldsymbol{x}_i(t^i_k) - \dot{\boldsymbol{x}}_i(t)$. From (5.48) and (4.1), one obtains that $\dot{\boldsymbol{x}}_i(t) = \boldsymbol{A}\boldsymbol{x}_i(t) + \boldsymbol{BK}\,\mathbb{X}_i(t)$. After simplifying one gets $\dot{\boldsymbol{e}}_i(t) = \boldsymbol{A}\boldsymbol{e}_i(t) - \boldsymbol{BK}\,\mathbb{X}_i(t)$, or $\|\dot{\boldsymbol{e}}_i(t)\| \leq \|\boldsymbol{A}\| \, \|\boldsymbol{e}_i(t)\| + \|\boldsymbol{BK}\| \, \|\mathbb{X}_i(t)\|$, $t \in [t^i_k, t^i_{k+1})$. It, then, follows that

$$\|\boldsymbol{e}_i(t)\| \leq \frac{\|\boldsymbol{BK}\| \, \|\mathbb{X}_i(t)\|}{\|\boldsymbol{A}\|} \, (\, e^{\|\boldsymbol{A}\|(t - t^i_k)} - 1). \tag{5.53}$$

The next event is triggered by (5.49) at $t = t^i_{k+1}$ where $\|\boldsymbol{\Phi}_1 \boldsymbol{e}_i(t^i_{k+1})\| = \phi_2 \|\mathbb{X}_i(t^i_{k+1})\| + \phi_3 \eta_i(t^i_{k+1})$. Then, from Lemma 3, it follows that $\|\boldsymbol{e}_i(t^i_{k+1})\| \geq \frac{\phi_2}{\|\boldsymbol{\Phi}_1\|} \|\mathbb{X}_i(t^i_{k+1})\| + \frac{\phi_3}{\|\boldsymbol{\Phi}_1\|} \eta_i(0) \, e^{-(\phi_4 + \phi_3 \frac{\phi_5}{\phi_2}) t^i_{k+1}}$. The latter inequality together with (5.53) leads to (5.51). The right hand side of (5.51) is strictly positive. Therefore, the minimum time between two events is strictly positive. Hence, DET (5.49) does not exhibit the Zeno behaviour. □

5.3.2 Denial of service attacks

The DoS model considered in ROCCET is similar to RQ-CEASE and R-PSEC. In particular, Assumptions 3 and 5, and expressions (5.5) and (5.6) hold for DoS.

5.3.3 Design objectives

ROCCET considers the the following important criteria as design objectives.

Reduce the frequency of transmissions: One approach to reduce the frequency of transmissions is to increase the value of MIET. Based on (5.51), the MIET depends on all of the design parameters. It can be shown that the derivative of MIET with respect to $\|\boldsymbol{K}\|$, $\|\boldsymbol{\Phi}_1\|$, and ϕ_4 is negative, implying that smaller values for $\|\boldsymbol{K}\|$, $\|\boldsymbol{\Phi}_1\|$, and ϕ_4 increase the value of MIET. On the other hand, the derivative of MIET with respect to ϕ_2, ϕ_3, and ϕ_5 is positive. Therefore, higher values for ϕ_2, ϕ_3, and ϕ_5 increase the MIET. This observation is used in developing the co-design approach in Theorems 5.4 and 5.5.

Control the convergence rate of consensus A desired exponential convergence rate as a *given* input is considered to control the consensus convergence rate. It is expected that the optimization reflects on the desired rate of convergence as such a higher rate of convergence leads to a larger number of transmissions (smaller MIET) and vice versa.

Tolerable amount of the DoS attacks: As mention in R-PSEC, it is of great importance to include the desired level of resilience to DoS in the parameter design stage. In this case, the optimization is expected to compute proper control and DET gains in response to the desired level of tolerance to DoS. In summary, the design objectives are as follows:

- Increase the MIET by simultaneously decreasing the values of $\{\|\boldsymbol{K}\|, \|\boldsymbol{\Phi}_1\|, \phi_4\}$, and increasing $\{\phi_2, \phi_3, \phi_5\}$ which together lead to an increase in MIET (5.51).
- Control the rate of consensus convergence as an exponential function.
- Govern the trade-off between the frequency of transmissions, consensus convergence rate, and the level of resilience to DoS attacks.

5.3.4 DoS formulation

This section formulates the DoS attacks. Many concepts are similar to Section 5.1.3, where DoS is formulated for RQ-CEASE. However, ROCCET is based on a continuous-time measurement and control updates. This makes the formulation of DoS relatively easier compared to RQ-CEASE and R-PSEC, where sampled-data measurement is considered.

If no update is received by the event-detector DoS is detected. Once DoS is detected, the transmission logic turns into a non-event-triggered mode, where periodic

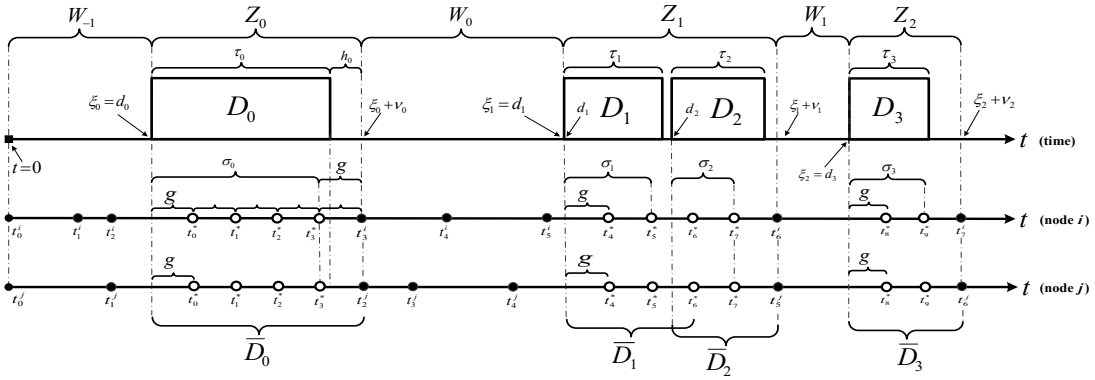

Figure 5.5: Schematic time diagram for a representative DoS sequence and event instants for nodes i and j. Successful transmissions are labeled with black circles while white circles show the periodic attempts to transmit after the DoS interval ends.

attempts (with a desired period time g) are made to transmit the state value to the neighbouring agents as soon as DoS is over. Depending on the length of the c-th DoS interval D_c, there might be multiple transmission attempts during D_c. Let $t_a^\star$, with sequence $a = 0, 1, \ldots$, denote the time instant when the a-th transmission attempt is made by the agents during DoS intervals. As shown in Fig 5.5, these periodic attempts produce a time delay h_c between the first successful transmission after D_c and the actual time when D_c is over. Time delay h_c, which satisfies $0 < h_c \leq g$, makes the 'effective' DoS interval larger than its actual length. To model the effective DoS intervals, define the following parameter

$$\sigma_c = \begin{cases} 0 & \text{if} \quad \nexists\, t_a^\star \in D_c, \\ \max\{t_a^\star \,|\, t_a^\star \in D_c\} - d_c & \text{otherwise.} \end{cases}$$

The c-th effective DoS interval is given by $\bar{D}_c = [\, d_c,\, d_c + \sigma_c + g\,)$. Two consecutive intervals for $\bar{D}_c$ have overlaps if they are not g seconds apart. To exclude such overlap, define Z_m as

$$Z_m = [\xi_m, \xi_m + \nu_m), \qquad m \in \mathbb{N}_0, \tag{5.54}$$

where parameter ξ_m is updated as follows

$$\xi_0 = d_0, \quad \xi_{m+1} = \inf\{d_c \,|\, d_c > \xi_m,\, d_c > d_{c-1} + \sigma_{c-1} + g\}.$$

Additionally, parameter ν_m is defined as

$$\nu_m = \sum_{\substack{c \in \mathbb{N}_0, \\ \xi_m \leq d_c < \xi_{m+1}}} |\bar{D}_c \backslash \bar{D}_{c+1}|. \tag{5.55}$$

Conceptually speaking, Z_m determines the m-th effective DoS interval which has no overlap with Z_{m-1} and Z_{m+1}. Based on Z_m, define the union of all effective and

disjoint attack intervals for $t \in [t_1, t_2)$ as

$$\bar{\mathcal{D}}(t_1, t_2) = \bigcup_{m \in \mathbb{N}_0} Z_m \cap [t_1, t_2]. \tag{5.56}$$

The complement of Z_m is W_m, which represents healthy intervals. More precisely,

$$W_{-1} = [0, \xi_0), \quad W_m = [\xi_m + \nu_m, \xi_{m+1}). \tag{5.57}$$

The union of all healthy intervals for $t \in [t_1, t_2)$ where ideal operation is guaranteed is given as follows

$$\bar{\mathcal{H}}(t_1, t_2) = \bigcup_{m \in \mathbb{N}_0} W_{m-1} \cap [\, t_1, t_2\,]. \tag{5.58}$$

Fig. 5.5 provides a schematic time diagram for the operation of ROCCET.

Let $|\bar{\mathcal{D}}(t_1, t_2)|$ and $|\bar{\mathcal{H}}(t_1, t_2)|$, respectively, denote the accumulative length of corresponding intervals for $t \in [t_1, t_2)$. Since $\bar{\mathcal{H}}(t_1, t_2)$ and $\bar{\mathcal{D}}(t_1, t_2)$ are complements of each other, the following expression holds true

$$|\bar{\mathcal{H}}(t_1, t_2)| = t_2 - t_1 - |\bar{\mathcal{D}}(t_1, t_2)|, \quad t_1 \leq t_2. \tag{5.59}$$

Inequality $|\bar{D}_c| \leq |D_c| + g$, $(c \in \mathbb{N}_0)$, holds true by construction and can be verified from Fig. 5.5. Considering t_1 and t_2 $(t_1 \leq t_2)$, the latter inequality gives way to the following relationship

$$|\bar{\mathcal{D}}(t_1, t_2)| \leq |\mathcal{D}(t_1, t_2)| + c(t_1, t_2) g. \tag{5.60}$$

5.3.5 Closed-loop system

Define the following global vectors

$$\begin{aligned} &\boldsymbol{x} = [\boldsymbol{x}_1^T(t), \ldots, \boldsymbol{x}_N^T(t)]^T, \ \tilde{\boldsymbol{x}} = [\boldsymbol{x}_1^T(t_k^1), \ldots, \boldsymbol{x}_N^T(t_k^N)]^T, \ \boldsymbol{e} = [\boldsymbol{e}_1^T(t), \ldots, \boldsymbol{e}_N^T(t)]^T, \\ &\boldsymbol{\eta} = [\eta_1(t), \ldots, \eta_N(t)]^T, \ \mathbb{X} = [\mathbb{X}_1^T(t), \ldots, \mathbb{X}_N^T(t)]^T, \boldsymbol{\Lambda} = \mathrm{diag}(\boldsymbol{\Lambda}_1(t), \ldots, \boldsymbol{\Lambda}_N(t)), \\ &\bar{\mathbb{X}} = [\, \|\mathbb{X}_1(t)\|, \ldots, \|\mathbb{X}_N(t)\| \,]^T. \end{aligned} \tag{5.61}$$

During $t \in Z_m$, the control input cannot be updated and remains zero. The control protocol can be viewed as follows

$$\boldsymbol{u}_i(t) = \begin{cases} \boldsymbol{K}\, \mathbb{X}_i(t), & t \in W_m, \\ \boldsymbol{0}, & t \in Z_m. \end{cases} \tag{5.62}$$

Considering both the healthy (W_m) and attack intervals (Z_m), the dynamic variable $\eta_i(t)$ is re-formulated as

$$\dot{\eta}_i(t) = \begin{cases} -\phi_4\, \eta_i(t) + \phi_5\, \|\mathbb{X}_i(t)\|, & t \in W_m, \\ 0, & t \in Z_m. \end{cases} \tag{5.63}$$

From (4.1) and (5.62), the closed-loop MAS is given below

$$\dot{\boldsymbol{x}}(t) = \begin{cases} (\boldsymbol{I}_N \otimes \boldsymbol{A} + \boldsymbol{L} \otimes \boldsymbol{B}\boldsymbol{K})\, \boldsymbol{x}(t) + \boldsymbol{L} \otimes \boldsymbol{B}\boldsymbol{K}\, \boldsymbol{e}(t), & t \in W_m, \\ (\boldsymbol{I}_N \otimes \boldsymbol{A})\, \boldsymbol{x}(t), & t \in Z_m. \end{cases} \tag{5.64}$$

To guarantee consensus in (5.64) the same state transformation used in (4.10) is used. This transformation is given below for ease of reference

$$\boldsymbol{r}(t) = (\tilde{\boldsymbol{W}} \otimes \boldsymbol{I}_n)\, \boldsymbol{x}(t). \tag{5.65}$$

It is proved in [100] that consensus is achieved in (5.64) iff $\lim_{t\to\infty} \boldsymbol{r}(t) = 0$. Using (5.65), system (5.64) is converted to

$$\dot{\boldsymbol{r}}(t) = \begin{cases} (\boldsymbol{I}_{N-1} \otimes \boldsymbol{A} + \tilde{\boldsymbol{J}} \otimes \boldsymbol{B}\boldsymbol{K})\, \boldsymbol{r}(t) + \tilde{\boldsymbol{J}}\tilde{\boldsymbol{W}} \otimes \boldsymbol{B}\boldsymbol{K}\, \boldsymbol{e}(t), & t \in W_m, \\ (\boldsymbol{I}_{N-1} \otimes \boldsymbol{A})\, \boldsymbol{r}(t), & t \in Z_m, \end{cases} \tag{5.66}$$

where $\tilde{\boldsymbol{J}} = \mathrm{diag}(\lambda_2, \ldots, \lambda_N)$.

5.3.6 Parameter design

This section develops an optimization algorithm that co-designs the control and DET parameters. In order to make the derivations easier to follow, the optimization for parameter design is presented in two theorems.

- Considering that there is no DoS attacks, Theorem 5.4 develops an optimization algorithm to co-design all unknown control and DET gains based on a given desired rate for consensus convergence.
- Based on Theorem 5.4, Theorem 5.5 studies the impact of DoS on the MAS and includes a *desired* level of tolerance to unknown DoS attacks within the co-design optimization.

Optimization: General framework

Initially, no DoS attack is considered in the setup. Theorem 5.5 extends the framework to incorporate DoS attacks. The optimization requires the eigenvalues and eigenvectors of the Laplacian matrix $\boldsymbol{L}$, which can be computed from Algorithm 3.4.

Theorem 5.4. Given a desired convergence rate ζ, the control gain and DET parameters are computed as follows

$$\begin{aligned} &\boldsymbol{K} = \boldsymbol{\Omega}\boldsymbol{P}^{-1}, \quad \boldsymbol{\Phi}_1 = (\boldsymbol{P}^{-1}\boldsymbol{S}_1\boldsymbol{P}^{-1})^{1/2}, \quad \phi_2 = \frac{1}{\sqrt{s_2}}, \\ &\phi_3 = \sqrt{s_3}, \qquad \phi_4 = s_4, \qquad \phi_5 = \frac{1}{\sqrt{s_5}}. \end{aligned} \tag{5.67}$$

The validity of (5.67) is conditioned on the existence of positive definite matrices $\boldsymbol{P}_{n\times n}>0$, $\boldsymbol{S}_{1_{n\times n}}>0$, matrix $\boldsymbol{\Omega}_{m\times n}$, positive scalars $s_j>0$, $(2\leq j\leq 5)$, and $\theta_c>0$, $(1\leq c\leq 7)$, satisfying the following constrained optimization

$$\min \qquad \mathbb{F}=\sum_{c=1}^{7}\theta_c, \tag{5.68}$$

subject to:

$$\boldsymbol{\Psi}=\begin{bmatrix}\boldsymbol{\Psi}_{11} & \boldsymbol{\Psi}_{12}\\ * & \boldsymbol{\Psi}_{22}\end{bmatrix}<0, \tag{5.69}$$

$$\boldsymbol{C}_1=\begin{bmatrix}\theta_1\boldsymbol{I} & \boldsymbol{I}\\ * & \boldsymbol{P}\end{bmatrix}>0,\quad \boldsymbol{C}_2=\begin{bmatrix}-\theta_2\boldsymbol{I} & \boldsymbol{S}_1\\ * & -\boldsymbol{I}\end{bmatrix}<0,\quad \boldsymbol{C}_3=\begin{bmatrix}-\theta_3 & s_2\\ * & -1\end{bmatrix}<0,\quad \boldsymbol{C}_4=\begin{bmatrix}\theta_4 & 1\\ * & s_3\end{bmatrix}>0,$$
$$\boldsymbol{C}_5=\begin{bmatrix}-\theta_5 & s_4\\ * & -1\end{bmatrix}<0,\quad \boldsymbol{C}_6=\begin{bmatrix}-\theta_6 & s_5\\ * & -1\end{bmatrix}<0,\quad \boldsymbol{C}_7=\begin{bmatrix}-\theta_7\boldsymbol{I} & \boldsymbol{\Omega}\\ * & -\boldsymbol{I}\end{bmatrix}<0, \tag{5.70}$$

where

$$\boldsymbol{\Psi}_{11}=\begin{bmatrix}\boldsymbol{\psi}_{11} & \tilde{\boldsymbol{J}}\tilde{\boldsymbol{W}}\otimes\boldsymbol{B}\boldsymbol{\Omega} & \boldsymbol{0}\\ * & -\boldsymbol{I}_N\otimes\boldsymbol{S}_1 & \boldsymbol{0}\\ * & * & (1-2s_4+s_3+\zeta)\boldsymbol{I}_N\end{bmatrix},$$
$$\boldsymbol{\Psi}_{12}=\begin{bmatrix}\sqrt{2}\tilde{\boldsymbol{J}}\otimes\boldsymbol{P} & \sqrt{2}\tilde{\boldsymbol{J}}\otimes\boldsymbol{P} & \boldsymbol{0} & \boldsymbol{0}\\ \boldsymbol{0} & \boldsymbol{0} & \sqrt{2}\lambda_N\boldsymbol{I}_N\otimes\boldsymbol{P} & \sqrt{2}\lambda_N\boldsymbol{I}_N\otimes\boldsymbol{P}\\ \boldsymbol{0} & \boldsymbol{0} & \boldsymbol{0} & \boldsymbol{0}\end{bmatrix},$$
$$\boldsymbol{\Psi}_{22}=\mathrm{diag}(-s_2\boldsymbol{I}_{(N-1)n},-s_5\boldsymbol{I}_{(N-1)n},-s_2\boldsymbol{I}_{Nn},-s_5\boldsymbol{I}_{Nn}),$$

and $\boldsymbol{\psi}_{11}=\boldsymbol{I}_{N-1}\otimes(\boldsymbol{A}\boldsymbol{P}+\boldsymbol{P}\boldsymbol{A}^T+\zeta\boldsymbol{P})+\tilde{\boldsymbol{J}}\otimes\boldsymbol{B}\boldsymbol{\Omega}+(\tilde{\boldsymbol{J}}\otimes\boldsymbol{B}\boldsymbol{\Omega})^T$. Using (5.67), the convergence rate of $\boldsymbol{r}(t)$ satisfies

$$\lambda_{\min}(\boldsymbol{P}^{-1})\boldsymbol{r}^T(t)\,\boldsymbol{r}(t)+\,\boldsymbol{\eta}^T(t)\,\boldsymbol{\eta}(t)\leq\mu e^{-\zeta t}, \tag{5.71}$$

where $\mu=\lambda_{\max}(\boldsymbol{P}^{-1})\,\boldsymbol{r}^T(0)\,\boldsymbol{r}(0)+\,\boldsymbol{\eta}^T(0)\,\boldsymbol{\eta}(0)$. By minimization of the objective function $\mathbb{F}$, the following bounds are guaranteed

$$\|\boldsymbol{K}\|\leq\theta_1\sqrt{\theta_7},\quad \|\boldsymbol{\Phi}_1\|\leq\theta_1\theta_2^{1/4},\quad \phi_2\geq\frac{1}{\sqrt{\theta_3}},\quad \phi_3\geq\frac{1}{\sqrt{\theta_4}},\quad \phi_4\leq\sqrt{\theta_5},\quad \phi_5\geq\frac{1}{\sqrt{\theta_6}}. \tag{5.72}$$

Proof. Proof of Theorem 5.4 is given in Appendix, Section 5.5.4. □

Optimization: Extension to DoS Attacks

The next theorem extends the optimization framework to cope with DoS attacks. A desired level of resilience to DoS is included as a given parameter.

Theorem 5.5. Select desired values for ideal convergence rate ζ, DoS resilience level $\gamma<1$, and period g for transmission attempts during DoS intervals. Let $\beta=\frac{\zeta(1-\gamma)}{\gamma}$. If there exist positive definite matrices $\boldsymbol{P}_{n\times n}>0$, $\boldsymbol{S}_{1_{n\times n}}>0$, matrix $\boldsymbol{\Omega}_{m\times n}$,

positive scalars $s_j > 0$, $(2 \leq j \leq 5)$, and $\theta_c > 0$, $(1 \leq c \leq 7)$, satisfying

$$\min \qquad \mathbb{F} = \sum_{c=1}^{7} \theta_c, \tag{5.73}$$

subject to:

$$\begin{aligned} &\boldsymbol{\Psi} < 0, \quad \boldsymbol{C}_1 > 0, \quad \boldsymbol{C}_2 < 0, \quad \boldsymbol{C}_3 < 0, \quad \boldsymbol{C}_4 > 0, \quad \boldsymbol{C}_5 < 0, \quad \boldsymbol{C}_6 < 0, \quad \boldsymbol{C}_7 < 0, \\ &\boldsymbol{A}\boldsymbol{P} + \boldsymbol{P}\boldsymbol{A}^T - \beta \boldsymbol{P} < 0. \end{aligned} \tag{5.74}$$

with $\boldsymbol{\Psi}$ and $\boldsymbol{C}_i$, $(1 \leq i \leq 7)$, defined in Theorem 5.4, then control gain $\boldsymbol{K}$ and DET gains $\boldsymbol{\Phi}_1$ and ϕ_2 to ϕ_5 are computed from the same equations given in (5.67). These parameters make MAS (5.66) resilient to DoS attacks satisfying

$$\frac{1}{T_1} + \frac{g}{F_1} < \gamma. \tag{5.75}$$

Using design parameters (5.67), system trajectories satisfy

$$\lambda_{\min}(\boldsymbol{P}^{-1}) \boldsymbol{r}^T(t)\, \boldsymbol{r}(t) + \boldsymbol{\eta}^T(t)\, \boldsymbol{\eta}(t) \leq \mu \rho\, e^{-\bar{\zeta} t}, \tag{5.76}$$

where $\mu = \lambda_{\max}(\boldsymbol{P}^{-1})\, \boldsymbol{r}^T(0)\, \boldsymbol{r}(0) + \boldsymbol{\eta}^T(0)\, \boldsymbol{\eta}(0)$ and

$$\rho = e^{(\zeta+\beta)(T_0 + g F_0)}, \qquad \bar{\zeta} = \zeta - (\zeta + \beta)\left(\frac{1}{T_1} + \frac{g}{F_1}\right). \tag{5.77}$$

Proof. Proof of Theorem 5.5 is given in Appendix, Section 5.5.5. □

Remark 5.12 (Design trade-offs in ROCCET)**.** Based on Theorem 5.5, the trade-off between the consensus convergence rate, frequency of transmissions, and tolerable strength of DoS attacks in ROCCET can be controlled as follows: As stated previously, optimization (5.73) is based on increasing MIET (5.51) with respect to the desired 'ideal' consensus convergence rate ζ. With higher values for ζ, computed parameters from optimization (5.73) tend to accelerate the rate of consensus convergence at the expense of more frequent transmissions. Converse statements are also true for smaller values of ζ. The desired resilience level to DoS (i.e., γ) provides an additional degree of freedom to control resilience to DoS attacks. By construction, increasing γ makes the MAS more resilient to DoS.

Remark 5.13 (Computation complexity of parameter design in PEC, PSEC, R-PSEC, and ROCCET)**.** Dimensions of the LMIs developed in PEC, PSEC, R-PSEC, and ROCCET are all dependent on the number size N. Thus, the computational complexity of the design state in all three implementations grows with N. As previously mentioned in Remark 3.11, this growth is in the order of $O(N^3)$. This remains as a future work to relax the dependency of the parameter design stage with preferably minimum loss to the advantageous features of the implementations.

Remark 5.14 (Extension to the leader-following consensus)**.** The proposed implementations in this chapter and Chapter 4 can be extended to the leader-following

Table 5.2: Comparison of different proposed ETC implementations.

Characteristics	**RQ-CEASE** [79]	**R-PSEC**	**ROCCET** [82]
Transmitter scheme	Sampled-data Event-triggered	Sampled-data Event-triggered	Event-triggered
Receiver scheme	Periodic	Periodic	Continuous-time
State Measurement scheme	Periodic	Periodic	Continuous-time
Control scheme	Sampled-data Event-triggered	Periodic	Continuous-time
Event monitoring	Periodic	Periodic	Continuous-time
Optimization for Design Parameters	No	No	Yes
Steady-state error	Yes	No	No
State Quantization	Yes	No	No
Control gain Design	No	Yes	Yes
Relative expected number of transmissions	High	Medium	Very Low
Resilience to DoS attacks	Yes	Yes	Yes
Network Topology	Undirected	Undirected	Undirected

consensus, where all agents (followers) are supposed to follow a certain agent labeled as the leader [148]. Two conditions are required for the leader following consensus: (i) The communication topology should contain a directed spanning tree with the leader as the root. (ii) While some nodes receive information from the leader, the leader does not receive information from any of the followers. The second condition implies that the leader is autonomous in its behaviour and does not interact with any of the followers. Therefore, the associated Laplacian matrix has a row with all entries equal zero.

5.4 Summary

This chapter proposes three resilient implementations for event-triggered consensus (ETC) in the presence of unknown denial of service (DoS) attacks. RQ-CEASE can be regarded as the extended version of Q-CEASE, which deals with unknown DoS attacks.

R-PSEC extends PSEC for the situation where the MAS is subject to unknown but bounded DoS attacks. R-PSEC includes a desired level of resilience to DoS, and the unknown control and ET parameters are computed based on the desired level of resilience. The parameter design in R-PSEC is a co-design LMI framework.

ROCCET deals with unknown DoS attacks in a similar fashion to R-PSEC. However, ROCCET benefits from a dynamic-event triggering (DET) scheme to further reduce the number of transmissions and computes required control and ET parameters based on an optimization. State measurement and monitoring of the ET condition in

ROCCET is continuous-time. Table 5.2 summarizes the main features of RQ-CEASE, R-PSEC, and ROCCET.

5.5 Appendix

In this section, the proofs of the theorems proposed in Chapter 5 are provided.

5.5.1 Proof of Theorem 5.1

Proof. Consider the following Lyaponuv candidate for (5.20)

$$V(t) = 0.5\, \boldsymbol{r}^T(t)\, \boldsymbol{r}(t). \tag{5.78}$$

Step I. Analysis for healthy intervals. Let $t \in W_m$. The time evolution of $\boldsymbol{r}(t)$ in healthy intervals is generated from (5.20) and is given below

$$\boldsymbol{r}(t) = -(t-nh)\boldsymbol{L}\,(\,\boldsymbol{r}_n + \boldsymbol{e}_n + \hat{\boldsymbol{\delta}}_n\,) + \boldsymbol{r}_n. \tag{5.79}$$

Using (5.79), the time derivative of $V(t)$ is expanded

$$\begin{aligned}\dot{V}(t) &= (t-nh)(\boldsymbol{r}_n+\boldsymbol{e}_n+\hat{\boldsymbol{\delta}}_n)^T\boldsymbol{L}^T\boldsymbol{L}(\boldsymbol{r}_n+\boldsymbol{e}_n+\hat{\boldsymbol{\delta}}_n)-\boldsymbol{r}_n^T\boldsymbol{L}(\boldsymbol{r}_n+\boldsymbol{e}_n+\hat{\boldsymbol{\delta}}_n)\\ &\leq h\lambda_N^2(\|\boldsymbol{r}_n\|+\|\boldsymbol{e}_n\|+\|\hat{\boldsymbol{\delta}}_n\|)^2-\lambda_2\|\boldsymbol{r}_n\|^2+\lambda_N\|\boldsymbol{r}_n\|\,\|\boldsymbol{e}_n\|+\lambda_N\|\boldsymbol{r}_n\|\,\|\hat{\boldsymbol{\delta}}_n\|.\end{aligned} \tag{5.80}$$

According to ET condition (5.15) with (5.16), in healthy intervals it holds that $|e_i(nh)| \leq \phi\,|\mathbb{X}_i(nh)|\,,\ (i \in \mathcal{V})$. Collectively, it is true that $\|\boldsymbol{e}_n\| \leq \phi\,\|\boldsymbol{L}\boldsymbol{q}(\hat{\boldsymbol{x}}_n)\|$, or equivalently $\|\boldsymbol{e}_n\| \leq \phi\,\|\boldsymbol{L}\|\,\|\boldsymbol{r}_n+\boldsymbol{e}_n+\hat{\boldsymbol{\delta}}_n\|$. Under $\phi < \frac{1}{\lambda_N}$, the former condition leads to

$$\|\boldsymbol{e}_n\| \leq \theta_1\,(\,\|\boldsymbol{r}_n\| + \|\hat{\boldsymbol{\delta}}_n\|\,), \tag{5.81}$$

with θ_1 defined previously. From (5.80) and (5.81), and considering $\|\hat{\boldsymbol{\delta}}_n\| \leq \delta_\star$ the following inequality is obtained

$$\begin{aligned}\dot{V}(t) \leq \Big(&-\lambda_2 + h\lambda_N^2(1+\theta_1)^2+\theta_1\lambda_N\Big)\,\|\boldsymbol{r}_n\|^2\\ &+2\Big(h\lambda_N^2(\theta_1^2+\theta_1+1)+\lambda_N/2(1+\theta_1)\Big)\,\|\boldsymbol{r}_n\|\,\delta_\star.\end{aligned}$$

It holds that $2\,\|\boldsymbol{r}_n\|\,\delta_\star \leq \delta_\star\,\|\boldsymbol{r}_n\|^2 + \delta_\star$. This gives way to

$$\begin{aligned}\dot{V}(t) \leq\ &\|\boldsymbol{r}_n\|^2\,\Big(-\lambda_2 + h\lambda_N^2(1+\theta_1)^2+\theta_1\lambda_N+\delta_\star\,h\lambda_N^2(\theta_1^2+\theta_1+1)+\delta_\star\lambda_N/2(1+\theta_1)\Big)\\ &+\delta_\star\,\Big(h\lambda_N^2(\theta_1^2+\theta_1+1)+\lambda_N/2(1+\theta_1)\,\Big), \qquad t \in W_m.\end{aligned} \tag{5.82}$$

The following condition is derived from (5.82)

$$\dot{V}(t) \leq -\,\omega_1 V(nh) + C_1, \quad t \in W_m, \tag{5.83}$$

where $C_1 = \delta_\star\,(h\lambda_N^2(\theta_1^2+\theta_1+1)+\lambda_N/2(1+\theta_1)\,)$. With $V(nh) = V(t) - (t-nh)\dot{V}(t)$,

(5.83) is revised as follows

$$\dot{V}(t) \leq -\omega_1 V(t) + C_2, \quad t \in W_m, \tag{5.84}$$

where $C_2 = \frac{C_1}{1-\omega_1 h}$. Inequality (5.84) leads to

$$V(t) \leq e^{-\omega_1(t-\xi_m-\nu_m)} V(\xi_m + \nu_m) + C_3, \quad t \in W_m, \tag{5.85}$$

where $C_3 = \frac{C_2}{\omega_1}$.

Step II. Analysis for DoS intervals. Now, let $t \in Z_m$. From (5.20) and (5.78), $\dot{V}(t)$ is derived as follows

$$\dot{V}(t) = \Big(-\boldsymbol{L}\left(\hat{\boldsymbol{r}}(\xi_m) + \hat{\boldsymbol{\delta}}(\xi_m)\right)\Big)^T \boldsymbol{r}(t) \leq \lambda_N \left\|\hat{\boldsymbol{r}}(\xi_m)\right\| \left\|\boldsymbol{r}(t)\right\| + \lambda_N \left\|\hat{\boldsymbol{\delta}}(\xi_m)\right\| \left\|\boldsymbol{r}(t)\right\|. \tag{5.86}$$

At the start of Z_m it holds that $\|\boldsymbol{e}(\xi_m)\| \leq \phi \|\boldsymbol{L}\boldsymbol{q}(\hat{\boldsymbol{r}}(\xi_m))\|$. Considering $\|\boldsymbol{e}(\xi_m)\| = \|\hat{\boldsymbol{r}}(\xi_m) - \boldsymbol{r}(\xi_m)\|$, it is obtained that

$$\|\hat{\boldsymbol{r}}(\xi_m) - \boldsymbol{r}(\xi_m)\| \leq \phi_1 \lambda_N (\|\hat{\boldsymbol{r}}(\xi_m)\| + \delta_\star). \tag{5.87}$$

With $\|\hat{\boldsymbol{r}}(\xi_m)\| - \|\boldsymbol{r}(\xi_m)\| \leq \|\hat{\boldsymbol{r}}(\xi_m) - \boldsymbol{r}(\xi_m)\|$, one obtains the following upper-bound for (5.87)

$$\|\hat{\boldsymbol{r}}(\xi_m)\| \leq \theta_2 \|\boldsymbol{r}(\xi_m)\| + \theta_1 \delta_\star, \tag{5.88}$$

where θ_2 is previously defined. Using (5.88), the following inequality is obtained from (5.86)

$$\dot{V}(t) \leq \lambda_N \theta_2 \left\|\boldsymbol{r}(\xi_m)\right\| \left\|\boldsymbol{r}(t)\right\| + \delta_\star \lambda_N (\theta_1 + 1) \left\|\boldsymbol{r}(t)\right\|. \tag{5.89}$$

Based on the values of $\boldsymbol{r}(t)$ and $\boldsymbol{r}(\xi_m)$ the following two scenarios are possible: (i) $\|\boldsymbol{r}(t)\| \leq \|\boldsymbol{r}(\xi_m)\|$, and (ii) $\|\boldsymbol{r}(t)\| \geq \|\boldsymbol{r}(\xi_m)\|$. First, it is assumed that $\|\boldsymbol{r}(t)\| \leq \|\boldsymbol{r}(\xi_m)\|$. Including $2\|\boldsymbol{r}(t)\|\delta_\star \leq \delta_\star \|\boldsymbol{r}(t)\|^2 + \delta_\star$ in (5.89), leads to $\dot{V}(t) \leq \omega_2 V(\xi_m) + C_4$, where $C_4 = 0.5\delta_\star \lambda_N(\theta_1 + 1)$ and ω_2 is given previously. Under scenario (i), the solution of $\dot{V}(t)$ is given below

$$V(t) \leq \omega_2 (t - \xi_m)(V(\xi_m) + C_4) + V(\xi_m). \tag{5.90}$$

Alternatively, if $\|\boldsymbol{r}(\xi_m)\| \leq \|\boldsymbol{r}(t)\|$, (5.89) results in $\dot{V}(t) \leq \omega_2 V(t) + C_4$ which has the following solution

$$V(t) \leq e^{\omega_2(t-\xi_m)} V(\xi_m) + e^{\omega_2(t-\xi_m)} C_5, \quad t \in Z_m, \tag{5.91}$$

where $C_5 = \frac{1}{\omega_2} C_4$. Since $1 + \epsilon \leq e^\epsilon$, $\forall \epsilon \geq 0$, the upper-bound in (5.91) is larger than (5.90). Therefore, $V(t)$ is upper-bounded by the right hand side of (5.91) for $t \in Z_m$.

Step III. Merging Healthy and DoS intervals. Combining (5.85) and (5.91),

the following condition can be obtained for $t \geq 0$, [32],

$$V(t) \leq e^{-\omega_1|\bar{\mathcal{H}}(0,t)|}e^{\omega_2|\bar{\mathcal{D}}(0,t)|}V(0) + C + 2C \sum_{\substack{m\in\mathbb{N}_0 \\ \xi_m \leq t}} e^{-\omega_1|\bar{\mathcal{H}}(\xi_m+v_m,t)|}e^{\omega_2|\bar{\mathcal{D}}(\xi_m,t)|}, \tag{5.92}$$

where $C = \max\{C_3, C_5\}$. From (5.7), (5.8), (5.12), and (5.13), the following upper-bound holds true

$$e^{-\omega_1|\bar{\mathcal{H}}(0,t)|}e^{\omega_2|\bar{\mathcal{D}}(0,t)|} \leq \eta_1\, e^{-\zeta_1 t}, \tag{5.93}$$

with η_1 and ζ_1 given in (5.23). Additionally, the summation in (5.92) lies withing the following bound [32, Lemma 4]

$$\sum_{\substack{m\in\mathbb{N}_0 \\ \xi_m \leq t}} e^{-\omega_1|\bar{\mathcal{H}}(\xi_m+v_m,t)|}e^{\omega_2|\bar{\mathcal{D}}(\xi_m,t)|} \leq \eta_1 \frac{e^{\zeta_1 F_0 F_1}}{1 - e^{-\zeta_1 F_1}}. \tag{5.94}$$

From (5.78), (5.93), and (5.94), expression (5.92) is revised:

$$\|\boldsymbol{r}(t)\| \leq \eta_1^{\frac{1}{2}}\, e^{-\frac{\zeta_1}{2}t}\, \|\boldsymbol{r}(0)\| + \sqrt{C}\left(1 + 2\eta_1 \frac{e^{\zeta_1 F_0 F_1}}{1 - e^{-\zeta_1 F_1}}\right)^{\frac{1}{2}}. \tag{5.95}$$

System (5.20) is ISS if $\zeta_1 > 0$. Two conditions are necessary for ζ_1 to be strictly positive: (i) $\omega_1 > 0$, and (ii) $\omega_1 > (\omega_1 + \omega_2)(\frac{1}{T_1} + \frac{h}{F_1})$. Condition (i) is satisfied if $a_0 > 0$ which leads to $h_{\max}$ and $\phi_{\max}$. Based on condition (ii), one concludes $\frac{1}{T_1} + \frac{h}{F_1} < \Omega_1$. It can be shown that $\max\{C_4, C_5\} = C_4$. The proof is complete by defining $C = C_4$. □

5.5.2 Proof of Theorem 5.2

Proof. Following (5.78), (5.79), and (5.80), the proof follows the same steps used in Theorem 5.1.

Step I. Let $t \in W_m$. According to (5.15) with the static threshold (5.17), it holds that $|e_i(nh)| \leq \phi$, $(i \in \mathcal{V})$, which leads to the following inequality in the global sense

$$\|\boldsymbol{e}_n\| \leq \phi_\star, \tag{5.96}$$

where $\phi_\star$ is given previously. Also $\|\hat{\boldsymbol{\delta}}_n\| \leq \delta_\star$. The following inequality is obtained from (5.80) and (5.96) for $t \in W_m$

$$\begin{aligned} \dot{V}(t) \leq & \left(h\lambda_N^2 - \lambda_2\right)\|\boldsymbol{r}_n\|^2 + \left(h\lambda_N^2 + \lambda_N\right)\|\boldsymbol{r}_n\|\,\delta_\star \\ & + \left(h\lambda_N^2 + \lambda_N\right)\|\boldsymbol{r}_n\|\,\phi_\star + h\lambda_N^2(\phi_\star + \delta_\star)^2. \end{aligned} \tag{5.97}$$

It holds that $2\|\boldsymbol{r}_n\|\,\delta_\star \leq \delta_\star\|\boldsymbol{r}_n\|^2 + \delta_\star$, and $2\|\boldsymbol{r}_n\|\,\phi_\star \leq \phi_\star\|\boldsymbol{r}_n\|^2 + \phi_\star$. Including these two inequalities in (5.97) leads to the following inequality for $t \in W_m$

$$\dot{V}(t) \leq -\omega_3 V(nh) + R_1, \tag{5.98}$$

where $R_1 = h\lambda_N^2(\delta_\star + \phi_\star)^2 + \lambda_N(h\lambda_N + 1)(\delta_\star + \phi_\star)$. With $V(nh) = V(t) - (t - nh)\dot{V}(t)$,

(5.98) is revised as follows

$$\dot{V}(t) \leq -\omega_3 V(t) + R_2, \quad (t \in W_m), \tag{5.99}$$

where $R_2 = \frac{R_1}{1-\omega_3 h}$.

Step II. Let $t \in Z_m$ for which $\dot{V}(t)$ is given in (5.86). At the start of Z_m it holds that $\|\boldsymbol{e}(\xi_m)\| \leq \phi_\star$ or equivalently $\|\hat{\boldsymbol{r}}(\xi_m) - \boldsymbol{r}(\xi_m)\| \leq \phi_\star$. Based on the former inequality, the following condition is obtained

$$\|\hat{\boldsymbol{r}}(\xi_m)\| \leq \phi_\star + \|\boldsymbol{r}(\xi_m)\|. \tag{5.100}$$

Using (5.100), the following inequality is obtained from (5.86)

$$\dot{V}(t) \leq \lambda_N \|\boldsymbol{r}(t)\| (\phi_\star + \|\boldsymbol{r}(\xi_m)\|) + \lambda_N \delta_\star \|\boldsymbol{r}(t)\|. \tag{5.101}$$

First, it is assumed that $\|\boldsymbol{r}(t)\| \leq \|\boldsymbol{r}(\xi_m)\|$ which results in the following inequality based on (5.101)

$$\dot{V}(t) \leq \omega_4 V(\xi_m) + R_3, \tag{5.102}$$

where $R_3 = \lambda_N(\delta_\star/2 + \phi_\star/2)$. Alternatively, if $\|\boldsymbol{r}(\xi_m)\| \leq \|\boldsymbol{r}(t)\|$, the following inequality is derived from (5.101)

$$\dot{V}(t) \leq \omega_4 V(t) + R_3. \tag{5.103}$$

Step III. Similar to Theorem 5.1, the solution of (5.103) is the comprehensive upper bound for $\dot{V}(t)$ when $t \in Z_m$. To derive stability conditions for $t \geq 0$, the same steps given in (5.92) to (5.94) are followed, which results in f_3 and f_4 given in (5.25). Two conditions are necessary for f_3 to be a class $\mathcal{KL}$ function: (i) $\omega_3 > 0$, and (ii) $\omega_3 > (\omega_3 + \omega_4)(\frac{1}{T_1} + \frac{h}{F_1})$. Condition (i) includes both h and ϕ. Based on condition (ii), inequality $\frac{1}{T_1} + \frac{h}{F_1} < \frac{\omega_3}{\omega_3+\omega_4}$ must be satisfied which completes the proof. □

5.5.3 Proof of Theorem 5.3

Proof. The proof is given in two steps.

Step I. Stability analysis in the presence of DoS: Let $d(t) \triangleq t - t_k$ represent an artificial time-varying time-delay that satisfies $0 \leq d(t) < h$. Using $d(t)$, system (5.40) is given below

$$\dot{\boldsymbol{\psi}}(t) = \begin{cases} (\boldsymbol{I}_{N-1} \otimes \boldsymbol{A})\boldsymbol{\psi}(t) + (\tilde{\boldsymbol{J}} \otimes \boldsymbol{B}(\boldsymbol{K} + \boldsymbol{\Delta}_k))\, \boldsymbol{\psi}(t - d(t)) \\ +(\tilde{\boldsymbol{J}}\tilde{\boldsymbol{W}} \otimes \boldsymbol{B}(\boldsymbol{K} + \boldsymbol{\Delta}_k))\, \boldsymbol{e}(t - d(t)), & t \in W_m, \\ \\ (\boldsymbol{I}_{N-1} \otimes \boldsymbol{A})\boldsymbol{\psi}(t), & t \in Z_m. \end{cases} \tag{5.104}$$

Consider LKF (4.56). From Theorem 4.3 with given ζ and LMIs $\boldsymbol{C}_1 < 0$, $\boldsymbol{C}_2 \geq 0$, and $\boldsymbol{C}_3 \geq 0$, it is guaranteed that $\dot{V}(t) < -\zeta V(t)$ for healthy intervals ($t \in W_m$). This

leads to

$$V(t) \leq e^{-\zeta(t-\xi_m-\nu_m)} V(\xi_m+\nu_m), \quad t \in W_m. \tag{5.105}$$

In the presence of DoS ($t \in Z_m$), system (5.104) is open loop and its states may diverge. In other words, there exists a positive scalar β such that $\dot{V}(t) < \beta V(t)$ for $t \in Z_m$. This inequality is expanded as follows

$$V(t) \leq e^{\beta(t-\xi_m)} V(\xi_m), \quad t \in Z_m. \tag{5.106}$$

By combining (5.105) and (5.106) the stability condition is obtained. If $t \in Z_m$, the following sequence of inequalities hold

$$\begin{aligned} V(t) \leq & e^{\beta(t-\xi_m)} V(\xi_m) \\ \leq & e^{\beta(t-\xi_m)} \left(e^{-\zeta(\xi_m-\xi_{m-1}-\nu_{m-1})} V(\xi_{m-1}+\nu_{m-1}) \right) \\ \leq & e^{\beta(t-\xi_m)} e^{-\zeta(\xi_m-\xi_{m-1}-\nu_{m-1})} e^{\beta(\xi_{m-1}+\nu_{m-1}-\xi_{m-2})} V(\xi_{m-2}) \\ \leq & \dots \\ \leq & e^{-\zeta|\bar{\mathcal{H}}(0,t)|} e^{\beta|\bar{\mathcal{D}}(0,t)|} V(0). \end{aligned} \tag{5.107}$$

From (5.29), (5.30), (5.38), and (5.39), it holds that

$$e^{-\zeta|\bar{\mathcal{H}}(0,t)|} e^{\beta|\bar{\mathcal{D}}(0,t)|} \leq \rho\, e^{-\bar{\zeta}t}, \tag{5.108}$$

with ρ and $\bar{\zeta}$ given in (5.46) [1]. Condition (5.108) gives way to

$$V(t) < \rho e^{-\bar{\zeta}t} V(0), \quad t \geq 0, \tag{5.109}$$

which is equivalent to (5.45). Let $\gamma = \zeta/(\zeta+\beta)$. Based on (5.109), if DoS attacks satisfy $(\frac{1}{T_1} + \frac{g}{F_1}) < \gamma$, system (5.104) is exponentially stable. Parameter γ is referred to as the DoS resilience, since its value defines the upper-bound for tolerable amount of DoS.

Step II. Parameter design with given DoS resilience: For healthy intervals ($t \in W_m$), the parameter design based on LKF (4.56) leads to the LMIs $\boldsymbol{C}_1 < 0$, $\boldsymbol{C}_2 \geq 0$, and $\boldsymbol{C}_3 \geq 0$ given in (5.41). Next, consider DoS intervals ($t \in Z_m$). Let $\gamma = \zeta/(\zeta+\beta)$ be a given DoS resilience level. Hence, $\beta = \frac{\zeta(1-\gamma)}{\gamma}$. The following expressions are considered for the derivatives of LKF (4.56) in $t \in Z_m$

$$\begin{aligned} \dot{V}_1 =& 2\dot{\boldsymbol{\psi}}^T(t)(\boldsymbol{I}_{N-1} \otimes \bar{\boldsymbol{P}})\boldsymbol{\psi}(t), \qquad \dot{V}_2 \leq \boldsymbol{\psi}^T(t)(\boldsymbol{I}_{N-1} \otimes \bar{\boldsymbol{Q}})\boldsymbol{\psi}(t), \\ \dot{V}_3 \leq & h^2 \dot{\boldsymbol{\psi}}^T(t)(\boldsymbol{I}_{N-1} \otimes \bar{\boldsymbol{Z}})\dot{\boldsymbol{\psi}}(t). \end{aligned} \tag{5.110}$$

The following null expression holds based on (5.104)

$$2\Big(\boldsymbol{\psi}^T(t)\boldsymbol{I}_{N-1} \otimes \boldsymbol{H}^{-1} + \dot{\boldsymbol{\psi}}^T(t)\boldsymbol{I}_{N-1} \otimes \boldsymbol{H}^{-1}\Big)\Big(\boldsymbol{I}_{N-1} \otimes \boldsymbol{A}\boldsymbol{\psi}(t) - \dot{\boldsymbol{\psi}}(t)\Big) = 0. \tag{5.111}$$

[1] It is straightforward to show that (5.107) also holds if $t \in W_m$.

Form (5.110), the following condition holds

$$\dot{V} - \beta V = \sum_{i=1}^{3} \dot{V}_i - \beta \sum_{i=1}^{3} V_i \leq \sum_{i=1}^{3} \dot{V}_i - \beta V_1. \tag{5.112}$$

Considering (5.110) and (5.111), expression (5.112) is revised as follows

$$\sum_{i=1}^{3} \dot{V}_i - \beta V_1 = \boldsymbol{\nu}_1^T (\bar{\boldsymbol{C}}_4 \otimes \boldsymbol{I}_{N-1}) \boldsymbol{\nu}_1, \tag{5.113}$$

where $\boldsymbol{\nu}_1 = [\boldsymbol{\psi}^T(t),\, \dot{\boldsymbol{\psi}}^T(t)]^T$ and

$$\bar{\boldsymbol{C}}_4 = \begin{bmatrix} \bar{\boldsymbol{c}}_1 & (\boldsymbol{H}^{-1}\boldsymbol{A})^T - \boldsymbol{H}^{-1} + \bar{\boldsymbol{P}} \\ * & h^2 \bar{\boldsymbol{Z}} - \boldsymbol{H}^{-1} - (\boldsymbol{H}^{-1})^T \end{bmatrix}, \tag{5.114}$$

with

$$\bar{\boldsymbol{c}}_1 = \boldsymbol{H}^{-1}\boldsymbol{A} + (\boldsymbol{H}^{-1}\boldsymbol{A})^T - \beta \bar{\boldsymbol{P}} + \bar{\boldsymbol{Q}}. \tag{5.115}$$

Considering (5.112) and (5.113), one concludes that if $\bar{\boldsymbol{C}}_4 < 0$, then $\dot{V}(t) - \beta V(t) < 0$ is guaranteed for $t \in Z_m$. As shown previously, combining $\dot{V}(t) + \zeta V(t) < 0$ for $t \in W_m$ and $\dot{V}(t) - \beta V(t) < 0$ for $t \in Z_m$ leads to (5.45). Pre- and post multiply $\bar{\boldsymbol{C}}_4$ by $\boldsymbol{T}$ and $\boldsymbol{T}^T$, where $\boldsymbol{T} = \boldsymbol{I}_2 \otimes \boldsymbol{H}$. Considering the same alternative variables used at the end of proof of Theorem 4.3 leads to LMI $\boldsymbol{C}_4 < 0$ given in (5.42). □

5.5.4 Proof of Theorem 5.4

Proof. To improve readability, the time argument t is removed in the proof. Global vectors used in the proof are defined in (5.61). Consider the following inequality

$$\dot{V} + \zeta\, V < 0, \tag{5.116}$$

where $V = V_1 + V_2$ with

$$V_1 = \boldsymbol{r}^T (\boldsymbol{I}_{N-1} \otimes \boldsymbol{P}^{-1})\, \boldsymbol{r}, \qquad V_2 = \boldsymbol{\eta}^T\, \boldsymbol{\eta}. \tag{5.117}$$

If (5.116) is guaranteed, condition (5.71) is satisfied.

Step I. (Time derivation of V): The time derivative for V_1 is obtained

$$\dot{V}_1 = \boldsymbol{r}^T\, \boldsymbol{\Xi}\, \boldsymbol{r} + 2\boldsymbol{r}^T\, (\tilde{\boldsymbol{J}}\tilde{\boldsymbol{W}} \otimes \boldsymbol{P}^{-1}\boldsymbol{B}\boldsymbol{K})\, \boldsymbol{e}, \tag{5.118}$$

where $\boldsymbol{\Xi} = \boldsymbol{I}_{N-1} \otimes (\boldsymbol{A}^T\boldsymbol{P}^{-1} + \boldsymbol{P}^{-1}\boldsymbol{A}) + 2\tilde{\boldsymbol{J}} \otimes \boldsymbol{P}^{-1}\boldsymbol{B}\boldsymbol{K}$. Expression $\dot{V}_2$ is expanded based on (5.50)

$$\dot{V}_2 = 2\, \boldsymbol{\eta}^T (-\phi_4\, \boldsymbol{\eta} + \phi_5 \bar{\mathbb{X}}). \tag{5.119}$$

From Young's inequality, it holds that $\boldsymbol{\eta}^T(\phi_5\bar{\mathbb{X}}) + (\phi_5\bar{\mathbb{X}})^T\boldsymbol{\eta} \leq \boldsymbol{\eta}^T\boldsymbol{\eta} + \phi_5^2\, \bar{\mathbb{X}}^T\bar{\mathbb{X}}$. In what follows, the upper-bound for (5.119) is obtained

$$\dot{V}_2 \leq (1 - 2\phi_4)\, \boldsymbol{\eta}^T\, \boldsymbol{\eta} + \phi_5^2\, \bar{\mathbb{X}}^T\bar{\mathbb{X}}. \tag{5.120}$$

The global from of (5.47) can be viewed as $\mathbb{X} = \boldsymbol{L} \otimes \boldsymbol{I}_n \boldsymbol{\Lambda} \tilde{\boldsymbol{x}}$. From $\boldsymbol{e} = \boldsymbol{\Lambda}\tilde{\boldsymbol{x}} - \boldsymbol{x}$ and $\boldsymbol{L} = \tilde{\boldsymbol{W}}^\dagger \tilde{\boldsymbol{J}} \tilde{\boldsymbol{W}}$, one obtains that

$$\mathbb{X} = (\boldsymbol{L} \otimes \boldsymbol{I}_n)\boldsymbol{e} + (\tilde{\boldsymbol{W}}^\dagger \tilde{\boldsymbol{J}} \otimes \boldsymbol{I}_n)\boldsymbol{r}. \tag{5.121}$$

Next, expression $\bar{\mathbb{X}}^T \bar{\mathbb{X}}$ is expanded as follows

$$\begin{aligned} \bar{\mathbb{X}}^T \bar{\mathbb{X}} = \mathbb{X}^T \mathbb{X} \leq & \boldsymbol{e}^T (2\boldsymbol{L}^2 \otimes \boldsymbol{I}_n)\boldsymbol{e} + \boldsymbol{r}^T (2\tilde{\boldsymbol{J}}^2 \otimes \boldsymbol{I}_n)\boldsymbol{r} \\ \leq & 2\lambda_N^2 \boldsymbol{e}^T \boldsymbol{e} + \boldsymbol{r}^T (2\tilde{\boldsymbol{J}}^2 \otimes \boldsymbol{I}_n)\boldsymbol{r}. \end{aligned} \tag{5.122}$$

The following upper-bound holds from (5.120) and (5.122)

$$\dot{V}_2 \leq (1 - 2\phi_4)\boldsymbol{\eta}^T \boldsymbol{\eta} + 2\phi_5^2 \lambda_N^2 \boldsymbol{e}^T \boldsymbol{e} + \boldsymbol{r}^T (2\phi_5^2 \tilde{\boldsymbol{J}}^2 \otimes \boldsymbol{I}_n)\boldsymbol{r}. \tag{5.123}$$

Let $\boldsymbol{\nu} = [\, \boldsymbol{r}^T, \boldsymbol{e}^T, \boldsymbol{\eta}^T \,]^T$. From (5.118) and (5.123), expression (5.116) is re-arranged as

$$\boldsymbol{\nu}^T \boldsymbol{\Psi}_1 \boldsymbol{\nu} < 0, \tag{5.124}$$

where

$$\boldsymbol{\Psi}_1 = \begin{bmatrix} \boldsymbol{\Psi}_{1,11} & \tilde{\boldsymbol{J}}\tilde{\boldsymbol{W}} \otimes \boldsymbol{P}^{-1}\boldsymbol{B}\boldsymbol{K} & \boldsymbol{0} \\ * & 2\phi_5^2 \lambda_N^2 \boldsymbol{I}_{Nn} & \boldsymbol{0} \\ * & * & (1 - 2\phi_4 + \zeta)\boldsymbol{I}_N \end{bmatrix},$$

and $\boldsymbol{\Psi}_{1,11} = \boldsymbol{\Xi} + \zeta \boldsymbol{I}_{N-1} \otimes \boldsymbol{P}^{-1} + 2\phi_5^2 \tilde{\boldsymbol{J}}^2 \otimes \boldsymbol{I}_n$.

Step II. (Incorporation of DET (5.49)): From (5.49), it holds that $\|\boldsymbol{\Phi}_1 \boldsymbol{e}_i(t)\| \leq \phi_2 \|\mathbb{X}_i(t)\| + \phi_3 \eta_i(t)$. Let $\bar{\boldsymbol{e}} = [\, \|\boldsymbol{\Phi}_1 \boldsymbol{e}_1(t)\|, \ldots, \|\boldsymbol{\Phi}_1 \boldsymbol{e}_N(t)\| \,]^T$. In a collective manner it holds that $\bar{\boldsymbol{e}} \leq \phi_2 \bar{\mathbb{X}} + \phi_3 \boldsymbol{\eta}$. To include this condition in (5.124), the following quadratic constraint is developed

$$\bar{\boldsymbol{e}}^T \bar{\boldsymbol{e}} = \boldsymbol{e}^T (\boldsymbol{I}_N \otimes \boldsymbol{\Phi}_1^2)\boldsymbol{e} \leq \phi_2^2 \bar{\mathbb{X}}^T \bar{\mathbb{X}} + \phi_3^2 \boldsymbol{\eta}^T \boldsymbol{\eta}. \tag{5.125}$$

Using (5.122), inequality (5.125) is expanded in what follows

$$\boldsymbol{\nu}^T \boldsymbol{\Psi}_2 \boldsymbol{\nu} \geq 0, \tag{5.126}$$

where $\boldsymbol{\Psi}_2 = \operatorname{diag}\left(2\phi_2^2(\tilde{\boldsymbol{J}}^2 \otimes \boldsymbol{I}_n),\ -\boldsymbol{I}_N \otimes \boldsymbol{\Phi}_1^2 + 2\phi_2^2 \lambda_N^2 \boldsymbol{I}_{Nn},\ \phi_3^2 \boldsymbol{I}_N\right)$. By incorporation of (5.126) with condition (5.124) one obtains the sufficient stability condition as follows

$$\boldsymbol{\nu}^T \boldsymbol{\Psi}_3 \boldsymbol{\nu} < 0, \tag{5.127}$$

where $\boldsymbol{\Psi}_3 = \boldsymbol{\Psi}_1 + \boldsymbol{\Psi}_2$. From (5.127), if $\boldsymbol{\Psi}_3 < 0$ stability for $\boldsymbol{r}$ is guaranteed.

Step III. (Convexification of $\boldsymbol{\Psi}_3 < 0$): Inequality $\boldsymbol{\Psi}_3 < 0$ is not affine with respect to all the decision variables. To derive an equivalent affine condition, the *Schur complement* Lemma is applied on $\boldsymbol{\Psi}_3 < 0$ multiple times which results in $\tilde{\boldsymbol{\Psi}} = \begin{bmatrix} \tilde{\boldsymbol{\Psi}}_{11} & \tilde{\boldsymbol{\Psi}}_{12} \\ * & \tilde{\boldsymbol{\Psi}}_{22} \end{bmatrix} <$

0, where

$$\tilde{\boldsymbol{\Psi}}_{11}=\begin{bmatrix}\boldsymbol{\Xi}+\zeta\boldsymbol{I}_{N-1}\otimes\boldsymbol{P}^{-1} & \tilde{\boldsymbol{J}}\tilde{\boldsymbol{W}}\otimes\boldsymbol{P}^{-1}\boldsymbol{B}\boldsymbol{K} & \boldsymbol{0}\\ * & -\boldsymbol{I}_N\otimes\boldsymbol{\Phi}_1^2 & \boldsymbol{0}\\ * & * & (1-2\phi_4+\phi_3^2+\zeta)\boldsymbol{I}_N\end{bmatrix},$$

$$\tilde{\boldsymbol{\Psi}}_{12}=\begin{bmatrix}\sqrt{2}\tilde{\boldsymbol{J}}\otimes\boldsymbol{I}_n & \sqrt{2}\tilde{\boldsymbol{J}}\otimes\boldsymbol{I}_n & \boldsymbol{0} & \boldsymbol{0}\\ \boldsymbol{0} & \boldsymbol{0} & \sqrt{2}\lambda_N\boldsymbol{I}_{Nn} & \sqrt{2}\lambda_N\boldsymbol{I}_{Nn}\\ \boldsymbol{0} & \boldsymbol{0} & \boldsymbol{0} & \boldsymbol{0}\end{bmatrix},$$

$$\tilde{\boldsymbol{\Psi}}_{22}=\mathrm{diag}(-\phi_2^{-2}\boldsymbol{I},-\phi_5^{-2}\boldsymbol{I},-\phi_2^{-2}\boldsymbol{I},-\phi_5^{-2}\boldsymbol{I}).$$

Pre- and post multiply inequality $\tilde{\boldsymbol{\Psi}}<0$ by $\boldsymbol{T}=\mathrm{diag}(\boldsymbol{I}_{N-1}\otimes\boldsymbol{P},\,\boldsymbol{I}_N\otimes\boldsymbol{P},\,\boldsymbol{I}_N,\boldsymbol{I}_{(N-1)n},\,\boldsymbol{I}_{(N-1)n},\,\boldsymbol{I}_{Nn},\,\boldsymbol{I}_{Nn})$. Denote the following alternative variables

$$\boldsymbol{\Omega}=\boldsymbol{K}\boldsymbol{P},\quad \boldsymbol{S}_1=\boldsymbol{P}\boldsymbol{\Phi}_1^2\boldsymbol{P},\quad s_2=\phi_2^{-2},\quad s_3=\phi_3^2,\quad s_4=\phi_4,\quad s_5=\phi_5^{-2}. \tag{5.128}$$

Using these alternative variables, the LMI $\boldsymbol{\Psi}<0$ given in (5.69) is obtained.

Step IV. (Formulation of objective function): Similar to the objective functions used in CEASE and PEC, a linear weighted-sum method is used to decrease/increase the design parameters based on their impact on MIET (5.51). To this end, the following constraints are considered

$$\begin{aligned}&\boldsymbol{P}^{-1}<\theta_1\boldsymbol{I},\qquad \boldsymbol{S}_1^T\boldsymbol{S}_1<\theta_2\boldsymbol{I},\qquad s_2^2<\theta_3,\qquad s_3^{-1}<\theta_4,\\ &s_4^2<\theta_5,\qquad s_5^2<\theta_6,\qquad \boldsymbol{\Omega}^T\boldsymbol{\Omega}<\theta_7\boldsymbol{I},\end{aligned} \tag{5.129}$$

where $\theta_c>0$, $(1\le c\le 7)$, are decision variables. Based on (5.129), if one decreases the values of $\theta_c>0$, $(1\le c\le 7)$, parameters $\{\|\boldsymbol{P}\|, s_3\}$ are increased and $\{\boldsymbol{S}_1, s_2, s_4, s_5, \|\boldsymbol{\Omega}\|\}$ are decreased. In return, parameters $\{\|\boldsymbol{K}\|, \|\boldsymbol{\Phi}_1\|, \phi_4\}$ are decreased and $\{\phi_2,\phi_3,\phi_5\}$ are increased based on alternative variables (5.128). This increases MIET (5.51). Inequalities (5.72) are as a result of (5.129). The objective function $\mathbb{F}$ in (5.68) minimizes a weighted sum of θ_c, $(1\le c\le 7)$, with all weights equal one. LMIs $\boldsymbol{C}_i$, $(1\le i\le 7)$, given in (5.70) are obtained from (5.129). Design parameters are computed from (5.67) once (5.68) is solved. □

5.5.5 Proof of Theorem 5.5

Proof. The proof is given in two steps.

Step I. Stability analysis in the presence of DoS: From Theorem 5.4, with given ζ and LMI $\boldsymbol{\Psi}<0$, it is guaranteed that $\dot{V}(t)<-\zeta V(t)$ for healthy intervals $(t\in W_m)$. This leads to

$$V(t)\le e^{-\zeta(t-\xi_m-\nu_m)}V(\xi_m+\nu_m),\quad t\in W_m. \tag{5.130}$$

In the presence of DoS $(t\in Z_m)$, MAS (5.66) is open loop and its states may diverge. Therefore, there exists a scalar β such that

$$\dot{V}(t)<\beta V(t),\quad (t\in Z_m). \tag{5.131}$$

This inequality is expanded as follows

$$V(t) \leq e^{\beta(t-\xi_m)} V(\xi_m), \quad (t \in Z_m). \tag{5.132}$$

By combining (5.130) and (5.132) the stability condition is obtained. If $t \in Z_m$, the following sequence of inequalities hold

$$\begin{aligned} V(t) &\leq e^{\beta(t-\xi_m)} V(\xi_m) \\ &\leq e^{\beta(t-\xi_m)} \left(e^{-\zeta(\xi_m - \xi_{m-1} - \nu_{m-1})} V(\xi_{m-1} + \nu_{m-1}) \right) \\ &\leq e^{\beta(t-\xi_m)} e^{-\zeta(\xi_m - \xi_{m-1} - \nu_{m-1})} e^{\beta(\xi_{m-1} + \nu_{m-1} - \xi_{m-2})} V(\xi_{m-2}) \\ &\leq \dots \\ &\leq e^{-\zeta |\bar{\mathcal{H}}(0,t)|} e^{\beta |\bar{\mathcal{D}}(0,t)|} V(0). \end{aligned} \tag{5.133}$$

From (5.7), (5.8), (5.59), and (5.60), it holds that

$$e^{-\zeta |\bar{\mathcal{H}}(0,t)|} e^{\beta |\bar{\mathcal{D}}(0,t)|} \leq \rho \, e^{-\bar{\zeta} t}, \tag{5.134}$$

with ρ and $\bar{\zeta}$ given in (5.77). Condition (5.134) gives way to

$$V(t) < \rho \, e^{-\bar{\zeta} t} V(0), \quad t \geq 0, \tag{5.135}$$

which is equivalent to (5.76). Let $\gamma = \zeta/(\zeta + \beta)$. Based on (5.135), if DoS attacks satisfy $(\frac{1}{T_1} + \frac{g}{F_1}) < \gamma$, MAS (5.66) is exponentially stable.

Step II. Parameter design with given DoS resilience: For healthy intervals ($t \in W_m$), the parameter design based on Lyapunov function (5.116) leads to the LMIs given in (5.69) and (5.70). Next, consider DoS intervals ($t \in Z_m$). Let $\gamma = \zeta/(\zeta + \beta)$ be a given DoS resilience level. Hence, $\beta = \frac{\zeta(1-\gamma)}{\gamma}$. Now, we work on (5.131) with Lyapunov candidate (5.117) for ($t \in Z_m$):

$$\dot{V} - \beta V = (\dot{V}_1 + \dot{V}_2) - \beta (V_1 + V_2) < 0. \tag{5.136}$$

If

$$(\dot{V}_1 + \dot{V}_2) - \beta V_1 < 0, \quad (t \in Z_m), \tag{5.137}$$

holds, condition (5.136) (or (5.131)) also holds. Based on (5.63), it holds that $\dot{\eta}_i = 0$, $(1 \leq i \leq N)$, for $t \in Z_m$. Therefore, $\dot{V}_2 = 0$ for $t \in Z_m$. Expression (5.137) is expanded based on (5.66) for $t \in Z_m$

$$\boldsymbol{r}^T \left(\boldsymbol{I}_{N-1} \otimes (\boldsymbol{A}^T \boldsymbol{P}^{-1} + \boldsymbol{P}^{-1} \boldsymbol{A} - \beta \boldsymbol{P}^{-1}) \right) \boldsymbol{r} < 0. \tag{5.138}$$

In summary, if (5.138) holds, then $\dot{V}(t) - \beta V(t) < 0$ is guaranteed for $t \in Z_m$. As shown previously, combining $\dot{V}(t) + \zeta V(t) < 0$ for $t \in W_m$ and $\dot{V}(t) - \beta V(t) < 0$ for $t \in Z_m$ leads to (5.76). Pre- and post multiply (5.138) by $\boldsymbol{I}_{N-1} \otimes \boldsymbol{P}$ which results in LMI (5.74). This completes the proof. □

Chapter 6

Event-triggered Formation-Containment

Recently, the formation-containment control (FCC) framework, which can be regarded as the combined problem of formation and containment for MASs, has arisen in several engineering applications [83–94]. In FCC, the leaders converge to a desired geometric formation. Simultaneously, the followers merge within the convex hull spanned by the leaders. As compared to solitary containment [12, 95–98] and solitary formation [99–101], FCC is more complex and is a topic of increasing interest in the control and signal processing community. A related application for FCC is the mixed containment-sensing problem [13] where the objective is to have a group of mobile agents (followers) cover and provide surveillance sequentially from one region of interest to another. In this application, the leaders steer the followers from one operational region (formation) to another and coordinate the sensing task for the followers. Formation-containment has been studied for agents with different dynamics, including second-order linear agents [83, 84], general linear agents [88, 89], heterogeneous agents [90, 91], Euler–Lagrange systems [92, 93], and a class of nonlinear agents [86]. All of these implementations impose the strict condition of real-time data transmissions between the agents. To preserve the limited energy allocated to each agent, event-triggered (ET) mechanisms [36, 39, 149–153] that reduce communications are of great interest in FCC applications.

The chapter proposes a formation-containment control approach using a dynamic event-triggered mechanism (FCC/DEME [102]) that offers optimality for design parameters, namely the control gains and dynamic event-triggering (DET) parameters. The leader-leader and follower-follower communications are reduced by utilizing a distributed DET framework. The main features of the proposed FCC/DEME [102] are listed below:

- FCC/DEME is the first implementation for formation-containment that utilizes the DET mechanism. This leads to considerable energy and communication savings for the MASs.
- Two different sets of control and DET parameters are introduced for: (i) formation

of the leaders, and; (ii) containment of the followers. To design these parameters, FCC/DEME utilizes two convex optimizations based on enabling a trade-off between the rate of convergence for formation-containment and the frequency of events.

Perhaps, the closest work to FCC/DEME is [94], where an ET scheme is proposed for the FCC problem. Unlike [94], the DET used in this paper is more general and adds additional degrees of freedom. As another difference, FCC/DEME (unlike [94]) is based on an optimization framework to develop a structured trade-off between the formation-containment convergence rate and frequency of the transmissions.

6.1 Multi-agent system

Consider the following general linear MAS

$$\dot{\boldsymbol{x}}_i(t) = \boldsymbol{A}\boldsymbol{x}_i(t) + \boldsymbol{B}\boldsymbol{u}_i(t), \quad i \in \mathcal{V} = \{1, \ldots, N{+}M\}, \tag{6.1}$$

where $\boldsymbol{x}_i(t) \in \mathbb{R}^n$ and $\boldsymbol{u}_i(t) \in \mathbb{R}^m$ are, respectively, the state and control input for agent i. Matrix pair $(\boldsymbol{A}, \boldsymbol{B})$ is controllable.

There exist two sets of agents in MAS (6.1), namely, the followers and leaders. The follower and leader sets are, respectively, denoted by $\mathcal{F} = \{i \in \mathcal{V} \,|\, 1 \leq i \leq N\}$ and $\mathcal{L} = \{i \in \mathcal{V} \,|\, N{+}1 \leq i \leq N{+}M\}$. For follower i, $(1 \leq i \leq N)$, notation $\mathcal{N}^i_{\mathcal{F}\leftarrow\mathcal{F}}$ is used to represent the set of its neighbours, which are also followers. The neighbours of follower i within the leaders' set are denoted by $\mathcal{N}^i_{\mathcal{F}\leftarrow\mathcal{L}}$. For leader i, $(N{+}1 \leq i \leq N{+}M)$, the set of its neighbours which are also leaders is denoted by $\mathcal{N}^i_{\mathcal{L}\leftarrow\mathcal{L}}$. Additionally, the neighbours of leader i within the followers' set is denoted by $\mathcal{N}^i_{\mathcal{L}\leftarrow\mathcal{F}}$.

Assumption 7. The follower-follower and leader-leader communication network topologies are connected and undirected. None of the leaders receive communication from the followers' set, i.e., $\mathcal{N}^i_{\mathcal{L}\leftarrow\mathcal{F}}$ is a null set for all leaders. In physical terms, this implies that the leaders are autonomous and are not restrained in their movement by the followers. There exists at least one directed path originating from one of the leaders to any follower in MAS (6.1).

Under Assumption 7, the associated Laplacian matrix $\boldsymbol{L} \in \mathbb{R}^{(N+M)\times(N+M)}$ with MAS (6.1) is given below

$$\boldsymbol{L} = \begin{bmatrix} \boldsymbol{L}_{\mathcal{F}_{(N\times N)}} & \boldsymbol{L}_{\mathcal{F}\mathcal{L}_{(N\times M)}} \\ \boldsymbol{0} & \boldsymbol{L}_{\mathcal{L}_{(M\times M)}} \end{bmatrix}. \tag{6.2}$$

Under Assumption 7, all eigenvalues of $\boldsymbol{L}_{\mathcal{F}}$ are positive real scalars. Each element in $-\boldsymbol{L}_{\mathcal{F}}^{-1}\boldsymbol{L}_{\mathcal{F}\mathcal{L}}$ is non-negative, and each row of $-\boldsymbol{L}_{\mathcal{F}}^{-1}\boldsymbol{L}_{\mathcal{F}\mathcal{L}}$ has a sum equal to one [12].

Illustrative example: To illustrate the graph notation used in this chapter, an example of a network with 10 agents (4 leaders, i.e., $M = 4$, and 6 followers, i.e., $N = 6$) is provided. This network is shown in Fig. 6.1. Based on Fig. 6.1, the neighbouring sets for agents 6 and 7, for example, are as follows: $\mathcal{N}^6_{\mathcal{F}\leftarrow\mathcal{F}} = \{1, 5\}$, $\mathcal{N}^6_{\mathcal{F}\leftarrow\mathcal{L}} = \{8\}$,

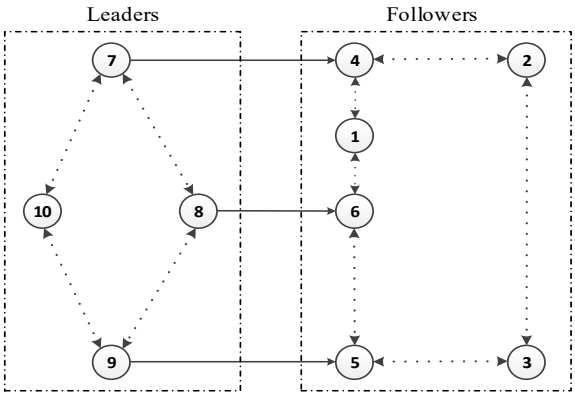

Figure 6.1: An illustrative network topology including leaders and followers.

$\mathcal{N}^7_{\mathcal{L}\leftarrow\mathcal{L}} = \{8, 10\}$, $\mathcal{N}^7_{\mathcal{L}\leftarrow\mathcal{F}} = \{\}$. The following blocks represent different partitions for the Laplacian matrix (6.2) corresponding to this network

$$\boldsymbol{L}_{\mathcal{F}}=\begin{bmatrix} 2 & 0 & 0 & -1 & 0 & -1 \\ 0 & 2 & -1 & -1 & 0 & 0 \\ 0 & -1 & 2 & 0 & -1 & 0 \\ -1 & -1 & 0 & 3 & 0 & 0 \\ 0 & 0 & -1 & 0 & 3 & -1 \\ -1 & 0 & 0 & 0 & -1 & 3 \end{bmatrix}, \boldsymbol{L}_{\mathcal{L}}=\begin{bmatrix} 2 & -1 & 0 & -1 \\ -1 & 2 & -1 & 0 \\ 0 & -1 & 2 & -1 \\ -1 & 0 & -1 & 2 \end{bmatrix}, \boldsymbol{L}_{\mathcal{FL}}=\begin{bmatrix} 0 & 0 & 0 & 0 \\ 0 & 0 & 0 & 0 \\ 0 & 0 & 0 & 0 \\ -1 & 0 & 0 & 0 \\ 0 & 0 & -1 & 0 \\ 0 & -1 & 0 & 0 \end{bmatrix}. \quad (6.3)$$

Definition 2 (Formation)**.** For a given formation vector $\boldsymbol{h}_i \in \mathbb{R}^n$, the leaders are said to achieve state formation if there exists a formation reference function $\boldsymbol{r}(t) \in \mathbb{R}^n$ such that $\lim_{t\to\infty}(\boldsymbol{x}_i(t) - \boldsymbol{h}_i - \boldsymbol{r}(t)) = 0$, $\forall i \in \mathcal{L}$, $\forall \boldsymbol{x}_i(0) \in \mathbb{R}^n$. As a result, it holds that $\lim_{t\to\infty}(\boldsymbol{x}_i(t) - \boldsymbol{x}_j(t)) = \boldsymbol{h}_i - \boldsymbol{h}_j$, $\forall i, j \in \mathcal{L}$. This chapter considers constant (time-invariant) formation vector $\boldsymbol{h}_i$, $\forall i \in \mathcal{L}$.

Note that the leaders can determine the desired state formation by selecting proper values for formation vector $\boldsymbol{h}_i$, $(i \in \mathcal{L})$. According to Definition 2, when formation is achieved it holds that $\lim_{t\to\infty}(\boldsymbol{x}_i(t) - \boldsymbol{h}_i) = \lim_{t\to\infty} \boldsymbol{r}(t)$, $\forall i \in \mathcal{L}$. This implies that the disagreements between $\boldsymbol{x}_i(t)$ and its corresponding formation vector $\boldsymbol{h}_i$ approaches the reference function $\boldsymbol{r}(t)$ for all leaders. Fig. 6.2 is provided to show the relationships between $\boldsymbol{x}_i(t)$, $\boldsymbol{h}_i$, and $\boldsymbol{r}(t)$ for an illustrative formation for 3 leaders. From Fig. 6.2, it is inferred that the formation reference $\boldsymbol{r}(t)$ describes the macroscopic movement of the whole formation, and $\boldsymbol{h}_i$ is the relative offset between $\boldsymbol{x}_i(t)$ and $\boldsymbol{r}(t)$. As shown later in Remark 6.3, the reference function $\boldsymbol{r}(t)$ is dependent on the initial state of the leaders and formation vectors $\boldsymbol{h}_i$.

Definition 3 (Containment)**.** Containment is said to be solved if starting from any initial states, the states of the followers converge to a convex hull formed by the leaders.

Definition 4 (Formation-Containment)**.** MAS (6.1) is said to achieve formation-containment if for any initial values, the leaders converge to the desired formation and simultaneously the followers achieve containment.

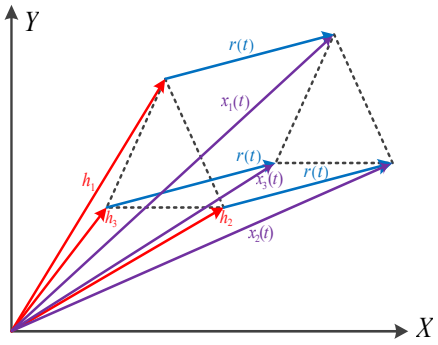

Figure 6.2: An illustrative example for 3 leaders forming a triangle. When formation is achieved, it holds that $\lim_{t\to\infty}(\boldsymbol{x}_i(t)-\boldsymbol{h}_i-\boldsymbol{r}(t))=0$, $(1\leq i\leq 3)$.

6.1.1 Dynamic event-triggering scheme and control protocol

The agents share their states within their neighbourhoods to achieve formation-containment. To reduce the amount of transmission, an event-detector is incorporated with each agent. The event-detector in agent i (leader or follower) monitors a 'dynamic event-triggering condition' to determine whether to transmit the state value $\boldsymbol{x}_i(t)$ within its neighbourhood. If the event detector detects an event at time instant t_k^i (superscript i indicates agent i, and subscript $k=0,1,\cdots$ denotes the sequence of events for agent i), then agent i transmits $\boldsymbol{x}_i(t_k^i)$ to its neighbours. Upon receiving $\boldsymbol{x}_i(t_k^i)$, agent j, (a neighbour of agent i), updates its previous database with the newly received state from agent i. This state value, i.e., $\boldsymbol{x}_i(t_k^i)$, is used at agent j until the next event is triggered by agent i. Let $\hat{\boldsymbol{x}}_i(t)\triangleq\boldsymbol{x}_i(t_k^i)$, $t\in[\,t_k^i,\,t_{k+1}^i\,)$. Denote the following disagreement vectors, for followers and leaders

$$\mathbb{X}_i(t)=\sum_{j\in\mathcal{N}_{\mathcal{L}\leftarrow\mathcal{L}}^i}a_{i,j}\Big((\boldsymbol{\Lambda}_i(t)\hat{\boldsymbol{x}}_i(t)-\boldsymbol{h}_i)-(\boldsymbol{\Lambda}_j(t)\hat{\boldsymbol{x}}_j(t)-\boldsymbol{h}_j)\Big),\qquad(\forall i\in\mathcal{L})\tag{6.4}$$

$$\mathbb{X}_i(t)=\sum_{j\in\mathcal{N}_{\mathcal{F}\leftarrow\mathcal{F}}^i}a_{i,j}\left(\boldsymbol{\Lambda}_i(t)\hat{\boldsymbol{x}}_i(t)-\boldsymbol{\Lambda}_j(t)\hat{\boldsymbol{x}}_j(t)\right)-\sum_{j\in\mathcal{N}_{\mathcal{F}\leftarrow\mathcal{L}}^i}a_{i,j}\boldsymbol{x}_j(t),\qquad(\forall i\in\mathcal{F})\tag{6.5}$$

where $a_{i,j}$ is element (i,j) in the weighted adjacency matrix and $\boldsymbol{\Lambda}_i(t)=e^{\boldsymbol{A}(t-t_k^i)}$.

Remark 6.1. Based on (6.4) and (6.5), the follower-follower and leader-leader state exchanges are event-triggered. Similar to [94–96, 153], the leader-to-follower transmission in FCC/DEME is continuous. Compared with the existing FCC implementations [83, 84, 86, 88–93] where all transmissions across the network are continuous, all in-neighbour transmissions in FCC/DEME except for the leader-to-follower communication are event-triggered. It should be noted that the leader-to-follower state transmission can be performed by a different subset of leaders during the formation-containment process (as shown later). This enhances the longevity of the leaders.

Let all agents transmit their initial state values $\boldsymbol{x}_i(0)$ to their neighbours, i.e., $t_0^i=0$, $\forall i\in\mathcal{F}\cup\mathcal{L}$. Denote the state error at time instant t by $\boldsymbol{e}_i(t)=\boldsymbol{\Lambda}_i(t)\hat{\boldsymbol{x}}_i(t)-\boldsymbol{x}_i(t)$, $\forall i\in\mathcal{F}\cup\mathcal{L}$, Motivated by [75], the next event instant after t_k^i, $\forall i\in\mathcal{F}\cup\mathcal{L}$, is triggered

based on the following DET condition

$$t^i_{k+1} = \inf\{t > t^i_k |\ \|\boldsymbol{\Phi}_c \boldsymbol{e}_i(t)\| \geq \alpha_c \|\mathbb{X}_i(t)\| + \beta_c \eta_i(t)\}, \tag{6.6}$$

where $\boldsymbol{\Phi}_c \in \mathbb{R}^{n\times n} > 0$, $\alpha_c > 0$, and $\beta_c > 0$ for $c \in \{1, 2\}$ are design parameters. In (6.6), if $i \in \mathcal{L}$ then $c = 1$ is used and if $i \in \mathcal{F}$ then $c = 2$. Parameter $\eta_i(t)$ satisfies

$$\dot{\eta}_i(t) = -\gamma_c \eta_i(t) + \rho_c \|\mathbb{X}_i(t)\|, \quad \forall i \in \mathcal{V}, \tag{6.7}$$

where $\eta_i(0) > 0$. Parameters $\gamma_c > 0$ and $\rho_c > 0$ are to be designed. Similar to (6.6), in (6.7) if $i \in \mathcal{L}$ then $c = 1$ and if $i \in \mathcal{F}$ then $c = 2$. The proposed distributed control protocol for the control input is given below

$$\boldsymbol{u}_i(t) = \begin{cases} \boldsymbol{K}_1 \mathbb{X}_i(t) + \boldsymbol{H} \sum\limits_{j \in \mathcal{N}^i_{\mathcal{L}\leftarrow\mathcal{L}}} a_{i,j}(\boldsymbol{h}_i - \boldsymbol{h}_j), & i \in \mathcal{L} \\ \boldsymbol{K}_2 \mathbb{X}_i(t), & i \in \mathcal{F}. \end{cases} \tag{6.8}$$

Matrices $\boldsymbol{K}_1 \in \mathbb{R}^{m\times n}$ and $\boldsymbol{K}_2 \in \mathbb{R}^{m\times n}$ are the control gains to be designed. Additionally, matrix $\boldsymbol{H} \in \mathbb{R}^{m\times n}$ is the formation gain which is also unknown and needs to be designed. As shown later in Remark 6.2, the term $\boldsymbol{H} \sum_{j\in\mathcal{N}^i_{\mathcal{L}\leftarrow\mathcal{L}}} a_{i,j}(\boldsymbol{h}_i - \boldsymbol{h}_j)$ is used in (6.8) to expand the set of possible formations that the leaders can achieve [100].

6.1.2 Design objectives

The design objectives in FCC/DEME are as follows:

1. Reduce the frequency of follower-follower and leader-leader state transmissions.
2. Add flexibility to control the rate of formation-containment convergence rate.
3. Govern the trade-off between the formation-containment convergence rate and the frequency of event-triggerings.
4. Compute unknown control and DET parameters in a co-design optimization framework based on an objective function to increase the inter-event interval.

6.2 Problem formulation

Define the following global vectors

$\boldsymbol{x}_{\mathcal{F}} = [\boldsymbol{x}^T_1(t), \ldots, \boldsymbol{x}^T_N(t)]^T$, $\boldsymbol{x}_{\mathcal{L}} = [\,\boldsymbol{x}^T_{N+1}(t), \ldots, \boldsymbol{x}^T_{N+M}(t)\,]^T$, $\hat{\boldsymbol{x}}_{\mathcal{F}} = [\hat{\boldsymbol{x}}^T_1(t), \ldots, \hat{\boldsymbol{x}}^T_N(t)]^T$,
$\hat{\boldsymbol{x}}_{\mathcal{L}} = [\hat{\boldsymbol{x}}^T_{N+1}(t), \ldots, \hat{\boldsymbol{x}}^T_{N+M}(t)]^T$, $\boldsymbol{e}_{\mathcal{F}} = [\boldsymbol{e}^T_1(t), \ldots, \boldsymbol{e}^T_N(t)]^T$, $\boldsymbol{e}_{\mathcal{L}} = [\boldsymbol{e}^T_{N+1}(t), \ldots, \boldsymbol{e}^T_{N+M}(t)]^T$,
$\boldsymbol{\eta}_{\mathcal{F}} = [\eta_1(t), \ldots, \eta_N(t)]^T$, $\boldsymbol{\eta}_{\mathcal{L}} = [\eta_{N+1}(t), \ldots, \eta_{N+M}(t)]^T$, $\mathbb{X}_{\mathcal{F}} = [\mathbb{X}^T_1(t), \ldots, \mathbb{X}^T_N(t)]^T$,
$\mathbb{X}_{\mathcal{L}} = [\mathbb{X}^T_{N+1}(t), \ldots, \mathbb{X}^T_{N+M}(t)]^T$, $\boldsymbol{\Lambda}_{\mathcal{F}} = \text{diag}(\boldsymbol{\Lambda}_1(t), \ldots, \boldsymbol{\Lambda}_N(t))$,
$\boldsymbol{\Lambda}_{\mathcal{L}} = \text{diag}(\boldsymbol{\Lambda}_{N+1}(t), \ldots, \boldsymbol{\Lambda}_{N+M}(t))$, $\bar{\mathbb{X}}_{\mathcal{F}} = [\,\|\mathbb{X}_1(t)\|, \ldots, \|\mathbb{X}_N(t)\|\,]^T$,
$\bar{\mathbb{X}}_{\mathcal{L}} = [\,\|\mathbb{X}_{N+1}(t)\|, \ldots, \|\mathbb{X}_{N+M}(t)\|\,]^T$, $\bar{\boldsymbol{e}}_{\mathcal{F}} = [\,\|\boldsymbol{e}_1(t)\|, \ldots, \|\boldsymbol{e}_N(t)\|\,]^T$,

$$\bar{\boldsymbol{e}}_{\mathcal{L}} = [\, \|\boldsymbol{e}_{N+1}(t)\| \,, \ldots, \|\boldsymbol{e}_{N+M}(t)\| \,]^T, \boldsymbol{h} = [\boldsymbol{h}_1, \ldots, \boldsymbol{h}_M]^T. \tag{6.9}$$

It holds that $\boldsymbol{e}_{\mathcal{L}} = \boldsymbol{\Lambda}_{\mathcal{L}}\hat{\boldsymbol{x}}_{\mathcal{L}} - \boldsymbol{x}_{\mathcal{L}}$ and $\boldsymbol{e}_{\mathcal{F}} = \boldsymbol{\Lambda}_{\mathcal{F}}\hat{\boldsymbol{x}}_{\mathcal{F}} - \boldsymbol{x}_{\mathcal{F}}$. The closed-loop system from (6.1) and (6.8) is given below

$$\dot{\boldsymbol{x}}_{\mathcal{L}} = (\boldsymbol{I}_M \otimes \boldsymbol{A} + \boldsymbol{L}_{\mathcal{L}} \otimes \boldsymbol{B}\boldsymbol{K}_1)\, \boldsymbol{x}_{\mathcal{L}} + \boldsymbol{L}_{\mathcal{L}} \otimes \boldsymbol{B}\boldsymbol{K}_1\, (\boldsymbol{e}_{\mathcal{L}} - \boldsymbol{h}) + (\boldsymbol{L}_{\mathcal{L}} \otimes \boldsymbol{B}\boldsymbol{H})\, \boldsymbol{h}. \tag{6.10}$$

$$\dot{\boldsymbol{x}}_{\mathcal{F}} = (\boldsymbol{I}_N \otimes \boldsymbol{A} + \boldsymbol{L}_{\mathcal{F}} \otimes \boldsymbol{B}\boldsymbol{K}_2)\, \boldsymbol{x}_{\mathcal{F}} + \boldsymbol{L}_{\mathcal{F}} \otimes \boldsymbol{B}\boldsymbol{K}_2\, \boldsymbol{e}_{\mathcal{F}} + \boldsymbol{L}_{\mathcal{F}\mathcal{L}} \otimes \boldsymbol{B}\boldsymbol{K}_2\, \boldsymbol{x}_{\mathcal{L}}. \tag{6.11}$$

6.2.1 System transformation

This section converts the FCC problem for the original closed-loop MAS (6.10) and (6.11) into the stability problem for a transformed system. System transformation is accomplished in the following 3 steps.

Step I: The first step converts the problem of formation for the leaders into an equivalent stability problem. Let $\boldsymbol{z} = \boldsymbol{x}_{\mathcal{L}} - \boldsymbol{h}$. Using $\boldsymbol{z}$, system (6.10) is expressed as

$$\dot{\boldsymbol{z}} = (\boldsymbol{I}_M \otimes \boldsymbol{A} + \boldsymbol{L}_{\mathcal{L}} \otimes \boldsymbol{B}\boldsymbol{K}_1)\, \boldsymbol{z} + \boldsymbol{L}_{\mathcal{L}} \otimes \boldsymbol{B}\boldsymbol{K}_1\, \boldsymbol{e}_{\mathcal{L}} + (\boldsymbol{I}_M \otimes \boldsymbol{A} + \boldsymbol{L}_{\mathcal{L}} \otimes \boldsymbol{B}\boldsymbol{H})\boldsymbol{h}. \tag{6.12}$$

To guarantee stability in (6.12), the eigenvalue decomposition of $\boldsymbol{L}_{\mathcal{L}}$, which was previously discussed in Section 4.1.3, is used. Let $0 < \lambda_{2,\mathcal{L}} \leq \ldots \leq \lambda_{M,\mathcal{L}}$ denote the eigenvalues of $\boldsymbol{L}_{\mathcal{L}}$ in the ascending order. Let matrix $\boldsymbol{W} = [w_{i,j}] \in \mathbb{R}^{M \times M}$ include the normalized eigenvectors of $\boldsymbol{L}_{\mathcal{L}}$ such that

$$\boldsymbol{W}\boldsymbol{J}_1\boldsymbol{W}^{-1} = \boldsymbol{L}_{\mathcal{L}}, \qquad \|\boldsymbol{W}\| = 1,$$

where $\boldsymbol{J}_1 = \mathrm{diag}(0, \lambda_{2,\mathcal{L}}, \ldots, \lambda_{M,\mathcal{L}})$ includes all eigenvalues of $\boldsymbol{L}_{\mathcal{L}}$. Let $\boldsymbol{W}^{-1} = [\tilde{w}_{i,j}]$. From $\boldsymbol{W}^{-1}$, the $(M-1)\times M$ dimensional matrix $\tilde{\boldsymbol{W}} = [\tilde{w}_{i,j}]$, for $2 \leq i \leq M$ and $1 \leq j \leq M$, is constructed. More precisely, $\tilde{\boldsymbol{W}}$ includes rows 2 to M of matrix $\boldsymbol{W}^{-1}$. Consider the following transformation

$$\boldsymbol{\psi}_{\mathcal{L}} = \tilde{\boldsymbol{W}} \otimes \boldsymbol{I}_n \boldsymbol{z}. \tag{6.13}$$

Using (6.13), system (6.12) is transformed to

$$\begin{aligned} \dot{\boldsymbol{\psi}}_{\mathcal{L}} = {} & (\boldsymbol{I}_{M-1} \otimes \boldsymbol{A} + \tilde{\boldsymbol{J}}_1 \otimes \boldsymbol{B}\boldsymbol{K}_1)\, \boldsymbol{\psi}_{\mathcal{L}} + \tilde{\boldsymbol{J}}_1\tilde{\boldsymbol{W}} \otimes \boldsymbol{B}\boldsymbol{K}_1\, \boldsymbol{e}_{\mathcal{L}} \\ & + (\tilde{\boldsymbol{W}} \otimes \boldsymbol{A})\boldsymbol{h} + (\tilde{\boldsymbol{W}} \otimes \boldsymbol{I}_n)(\boldsymbol{L}_{\mathcal{L}} \otimes \boldsymbol{B}\boldsymbol{H})\boldsymbol{h}. \end{aligned} \tag{6.14}$$

where $\tilde{\boldsymbol{J}}_1 = \mathrm{diag}(\lambda_{2,\mathcal{L}}, \ldots, \lambda_{M,\mathcal{L}})$. In fact, $\boldsymbol{\psi}_{\mathcal{L}}$ is a disagreement between the state of the leaders and their respective formation vectors. It is proved in [100, Theorem 1] that formation is achieved in (6.10) if and only if $\lim_{t\to\infty} \boldsymbol{\psi}_{\mathcal{L}} = 0$. Similar to [88,89,91,100], the term $(\tilde{\boldsymbol{W}} \otimes \boldsymbol{A})\boldsymbol{h} + (\tilde{\boldsymbol{W}} \otimes \boldsymbol{I}_n)(\boldsymbol{L}_{\mathcal{L}} \otimes \boldsymbol{B}\boldsymbol{H})\boldsymbol{h}$ in (6.14) should be made zero to guarantee $\lim_{t\to\infty} \boldsymbol{\psi}_{\mathcal{L}} = 0$. More precisely, the following condition, which is known as the formability condition, should be satisfied.

Formability Condition: For given formation vectors $\boldsymbol{h}_i$, $(i \in \mathcal{L})$, if there exists a

formation gain $\boldsymbol{H}$ such that the following condition is satisfied

$$(\boldsymbol{A}+\boldsymbol{BH})\sum_{j\in\mathcal{N}^i_{\mathcal{L}\leftarrow\mathcal{L}}} a_{i,j}(\boldsymbol{h}_i-\boldsymbol{h}_j)=\boldsymbol{0},\quad(\forall i\in\mathcal{L}), \tag{6.15}$$

then formation for leaders is feasible with respect to $\boldsymbol{h}_i$. For proof of (6.15), refer to [100, Theorem 2]. Under (6.15), expression (6.14) reduces to

$$\dot{\boldsymbol{\psi}}_{\mathcal{L}}=(\boldsymbol{I}_{M-1}\otimes\boldsymbol{A}+\tilde{\boldsymbol{J}}_1\otimes\boldsymbol{BK}_1)\,\boldsymbol{\psi}_{\mathcal{L}}+\tilde{\boldsymbol{J}}_1\tilde{\boldsymbol{W}}\otimes\boldsymbol{BK}_1\,\boldsymbol{e}_{\mathcal{L}}. \tag{6.16}$$

Step II: Let

$$\boldsymbol{\psi}_{\mathcal{F}}=\boldsymbol{x}_{\mathcal{F}}+(\boldsymbol{L}_{\mathcal{F}}^{-1}\boldsymbol{L}_{\mathcal{FL}})\otimes\boldsymbol{I}_n\boldsymbol{x}_{\mathcal{L}}. \tag{6.17}$$

If $\lim_{t\to\infty}\boldsymbol{\psi}_{\mathcal{F}}=0$, it holds that

$$\lim_{t\to\infty}[\boldsymbol{x}_{\mathcal{F}}+(\boldsymbol{L}_{\mathcal{F}}^{-1}\boldsymbol{L}_{\mathcal{FL}})\otimes\boldsymbol{I}_n\boldsymbol{x}_{\mathcal{L}}]=0.$$

Since the row sum of $-\boldsymbol{L}_{\mathcal{F}}^{-1}\boldsymbol{L}_{\mathcal{FL}}$ equals one, the term $(\boldsymbol{L}_{\mathcal{F}}^{-1}\boldsymbol{L}_{\mathcal{FL}})\otimes\boldsymbol{I}_n\boldsymbol{x}_{\mathcal{L}}$ expresses a convex hull of the leaders' states to which $\boldsymbol{x}_{\mathcal{F}}$ converges. Therefore, containment is achieved in the sense of Definition 3 if $\lim_{t\to\infty}\boldsymbol{\psi}_{\mathcal{F}}=0$. Next, expression (6.11) is transformed under transformation (6.17) and formability condition (6.15)

$$\begin{aligned}\dot{\boldsymbol{\psi}}_{\mathcal{F}}=&(\boldsymbol{I}_N\otimes\boldsymbol{A}+\boldsymbol{L}_{\mathcal{F}}\otimes\boldsymbol{BK}_2)\,\boldsymbol{\psi}_{\mathcal{F}}+\boldsymbol{L}_{\mathcal{F}}\otimes\boldsymbol{BK}_2\,\boldsymbol{e}_{\mathcal{F}}+(\boldsymbol{I}_N\otimes\boldsymbol{BK}_1)(\boldsymbol{L}_{\mathcal{F}}^{-1}\boldsymbol{L}_{\mathcal{FL}}\boldsymbol{L}_{\mathcal{L}}\otimes\boldsymbol{I}_n)\,\boldsymbol{z}\\&+(\boldsymbol{I}_N\otimes\boldsymbol{BK}_1)(\boldsymbol{L}_{\mathcal{F}}^{-1}\boldsymbol{L}_{\mathcal{FL}}\boldsymbol{L}_{\mathcal{L}}\otimes\boldsymbol{I}_n)\,\boldsymbol{e}_{\mathcal{L}}.\end{aligned} \tag{6.18}$$

Step III: If $\lim_{t\to\infty}\boldsymbol{\psi}_{\mathcal{L}}=0$, formation is achieved for the leaders with respect to Definition 2. As a result, it holds that $\lim_{t\to\infty}\boldsymbol{z}=\boldsymbol{x}_{\mathcal{L}}-\boldsymbol{h}=\boldsymbol{1}_M\otimes\boldsymbol{r}(t)$. Therefore, the third term in the right hand side of (6.18) approaches $(\boldsymbol{I}_N\otimes\boldsymbol{BK}_1)(\boldsymbol{L}_{\mathcal{F}}^{-1}\boldsymbol{L}_{\mathcal{FL}}\boldsymbol{L}_{\mathcal{L}}\otimes\boldsymbol{I}_n)\,\boldsymbol{1}_M\otimes\boldsymbol{r}(t)$. Since $\boldsymbol{L}_{\mathcal{L}}\boldsymbol{1}_M=\boldsymbol{0}$, it holds that

$$\lim_{t\to\infty}(\boldsymbol{I}_N\otimes\boldsymbol{BK}_1)(\boldsymbol{L}_{\mathcal{F}}^{-1}\boldsymbol{L}_{\mathcal{FL}}\boldsymbol{L}_{\mathcal{L}}\otimes\boldsymbol{I}_n)\,\boldsymbol{z}=\boldsymbol{0}. \tag{6.19}$$

The state error for leaders $\boldsymbol{e}_{\mathcal{L}}$ approaches zero, i.e., $\lim_{t\to\infty}\boldsymbol{e}_{\mathcal{L}}=0$. This fact together with (6.19) imply that the asymptotic stability for (6.18) can be simplified to the asymptotic stability of the following system

$$\dot{\boldsymbol{\psi}}_{\mathcal{F}}=(\boldsymbol{I}_N\otimes\boldsymbol{A}+\boldsymbol{L}_{\mathcal{F}}\otimes\boldsymbol{BK}_2)\,\boldsymbol{\psi}_{\mathcal{F}}+\boldsymbol{L}_{\mathcal{F}}\otimes\boldsymbol{BK}_2\,\boldsymbol{e}_{\mathcal{F}}. \tag{6.20}$$

A similar eigenvalue decomposition is used for (6.20). Let matrix $\boldsymbol{V}$ be the normalized eigenvector matrix for $\boldsymbol{L}_{\mathcal{F}}$ such that

$$\boldsymbol{VJ}_2\boldsymbol{V}^{-1}=\boldsymbol{L}_{\mathcal{F}},\qquad\|\boldsymbol{V}\|=1, \tag{6.21}$$

where $\boldsymbol{J}_2=\mathrm{diag}(\lambda_{1,\mathcal{F}},\ldots,\lambda_{N,\mathcal{F}})$ includes all eigenvalues of $\boldsymbol{L}_{\mathcal{F}}$. The following transformation is considered

$$\tilde{\boldsymbol{\psi}}_{\mathcal{F}}=\boldsymbol{V}^{-1}\otimes\boldsymbol{I}_n\boldsymbol{\psi}_{\mathcal{F}}. \tag{6.22}$$

Using (6.22), system (6.20) is transformed to

$$\dot{\tilde{\boldsymbol{\psi}}}_{\mathcal{F}} = (\boldsymbol{I}_N \otimes \boldsymbol{A} + \boldsymbol{J}_2 \otimes \boldsymbol{B}\boldsymbol{K}_2)\,\tilde{\boldsymbol{\psi}}_{\mathcal{F}} + (\boldsymbol{J}_2\boldsymbol{V}^{-1} \otimes \boldsymbol{B}\boldsymbol{K}_2)\,\boldsymbol{e}_{\mathcal{F}}. \tag{6.23}$$

In conclusion, the formation-containment problem for MAS (6.1) is solved if systems (6.16) and (6.23) are stable.

It should be noted that, unlike $\boldsymbol{L}_{\mathcal{L}}$, all eigenvalues of $\boldsymbol{L}_{\mathcal{F}}$ are strictly positive. Therefore, the transformation used in (6.22) is based on all eigenvectors included in $\boldsymbol{V}$. In contrast, in (6.13) the corresponding eigenvector to eigenvalue of zero is excluded.

Remark 6.2. According to the formability condition (6.15), linear MASs cannot achieve all the formation vectors due to the dynamic constraints of the agents. Similar observations for formability in general linear MASs have been made in other implementations including [88, 89, 91, 100]. The physical interpretation of (6.15) is that the expected formation should comply with the dynamics of the leaders [88]. It is worth mentioning that if $\boldsymbol{H} = \boldsymbol{0}$ in control protocol (6.8), the formability condition (6.15) reduces to $\boldsymbol{A}\sum_{j\in\mathcal{N}^i_{\mathcal{L}\leftarrow\mathcal{L}}} a_{i,j}(\boldsymbol{h}_i - \boldsymbol{h}_j) = \boldsymbol{0}$. Therefore, including the formation gain $\boldsymbol{H}$ expands the set of feasible formations that the leaders can achieve. It should be noted that for some formation vectors and agent dynamics, the formation gain $\boldsymbol{H}$ may be unnecessary (i.e., $\boldsymbol{H}$ can be zero).

Remark 6.3. It is worth mentioning that if formation is achieved (i.e., $\lim_{t\to\infty}\boldsymbol{\psi}_{\mathcal{L}} = 0$), the explicit expression for formation reference function $\boldsymbol{r}(t)$ satisfies

$$\lim_{t\to\infty}\left(\boldsymbol{r}(t) - \boldsymbol{r}_0(t) - \boldsymbol{r}_h(t)\right) = 0, \tag{6.24}$$

where

$$\begin{aligned}
\boldsymbol{r}_0(t) &= e^{\boldsymbol{A}t}(\tilde{\boldsymbol{w}}_1 \otimes \boldsymbol{I}_n)\boldsymbol{x}_{\mathcal{L}}(0),\\
\boldsymbol{r}_h(t) &= -e^{\boldsymbol{A}t}(\tilde{\boldsymbol{w}}_1 \otimes \boldsymbol{I}_n)\boldsymbol{h} + \int_0^t e^{\boldsymbol{A}(t-v)}((\tilde{\boldsymbol{w}}_1 \otimes \boldsymbol{I}_n)(\boldsymbol{I}_M \otimes \boldsymbol{A} + \boldsymbol{L}_{\mathcal{L}}\boldsymbol{B}\boldsymbol{H}))\,\boldsymbol{h}\,dv,
\end{aligned}$$

and $\tilde{\boldsymbol{w}}_1$ is row 1 of $\boldsymbol{W}^{-1}$. For proof of (6.24) refer to [100, Theorem 3]. Based on (6.24), the formation reference function $\boldsymbol{r}(t)$ depends on both the leaders' initial states $\boldsymbol{x}_{\mathcal{L}}(0)$ and global formation vector $\boldsymbol{h}$. In particular, $\boldsymbol{r}_0(t)$ is the impact of $\boldsymbol{x}_{\mathcal{L}}(0)$ on $\boldsymbol{r}(t)$, while $\boldsymbol{r}_h(t)$ shows how different choices of $\boldsymbol{h}_i$ impact $\boldsymbol{r}(t)$.

6.3 Main results

In this section, first the possibility of Zeno-behaviour for DET scheme (6.6) is excluded by obtaining a lower bound for the interval between two successive events. It is explained how this lower bound relates to the design objectives mentioned in Section 6.1.2. Two separate optimizations are then developed to co-design unknown parameters. The first optimization simultaneously computes all design parameters ($\boldsymbol{K}_1$, $\boldsymbol{\Phi}_1$ α_1, β_1, γ_1, and ρ_1) for the leaders. The second optimization co-designs all design parameters ($\boldsymbol{K}_2$, $\boldsymbol{\Phi}_2$ α_2, β_2, γ_2, and ρ_2) for the followers.

6.3.1 Exclusion of Zeno-behaviour

This section begins with the following Lemma which will be used for the exclusion of the Zeno-behaviour.

Lemma 5. It holds that $\eta_i(t) > \eta_i(0)\, e^{-(\gamma_c+\beta_c\frac{\rho_c}{\alpha_c})t}$, $\forall t \geq 0$, $\forall i \in \mathcal{V}$, and $c \in \{1,2\}$. Hence, $\eta_i(t)$ remains positive over time.

Proof. Based on (6.6), for $t \in [t_k^i, t_{k+1}^i)$, it holds that $\|\boldsymbol{\Phi}_c \boldsymbol{e}_i(t)\| - \beta_c \eta_i(t) \leq \alpha_c \|\mathbb{X}_i(t)\|$. Therefore, $\frac{\rho_c}{\alpha_c}\|\boldsymbol{\Phi}_c \boldsymbol{e}_i(t)\| - \beta_c \frac{\rho_c}{\alpha_c}\eta_i(t) \leq \rho_c \|\mathbb{X}_i(t)\|$. Incorporating this inequality in (6.7), results in $\dot{\eta}_i(t) \geq -(\gamma_c + \beta_c \frac{\rho_c}{\alpha_c})\eta_i(t) + \frac{\rho_c}{\alpha_c}\|\boldsymbol{\Phi}_c \boldsymbol{e}_i(t)\|$. Hence, $\dot{\eta}_i(t) \geq -(\gamma_c + \beta_c \frac{\rho_c}{\alpha_c})\eta_i(t)$. Thus, $\eta_i(t) > \eta_i(t_k^i)\, e^{-(\gamma_c+\beta_c\frac{\rho_c}{\alpha_c})(t-t_k^i)}$. By induction and moving back through all events t_k^i, t_{k-1}^i, ..., $t_0^i = 0$, one obtains $\eta_i(t) > \eta_i(0)\, e^{-(\gamma_c+\beta_c\frac{\rho_c}{\alpha_c})t}$ referring to its positive value. □

Next, the minimum inter-event time (MIET) for leaders is obtained which excludes the Zeno-behaviour. The MIET for followers can be obtained in a similar way.

Theorem 6.1. The minimum inter-event time for leader i, $(\forall i \in \mathcal{L})$, is strictly positive and lower-bounded by

$$t_{k+1}^i - t_k^i \geq \frac{1}{\|\boldsymbol{A}\|} \ln\left(1 + \|\boldsymbol{A}\|\,(\kappa_{1i} + \kappa_{2i})\right), \quad (i \in \mathcal{L}), \tag{6.25}$$

where

$$\kappa_{1i} = \frac{\alpha_1}{\kappa_{3i}}\left\|\mathbb{X}_i(t_{k+1}^i)\right\|, \qquad \kappa_{2i} = \frac{\beta_1}{\kappa_{3i}}\,\eta_i(0)\, e^{-(\gamma_1+\beta_1\frac{\rho_1}{\alpha_1})t_{k+1}^i},$$
$$\kappa_{3i} = \|\boldsymbol{\Phi}_1\|\left(\|\boldsymbol{B}\boldsymbol{K}_1\|\,\|\mathbb{X}_i(t_{k+1}^i)\| + \kappa_{4i}\right), \quad \kappa_{4i} = \|\boldsymbol{B}\boldsymbol{H}\sum_{j\in\mathcal{N}_{\mathcal{L}\leftarrow\mathcal{L}}^i} a_{i,j}(\boldsymbol{h}_i - \boldsymbol{h}_j)\|. \tag{6.26}$$

Proof. Consider t_k^i and t_{k+1}^i as two consecutive events for leader i. From (6.6), it holds that $\|\boldsymbol{e}_i(t_k^i)\| = 0$. For $t \geq t_k^i$, the state error $\boldsymbol{e}_i(t)$ evolves from zero until the next event is triggered at $t = t_{k+1}^i$ which fulfills (6.6). From $\boldsymbol{e}_i(t) = \boldsymbol{\Lambda}_i(t)\hat{\boldsymbol{x}}_i(t) - \boldsymbol{x}_i(t)$, it follows that $\dot{\boldsymbol{e}}_i(t) = \boldsymbol{A}\boldsymbol{\Lambda}_i(t)\hat{\boldsymbol{x}}_i(t) - \dot{\boldsymbol{x}}_i(t)$. From (6.8) and (6.1), one obtains that $\dot{\boldsymbol{x}}_i(t) = \boldsymbol{A}\boldsymbol{x}_i(t) + \boldsymbol{B}\boldsymbol{K}_1\,\mathbb{X}_i(t) + \boldsymbol{B}\boldsymbol{H}\sum_{j\in\mathcal{N}_{\mathcal{L}\leftarrow\mathcal{L}}^i} a_{i,j}(\boldsymbol{h}_i - \boldsymbol{h}_j)$. After simplifying one gets $\dot{\boldsymbol{e}}_i(t) = \boldsymbol{A}\boldsymbol{e}_i(t) - \boldsymbol{B}\boldsymbol{K}_1\,\mathbb{X}_i(t) - \boldsymbol{B}\boldsymbol{H}\sum_{j\in\mathcal{N}_{\mathcal{L}\leftarrow\mathcal{L}}^i} a_{i,j}(\boldsymbol{h}_i - \boldsymbol{h}_j)$, or $\|\dot{\boldsymbol{e}}_i(t)\| \leq \|\boldsymbol{A}\|\,\|\boldsymbol{e}_i(t)\| + \|\boldsymbol{B}\boldsymbol{K}_1\|\,\|\mathbb{X}_i(t)\| + \kappa_{4i}$, $t \in [t_k^i, t_{k+1}^i)$. It, then, follows that

$$\|\boldsymbol{e}_i(t)\| \leq \frac{\|\boldsymbol{B}\boldsymbol{K}_1\|\,\|\mathbb{X}_i(t)\| + \kappa_{4i}}{\|\boldsymbol{A}\|}\,(\,e^{\|\boldsymbol{A}\|(t-t_k^i)} - 1). \tag{6.27}$$

The next event is triggered by (6.6) at $t = t_{k+1}^i$ where

$$\|\boldsymbol{\Phi}_1 \boldsymbol{e}_i(t_{k+1}^i)\| = \alpha_1 \|\mathbb{X}_i(t_{k+1}^i)\| + \beta_1 \eta_i(t_{k+1}^i).$$

From Lemma 5, it follows that $\|\boldsymbol{e}_i(t_{k+1}^i)\| \geq \frac{\alpha_1}{\|\boldsymbol{\Phi}_1\|}\|\mathbb{X}_i(t_{k+1}^i)\| + \frac{\beta_1}{\|\boldsymbol{\Phi}_1\|}\eta_i(0)\, e^{-(\gamma_1+\beta_1\frac{\rho_1}{\alpha_1})t_{k+1}^i}$. The latter inequality together with (6.27) leads to (6.25). The right hand side of (6.25)

is strictly positive. Therefore, the minimum time between two events is strictly positive. Hence, DET (6.6) does not exhibit the Zeno behaviour. □

Corollary 1. It is straightforward to show that the MIET for followers is obtained from (6.25) by considering $\kappa_{4i}=0$, $(i \in \mathcal{F})$, and replacing the followers' parameters $\boldsymbol{K}_2$, $\boldsymbol{\Phi}_2$, α_2, β_2, γ_2, and ρ_2.

How design objectives are related to MIET (6.25)**?**

One approach to reduce the frequency of events (Design objective 1 mentioned in Section 6.1.2), is to increase the value of MIET (6.25). To this end, one should limit $\{\|\boldsymbol{K}_c\|, \|\boldsymbol{\Phi}_c\|, \gamma_c\}$ and increase $\{\alpha_c, \beta_c, \rho_c\}$ for $c \in \{1,2\}$. On the other hand, the formation-containment convergence rate (Design objective 2) is impacted by $\|\boldsymbol{K}_c\|$. Accelerating the convergence rate, for example, tends to increase $\|\boldsymbol{K}_c\|$, which decreases MIET (6.25). As mentioned previously, increasing the MIET tends to reduce $\|\boldsymbol{K}_c\|$, which may lead to a conservative convergence rate. To cope with the trade-off between the frequency of the events and convergence of the MAS, it is desirable to design unknown parameters using an optimization framework (Design objectives 3 and 4) based on an objective function that increases the value of MIET for a desired convergence rate for formation-containment.

6.3.2 Parameter design

Parameter design for leaders: This section proposes an optimization to co-design all required parameters ($\boldsymbol{K}_1$, $\boldsymbol{\Phi}_1$ α_1, β_1, γ_1, and ρ_1) for the leaders. To solve the optimization, each leader should locally compute the eigenvalues of $\boldsymbol{L}_{\mathcal{L}}$ (included in $\tilde{\boldsymbol{J}}_1$) and its matrix of eigenvectors $\boldsymbol{W}$ as a preliminary step. These eigenparameters can be computed in a distributed fashion using Algorithm 3.4.

Theorem 6.2. Let the formation gain $\boldsymbol{H}$ and formation vectors $\boldsymbol{h}_i$ satisfy the formability condition (6.15). Given (6.15) and a desired convergence rate ζ_1, if there exist matrices $\boldsymbol{P} \in \mathbb{R}^{n\times n}>0$, $\tilde{\boldsymbol{\Phi}} \in \mathbb{R}^{n\times n}>0$, $\boldsymbol{\Omega} \in \mathbb{R}^{m\times n}$, positive scalars $\tilde{\alpha}$, $\tilde{\beta}$, $\tilde{\gamma}$, $\tilde{\rho}$, τ_1, τ_2, and θ_c, $(1 \le c \le 7)$, satisfying the following optimization

$$\min \qquad \mathbb{F}_1 = \sum_{c=1}^{7} \theta_c, \tag{6.28}$$

subject to:

$$\boldsymbol{\Xi} = \begin{bmatrix} \boldsymbol{\Xi}_{11} & \tilde{\boldsymbol{J}}_1\tilde{\boldsymbol{W}}\otimes\boldsymbol{B}\boldsymbol{\Omega} & \tilde{\boldsymbol{J}}_1\otimes\boldsymbol{P} & \boldsymbol{0} \\ * & -\boldsymbol{I}_M\otimes\tilde{\boldsymbol{\Phi}} & \boldsymbol{0} & \boldsymbol{I}_M\otimes\boldsymbol{P} \\ * & * & -\tau_1\boldsymbol{I} & \boldsymbol{0} \\ * & * & * & -\tau_2\boldsymbol{I} \end{bmatrix} < 0,$$

$$\pi_1 = 1 - 2\tilde{\gamma} + 2\tilde{\beta} + 2\zeta_1 < 0, \qquad \pi_2 = 4\tilde{\alpha} + 2\tilde{\rho} + (-2+\tau_1) < 0,$$

$$\boldsymbol{\pi}_3 = (4\tilde{\alpha} + 2\tilde{\rho})\tilde{\boldsymbol{J}}_1^2 + (-2+\tau_2)\boldsymbol{I}_{M-1} < 0,$$

$$\boldsymbol{C}_1=\begin{bmatrix}\theta_1\boldsymbol{I} & \boldsymbol{I}\\ * & \boldsymbol{P}\end{bmatrix}>0,\ \boldsymbol{C}_2=\begin{bmatrix}-\theta_2\boldsymbol{I} & \tilde{\boldsymbol{\Phi}}\\ * & -\boldsymbol{I}\end{bmatrix}<0,\ \boldsymbol{C}_3=\begin{bmatrix}\theta_3 & 1\\ * & \tilde{\alpha}\end{bmatrix}>0,\ \boldsymbol{C}_4=\begin{bmatrix}\theta_4 & 1\\ * & \tilde{\beta}\end{bmatrix}>0,$$
$$\boldsymbol{C}_5=\begin{bmatrix}-\theta_5 & \tilde{\gamma}\\ * & -1\end{bmatrix}<0,\quad \boldsymbol{C}_6=\begin{bmatrix}\theta_6 & 1\\ * & \tilde{\rho}\end{bmatrix}>0,\quad \boldsymbol{C}_7=\begin{bmatrix}-\theta_7\boldsymbol{I} & \boldsymbol{\Omega}\\ * & -\boldsymbol{I}\end{bmatrix}<0, \tag{6.29}$$

where $\boldsymbol{\Xi}_{11}=\boldsymbol{I}_{M-1}\otimes(\boldsymbol{P}\boldsymbol{A}^T+\boldsymbol{A}\boldsymbol{P})+\tilde{\boldsymbol{J}}_1\otimes\boldsymbol{B}\boldsymbol{\Omega}+(\tilde{\boldsymbol{J}}_1\otimes\boldsymbol{B}\boldsymbol{\Omega})^T+2\zeta_1\boldsymbol{I}_{M-1}\otimes\boldsymbol{P}$, then design parameters for leaders are computed as

$$\boldsymbol{K}_1=\boldsymbol{\Omega}\boldsymbol{P}^{-1},\quad \boldsymbol{\Phi}_1=(\boldsymbol{P}^{-1}\tilde{\boldsymbol{\Phi}}\boldsymbol{P}^{-1})^{1/2},\quad \alpha_1=\sqrt{\tilde{\alpha}},\quad \beta_1=\sqrt{\tilde{\beta}},\quad \gamma_1=\tilde{\gamma},\quad \rho_1=\sqrt{\tilde{\rho}}. \tag{6.30}$$

Using design parameters (6.30), system trajectories converge at a rate which satisfies

$$\lambda_{\min}(\boldsymbol{P}^{-1})\,\boldsymbol{\psi}_{\mathcal{L}}^T(t)\,\boldsymbol{\psi}_{\mathcal{L}}(t)+\,\boldsymbol{\eta}_{\mathcal{L}}^T(t)\,\boldsymbol{\eta}_{\mathcal{L}}(t)\leq\mu e^{-2\zeta_1 t}, \tag{6.31}$$

where $\mu=\lambda_{\max}(\boldsymbol{P}^{-1})\,\boldsymbol{\psi}_{\mathcal{L}}^T(0)\,\boldsymbol{\psi}_{\mathcal{L}}(0)+\,\boldsymbol{\eta}_{\mathcal{L}}^T(0)\,\boldsymbol{\eta}_{\mathcal{L}}(0)$. The following bounds are guaranteed by minimizing $\mathbb{F}_1$

$$\|\boldsymbol{K}_1\|\leq\theta_1\sqrt{\theta_7},\ \ \|\boldsymbol{\Phi}_1\|\leq\theta_1\theta_2^{1/4},\ \ \alpha_1\geq\frac{1}{\sqrt{\theta_3}},\ \ \beta_1\geq\frac{1}{\sqrt{\theta_4}},\ \ \gamma_1\leq\sqrt{\theta_5},\quad \rho_1\geq\frac{1}{\sqrt{\theta_6}}. \tag{6.32}$$

Proof. The proof is included in Appendix, Section 6.5.1. □

Parameter design for followers: The following theorem co-designs all required parameters ($\boldsymbol{K}_2$, $\boldsymbol{\Phi}_2$ α_2, β_2, γ_2, and ρ_2) for the followers. The following optimization is based on the knowledge of the eigenvalues and eigenvectors of $\boldsymbol{L}_{\mathcal{F}}$. The eigenvalues of $\boldsymbol{L}_{\mathcal{F}}$ are equal to non-zero eigenvalues of $\boldsymbol{L}_{\text{est}}=[\boldsymbol{L}_{\mathcal{F}}\ \ \boldsymbol{L}_{\mathcal{F}\mathcal{L}};\boldsymbol{0}\ \ \boldsymbol{0}]$. The eigenvalues of $\boldsymbol{L}_{\text{est}}$ can be computed by the followers in a distributed fashion using [112].

Theorem 6.3. Let the formability condition (6.15) hold. Given (6.15) and a desired convergence rate ζ_2, if there exist matrices $\boldsymbol{P}\in\mathbb{R}^{n\times n}>0$, $\tilde{\boldsymbol{\Phi}}\in\mathbb{R}^{n\times n}>0$, $\boldsymbol{\Omega}\in\mathbb{R}^{m\times n}$, positive scalars $\tilde{\alpha}$, $\tilde{\beta}$, $\tilde{\gamma}$, $\tilde{\rho}$, τ_1, τ_2, and θ_c, $(1\leq c\leq 7)$, satisfying the following optimization[1]

$$\min\qquad \mathbb{F}_2=\sum_{c=1}^{7}\theta_c, \tag{6.33}$$

subject to:

$$\boldsymbol{\Xi}=\begin{bmatrix}\boldsymbol{\Xi}_{11} & \boldsymbol{J}_2\boldsymbol{V}^{-1}\otimes\boldsymbol{B}\boldsymbol{\Omega} & \boldsymbol{I}_N\otimes\boldsymbol{P} & \boldsymbol{0}\\ * & -\boldsymbol{I}_N\otimes\tilde{\boldsymbol{\Phi}} & \boldsymbol{0} & \boldsymbol{I}_N\otimes\boldsymbol{P}\\ * & * & -\tau_1\boldsymbol{I} & \boldsymbol{0}\\ * & * & * & -\tau_2\boldsymbol{I}\end{bmatrix}<0,$$
$$\pi_1=1-2\tilde{\gamma}+2\tilde{\beta}+2\zeta_2<0,\qquad \pi_2=4\tilde{\alpha}+2\tilde{\rho}+(-2+\tau_1)<0,$$
$$\boldsymbol{\pi}_3=(4\tilde{\alpha}+2\tilde{\rho})\boldsymbol{J}_2^2+(-2+\tau_2)\boldsymbol{I}_N<0,$$

[1]To improve comprehension, common notation used for leaders and followers is intentionally kept the same in Theorems 6.2 and 6.3. For example, $\boldsymbol{\Xi}$ in Theorem 6.2 corresponds to the constraint matrix for the leaders. Likewise, $\boldsymbol{\Xi}$ in Theorem 6.3 corresponds to the constraint matrix for the followers. The difference between them is evident from the context where the symbols are used.

Algorithm 6.10 . FCC/DEME

I(a). Parameter Design (Leaders): (D1 -D3)

D1. Formation gain $\boldsymbol{H}$ is selected such that the formability condition (6.15) is satisfied for formation vectors $\boldsymbol{h}_i$.

D2. Each leader uses a distributed approach such as Algorithm 3.4 to locally compute the eigenvalues and eigenvectors of $\boldsymbol{L}_{\mathcal{L}}$. Then, they construct $\tilde{\boldsymbol{J}}_1$ and $\tilde{\boldsymbol{W}}$ following Section 6.2.1.

D3. Each leader solves optimization (6.28) for an agreed value of ζ_1. The control gain and dynamic event-triggering parameters are computed from (6.30).

I(b). Parameter Design (Followers): (D1 -D2)

D1. Each follower uses a distributed approach [112, 127] to locally compute the eigenvalues and eigenvectors of $\boldsymbol{L}_{\mathcal{F}}$.

D2. Followers solve optimization (6.33) for an agreed value of ζ_2. The control gain and dynamic event-triggering parameters are computed from (6.35).

II. Execution: (E1 and E2)

E1. Leaders and followers transmit their initial state values $\boldsymbol{x}_i(0)$ to their neighbourhoods.

E2. Using designed parameters the states of the leaders approach the desired formation specified by formation vectors $\boldsymbol{h}_i$. The followers achieve the event-triggered containment.

$$\boldsymbol{C}_1=\begin{bmatrix}\theta_1\boldsymbol{I} & \boldsymbol{I}\\ * & \boldsymbol{P}\end{bmatrix}>0,\ \boldsymbol{C}_2=\begin{bmatrix}-\theta_2\boldsymbol{I} & \tilde{\boldsymbol{\Phi}}\\ * & -\boldsymbol{I}\end{bmatrix}<0,\ \boldsymbol{C}_3=\begin{bmatrix}\theta_3 & 1\\ * & \tilde{\alpha}\end{bmatrix}>0,\ \boldsymbol{C}_4=\begin{bmatrix}\theta_4 & 1\\ * & \tilde{\beta}\end{bmatrix}>0,$$
$$\boldsymbol{C}_5=\begin{bmatrix}-\theta_5 & \tilde{\gamma}\\ * & -1\end{bmatrix}<0,\quad \boldsymbol{C}_6=\begin{bmatrix}\theta_6 & 1\\ * & \tilde{\rho}\end{bmatrix}>0,\quad \boldsymbol{C}_7=\begin{bmatrix}-\theta_7\boldsymbol{I} & \boldsymbol{\Omega}\\ * & -\boldsymbol{I}\end{bmatrix}<0, \tag{6.34}$$

where $\boldsymbol{\Xi}_{11}=\boldsymbol{I}_N\otimes(\boldsymbol{P}\boldsymbol{A}^T+\boldsymbol{A}\boldsymbol{P})+\boldsymbol{J}_2\otimes\boldsymbol{B}\boldsymbol{\Omega}+(\boldsymbol{J}_2\otimes\boldsymbol{B}\boldsymbol{\Omega})^T+2\zeta_2\boldsymbol{I}_N\otimes\boldsymbol{P}$, then design parameters for followers are computed as

$$\boldsymbol{K}_2=\boldsymbol{\Omega}\boldsymbol{P}^{-1},\quad \boldsymbol{\Phi}_2=(\boldsymbol{P}^{-1}\tilde{\boldsymbol{\Phi}}\boldsymbol{P}^{-1})^{1/2},\quad \alpha_2=\sqrt{\tilde{\alpha}},\quad \beta_2=\sqrt{\tilde{\beta}},\quad \gamma_2=\tilde{\gamma},\quad \rho_2=\sqrt{\tilde{\rho}}. \tag{6.35}$$

The following bounds are guaranteed by minimizing $\mathbb{F}_2$

$$\|\boldsymbol{K}_2\|\leq\theta_1\sqrt{\theta_7},\ \ \|\boldsymbol{\Phi}_2\|\leq\theta_1\theta_2^{1/4},\ \ \alpha_2\geq\frac{1}{\sqrt{\theta_3}},\ \ \beta_2\geq\frac{1}{\sqrt{\theta_4}},\ \ \gamma_2\leq\sqrt{\theta_5},\quad \rho_2\geq\frac{1}{\sqrt{\theta_6}}. \tag{6.36}$$

Proof. The proof is included in Appendix, Section 6.5.2. □

Based on Theorems 6.2 and 6.3, the proposed formation-containment control using dynamic event-triggered mechanism (FCC/DEME) is summarized in Algorithm 6.10.

Remark 6.4. It should be noted that the parameter design stage in FCC/DEME is independent of $\boldsymbol{L}_{\mathcal{FL}}$. Therefore, the communication topology between the leaders and followers can change during the formation-containment process without requiring a re-design of the control and event-triggering parameters. In other words, the leader-to-follower transmission can be performed by different leaders at each period of time. This prolongs the leaders' communication energy resources since one subset of leaders can transmit to the followers for a certain time interval. Then, this subset ceases the leader-to-follower transmission and another subset takes the responsibility of transmitting to the followers.

6.4 Summary

Referred to as the FCC/DEME, this chapter proposes a formation-containment control (FCC) implementation using the dynamic event-triggered (DET) strategy for multi-agent systems. To achieve formation for the leaders and containment for the followers, the formation and containment formulations are converted to stability problems of equivalent systems. The Lyapunov stability theorem is used to develop sufficient conditions to guarantee formation-containment. An objective function is proposed for optimal parameters design. Namely, the control gains and DET parameters, are computed through a constrained convex optimization framework.

6.5 Appendix

6.5.1 Proof of Theorem 6.2

Proof. Consider the following inequality

$$\dot{V} + 2\,\zeta_1\, V < 0, \tag{6.37}$$

where $V = V_1 + V_2$ with

$$V_1 = \boldsymbol{\psi}_{\mathcal{L}}^T (\boldsymbol{I}_{M-1} \otimes \boldsymbol{P}^{-1})\, \boldsymbol{\psi}_{\mathcal{L}}, \qquad V_2 = \boldsymbol{\eta}_{\mathcal{L}}^T\, \boldsymbol{\eta}_{\mathcal{L}}. \tag{6.38}$$

Inequality (6.37) leads to the exponential convergence rate specified in (6.31). The time derivative for V_1 is obtained as follows

$$\dot{V}_1 = \boldsymbol{\psi}_{\mathcal{L}}^T\, \bar{\boldsymbol{\Xi}}_{11}\, \boldsymbol{\psi}_{\mathcal{L}} + 2\boldsymbol{\psi}_{\mathcal{L}}^T\, \bar{\boldsymbol{\Xi}}_{12}\, \boldsymbol{e}_{\mathcal{L}}, \tag{6.39}$$

where

$$\bar{\boldsymbol{\Xi}}_{11} = \boldsymbol{I}_{M-1} \otimes (\boldsymbol{A}^T \boldsymbol{P}^{-1} + \boldsymbol{P}^{-1}\boldsymbol{A}) + 2\tilde{\boldsymbol{J}}_1 \otimes \boldsymbol{P}^{-1}\boldsymbol{B}\boldsymbol{K}_1, \qquad \bar{\boldsymbol{\Xi}}_{12} = \tilde{\boldsymbol{J}}_1 \tilde{\boldsymbol{W}} \otimes \boldsymbol{P}^{-1}\boldsymbol{B}\boldsymbol{K}_1.$$

In what follows, $\dot{V}_2$ is expanded based on (6.7)

$$\dot{V}_2 = 2\,\boldsymbol{\eta}_{\mathcal{L}}^T(-\gamma_1\, \boldsymbol{\eta}_{\mathcal{L}} + \rho_1 \bar{\mathbb{X}}_{\mathcal{L}}). \tag{6.40}$$

From Young's inequality, it holds that $\boldsymbol{\eta}_{\mathcal{L}}^T(\rho_1 \bar{\mathbb{X}}_{\mathcal{L}}) + \rho_1 \bar{\mathbb{X}}_{\mathcal{L}}^T \boldsymbol{\eta}_{\mathcal{L}} \leq \boldsymbol{\eta}_{\mathcal{L}}^T \boldsymbol{\eta}_{\mathcal{L}} + \rho_1^2 \bar{\mathbb{X}}_{\mathcal{L}}^T \bar{\mathbb{X}}_{\mathcal{L}}$. The following upper-bound for (6.40) is obtained

$$\dot{V}_2 \leq (1 - 2\,\gamma_1)\, \boldsymbol{\eta}_{\mathcal{L}}^T\, \boldsymbol{\eta}_{\mathcal{L}} + \rho_1^2\, \bar{\mathbb{X}}_{\mathcal{L}}^T \bar{\mathbb{X}}_{\mathcal{L}}. \tag{6.41}$$

The global form of (6.4) for leaders can be viewed as follows

$$\mathbb{X}_{\mathcal{L}} = \boldsymbol{L}_{\mathcal{L}} \otimes \boldsymbol{I}_n(\boldsymbol{\Lambda}_{\mathcal{L}} \hat{\boldsymbol{x}}_{\mathcal{L}} - \boldsymbol{h}). \tag{6.42}$$

From $\boldsymbol{e}_{\mathcal{L}} = \boldsymbol{\Lambda}_{\mathcal{L}} \hat{\boldsymbol{x}}_{\mathcal{L}} - \boldsymbol{x}_{\mathcal{L}}$, $\boldsymbol{z} = \boldsymbol{x}_{\mathcal{L}} - \boldsymbol{h}$, and $\boldsymbol{L}_{\mathcal{L}} = \tilde{\boldsymbol{W}}^{\dagger} \tilde{\boldsymbol{J}}_1 \tilde{\boldsymbol{W}}$, the following expression from (6.13) and (6.42) is derived

$$\mathbb{X}_{\mathcal{L}} = (\tilde{\boldsymbol{W}}^{\dagger} \tilde{\boldsymbol{J}}_1) \otimes \boldsymbol{I}_n \boldsymbol{\psi}_{\mathcal{L}} + (\tilde{\boldsymbol{W}}^{\dagger} \tilde{\boldsymbol{J}}_1 \tilde{\boldsymbol{W}}) \otimes \boldsymbol{I}_n \boldsymbol{e}_{\mathcal{L}}. \tag{6.43}$$

Considering that $\tilde{\boldsymbol{W}}^{\dagger^T}\tilde{\boldsymbol{W}}^{\dagger}=\boldsymbol{I}$, expression $\bar{\mathbb{X}}_{\mathcal{L}}^T\bar{\mathbb{X}}_{\mathcal{L}}$ is expanded below

$$\bar{\mathbb{X}}_{\mathcal{L}}^T\bar{\mathbb{X}}_{\mathcal{L}}=\mathbb{X}_{\mathcal{L}}^T\mathbb{X}_{\mathcal{L}}\leq 2\boldsymbol{\sigma}_1^T\boldsymbol{\sigma}_1+2\boldsymbol{\sigma}_2^T(\tilde{\boldsymbol{J}}_1^2\otimes\boldsymbol{I}_n)\boldsymbol{\sigma}_2, \tag{6.44}$$

where $\boldsymbol{\sigma}_1=(\tilde{\boldsymbol{W}}^{\dagger}\tilde{\boldsymbol{J}}_1)\otimes\boldsymbol{I}_n\boldsymbol{\psi}_{\mathcal{L}}$ and $\boldsymbol{\sigma}_2=\tilde{\boldsymbol{W}}\otimes\boldsymbol{I}_n\boldsymbol{e}_{\mathcal{L}}$. The following upper-bound holds from (6.41) and (6.44)

$$\dot{V}_2\leq(1-2\,\gamma_1)\boldsymbol{\eta}_{\mathcal{L}}^T\boldsymbol{\eta}_{\mathcal{L}}+2\rho_1^2\boldsymbol{\sigma}_1^T\boldsymbol{\sigma}_1+2\rho_1^2\boldsymbol{\sigma}_2^T(\tilde{\boldsymbol{J}}_1^2\otimes\boldsymbol{I}_n)\boldsymbol{\sigma}_2. \tag{6.45}$$

The following two equalities hold by definition

$$\tau_1^{-1}\left(\boldsymbol{\psi}_{\mathcal{L}}^T(\tilde{\boldsymbol{J}}_1^2\otimes\boldsymbol{I}_n)\boldsymbol{\psi}_{\mathcal{L}}-\boldsymbol{\sigma}_1^T\boldsymbol{\sigma}_1\right)=0, \tag{6.46}$$

$$\tau_2^{-1}(\boldsymbol{e}_{\mathcal{L}}^T\boldsymbol{e}_{\mathcal{L}}-\boldsymbol{\sigma}_2^T\boldsymbol{\sigma}_2)\geq 0, \tag{6.47}$$

where $\tau_1{>}0$ and $\tau_2{>}0$ are decision variables. Based on (6.6), it holds that $\|\boldsymbol{\Phi}_1\boldsymbol{e}_i(t)\|\leq\alpha_1\|\mathbb{X}_i(t)\|+\beta_1\eta_i(t)$. Let $\boldsymbol{a}_1=[\,\|\boldsymbol{\Phi}_1\boldsymbol{e}_{N+1}(t)\|,\ldots,\|\boldsymbol{\Phi}_1\boldsymbol{e}_{N+M}(t)\|\,]^T$. In a collective fashion it holds that $\boldsymbol{a}_1\leq\alpha_1\bar{\mathbb{X}}_{\mathcal{L}}+\beta_1\boldsymbol{\eta}_{\mathcal{L}}$, which is equivalent to

$$\begin{aligned}\boldsymbol{a}_1^T\boldsymbol{a}_1=\boldsymbol{e}_{\mathcal{L}}^T(\boldsymbol{I}_M\otimes\boldsymbol{\Phi}_1^2)\boldsymbol{e}_{\mathcal{L}}&\leq(\alpha_1\bar{\mathbb{X}}_{\mathcal{L}}+\beta_1\boldsymbol{\eta}_{\mathcal{L}})^T(\alpha_1\bar{\mathbb{X}}_{\mathcal{L}}+\beta_1\boldsymbol{\eta}_{\mathcal{L}})\\&\leq 2\alpha_1^2\bar{\mathbb{X}}_{\mathcal{L}}^T\bar{\mathbb{X}}_{\mathcal{L}}+2\beta_1^2\boldsymbol{\eta}_{\mathcal{L}}^T\boldsymbol{\eta}_{\mathcal{L}}.\end{aligned} \tag{6.48}$$

Using (6.44), the following expression holds from (6.48)

$$\boldsymbol{e}_{\mathcal{L}}^T(\boldsymbol{I}_M\otimes\boldsymbol{\Phi}_1^2)\boldsymbol{e}_{\mathcal{L}}\leq 4\alpha_1^2\boldsymbol{\sigma}_1^T\boldsymbol{\sigma}_1+4\alpha_1^2\boldsymbol{\sigma}_2^T(\tilde{\boldsymbol{J}}_1^2\otimes\boldsymbol{I}_n)\boldsymbol{\sigma}_2+2\beta_1^2\boldsymbol{\eta}_{\mathcal{L}}^T\boldsymbol{\eta}_{\mathcal{L}}. \tag{6.49}$$

Let $\boldsymbol{\nu}=[\,\boldsymbol{\psi}_{\mathcal{L}}^T,\boldsymbol{e}_{\mathcal{L}}^T,\boldsymbol{\eta}_{\mathcal{L}}^T,\boldsymbol{\sigma}_1^T,\,\boldsymbol{\sigma}_2^T\,]^T$. Based on (6.39), (6.45), (6.46), (6.47), and (6.49), expression (6.37) is re-arranged as follows

$$\boldsymbol{\nu}^T\begin{bmatrix}\tilde{\boldsymbol{\Xi}} & \boldsymbol{0}\\ * & \tilde{\boldsymbol{\Pi}}\end{bmatrix}\boldsymbol{\nu}<0, \tag{6.50}$$

where $\tilde{\boldsymbol{\Xi}}=\begin{bmatrix}\tilde{\boldsymbol{\Xi}}_{11} & \tilde{\boldsymbol{\Xi}}_{12}\\ * & \tilde{\boldsymbol{\Xi}}_{22}\end{bmatrix}$ and $\tilde{\boldsymbol{\Pi}}=\mathrm{diag}(\tilde{\boldsymbol{\pi}}_1,\tilde{\boldsymbol{\pi}}_2,\tilde{\boldsymbol{\pi}}_3)$ and

$$\begin{aligned}\tilde{\boldsymbol{\Xi}}_{11}&=\bar{\boldsymbol{\Xi}}_{11}+\tau_1^{-1}\tilde{\boldsymbol{J}}_1^2\otimes\boldsymbol{I}_n+2\zeta_1\boldsymbol{I}_{M-1}\otimes\boldsymbol{P}^{-1},\qquad \tilde{\boldsymbol{\Xi}}_{22}=-\boldsymbol{I}_M\otimes\boldsymbol{\Phi}_1^2+\tau_2^{-1}\boldsymbol{I}_{Mn},\\ \tilde{\boldsymbol{\pi}}_1&=(1-2\gamma_1+2\beta_1^2+2\zeta_1)\boldsymbol{I}_M,\qquad \tilde{\boldsymbol{\pi}}_2=(2\rho_1^2-\tau_1^{-1}+4\alpha_1^2)\boldsymbol{I}_{Mn},\\ \tilde{\boldsymbol{\pi}}_3&=-\tau_2^{-1}\boldsymbol{I}+(4\alpha_1^2+2\rho_1^2)(\tilde{\boldsymbol{J}}_1^2\otimes\boldsymbol{I}_n).\end{aligned} \tag{6.51}$$

Based on (6.50), inequality (6.37) is guaranteed if $\tilde{\boldsymbol{\Xi}}{<}0$ and $\tilde{\boldsymbol{\Pi}}{<}0$. Pre- and post multiply inequality $\tilde{\boldsymbol{\Xi}}$ by $\boldsymbol{T}=\mathrm{diag}(\boldsymbol{I}_{M-1}\otimes\boldsymbol{P},\boldsymbol{I}_M\otimes\boldsymbol{P})$ which results in $\hat{\boldsymbol{\Xi}}=\begin{bmatrix}\hat{\boldsymbol{\Xi}}_{11} & \hat{\boldsymbol{\Xi}}_{12}\\ * & \hat{\boldsymbol{\Xi}}_{22}\end{bmatrix}<0$ where

$$\begin{aligned}\hat{\boldsymbol{\Xi}}_{11}&=\boldsymbol{I}_{M-1}\otimes(\boldsymbol{P}\boldsymbol{A}^T+\boldsymbol{A}\boldsymbol{P})+2\tilde{\boldsymbol{J}}_1\otimes\boldsymbol{B}\boldsymbol{K}_1\boldsymbol{P}+\tau_1^{-1}(\tilde{\boldsymbol{J}}_1\otimes\boldsymbol{P})^2+2\zeta_1\boldsymbol{I}_{M-1}\otimes\boldsymbol{P},\\ \hat{\boldsymbol{\psi}}_{12}&=\tilde{\boldsymbol{J}}_1\tilde{\boldsymbol{W}}\otimes\boldsymbol{B}\boldsymbol{K}_1\boldsymbol{P},\qquad \hat{\boldsymbol{\psi}}_{22}=-\boldsymbol{I}_M\otimes(\boldsymbol{P}\boldsymbol{\Phi}_1^2\boldsymbol{P})+\tau_2^{-1}\boldsymbol{I}_M\otimes\boldsymbol{P}^2.\end{aligned} \tag{6.52}$$

Denote $\boldsymbol{\Omega}=\boldsymbol{K}_1\boldsymbol{P}$ and $\tilde{\boldsymbol{\Phi}}=\boldsymbol{P}\boldsymbol{\Phi}_1^2\boldsymbol{P}$ as alternative variables. Then, the *Schur complement* is applied on $\hat{\boldsymbol{\Xi}}$ which results in $\boldsymbol{\Xi}{<}0$ given in the statement of the theorem.

Denote $\tilde{\alpha}=\alpha_1^2$, $\tilde{\beta}=\beta_1^2$, $\tilde{\gamma}=\gamma_1$, and $\tilde{\rho}=\rho_1^2$. The following inequality is also considered

$$-\tau_i^{-1} \leq -2+\tau_i, \qquad i \in \{1,2\}. \tag{6.53}$$

Using $\tilde{\alpha}$, $\tilde{\beta}$, $\tilde{\gamma}$, $\tilde{\rho}$, and considering (6.53), inequalities $\pi_1<0$, $\pi_2<0$, and $\boldsymbol{\pi}_3<0$ given in the statement of the theorem are obtained. The relations between design parameters and decision variables are given in (6.30).

Motivated by [116, Sec. 2.2] and similar to [36, 40], a linear scalarization method is used to decrease/increase the decision variables used in $\boldsymbol{K}_1$, $\boldsymbol{\Phi}_1$, α_1, β_1, γ_1, and ρ_1 (see (6.30)). To this end, consider the following constraints

$$\begin{aligned} &\boldsymbol{P}^{-1}<\theta_1\boldsymbol{I}, \qquad \tilde{\boldsymbol{\Phi}}^T\tilde{\boldsymbol{\Phi}}<\theta_2\boldsymbol{I}, \qquad \tilde{\alpha}^{-1}<\theta_3, \qquad \tilde{\beta}^{-1}<\theta_4,\\ &\tilde{\gamma}^2<\theta_5, \qquad \tilde{\rho}^{-1}<\theta_6, \qquad \boldsymbol{\Omega}^T\boldsymbol{\Omega}<\theta_7\boldsymbol{I}, \end{aligned} \tag{6.54}$$

where $\theta_c>0$, $(1\leq c\leq 7)$, are decision variables. Based on inequalities (6.54), if one decreases θ_c, $(1\leq c\leq 7)$, parameters $\{\|\tilde{\boldsymbol{\Phi}}\|, \tilde{\gamma}, \|\boldsymbol{\Omega}\|\}$ are decreased and parameters $\{\|\boldsymbol{P}\|, \tilde{\alpha}, \tilde{\beta}, \tilde{\rho}\}$ are increased. Therefore, design parameters $\{\|\boldsymbol{K}_1\|, \|\boldsymbol{\Phi}_1\|, \gamma_1\}$ are decreased and $\{\alpha_1, \beta_1, \rho_1\}$ are increased based on (6.30). These together increase MIET (6.25). Inequalities (6.32) are obtained from (6.54). The objective function $\mathbb{F}_1$ in (6.28) minimizes a weighted sum of the decision variables θ_c with all weights equal to 1. The LMIs given in (6.29) that include θ_c, $(1\leq c\leq 7)$, are equivalent to (6.54) using Schur complement. Once (6.28) is solved, design parameters are computed from (6.30) and that completes the proof. □

6.5.2 Proof of Theorem 6.3

Proof. The proof follows the same steps given in the proof of Theorem 6.2. Consider the following inequality

$$\dot{V}+2\,\zeta_2\,V<0, \tag{6.55}$$

where $V=V_1+V_2$ with

$$V_1=\tilde{\boldsymbol{\psi}}_{\mathcal{F}}^T(\boldsymbol{I}_N\otimes\boldsymbol{P}^{-1})\,\tilde{\boldsymbol{\psi}}_{\mathcal{F}}, \qquad V_2=\boldsymbol{\eta}_{\mathcal{F}}^T\,\boldsymbol{\eta}_{\mathcal{F}}. \tag{6.56}$$

From (6.23) and (6.56), it follows that

$$\dot{V}_1=\tilde{\boldsymbol{\psi}}_{\mathcal{F}}^T\,\bar{\boldsymbol{\Xi}}_{11}\,\tilde{\boldsymbol{\psi}}_{\mathcal{F}}+2\tilde{\boldsymbol{\psi}}_{\mathcal{F}}^T\,\bar{\boldsymbol{\Xi}}_{12}\,\boldsymbol{e}_{\mathcal{F}}, \tag{6.57}$$

where

$$\begin{aligned} &\bar{\boldsymbol{\Xi}}_{11}=\boldsymbol{I}_N\otimes(\boldsymbol{A}^T\boldsymbol{P}^{-1}+\boldsymbol{P}^{-1}\boldsymbol{A})+2\boldsymbol{J}_2\otimes\boldsymbol{P}^{-1}\boldsymbol{B}\boldsymbol{K}_2,\\ &\bar{\boldsymbol{\Xi}}_{12}=\boldsymbol{J}_2\boldsymbol{V}^{-1}\otimes\boldsymbol{P}^{-1}\boldsymbol{B}\boldsymbol{K}_2, \end{aligned} \tag{6.58}$$

In what follows, $\dot{V}_2$ is expanded based on (6.7)

$$\dot{V}_2=2\,\boldsymbol{\eta}_{\mathcal{F}}^T(-\gamma_2\,\boldsymbol{\eta}_{\mathcal{F}}+\rho_2\bar{\mathbb{X}}_{\mathcal{F}}). \tag{6.59}$$

Similar to (6.41) the following condition holds from (6.59)

$$\dot{V}_2 \leq (1-2\,\gamma_2)\,\boldsymbol{\eta}_{\mathcal{F}}^T\boldsymbol{\eta}_{\mathcal{F}} + \rho_2^2\,\bar{\mathbb{X}}_{\mathcal{F}}^T\bar{\mathbb{X}}_{\mathcal{F}}. \tag{6.60}$$

The global form of (6.4) for followers is given below

$$\mathbb{X}_{\mathcal{F}} = \boldsymbol{L}_{\mathcal{G}}\otimes\boldsymbol{I}_n\boldsymbol{\Lambda}_{\mathcal{F}}\hat{\boldsymbol{x}}_{\mathcal{F}} + \boldsymbol{L}_{\mathcal{FL}}\otimes\boldsymbol{I}_n\boldsymbol{x}_{\mathcal{L}}. \tag{6.61}$$

Considering $\boldsymbol{e}_{\mathcal{F}} = \boldsymbol{\Lambda}_{\mathcal{F}}\hat{\boldsymbol{x}}_{\mathcal{F}} - \boldsymbol{x}_{\mathcal{F}}$, $\boldsymbol{V}\boldsymbol{J}_2\boldsymbol{V}^{-1} = \boldsymbol{L}_{\mathcal{G}}$, and transformation (6.17), the following expression is developed from (6.61)

$$\mathbb{X}_{\mathcal{F}} = \boldsymbol{\psi}_{\mathcal{G}} + (\boldsymbol{V}\boldsymbol{J}_2\otimes\boldsymbol{I}_n)\boldsymbol{\sigma}. \tag{6.62}$$

where $\boldsymbol{\sigma} = (\boldsymbol{V}^{-1}\otimes\boldsymbol{I}_n)\boldsymbol{e}_{\mathcal{F}}$. Recalling that $\boldsymbol{V}^T\boldsymbol{V} = \boldsymbol{I}$ (symmetric matrices have orthogonal eigenvectors), we expand $\bar{\mathbb{X}}_{\mathcal{F}}^T\bar{\mathbb{X}}_{\mathcal{F}}$

$$\bar{\mathbb{X}}_{\mathcal{F}}^T\bar{\mathbb{X}}_{\mathcal{F}} = \mathbb{X}_{\mathcal{G}}^T\mathbb{X}_{\mathcal{G}} = 2\boldsymbol{\psi}_{\mathcal{G}}^T\boldsymbol{\psi}_{\mathcal{G}} + 2\boldsymbol{\sigma}^T(\boldsymbol{J}_2\otimes\boldsymbol{I}_n)^2\boldsymbol{\sigma}. \tag{6.63}$$

The following upper-bound holds from (6.60) and (6.63)

$$\dot{V}_2 \leq (1-2\,\gamma_2)\,\boldsymbol{\eta}_{\mathcal{F}}^T\boldsymbol{\eta}_{\mathcal{F}} + 2\rho_2^2\boldsymbol{\psi}_{\mathcal{G}}^T\boldsymbol{\psi}_{\mathcal{G}} + 2\rho_2^2\boldsymbol{\sigma}^T(\boldsymbol{J}_2\otimes\boldsymbol{I}_n)^2\boldsymbol{\sigma}. \tag{6.64}$$

Based on (6.6), it holds that $\|\boldsymbol{\Phi}_2\boldsymbol{e}_i(t)\| \leq \alpha_2\|\mathbb{X}_i(t)\| + \beta_2\eta_i(t)$. Let $\boldsymbol{a}_1 = [\|\boldsymbol{\Phi}_2\boldsymbol{e}_1(t)\|, \ldots, \|\boldsymbol{\Phi}_2\boldsymbol{e}_N(t)\|]^T$. Collectively, it holds that $\boldsymbol{a}_1 \leq \alpha_2\bar{\mathbb{X}}_{\mathcal{F}} + \beta_2\boldsymbol{\eta}_{\mathcal{F}}$, or

$$\begin{aligned}\boldsymbol{a}_1^T\boldsymbol{a}_1 = \boldsymbol{e}_{\mathcal{F}}^T(\boldsymbol{I}_N\otimes\boldsymbol{\Phi}_2^2)\boldsymbol{e}_{\mathcal{F}} &\leq (\alpha_2\bar{\mathbb{X}}_{\mathcal{F}} + \beta_2\boldsymbol{\eta}_{\mathcal{F}})^T(\alpha_2\bar{\mathbb{X}}_{\mathcal{F}} + \beta_2\boldsymbol{\eta}_{\mathcal{F}}) \\ &\leq 2\alpha_2^2\bar{\mathbb{X}}_{\mathcal{F}}^T\bar{\mathbb{X}}_{\mathcal{F}} + 2\beta_2^2\boldsymbol{\eta}_{\mathcal{F}}^T\boldsymbol{\eta}_{\mathcal{F}}.\end{aligned} \tag{6.65}$$

Using (6.63) the following expression holds from (6.65)

$$\boldsymbol{e}_{\mathcal{F}}^T(\boldsymbol{I}_N\otimes\boldsymbol{\Phi}_2^2)\boldsymbol{e}_{\mathcal{F}} \leq 4\alpha_2^2\boldsymbol{\psi}_{\mathcal{G}}^T\boldsymbol{\psi}_{\mathcal{G}} + 4\alpha_2^2\boldsymbol{\sigma}^T(\boldsymbol{J}_2\otimes\boldsymbol{I}_n)^2\boldsymbol{\sigma} + 2\beta_2^2\boldsymbol{\eta}_{\mathcal{F}}^T\boldsymbol{\eta}_{\mathcal{F}}. \tag{6.66}$$

The following equality holds by definition

$$\tau_1^{-1}(\tilde{\boldsymbol{\psi}}_{\mathcal{G}}^T\tilde{\boldsymbol{\psi}}_{\mathcal{G}} - \boldsymbol{\psi}_{\mathcal{G}}^T\boldsymbol{\psi}_{\mathcal{G}}) = 0, \tag{6.67}$$

$$\tau_2^{-1}\left(\boldsymbol{e}_{\mathcal{F}}^T\boldsymbol{e}_{\mathcal{F}} - \boldsymbol{\sigma}^T\boldsymbol{\sigma}\right) \geq 0, \tag{6.68}$$

where $\tau_1{>}0$ and $\tau_2{>}0$ are decision variables. Let $\boldsymbol{\nu} = [\,\tilde{\boldsymbol{\psi}}_{\mathcal{F}}^T, \boldsymbol{e}_{\mathcal{F}}^T, \boldsymbol{\eta}_{\mathcal{F}}^T, \boldsymbol{\psi}_{\mathcal{F}}^T, \boldsymbol{\sigma}^T]^T$. Based on (6.57), (6.64), (6.67), (6.68) and (6.66), we re-arrange (6.55) as follows

$$\boldsymbol{\nu}^T\begin{bmatrix}\tilde{\boldsymbol{\Xi}} & \boldsymbol{0}\\ * & \tilde{\boldsymbol{\Pi}}\end{bmatrix}\boldsymbol{\nu} < 0, \tag{6.69}$$

where $\tilde{\boldsymbol{\Xi}} = \begin{bmatrix}\tilde{\boldsymbol{\Xi}}_{11} & \bar{\boldsymbol{\Xi}}_{12}\\ * & \bar{\boldsymbol{\Xi}}_{22}\end{bmatrix}$ and $\tilde{\boldsymbol{\Pi}} = \mathrm{diag}(\tilde{\boldsymbol{\pi}}_1, \tilde{\boldsymbol{\pi}}_2, \tilde{\boldsymbol{\pi}}_3)$ and

$$\begin{aligned}&\tilde{\boldsymbol{\Xi}}_{11} = \bar{\boldsymbol{\Xi}}_{11} + \tau_1^{-1}\boldsymbol{I}_{Nn} + 2\zeta_2\boldsymbol{I}_N\otimes\boldsymbol{P}^{-1}, \qquad \tilde{\boldsymbol{\Xi}}_{22} = -\boldsymbol{I}_N\otimes\boldsymbol{\Phi}_2^2 + \tau_2^{-1}\boldsymbol{I}_{Nn},\\ &\tilde{\boldsymbol{\pi}}_1 = (1-2\gamma_2+2\beta_2^2+2\zeta_2)\boldsymbol{I}_N, \qquad \tilde{\boldsymbol{\pi}}_2 = (2\rho_2^2-\tau_1^{-1}+4\alpha_2^2)\boldsymbol{I}_{Nn},\\ &\tilde{\boldsymbol{\pi}}_3 = -\tau_2^{-1}\boldsymbol{I}_{Nn} + (4\alpha_2^2+2\rho_2^2)(\boldsymbol{J}_2^2\otimes\boldsymbol{I}_n).\end{aligned} \tag{6.70}$$

Following the same steps given in (6.52), (6.53), and (6.54) leads to the LMIs given in the statement of the Theorem. The proposed objective function (6.33) follows the same logic explained in Theorem 6.2 and that completes the proof. □

Chapter 7

Experimental Results

In this section, different MASs are considered to provide comprehensive experimental results on the performance of the proposed algorithms in the thesis. Different values for the initialization parameters are considered to fully observe their influence on the MAS and find potential trade-offs between important features of the event-triggered consensus. To solve the optimization stages included in some algorithms, the YALMIP parser [154] and SDPT3 solver [155] are used in Matlab environment.

7.1 CEASE

To illustrate the implementation of Algorithm 3.1, a network with 10 nodes is considered. The corresponding Laplacian matrix to this network is given below

$$\boldsymbol{L}=\begin{bmatrix} 7 & -1 & -1 & -1 & -1 & 0 & -1 & 0 & -1 & -1 \\ -1 & 4 & 0 & -1 & 0 & -1 & -1 & 0 & 0 & 0 \\ -1 & 0 & 5 & 0 & -1 & -1 & 0 & 0 & -1 & -1 \\ -1 & -1 & 0 & 4 & 0 & 0 & -1 & 0 & -1 & 0 \\ -1 & 0 & -1 & 0 & 4 & 0 & 0 & 0 & -1 & -1 \\ 0 & -1 & -1 & 0 & 0 & 4 & 0 & -1 & -1 & 0 \\ -1 & -1 & 0 & -1 & 0 & 0 & 4 & 0 & 0 & -1 \\ 0 & 0 & 0 & 0 & 0 & -1 & 0 & 2 & -1 & 0 \\ -1 & 0 & -1 & -1 & -1 & -1 & 0 & -1 & 7 & -1 \\ -1 & 0 & -1 & 0 & -1 & 0 & -1 & 0 & -1 & 5 \end{bmatrix}. \tag{7.1}$$

It can be verified that $\lambda_2 = 1.5617$ and $\lambda_N = 8.4398$. To initialize optimization (3.11), convergence rate is set at $\zeta = 0.30$ and sampling period at $h = 0.01$ sec. It takes 24 iterations for the interior-point method used by SDPT3 to solve (3.11). The solution of optimization (3.11) for this setting is given below:

$$p = 2.1072, \alpha = 189.1258, \epsilon_1 = 2.2304, \epsilon_2 = 0.0134,\ \mu = 1.2740, \gamma = 188.2934. \tag{7.2}$$

Using (7.2), consensus design parameters are computed as $\mathcal{K} = 0.6046$ and $\phi_1 = 0.0053$. Additionally, the objective function (3.11) is computed as $\mathcal{F} = 376.58$. The maximum possible consensus error is obtained from (3.13) as $C = 0.5022$.

Let $x_i(0) = 2 \times i$, $(1 \leq i \leq 10)$. The constant threshold in the ET scheme (3.5) is

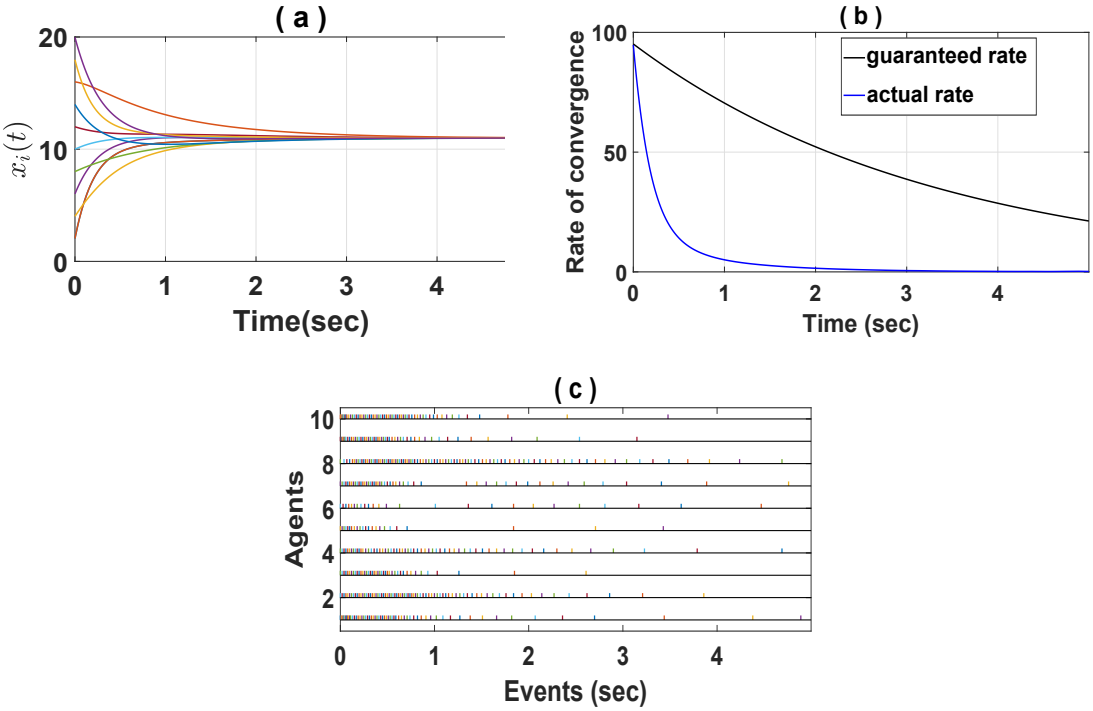

Figure 7.1: Consensus trajectories using Algorithm 3.1 (a): Average consensus for $x_i(t)$, (b): Expected and actual trajectories for $\|\boldsymbol{r}(t)\|$, (c): Events for each agent.

considered as $\phi_2 = 0.03$. Consensus iterations are run for 5 seconds. The evolutions of $x_i(t)$ in (3.1) for the 10 nodes are shown in Figs. 7.1(a). Based on Fig.7.1(a), the states $x_i(t)$ converge to the average value of the initial parameter. Fig.7.1(b) compares the theoretical (guaranteed) rate of consensus and its actual rate. As expected the actual rate is below the guaranteed rate. In this example, the nodes, respectively, trigger 59, 74, 40, 59, 22, 24, 48, 91, 49, and 58 event samples. These event instants are shown in Fig. 7.1(b). The average number of events (AE) for the 10 nodes is 52.40. Notice that if the ET scheme was not used, the nodes would transmit 5/0.01=500 packets. However, using the ET scheme only 52.40/500 $\approx$ 10% of the total packets is transmitted. The average inter-event time (AIET), which shows the average frequency of the event-triggering, is computed as AIET $= 5/\text{AE}$. In this exampled, AIET= 0.0954. The consensus error at $t = 5$ sec, which is denoted by $\|\boldsymbol{r}(5)\|$, is also reported. The consensus error in this example is $\|\boldsymbol{r}(5)\| = 0.0414$. As expected the actual consensus error is lower than the theoretical one, i.e., $\|\boldsymbol{r}(5)\| \leq C$.

7.1.1 Impact of convergence rate ζ

In this section, the impact of different convergence rates ζ on consensus features is investigated. The sampling period h is fixed at $h = 0.01$ sec. The desired convergence rate ζ is increased with steps of 0.1 and optimization (3.11) is solved while other

Table 7.1: CEASE with varying ζ and fixed $h=0.01$, $\phi_2=0.03$.

ζ	$\mathcal{K}$	ϕ_1	T_s	$\|\boldsymbol{r}(T_s)\|$	AE	AIET	$\mathcal{F}$
0.10	0.3242	0.0086	6.5910	0.1914	46.2	0.1427	229.9806
0.20	0.4819	0.0067	5.0250	0.1154	50.9	0.0987	295.7997
0.30	0.6046	0.0053	4.2410	0.0877	51.8	0.0819	376.5860
0.40	0.7101	0.0041	3.6800	0.0824	58.1	0.0633	488.0071
0.50	0.8049	0.0030	3.3860	0.0691	58.5	0.0579	659.0263
0.60	0.8921	0.0021	3.0570	0.0664	60.7	0.0504	963.3216

parameters remain fixed. Consensus results for varying ζ and fixed h are listed in Table 7.1. Starting from initial values $x_i(0)=2\times i$, $(1\leq i\leq 10)$, CEASE is run until the settling time T_s, where

$$T_s=\min_{t=nh}\{\ t\ \mid\quad |\,\|\boldsymbol{r}((n+1)h)\|-\|\boldsymbol{r}(nh)\|\,|\leq 0.0001\} \tag{7.3}$$

In fact, the settling time T_s denote the time that consensus is reached within its steady-state error. From Table 7.1 one observes that:

- The settling time T_s gets steadily reduced as ζ is increased;
- Faster convergence rate is achieved with a higher minimized objective function $\mathcal{F}$, which implies obtaining a larger $\mathcal{K}$ and a smaller ϕ_1. In fact, a smaller value of the objective function translates to having larger values for AIET;
- The steady-state consensus error $\|\boldsymbol{r}(T_s)\|$ becomes smaller with higher convergence rates.

It is worth mentioning that in this configuration with $h=0.01$, the optimization problem (3.11) becomes infeasible for $\zeta\geq 0.82$, i.e., no consensus convergence rate higher than $\zeta=0.82$ is guaranteed for a sampling period of $h=0.01$ in this network.

7.1.2 Impact of sampling period h

In this section, we fix $\zeta=0.30$, $\phi_2=0.03$ and vary h. Consensus results are listed in Table 7.2, where it is observed that

- Increasing h leads to smaller values for both ϕ_1 and $\mathcal{K}$, and a larger value for the objective function $\mathcal{F}$.

Table 7.2: CEASE with varying h and fixed $\zeta=0.3$, $\phi_2=0.03$.

h	$\mathcal{K}$	ϕ_1	T_s	$\|\boldsymbol{r}(T_s)\|$	AE	AIET	$\mathcal{F}$
0.001	1.7609	0.0106	1.5600	0.0646	44.40	0.0351	188.7839
0.005	0.8271	0.0076	3.2060	0.0735	48.0	0.0668	263.4882
0.015	0.5054	0.0035	4.7860	0.1189	58.4	0.0820	562.3605
0.025	0.4051	0.0008	5.7010	0.1429	59.5	0.0958	2558.6431

Table 7.3: CEASE with different constant values for ϕ_2 and fixed $\zeta = 0.3$, $h = 0.01$.

ϕ_2	$\mathcal{K}$	ϕ_1	T_s	$\|\boldsymbol{r}(T_s)\|$	AE	AIET	$\mathcal{F}$
0.01	0.6046	0.0053	4.3510	0.0907	88.10	0.0494	376.58
0.02	0.6046	0.0053	4.2110	0.0974	63.80	0.0660	376.58
0.05	0.6046	0.0053	4.0300	0.1067	38.90	0.1036	376.58
0.10	0.6046	0.0053	3.6210	0.1744	26.90	0.1346	376.58

Table 7.4: CEASE for a large network with $N = 100$, and $\phi_2 = 0.01$, $h = 0.01$.

ζ	$\mathcal{K}$	ϕ_1	T_s	$\|\boldsymbol{r}(T_s)\|$	AE	AIET	$\mathcal{F}$
0.3	0.1029	0.0036	4.6510	0.2274	77.23	0.0602	547.79
0.4	0.1236	0.0034	4.3301	0.1933	85.46	0.0507	586.77
0.5	0.1417	0.0032	4.2213	0.1691	88.17	0.0479	624.9473

- With smaller values of h, consensus is reached faster.
- The AIET is increased with larger values of h.
- With larger values of h the steady-state consensus error $\|\boldsymbol{r}(T_s)\|$ becomes larger.

With $\zeta = 0.30$, the optimization problem (3.11) becomes infeasible for $h \geq 0.031$, implying that the largest sampling period that can guarantee 0.30-exponential rate of convergence in this configuration is $h = 0.031$ sec.

7.1.3 Impact of constant threshold ϕ_2

Next, the impact of the constant threshold ϕ_2 on the consensus features is studied. Consensus results for incrementally increasing values of ϕ_2 and fixed $\zeta = 0.3$ and $h = 0.01$ are reported in Table 7.3. It should be reminded that parameter ϕ_2 is not involved in the optimization (3.11). Hence, parameters $\mathcal{K}$ and ϕ_1 are similar in all rows of Table 7.3. According to Table 7.3, the AIET is increased with higher values of ϕ_2 at the expense of higher errors in consensus. It should be noted that increasing ϕ_2 decreases the settling time.

7.1.4 Large networks

In the final experiment, CEASE is evaluated over a large random network. To this end, a connected network of 100 nodes, i.e., $N = 100$, is randomly generated with $\Pr\{a_{ij} = 1\} = 0.25$ and $\Pr\{a_{ij} = 0\} = 0.75$. Necessary eigenvalues of the Laplacian matrix corresponding to this network are $\lambda_2 = 15.5772$ and $\lambda_N = 39.8007$. Considering $h = 0.01$ sec, $\phi_2 = 0.01$, and given values of ζ in Table 7.4, consensus parameters are computed using (3.11). The results are listed in Table 7.4. Similar to previous experiments, computed values of $\mathcal{K}$ and ϕ for this large network correspond to the desired exponential rate ζ.

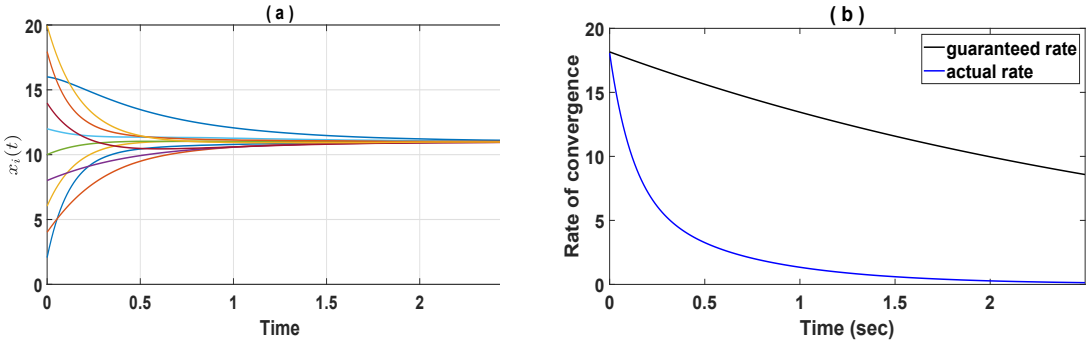

Figure 7.2: (a): Average consensus using Q-CEASE, (b): The guaranteed (theoretical) rate of convergence vs the actual rate of convergence.

Table 7.5: Q-CEASE performance for differnet $\{h, \phi, \delta\}$.

$h/h_{\max}$	$\phi/\phi_{\max}$	δ	M	T_s	$\|\boldsymbol{r}(T_s)\|$	AE
0.1	0.5	0.05	0.93	2.01	0.1145	202.91
0.5	0.5	0.05	1.34	1.99	0.1521	238.78
0.9	0.5	0.05	1.95	2.00	0.1649	164.76
0.5	0.1	0.05	1.15	1.94	0.1205	204.25
0.5	0.5	0.05	2.04	1.95	0.1354	206.84
0.5	0.9	0.05	9.40	2.03	0.1414	196.15
0.5	0.5	0.01	0.41	1.98	0.0845	212.01
0.5	0.5	0.10	3.95	1.83	0.1754	197.93
0.5	0.5	0.40	21.41	1.63	0.4492	219.63

7.2 Q-CEASE

This sections evaluate the proposed Q-CEASE implementation. Consider the same 10-node network with Laplacian matrix (7.1) with $\lambda_2 = 1.5617$ and $\lambda_{10} = 8.4398$. Select the quantization level as $\delta = 0.05$ and convergence rate $\zeta = 0.3$ From (3.19), $h_{\max} = 0.0177$. Select $h \approx 0.2 h_{\max} = 0.004$, which leads to $\phi_{\max} = 0.0115$. To keep M small enough, select $\phi = 0.9\phi_{\max}$, which results in $\phi = 0.0104$. For these values, $M = 4.2276$. Starting from initial values $x_i(0) = 2 \times i$, $(1 \leq i \leq 10)$, the Q-CEASE algorithm is run until T_s, where T_s is defined in (7.3). The evolution of the states $x_i(t)$ for the ten nodes is shown in Fig. 7.2(a). For this setting, $T_s = 2.499$ sec, which is equivalent to a total number of $2.499/0.004 \approx 625$ samples. However, the ten nodes, respectively, trigger 210, 208, 225, 224, 225, 204, 220, 208, 211, and 209 events, leading to an average event of AE=214.40 per node. The ratio of the average events to total samples for this setting is, therefore, $214.40/625 = 0.3430$. The norm of $\boldsymbol{r}(T_s)$ which shows how close the nodes have reached $\bar{x}(0)$ is calculated as $\|\boldsymbol{r}(T_s)\| = 0.1349$. As expected, $\|\boldsymbol{r}(T_s)\| \leq M$. In Fig. 7.2(b), the guaranteed rate $e^{-0.3t}\|\boldsymbol{r}(0)\|$ is compared with the actual rate $\|\boldsymbol{r}(t)\|$, which satisfies $\|\boldsymbol{r}(t)\| \leq e^{-0.3t}\|\boldsymbol{r}(0)\|$ for all $t > 0$.

Compared to CEASE, Q-CEASE transmits more samples.

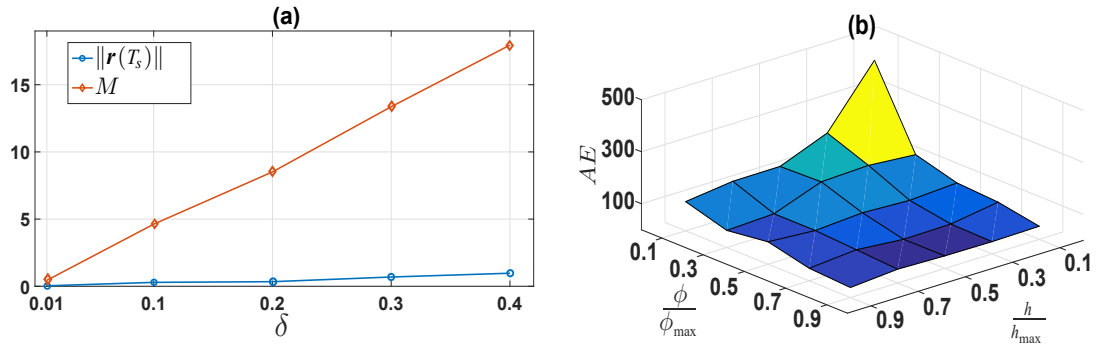

Figure 7.3: (a): Actual ($\|\boldsymbol{r}(T_s)\|$) and maximum theoretical quantization error (M), (b): Average number of transmissions AE versus $\{h/h_{\max}, \phi/\phi_{\max}\}$.

7.2.1 Random networks

Next, the scalability of the Q-CEASE algorithm is investigated for random networks with $N=10$ and varying parameters h, ϕ, and δ. Networks are generated with $\mathbb{E}\{\lambda_2\}=2$ and $\mathbb{E}\{\lambda_{10}\}=8$, where $\mathbb{E}$ returns the expected value. For given values of $h/h_{\max}$, $\phi/\phi_{\max}$, and δ in each row of Table 7.5, the Q-CEASE algorithm is run with $\zeta=0.3$ over 25 random networks. The results for M, T_s, $\|\boldsymbol{r}(T_s)\|$, and AE are calculated based on the average values for all 25 networks. According to Table 7.5, one concludes that:

- For fixed $\phi/\phi_{\max}$ and δ, increasing $h/h_{\max}$ results in smaller values for AE at the expense of a higher quantization error (larger $\|\boldsymbol{r}(T_s)\|$).
- For fixed $h/h_{\max}$ and δ, increasing $\phi/\phi_{\max}$ decreases the AE, however quantization error is slightly increased.
- As expected, increasing δ results in higher values for $\|\boldsymbol{r}(T_s)\|$ which is translated to a higher error in average consensus.

7.2.2 Large networks

In this section, larger random networks with $N=50$, $\mathbb{E}\{\lambda_2\}=9$, and $\mathbb{E}\{\lambda_{50}\}=27$ are considered. Let $\zeta=0.3$. Fig. 7.3(a) shows $\|\boldsymbol{r}(T_s)\|$ and M with respect to δ for fixed $h/h_{\max}=\phi/\phi_{\max}=0.5$. According to Fig. 7.3(a), the actual quantization error $\|\boldsymbol{r}(T_s)\|$ is much lower than the worst-case error (M), especially for larger δ. In Fig. 7.3(b), the 3D graph for AE is shown with respect to different ratios of $h/h_{\max}$ and $\phi/\phi_{\max}$, ($\delta=0.05$). Based on Fig. 7.3(b), the least amount for AE happens when both ϕ and h are chosen close to their maximum allowable values from (3.19), i.e., $\phi\to\phi_{\max}$ and $h\to h_{\max}$, which is at the expense of a higher quantization error.

7.3 DEASE

Experimental results for DEASE are included in this section. The 10-node network given in (7.1) is considered. To compute consensus parameters required in DEASE, set $h = 0.01$ and solve optimization (3.31). The following parameters are computed

$$\phi_1 = 6.2444, \quad \phi_2 = 0.0309, \quad \phi_3 = 0.0219. \tag{7.4}$$

The objective function is calculated as $\mathbb{F} = 117.03$. The same initial states considered in CEASE are considered, i.e., $x_i(0) = 2 \times i$, $(1 \leq i \leq 10)$. Additionally, the initial states consider for the dynamic threshold η is $\eta_i(0) = 0.1$, $(1 \leq i \leq 10)$. Consensus iteration is run for 5 seconds. The evolution of $x_i(t)$ and $\eta_i(t)$, $(1 \leq i \leq 10)$, for the 10 nodes are shown in Fig. 7.4(a). As shown in Fig. 7.4(b), $\eta_i(t)$ rises from the initial value of 0.1 and provides a considerable threshold for (3.24). Variable $\eta_i(t)$ converges zero and does not cause steady state error in consensus. Fig. 7.4(c) shows the transmission instants triggered by each node. The agents trigger 19, 24, 14, 32, 16, 27, 28, 39, 18, and 16 events during consensus, which leads to an average transmission value of AE=23.30. Compared to CEASE, where AE=52.4, the value of AE using DEASE is lower. Based on the number of transmissions, it can be concluded that DEASE outperforms CEASE in communication savings. Additionally, at $t = 5$ sec, the consensus error [1] in DEASE is $\|\boldsymbol{r}(5)\| = 0.000958$, which is way lower than the error computed for CEASE. Compared to CEASE, DEASE provides a more efficient framework both in terms of transmission saving and consensus error.

7.3.1 Impact of h

This section investigates the impact of h on consensus features. The network configuration and initial conditions are kept the same. Consensus time horizon is set at 5s. In this MAS setting, the maximum allowable h which computes feasible solution for optimization (3.31) is $h = 0.12s$. Compared to CEASE, where the maximum allowable sampling period is obtained as $h = 0.031$, DEASE is more powerful in allowing larger values for the sampling period. The reason lies within the fact that DEASE uses all eigenvalues of the Laplacian matrix. However, CEASE is based on the extreme eigenvalues which makes the feasibility region limited at the expenses of scalability to the network size.

[1] It should be reminded that the consensus error in DEASE asymptotically approaches zero. In this example, $\|\boldsymbol{r}(5)\|$ is reported for DEASE just for the sake of comparison with CEASE.

Table 7.6: Consensus using DEASE with varying h.

h	ϕ_1	ϕ_2	ϕ_3	AE	AIET	$\mathbb{F}$
0.01	6.2444	0.0309	0.0219	23.3	0.2146	117.0310
0.05	7.8971	0.0194	0.0137	27.2	0.1835	187.1074
0.08	9.9334	0.0122	0.0086	24.7	0.2020	296.0299
0.10	12.1757	0.0081	0.0058	42.0	0.1188	444.7712

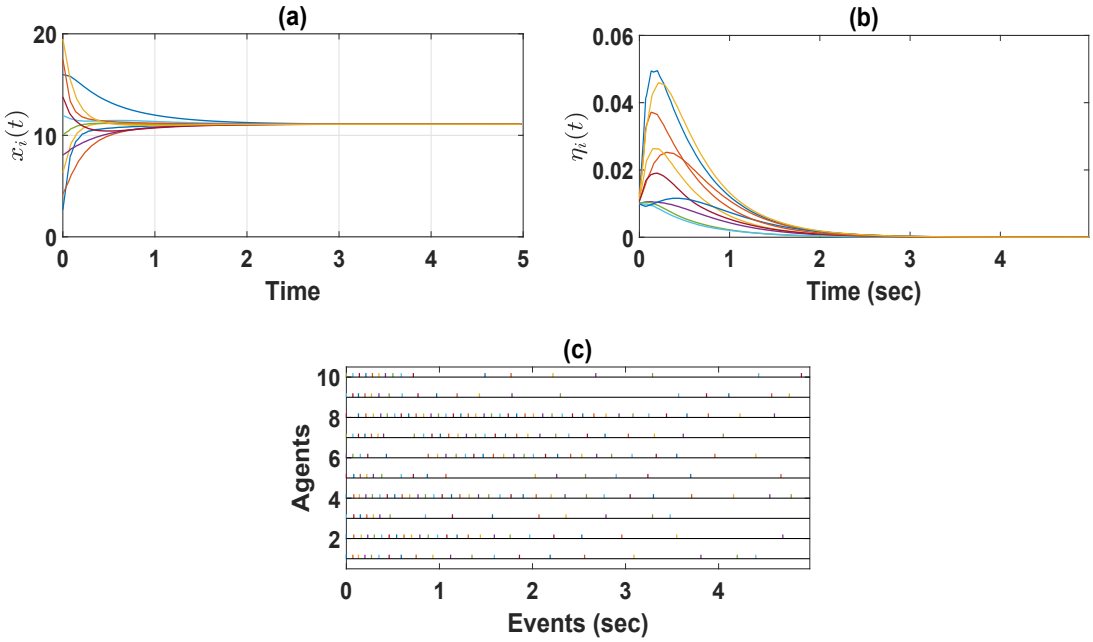

Figure 7.4: Consensus trajectories using Algorithm 3.3 (a): Average consensus for $x_i(t)$, (b): Trajectories of the dynamic threshold $\eta_i(t)$, (c): Events for each agent.

7.3.2 Comparison with Reference [122]

This section compares DEASE and implementation [122] from different aspects. Reference [122] proposes a sampled-data ET scheme for consensus in first-order agents. Denote t_k^i as the k-th event instant for agent i. With some minor modification in notation, the following ET condition is used in [122] to detect and trigger the next event instant

$$t_{k+1}^i = t_k^i + h \inf\{n \,|\, e_i^2(t_k^i + nh) \geq \sigma_i \, z_i^2(t_k^i + nh)\}, \tag{7.5}$$

where $e_i(t_k^i+nh) = x_i(t_k^i) - x_i(t_k^i+nh)$ and $z_i(t_k^i+nh) = \sum_{j\in\mathcal{N}_i}(x_i(t_k^i+nh) - x_j(t_k^i+nh))$, with given sampling period h. Scalar $\sigma_i \geq 0$ is the ET parameter and needs to be designed. Note that the ET scheme (7.5) is only used for reducing the number of 'control updates' and transmission between the agents is conducted periodically (not event-triggered). In contrast, both the control updates and neighbouring transmissions in DEASE are sampled-data event-triggered. According to [122, Theorem 8], the operating regions for h and σ_i are as follows

$$0 < h \leq \frac{1}{2\lambda_N}, \qquad 0 < \sigma_i < \frac{1}{\lambda_N^2}. \tag{7.6}$$

The same network used in [122] is considered

$$\boldsymbol{L} = \begin{bmatrix} 2 & -1 & -1 & 0 \\ -1 & 2 & -1 & 0 \\ -1 & -1 & 3 & -1 \\ 0 & 0 & -1 & 1 \end{bmatrix}. \tag{7.7}$$

For (7.7) it holds that $\lambda_4 = 4$. Hence, one obtains that $0 < h \leq 0.125$ and $\sigma_i < 0.0625$. To observe the fewest number of events triggered by [122], let $h = 0.125$ and $\sigma_i = 0.0625$, $i = 1, ..., 4$. Initial conditions are set as $\boldsymbol{x}(0) = [0.4773, -0.3392, 0.5, -0.6381]^T$. The agents trigger 41, 40, 39, and 41 events (AE=40.25) in a time horizon of 10 seconds.

With $h = 0.125$, the following parameters are obtained from DEASE for network (7.7)

$$\phi_1 = 5.2062, \qquad \phi_2 = 0.0445, \qquad \phi_3 = 0.0315. \tag{7.8}$$

Let $\eta_i(0) = 0.1$. Consensus is run using DEASE with above parameters. The agents trigger 20, 19, 12, and 23 events (AE= 18.50) in 10 seconds. This implies that DEASE triggers fewer number of events than [122].

In another experiment, the maximum allowable sampling period in DEASE is computed as $h_{\max} = 0.264$. Comparing this value with 0.125 shows that the maximum sampling period supported by DEASE is much higher.

In fact, these two observations (i.e., fewer number of events and higher admissible h in DEASE) were expected since i) The dynamic event-triggering scheme used in DEASE is more advanced; and ii) In DEASE all eigenvalues of the Laplacian matrix are used to compute necessary parameters. However, implementation [122] is based on the extreme eigenvalue λ_N and its design is irrespective of network size N.

7.4 PEC

To evaluate the performance of PEC, the following MAS is considered

$$\left.\begin{aligned} \dot{r}_i(t) &= v_i(t), \\ \dot{v}_i(t) &= -\mu_k v_i(t) + u_i(t) \end{aligned}\right\} \quad 1 \leq i \leq 6, \tag{7.9}$$

where $r_i(t) \in \mathbb{R}$ and $v_i(t) \in \mathbb{R}$, respectively, denote the position and velocity of agent i. Scalar $\mu_k > 0$ denotes the velocity damping and $u_i(t)$ is the control input. Considering $\mu_k = 0.5$, the state space representation for (7.9) in the form of linear agent (4.1) is given by

$$\boldsymbol{A} = \begin{bmatrix} 0 & 1 \\ 0 & -0.5 \end{bmatrix}, \qquad \boldsymbol{B} = \begin{bmatrix} 0 \\ 1 \end{bmatrix}, \tag{7.10}$$

where $\boldsymbol{x}_i(t) = [r_i(t), v_i(t)]^T$. The network topology associated with MAS (7.9) is represented by the following Laplacian matrix

$$\boldsymbol{L} = \begin{bmatrix} 2 & -1 & 0 & 0 & 0 & -1 \\ -1 & 2 & -1 & 0 & 0 & 0 \\ 0 & -1 & 2 & -1 & 0 & 0 \\ 0 & 0 & -1 & 2 & -1 & 0 \\ 0 & 0 & 0 & -1 & 2 & -1 \\ -1 & 0 & 0 & 0 & -1 & 2 \end{bmatrix}. \tag{7.11}$$

Considering the eigenvalue decomposition in (4.9), one can verify that the following parameters hold for Laplacian matrix (7.11)

$$\begin{aligned} &\boldsymbol{J} = \text{diag}(0,1,1,3,3,4), \qquad \tilde{\boldsymbol{J}} = \text{diag}(1,1,3,3,4), \\ &\boldsymbol{W} = \begin{bmatrix} 0.4082 & 0.2887 & 0.5 & 0.2887 & -0.5 & 0.4082 \\ 0.4082 & -0.2887 & 0.5 & 0.2887 & 0.5 & -0.4082 \\ 0.4082 & -0.5774 & 0 & -0.5774 & 0 & 0.4082 \\ 0.4082 & -0.2887 & -0.5 & 0.2887 & -0.5 & -0.4082 \\ 0.4082 & 0.2887 & -0.5 & 0.2887 & 0.5 & 0.4082 \\ 0.4082 & 0.5774 & 0 & -0.5774 & 0 & -0.4082 \end{bmatrix}, \\ &\tilde{\boldsymbol{W}} = \begin{bmatrix} 0.2887 & -0.2887 & -0.5774 & -0.2887 & 0.2887 & 0.5774 \\ 0.5 & 0.5 & 0 & -0.5 & -0.5 & 0 \\ 0.2887 & 0.2887 & -0.5774 & 0.2887 & 0.2887 & -0.5774 \\ -0.5 & 0.5 & 0 & -0.5 & 0.5 & 0 \\ 0.4082 & -0.4082 & 0.4082 & -0.4082 & 0.4082 & -0.4082 \end{bmatrix}. \end{aligned} \tag{7.12}$$

Parameter design: To solve consensus using Algorithm 4.5, select $\zeta = 0.3$ and $\delta = 0.01$. For an accuracy of $\epsilon_g = 10^{-5}$, it takes 22 iterations for the SDPT3 solver to solve (4.13) with the following solution

$$\begin{aligned} &\boldsymbol{P} = \begin{bmatrix} 0.0737 & -0.0611 \\ -0.0611 & 0.2481 \end{bmatrix}, \boldsymbol{\Omega} = \begin{bmatrix} -0.0186 & -0.3514 \end{bmatrix}, \tilde{\boldsymbol{\Phi}} = \begin{bmatrix} 1.1764 & -0.0116 \\ -0.0116 & 1.3330 \end{bmatrix}, \quad \tilde{\alpha} = 0.058027, \\ &\tau_1 = 1.8839, \quad \tau_2 = 0.14314, \quad \epsilon_1 = 32.3787, \quad \epsilon_2 = 10.6587, \quad \theta_1 = 18.3983, \\ &\theta_2 = 1.7791, \quad \theta_3 = 17.2334, \quad \theta_4 = 0.1238. \end{aligned} \tag{7.13}$$

Using (4.15) and solution (7.13), consensus parameters are calculated as follows

$$\boldsymbol{K} = \begin{bmatrix} -1.7953 & -1.8586 \end{bmatrix}, \quad \boldsymbol{\Phi} = \begin{bmatrix} 18.5377 & 4.5921 \\ 4.5921 & 5.7849 \end{bmatrix}, \quad \alpha = 0.2409. \tag{7.14}$$

From solution (7.13) and considering the convergence rate in PEC, i.e., expression (4.16), the rate of consensus is obtained as follows

$$\boldsymbol{\psi}^T(t)\,\boldsymbol{\psi}(t) \leq 2.2181\, e^{-0.6t}\, \boldsymbol{\psi}^T(0)\,\boldsymbol{\psi}(0). \tag{7.15}$$

Additionally, the objective function $\mathbb{F}$ in (4.13) is computed as $\mathbb{F} = 37.5346$.

Consensus iterations: Let $\boldsymbol{x}_i(0) = [10 \times i,\ i]^T$, $(1 \leq i \leq 6)$. The uncertainty in control gain is assumed as $\boldsymbol{\Delta}_K = 0.01 \sin(i \times t)$, $(1 \leq i \leq 6)$. Note that the control gain uncertainty satisfies Assumption 2 with $\delta = 0.01$. The following criterion is used to

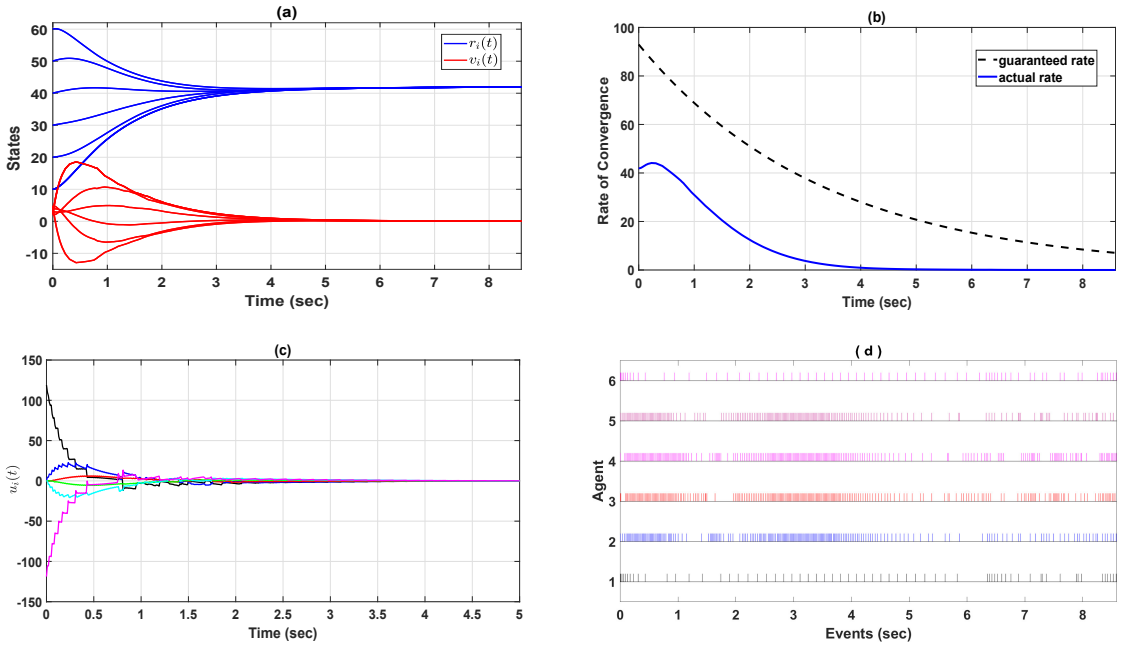

Figure 7.5: Trajectories of MAS (7.9) using PEC; (a): State consensus, (b): The guaranteed consensus rate vs the actual rate, (c) The control inputs $\boldsymbol{u}_i(t)$, $(1 \leq i \leq 6)$, (d) The event instants for each agent.

---

determine $t^\star$, which is the time when consensus is achieved. Time $t^\star$ is determined as

$$t^\star = \inf\{\ t \mid \frac{\|\boldsymbol{\psi}(t)\|}{\|\boldsymbol{\psi}(0)\|} \leq 0.0001\ \}. \tag{7.16}$$

Conceptually speaking, time $t^\star$ is the smallest time when the disagreement between the agents $\|\boldsymbol{\psi}(t)\|$ reaches within the 0.0001 of its initial value $\|\boldsymbol{\psi}(0)\|$. A lower value for $t^\star$ is translated to a faster rate of consensus convergence. Based on (7.16), it takes 8.60 sec to reach consensus in MAS (7.9). In Fig. 7.5, the trajectories of MAS (7.9) using the PEC implementation are plotted. Fig. 7.5(a) shows the evolution of the states to reach a consensus. As shown in Fig. 7.5(a), the disagreement between the position states $r_i(t)$ for all agents approaches zero as consensus is achieved. Additionally, all velocities approach zero as consensus is reached. Fig. 7.5(b) is included to verify that the obtained consensus parameters are capable of ensuring 0.3-exponential consensus and satisfy (7.15). In Fig. 7.5(c), the control input used to achieve consensus is plotted. Simulation results show that the six agents, respectively, trigger 64, 209, 237, 235, 201, and 68 events (transmissions) during the process. These event instants are shown in Fig. 7.5(d). The average number of events is AE=169.00. Let AIET $= t^\star/\text{AE}$ define the average inter-event time. In this example, AIET $= 0.0509$. This implies that the agents transmit every 0.0509 sec at average.

7.4.1 Impact of ζ and δ on PEC

Next, the impact of different values of ζ and δ on consensus features is investigated. To this end, optimization (4.13) is solved for given values of ζ and δ listed in Table 7.7. In the first half of Table 7.7, parameter δ is fixed at $\delta = 0.01$ and ζ is incrementally increased. In the second half of Table 7.7, $\zeta = 0.3$ is fixed and δ is increased. Simulation is conducted for (7.9) with corresponding computed parameters. The following facts are observed according to Table 7.7:

- As expected, with higher values for ζ the rate of convergence is increased and thus $t^\star$ steadily gets reduced.
- A larger ζ leads to a larger $\|\boldsymbol{K}\|$. This is consistent with the fact that increasing the desired convergence rate requires higher values for the control input $\boldsymbol{u}_i(t)$.
- A larger value for ζ leads to smaller values for α and higher values for $\boldsymbol{\Phi}$ to increase the events density and cope with the desired rate of convergence. Therefore, the AIET becomes smaller (i.e., more frequent events) as ζ is increased.
- The value of the objective function $\mathbb{F}$ is constantly increased with increments in ζ. It is reminded that $\mathbb{F}$ (4.13) is formulated based on increasing MIET (4.6). Hence, with a higher value of $\mathbb{F}$ one expects a smaller AIET and that can be observed in Table 7.7.
- A larger value for δ results in a larger $\|\boldsymbol{K}\|$ to compensate the impact of larger uncertainty. Additionally, the ET parameters $\boldsymbol{\Phi}$ and α are computed, respectively, larger and smaller to let more transmission.
- Although larger values for δ lead to larger control gains but the convergence time $t^\star$ does not necessarily gets reduced. This is due to the impact of uncertainty in the nominal control gains which adversely affects the convergence rate.
- No specific trend is observed in AE and AIET with changes in δ.

These results verify the flexibility and effectiveness of the proposed PEC algorithm in maintaining an event-triggered consensus with two performance related initializations.

Table 7.7: Consensus performance using PEC; different values for ζ and δ.

ζ	δ	$\|\boldsymbol{K}\|$	$\|\boldsymbol{\Phi}\|$	α	$t^\star$	AE	AIET	$\mathbb{F}$
0.0	0.01	1.2669	11.7086	0.2427	14.80	125.33	0.1181	30.5293
0.2	0.01	2.1113	16.8325	0.2415	9.73	136.17	0.0715	34.9227
0.4	0.01	3.0937	23.6438	0.2402	7.43	183.00	0.0406	40.4270
0.6	0.01	4.2342	32.4615	0.2388	6.89	240.17	0.0287	47.0449
0.3	0.01	2.5840	20.0191	0.2409	8.60	169.00	0.0509	37.5346
0.3	0.05	2.5941	20.9679	0.2409	8.51	175.33	0.0485	38.1213
0.3	0.10	2.6290	22.3003	0.2410	8.81	166.83	0.0528	38.9620

7.5 PSEC

To evaluate the effectiveness of PSEC, the same MAS given in (7.9) is considered with Laplacian matrix (7.11).

Parameter design: To solve consensus using Algorithm 4.6, initial parameters are selected as $h=0.05$, $\zeta=0.3$, and $\delta=0.01$. For the accuracy of $\epsilon_g=10^{-5}$, it takes 10 iterations for the SDPT3 solver to solve the LMIs in Theorem 4.3 with the following solution

$$\begin{aligned}
&\boldsymbol{V}=\begin{bmatrix}-0.0223 & -3.0502\end{bmatrix},\quad \boldsymbol{H}=\begin{bmatrix}5.3156 & -4.5884\\ -3.2413 & 5.5064\end{bmatrix},\quad \boldsymbol{Y}_{11}=\begin{bmatrix}199.7110 & 5.2908\\ 5.2908 & 231.8874\end{bmatrix},\\
&\boldsymbol{Y}_{12}=\begin{bmatrix}-182.5239 & -13.5311\\ -19.9524 & -190.4797\end{bmatrix},\quad \boldsymbol{Y}_{22}=\begin{bmatrix}194.8548 & -0.8846\\ -0.8846 & 205.6827\end{bmatrix},\quad \boldsymbol{F}_1=\begin{bmatrix}-8.2771 & 5.8829\\ 5.0067 & -9.2585\end{bmatrix},\\
&\boldsymbol{F}_2=\begin{bmatrix}-7.9583 & 4.9631\\ 5.6608 & -9.1558\end{bmatrix},\quad \boldsymbol{G}_1=\begin{bmatrix}-29.3485 & 2.8433\\ 10.2084 & -42.6486\end{bmatrix},\quad \boldsymbol{G}_2=\begin{bmatrix}17.7108 & 5.7674\\ -3.7916 & 23.4150\end{bmatrix},\\
&\boldsymbol{P}=\begin{bmatrix}11.8711 & -7.2267\\ -7.2267 & 11.2479\end{bmatrix},\quad \boldsymbol{Q}=\begin{bmatrix}17.8488 & -12.3498\\ -12.3498 & 20.5883\end{bmatrix},\quad \boldsymbol{Z}=\begin{bmatrix}476.0677 & -261.7300\\ -261.7300 & 423.7600\end{bmatrix},\\
&\boldsymbol{M}_1=\begin{bmatrix}19.7385 & 16.9919\\ 16.9919 & 16.4037\end{bmatrix},\quad \boldsymbol{M}_2=\begin{bmatrix}0.0099 & 0.0035\\ 0.0035 & 0.0108\end{bmatrix},\quad \epsilon_1=71.3307,\quad \epsilon_2=71.7854,\\
&\epsilon_3=63.4235.
\end{aligned}\tag{7.17}$$

Using (4.25) and (7.17), consensus parameters for PSEC are computed as follows

$$\boldsymbol{K}=\begin{bmatrix}-0.9806 & -1.1312\end{bmatrix},\ \boldsymbol{\Phi}_1=\begin{bmatrix}19.7385 & 16.9919\\ 16.9919 & 16.4037\end{bmatrix},\ \boldsymbol{\Phi}_2=\begin{bmatrix}0.0099 & 0.0035\\ 0.0035 & 0.0108\end{bmatrix}\tag{7.18}$$

From solution (7.17) and considering the convergence rate in PSEC, i.e., expression (4.26), the rate of consensus is obtained as follows

$$\|\boldsymbol{\psi}(t)\|^2\leq 3.1995\,e^{-0.6t}\ \|\boldsymbol{\psi}(0)\|^2.\tag{7.19}$$

Comparing (7.19) with the one obtained for PEC, i.e., (7.15), one can conclude that the guaranteed bound in PSEC is more conservative, since the exponential coefficient for PSEC is higher ($3.1995 > 2.2181$). Therefore, it is expected that consensus in PSEC reaches slower than PEC with the same values of ζ and δ. This is one of the trade-offs for incorporation of a sampler in PSEC.

Consensus iterations: Consider the same initial conditions $\boldsymbol{x}_i(0)$ and control gain uncertainty $\boldsymbol{\Delta}_K$ given for PEC. Consensus is run until the same termination point determined by (7.16). Based on (7.16), it takes 12.44 sec for the PSEC algorithm to reach consensus in MAS (7.9). In Fig.7.6(a), trajectories of (7.9) reaching consensus are plotted. Note that the value for $t^\star$ was 8.60 sec for PEC, which implies that consensus reaches more slowly in PSEC. Fig.7.6(b) verifies that expression (7.15) holds between the guaranteed rate and actual rate of consensus. In Fig.7.6(c), the control input used to achieve consensus is plotted. As shown in Fig.7.6(d), the six agents, respectively, transmit on 94, 157, 107, 182, 134, and 95 occasions. The average number of events is AE=128.17. Compared to PEC, fewer number of events are triggered in PSEC. This is because the sampling period itself adds to the interval between the events. Note that if no ET scheme was utilized, each agent would transmit on

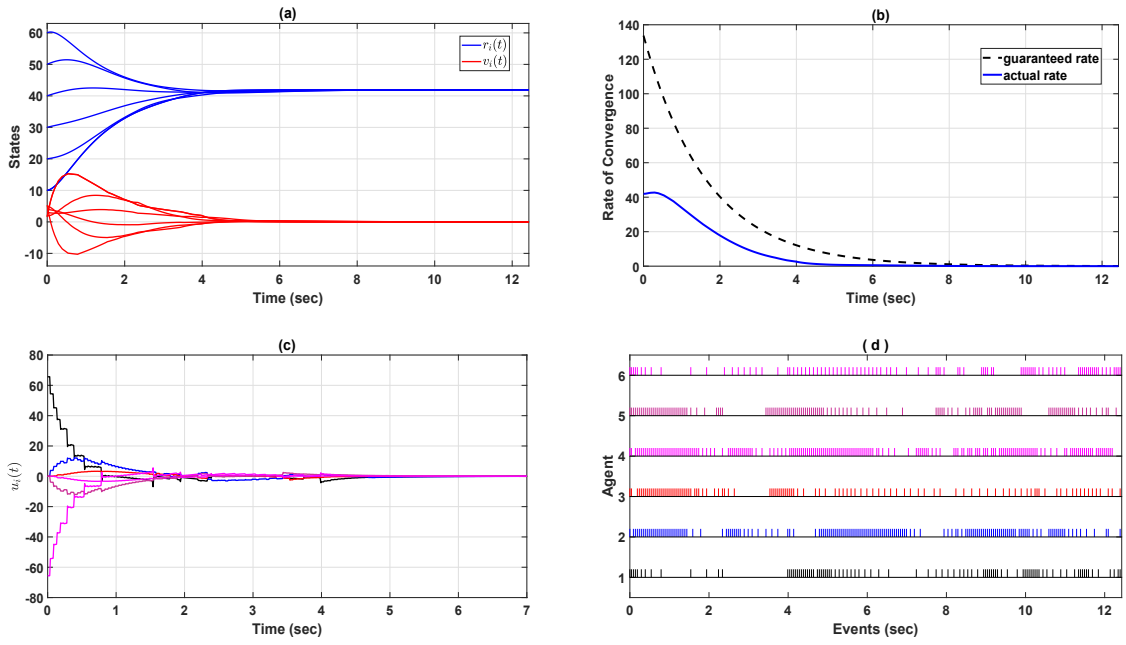

Figure 7.6: Trajectories of MAS (7.9) using PSEC; (a): State consensus, (b): The guaranteed consensus rate vs the actual rate, (c) The control inputs $\boldsymbol{u}_i(t)$, $(1 \leq i \leq 6)$, (d) The event instants for each agent.

$12.44/0.05 \approx 249$ occasions. However, with the ET scheme the average number of transmissions is 128.17. This implies that $128.17/249 \approx 50\%$ of the total packets are saved from transmissions. In this example, the AIET is computed as AIET $= 0.0971$.

7.5.1 Impact of ζ, δ, and h on PSEC

This section studies the impact of different desired initial values, i.e., convergence rate ζ, sampling period h, and non-fragility level δ, on the consensus features. To this end, the LMIs obtained in Theorem 4.3 are solved for given values of ζ, δ, and h listed in each row of Table 7.8. The table is divided into three sections. Out of the three parameters ζ, δ, and h, one is varying in each section and the remaining two are fixed. Consensus is run for (7.9) with corresponding computed parameters for each row of Table 7.8. The results are summarized below.

- The impact of varying ζ and δ on consensus is similar to the discussion given for PEC in Section 7.4.1.
- By increasing the value of the sampling period h (last section in Table 7.8), the AIET is increased. This is due to the fact that a larger sampling period helps in increasing the interval between events and saves more transmissions.

- Increasing the sampling period h, leads to control gains with smaller norms. Therefore, reaching consensus may be slower with increased values of h.

7.6 RQ-CEASE

This section quantifies the performance of the RQ-CEASE algorithms. The network with $N=6$ is described by

$$\boldsymbol{L}=\begin{bmatrix} 2 & -1 & 0 & 0 & 0 & -1 \\ -1 & 3 & 0 & -1 & -1 & 0 \\ 0 & 0 & 2 & -1 & 0 & -1 \\ 0 & -1 & -1 & 3 & 0 & -1 \\ 0 & -1 & 0 & 0 & 2 & -1 \\ -1 & 0 & -1 & -1 & -1 & 4 \end{bmatrix}. \tag{7.20}$$

It can be verified that $\lambda_2=1.4384$ and $\lambda_6=5.5616$. Let $\boldsymbol{x}(0)=[111.0,\ 211.1,\ 121.3,\ 102.9,\ 202.0,\ 150.0]^T$. The following DoS sequence considered in [32] is used

$$\begin{aligned} &d_c=(c+1)+0.5c(c+1)-\alpha^{-1}(c+1),\\ &\tau_c=\alpha^{-1}(c+1), \qquad\qquad c\in\mathbb{N}_0 \end{aligned} \tag{7.21}$$

where $\alpha\in\mathbb{R}_{\geq 1}$. This DoS sequence satisfies Assumption 5 with $T_0=0$, $T_1=\alpha$, $F_0=1$, and $F_1=1$, [32].

Algorithm 5.7: Let $\bar{\delta}=0.01$. Using λ_2, λ_6, $\bar{\delta}$, and N the upper bound for h is calculated as $h_M=0.0457$. Select $h=0.01$ which satisfies $h<h_M$. Based on the selected value for h, the maximum ET parameter is $\phi_M=0.0266$. Let $\phi=0.01$. It is obtained that $\omega_1=0.7240$, $\omega_2=5.9251$, and $\Omega_1=0.1089$. With $\alpha=15$ it holds that $\frac{1}{T_1}+\frac{h}{F_1}=0.0867$. Hence, $\frac{1}{T_1}+\frac{h}{F_1}<\Omega_1$. With such values $\eta_1=1.1422$, $\zeta_1=0.1478$, and $f_2=1.0635$. Consensus iteration is run for a time horizon of 7sec, i.e., $t\in[0,7]$. The evolution of $x_i(t)$ to reach average consensus is shown in Fig. 7.7(a). Fig. 7.7(b)

Table 7.8: Consensus performance using PSEC; different values for ζ, δ, and h.

ζ	δ	h	$\|\boldsymbol{K}\|$	$\|\boldsymbol{\Phi}_1\|$	$\|\boldsymbol{\Phi}_2\|$	$t^\star$	AE	AIET
0.0	0.01	0.05	0.9717	4.4841	0.1647	16.04	80.50	0.1993
0.2	0.01	0.05	1.3230	6.6025	0.1615	11.50	108.17	0.1063
0.4	0.01	0.05	1.7544	9.5932	0.1410	10.44	131.83	0.0792
0.6	0.01	0.05	1.9811	12.4167	0.1216	9.30	124.83	0.0745
0.3	0.05	0.05	1.5931	7.1564	0.1493	12.63	121.33	0.1041
0.3	0.10	0.05	1.9523	6.7090	0.1429	9.73	99.17	0.0981
0.3	0.15	0.05	2.2132	5.3403	0.1200	9.90	98.50	0.1005
0.3	0.01	0.04	1.5737	8.4731	0.1553	11.82	156.00	0.0758
0.3	0.01	0.08	1.5123	7.9054	0.1538	12.26	93.67	0.1309
0.3	0.01	0.12	1.4429	7.6928	0.1484	12.94	75.67	0.1710
0.3	0.01	0.20	1.1600	7.1621	0.1260	12.99	48.00	0.2558

compares the guaranteed theoretical trajectory for $\|\boldsymbol{r}(t)\|$ given in (5.22) with the actual rate $\|\boldsymbol{r}(t)\|$. As expected, the actual rate is below the theoretical bound. Parameter $\|\boldsymbol{r}(7)\|$ is used as an indication of how close the nodes have reached average consensus. In this experiment $\|\boldsymbol{r}(7)\| = 0.0045$. For this setting, a total number of 700 samples are used in $t \in [0, 7]$. The six nodes, however, trigger 492, 388, 463, 395, 478, and 419 events respectively, leading to an average event AE of 439.17 per node. The events are shown in Fig. 7.7(c).

Next, the performance of RQ-CEASE is investigated for the same network against DoS (7.21) using different design parameters. For the given values of h, ϕ, and $\bar{\delta}$ specified in each row of Table 7.9, a separate consensus is run and corresponding results are recorded. According to Table 7.9, one concludes that: (i) Increasing any of h, ϕ, or $\bar{\delta}$ reduces the resilience of the network to DoS attacks since Ω_1 is decreased; (ii) For fixed values of h and $\bar{\delta}$, increasing ϕ decreases AE since the ET threshold becomes larger. (iii) As expected, increasing $\bar{\delta}$ results in higher values for $\|\boldsymbol{r}(7)\|$, which is translated to higher consensus errors.

Algorithm 5.8: Next, the performance of RQ-CEASE with the state-independent ET threshold (Algorithm 5.8) is investigated for the same network against DoS (7.21) using different design parameters. Let $h = \phi = \bar{\delta} = 0.01$ and $\alpha = 15$. These values result in $\Omega_2 = 0.1551$, $\eta_2 = 1.1408$, $\zeta_2 = 0.4506$ and $f_4 = 1.5245$. As expected, $\Omega_2 > \Omega_1$ which implies more resilience of Algorithm 5.8.

Using Algorithm 5.8, consensus is run with the previously given initial conditions. The nodes, respectively, trigger on 188, 268, 322, 268, 307, and 194 occasions which leads to AE = 257.83. In addition, $\|\boldsymbol{r}(7)\| = 0.0062$. System trajectories are shown in Fig. 7.8. Comparing Fig. 7.7(c) with Fig. 7.8(c), one observes that the density of events remains almost the same when using Algorithm 5.7. However, Algorithm 5.8 detects very few events as consensus approaches the error bound. This phenomenon was expected since $\mathbb{X}_i(0) > 1$ for all nodes. Table 7.10 is provided to study the impact of different parameters on Algorithm 5.8. In addition to the observations made for Algorithm 5.7, it is noted that: (i) The values for Ω_2 are larger than Ω_1 in all corresponding rows of Tables 7.9 and 7.10 which verify higher resilience offered by Algorithm 5.8 (Note that $\lambda_6 > 0.5\sqrt{6}$). (ii) The recorded AE values are smaller for Algorithm 5.8, implying higher transmission savings for Algorithm 5.8 at this setting.

Table 7.9: Performance of Algorithm 5.7 for different parameters.

h	ϕ	$\bar{\delta}$	Ω_1	AE	$\|\boldsymbol{r}(7)\|$
0.004	0.010	0.010	0.1362	605.50	0.0042
0.008	0.010	0.010	0.1182	422.16	0.0043
0.012	0.010	0.010	0.0994	525.66	0.0045
0.010	0.004	0.010	0.1423	633.00	0.0045
0.010	0.008	0.010	0.1203	633.00	0.0045
0.010	0.012	0.010	0.0971	341.16	0.0042
0.010	0.010	0.001	0.1143	446.17	0.0021
0.010	0.010	0.015	0.1059	442.33	0.0155
0.010	0.010	0.025	0.0999	444.66	0.0174

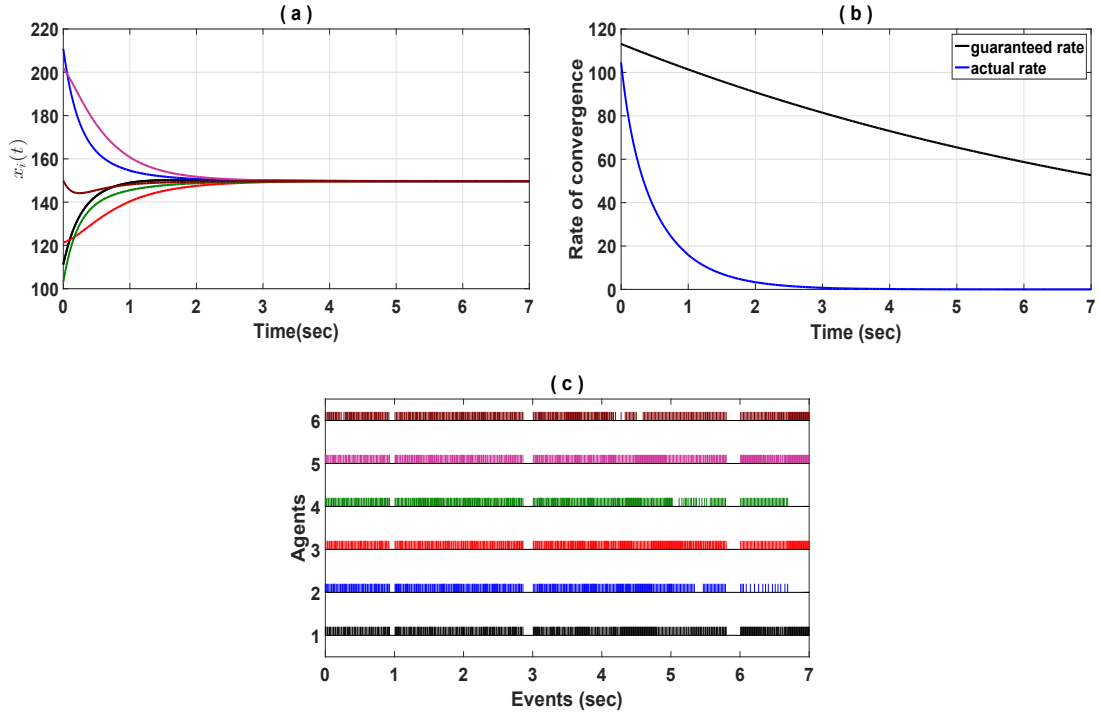

Figure 7.7: Consensus trajectories using Algorithm 5.7 (a): Average consensus for $x_i(t)$, (b): Expected and actual trajectories for $\|\boldsymbol{r}(t)\|$, (c): Events for each agent.

(iii) $\|\boldsymbol{r}(7)\|$ is larger in Algorithm 5.8. This is consistent with the steady-state error upper-bounds f_2 and f_4, where the scale of f_4 (unlike f_2) depends on $\delta_\star + \phi_\star$.

7.6.1 Randomized initial conditions

Finally, the impact of randomized initial state values $x_i(0)$ is investigated on the RQ-CEASE performance. To this end, select the 10-node network that was already considered in (7.1). Initial values are picked at random from normal distribution with zero mean and σ^2 variance, i.e. $x_i(0) \sim \mathcal{N}(0, \sigma^2)$ for $(1 \leq i \leq 10)$. Let

Table 7.10: Performance of Algorithm 5.8 for different parameters.

h	ϕ	$\bar{\delta}$	Ω_2	AE	$\|\boldsymbol{r}(7)\|$
0.004	0.010	0.010	0.1787	510.66	0.0100
0.008	0.010	0.010	0.1631	304.83	0.0116
0.012	0.010	0.010	0.1469	222.66	0.0108
0.010	0.004	0.010	0.1606	314.66	0.0096
0.010	0.008	0.010	0.1569	270.50	0.0104
0.010	0.012	0.010	0.1532	246.50	0.0155
0.010	0.010	0.001	0.1592	257.16	0.0109
0.010	0.010	0.015	0.1528	256.50	0.0131
0.010	0.010	0.025	0.1481	258.66	0.0132

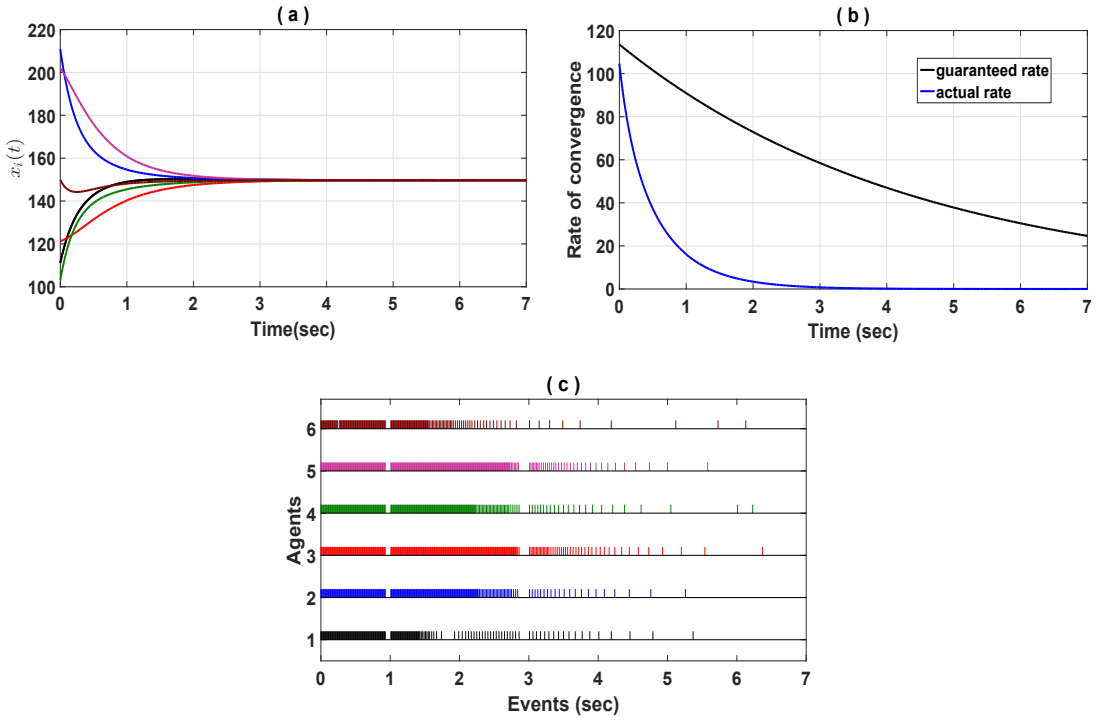

Figure 7.8: Consensus trajectories using Algorithm 5.8 (a): Average consensus for $x_i(t)$, (b): Expected and actual trajectories for $\|\boldsymbol{r}(t)\|$, (c): Events for each agent.

$\sigma^2 \in \{0.1, 0.5, 1, 5, 15\}$. For each value of σ^2, 100 sets of initial values $\{x_1(0), \ldots, x_{10}(0)\}$ are selected from $\mathcal{N}(0, \sigma^2)$. Then, consensus is run for each set of initial values using both Algorithms 5.7 and 5.8 with $h = 0.005$, $\phi = 0.01$, and $\bar{\delta} = 0.01$ under DoS sequence (7.21) with $\alpha = 12$. Fig. 7.9(a) compares the average transmissions using Algorithms 5.7 and 5.8. Each trajectory in Fig. 7.9(a) is the average number of events for the ten nodes and for randomized initial conditions at a particular time. According to Fig. 7.9(a), Algorithm 5.7 triggers fewer number of events at the start of process. However, Algorithm 5.8 transmits less samples afterwards and, unlike Algorithm 5.7, remains almost monotonous. Likewise, Fig. 7.9(b) compares the average values for $\|\boldsymbol{r}(t)\|$ calculated from the two algorithms. According to Fig. 7.9(b), the rates of $\|\boldsymbol{r}(t)\|$ converging to the error-bound are very close for the two algorithms. However, using Algorithm 5.8 the steady-state error for consensus, i.e., $\lim_{t\to\infty} \|\boldsymbol{r}(t)\|$, is larger than Algorithm 5.7.

7.7 R-PSEC

Consider the same network topology given in PEC and PSEC with the Laplacian matrix (7.11). Let $\boldsymbol{r}_i(t) = [\tilde{x}_i(t),\ \tilde{y}_i(t),\ \tilde{z}_i(t)]$ and $\boldsymbol{u}_i(t) = [u_{i,x}(t),\ u_{i,y}(t),\ u_{i,z}(t)\,]$, respectively, denote the position and control vectors for spacecraft i in the Cartesian coordinate system. The linearized equations of the relative dynamics for spacecraft i,

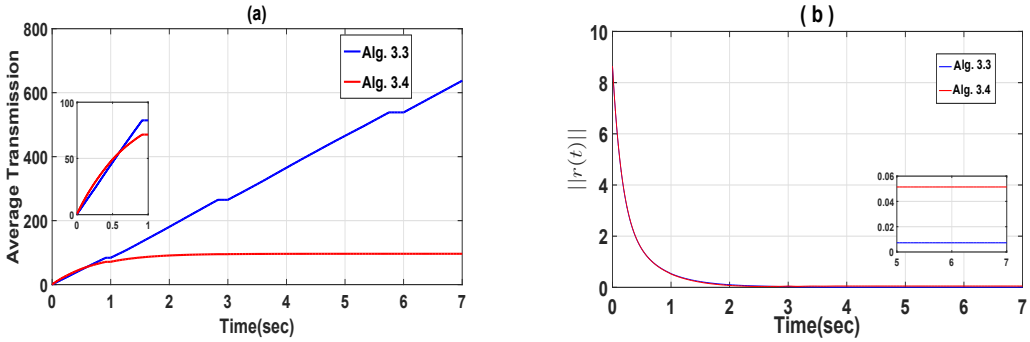

Figure 7.9: Comparing (a): the average number of events (transmissions) over time, (b): The norm of disagreement ($\|\boldsymbol{r}(t)\|$).

$(1 \leq i \leq 6)$ is written as follows [64]

$$\dot{\boldsymbol{x}}_i(t) = \begin{bmatrix} \boldsymbol{0}_3 & \boldsymbol{I}_3 \\ \boldsymbol{A}_1 & \boldsymbol{A}_2 \end{bmatrix} \boldsymbol{x}_i(t) + \begin{bmatrix} \boldsymbol{0}_3 \\ \boldsymbol{I}_3 \end{bmatrix} \boldsymbol{u}_i(t), \qquad (1 \leq i \leq 6), \tag{7.22}$$

where $\boldsymbol{x}_i = [\, \boldsymbol{r}_i^T(t),\, \dot{\boldsymbol{r}}_i^T(t)\,]^T$ and

$$\boldsymbol{A}_1 = \begin{bmatrix} 0 & 0 & 0 \\ 0 & 3\omega_0^2 & 0 \\ 0 & 0 & -\omega_0^2 \end{bmatrix}, \qquad \boldsymbol{A}_2 = \begin{bmatrix} 0 & 3\omega_0^2 & 0 \\ 0 & -2\omega_0^2 & 0 \\ 0 & 0 & 0 \end{bmatrix}. \tag{7.23}$$

Parameter $\omega_0 = 0.001$ is the angular rate of the spacecraft [64]. The spacecrafts are said to achieve formation flying if the velocity vectors converge to the same value, i.e., $\dot{\boldsymbol{r}}_i(t) \rightarrow \dot{\boldsymbol{r}}_j(t)$, and the positions maintain a prescribed separation, i.e., $\boldsymbol{r}_i(t) - \boldsymbol{h}_i \rightarrow \boldsymbol{r}_j(t) - \boldsymbol{h}_j$, $(1 \leq i, j \leq 6)$ [64].

Consensus-based formation: The spacecrafts are desired to form a regular hexagon. Formation is achieved if $\lim_{t\to\infty}[\boldsymbol{x}_i(t) - \boldsymbol{x}_j(t)] = \boldsymbol{h}_i - \boldsymbol{h}_j$, $(1 \leq i, j \leq 6)$. Formation can be achieved in (7.22) using the R-PSEC algorithm with the following disagreement

$$\mathbb{X}_i(t) = \sum_{j \in \mathcal{N}_i} a_{i,j} \Big((\boldsymbol{\Lambda}_i(t_k)\hat{\boldsymbol{x}}_i(t_k) - \boldsymbol{h}_i) - (\boldsymbol{\Lambda}_j(t_k)\hat{\boldsymbol{x}}_j(t_k) - \boldsymbol{h}_j) \Big), \tag{7.24}$$

Consider similar steady-state *velocity* for (7.22), (i.e., $\lim\limits_{t\to\infty}[\dot{\boldsymbol{r}}_i(t) - \dot{\boldsymbol{r}}_j(t)] \rightarrow \boldsymbol{0}$, $1 \leq i, j \leq 6$). Additionally, it is assumed that the steady-state value $\tilde{y}_i(t)$ is the same for all spacecrafts, (i.e., $\lim\limits_{t\to\infty}[\tilde{y}_i(t) - \tilde{y}_j(t)] \rightarrow 0$, $1 \leq i, j \leq 6$). This implies that the regular hexagon will be achieved while the spacecrafts have equal velocity and equal $\tilde{y}_i(t)$. Note that the N vertices of a 2-dimensional N-sided regular polygon with radius d, centered at $(0, 0)$, can be given by $p_i = (\tilde{x}_i, \tilde{z}_i)$, where $\tilde{x}_i = d\cos(2\pi i/N)$ and $\tilde{z}_i = d\sin(2\pi i/N)$ for $(1 \leq i \leq N)$. By definition, when formation is achieved it holds that

$$\lim_{t\to\infty}[\boldsymbol{x}_i(t) - \boldsymbol{x}_{i+1}(t)] = \boldsymbol{h}_i - \boldsymbol{h}_{i+1}. \tag{7.25}$$

Based on (7.25) and with $\boldsymbol{h}_1=[0,0,0,0,0,0]^T$, the remaining formation vectors are computed as follows

$$\boldsymbol{h}_{i+1}=\boldsymbol{h}_i-\boldsymbol{b}_i,\quad (1\leq i\leq N-1), \tag{7.26}$$

where $\boldsymbol{b}_i$ can be obtained from (7.25) as follows

$$\boldsymbol{b}_i=d\,[\,\cos(2\pi i/N)-\cos(2\pi(i+1)/N),\,0,\,\sin(2\pi i/N)-\sin(2\pi(i+1)/N),0,\,0,\,0\,]^T.$$

For $N=6$ and $d=5$, the agents in this example form a regular hexagon with an edge of $d=5$m.

Parameter design: Consider $h=0.05$, $\zeta=0.3$, and $\delta=0.01$. The desired level of resilience to DoS is selected as $\gamma=0.25$. The following control gain and ET parameters are computed from Theorem 5.3

$$\boldsymbol{K}=\begin{bmatrix}-0.5385 & 0.0011 & 0 & -1.2024 & 0 & 0\\ -0.0011 & -0.5385 & 0 & 0 & -1.2024 & 0\\ 0 & 0 & -0.5385 & 0 & 0 & -1.2024\end{bmatrix},$$

$$\boldsymbol{\Phi}_1=\begin{bmatrix}10.6590 & -0.0002 & 0 & 15.3019 & 0.0282 & 0\\ -0.0002 & 10.6618 & 0 & -0.0287 & 15.3091 & 0\\ 0 & 0 & 10.6583 & 0 & 0 & 15.3004\\ 15.3019 & -0.0287 & 0 & 24.8012 & -0.0005 & 0\\ 0.0282 & 15.3091 & 0 & -0.0005 & 24.8163 & 0\\ 0 & 0 & 15.3004 & 0 & 0 & 24.7979\end{bmatrix},$$

$$\boldsymbol{\Phi}_2=\begin{bmatrix}0.0015 & 0 & 0 & 0.0011 & 0 & 0\\ 0 & 0.0015 & 0 & 0 & 0.0011 & 0\\ 0 & 0 & 0.0015 & 0 & 0 & 0.0011\\ 0.0011 & 0 & 0 & 0.0036 & 0 & 0\\ 0 & 0.0011 & 0 & 0 & 0.0036 & 0\\ 0 & 0 & 0.0011 & 0 & 0 & 0.0036\end{bmatrix}. \tag{7.27}$$

Formation iterations: Similar to (4.10), the formation disagreement is defined as $\boldsymbol{z}(t)=(\tilde{\boldsymbol{W}}\otimes\boldsymbol{I}_n)\,(\boldsymbol{x}(t)-\boldsymbol{h})$, where $\boldsymbol{h}=[\boldsymbol{h}_1^T,\ldots,\boldsymbol{h}_6^T]^T$. Let $\boldsymbol{x}_1(0)=[30,10,20,0,1,0]^T$, $\boldsymbol{x}_2(0)=[15,15,12,0,1,0]^T$, $\boldsymbol{x}_3(0)=[-5,6,15,0,1,0]^T$, $\boldsymbol{x}_4(0)=[8,22,45,0,1,0]^T$, $\boldsymbol{x}_5(0)=[10,8,55,0,1,0]^T$ and $\boldsymbol{x}_6(0)=[12,-8,30,0,1,0]^T$. The consensus-based formation is run until time $t^\star$, where

$$t^\star=\inf\{\ t\mid \|\boldsymbol{z}(t)\|\leq 5\times 10^{-4}\,\|\boldsymbol{z}(0)\|\,\}. \tag{7.28}$$

DoS attacks: Consider the following DoS sequence [32],

$$\begin{aligned} &d_c=(c+1)+0.5c(c+1)-a^{-1}(c+1),\\ &\tau_c=a^{-1}(c+1), \qquad\qquad c\in\mathbb{N}_0,\qquad a\in\mathbb{R}_{\geq 1}. \end{aligned} \tag{7.29}$$

With $T_0=0$, $T_1=a$, and $F_0=F_1=1$, Assumption 5 is satisfied for (7.29), [32]. Let the period for transmission attempts during DoS be $g=0.01$s. With $T_1=a=4.5$, it

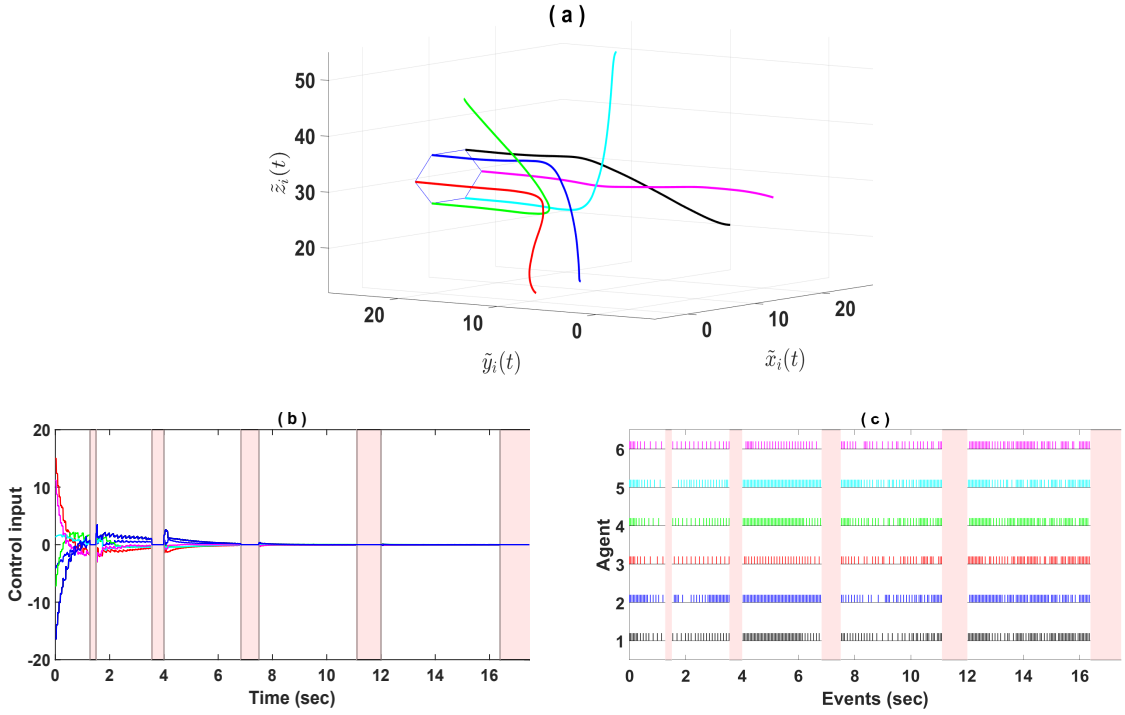

Figure 7.10: Trajectories of MAS (7.22) using R-PSEC; (a): The spacecrafts reach formation flying on a regular hexagon, (b): The control input generated to reach formation, (c) The event instants for each agent. Highlighted areas in figures (b) and (c) show DoS intervals (7.29).

---

holds that $\frac{1}{T_1} + \frac{g}{F_1} = 0.2322 < \gamma = 0.25$. Using designed parameters (7.27), consensus-based formation is simulated in the presence of DoS (7.29). Fig. 7.10(a) shows the trajectories of the spacecrafts reach a formation of a regular hexagon. Based on the termination time defined in (7.28), it takes 17.48 sec for the MASs to reach formation in the presence of DoS. The control inputs $\boldsymbol{u}_i(t)$ are shown in Fig. 7.10(b). The highlighted areas in Pink color show the DoS intervals. Note that the control inputs are kept zero during the DoS attacks. The spacecrafts, respectively, transmit 187, 216, 150, 191, 206, and 148 times during the process. The event-triggerings are shown in Fig. 7.10(c). The average number of events is AE=183.00. To compute the AIET in the presence of DoS, the following expression is used

$$\text{AIET} = \frac{t^\star - |\mathcal{D}(0, t^\star)|}{\text{AE}}. \tag{7.30}$$

In fact, in AIET (7.30) the total DoS duration from time 0 to $t^\star$, denoted by $|\mathcal{D}(0, t^\star)|$, is omitted from the total formation time $t^\star$. In other words, AIET is computed only based on the healthy intervals. Using (7.30), for this example AIET=0.0775.

Formation indices in the absence of DoS: It is interesting to observe how the formation indices (i.e., the settling time $t^\star$, AE, and AIET) are impacted when DoS never occurs. To this end, the same parameters obtained in (7.27) are used and

no DoS attack is considered. Simulation results lead to $t^\star = 14.86$, AE=173.83, and AIET=0.0855. As expected, formation is reached faster with lower number of events and larger interval between the events.

7.7.1 Impact of DoS resilience level γ

This section studies the impact of the desired DoS resilience level γ on computed parameters and consensus features. Consider fixed values $\zeta = 0.3$, $h = 0.05$, and $g = 0.01$. The DoS pattern is considered the same as (7.29), with $T_0 = 0$, $T_1 = a$, and $F_0 = F_1 = 1$. Parameter a in (7.29) is selected such as $\frac{1}{T_1} + \frac{g}{F_1} = \gamma$, where $g = 0.01$. Note that $\frac{1}{T_1} + \frac{g}{F_1} = \gamma$ implies an asymptotic convergence based on Theorem 5.3. The obtained results are listed in Table 7.11, where the following observations are made

- Higher values for γ lead to smaller values for $\|\boldsymbol{K}\|$ and a more conservative consensus (formation) is obtained. In fact, the LMIs in Theorem 5.3 return a smaller control gain to accommodate for a stronger attack. The settling time $t^\star$ is, therefore, increased with larger γ.
- The rate of change for AE and AIET is not monotonic. However, the pattern is that with larger γ more transmission is made (larger AE) and AIET is decreased.

7.8 ROCCET

To evaluate the performance of ROCCET, two different experiments are conducted. In the first experiment, the formation control for non-holonomic mobile robots is studied. The second experiment considers the leader-following application for a second-order oscillatory MAS.

7.8.1 Formation in nonholonomic mobile robots

The dynamics of mobile robot i shown in Fig. 7.11 is given by [156]

$$\dot{\bar{\boldsymbol{x}}}_i = \boldsymbol{f}(\bar{\boldsymbol{x}}_i) + \bar{\boldsymbol{B}}\bar{\boldsymbol{u}}_i, \quad (1 \leq i \leq 5), \tag{7.31}$$

Table 7.11: Consensus performance using R-PSEC; different desired resilience γ with $\zeta = 0.3$, $h = 0.05$, and $\delta = 0.01$.

γ	$\|\boldsymbol{K}\|$	$\|\boldsymbol{\Phi}_1\|$	$\|\boldsymbol{\Phi}_2\|$	$t^\star$	AE	AIET
0.05	1.6123	7.7199	0.1309	12.56	163.17	0.0741
0.10	1.5528	7.5549	0.1394	13.20	160.17	0.0763
0.15	1.5012	5.8258	0.1191	16.21	190.33	0.0773
0.25	1.3175	8.2125	0.0850	19.91	215.00	0.0754
0.33	1.2489	54.2063	0.0547	20.90	313.50	0.0508

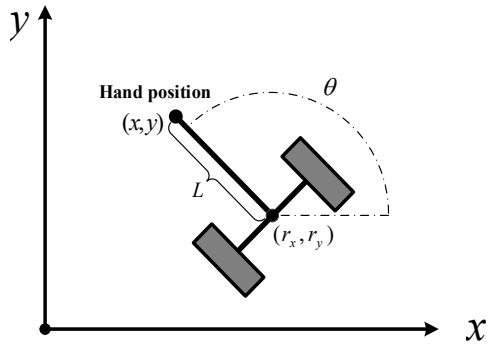

Figure 7.11: Non-holonomic mobile robot coordinates.

where

$$\bar{\boldsymbol{x}}_i = [\, r_{x,i},\, r_{y,i},\, \theta_i,\, v_i,\, \omega_i \,]^T, \qquad \boldsymbol{f}(\bar{\boldsymbol{x}}_i) = [\, v_i \cos(\theta_i),\, v_i \sin(\theta_i),\, \omega_i,\, 0,\, 0 \,]^T,$$
$$\bar{\boldsymbol{B}} = \begin{bmatrix} 0 & 0 & 0 & 0 & \frac{1}{J} \\ 0 & 0 & 0 & \frac{1}{m} & 0 \end{bmatrix}^T, \qquad \bar{\boldsymbol{u}}_i = [\, f_i,\, \tau_i \,]^T.$$

For robot i, parameters $r_{x,i}$ and $r_{y,i}$ are the inertial positions; θ_i is the orientation; v_i is the linear speed; ω_i is the angular speed; τ_i is the applied torque; f_i is the applied force; $m = 10.1$kg is the mass; and $J = 0.13$kg.m^2 is the moment of inertia. The network is described by the following Laplacian matrix

$$\boldsymbol{L} = \begin{bmatrix} 2 & -1 & 0 & 0 & -1 \\ -1 & 2 & -1 & 0 & 0 \\ 0 & -1 & 2 & -1 & 0 \\ 0 & 0 & -1 & 2 & -1 \\ -1 & 0 & 0 & -1 & 2 \end{bmatrix}. \tag{7.32}$$

As described later, the objective is that the five robots in (7.31) form a regular pentagon.

Feedback linearization: Denoting the following variables, robot (7.31) is state feedback linearizable [156]

$$x_{1,i} = r_{x,i} + L\cos(\theta_i), \qquad x_{2,i} = r_{y,i} + L\sin(\theta_i),$$
$$x_{3,i} = v_i\cos(\theta_i) - L\omega_i\sin(\theta_i), \quad x_{4,i} = v_i\sin(\theta_i) + L\omega_i\cos(\theta_i), \qquad x_{5,i} = \theta_i, \tag{7.33}$$

where $L = 0.12$m is an internal distance in the structure of the robot. Now, consider the following linear system

$$\dot{\boldsymbol{x}}_i = \boldsymbol{A}\boldsymbol{x}_i + \boldsymbol{B}\boldsymbol{u}_i, \quad (1 \leq i \leq 5), \tag{7.34}$$

where $\boldsymbol{x}_i = [\, x_{1,i},\, x_{2,i},\, x_{3,i},\, x_{4,i} \,]^T$ and

$$\boldsymbol{A} = \begin{bmatrix} \boldsymbol{0}_{2\times2} & \boldsymbol{I}_2 \\ \boldsymbol{0}_{2\times2} & \boldsymbol{0}_{2\times2} \end{bmatrix}, \qquad \boldsymbol{B} = \begin{bmatrix} \boldsymbol{0}_{2\times2} \\ \boldsymbol{I}_2 \end{bmatrix}.$$

The feedback linearizing control for robot i is

$$\bar{\boldsymbol{u}}_i = \begin{bmatrix} \frac{1}{m}\cos(\theta_i) & -\frac{L}{J}\sin(\theta_i) \\ \frac{1}{m}\sin(\theta_i) & \frac{L}{J}\cos(\theta_i) \end{bmatrix}^{-1} \left(\boldsymbol{u}_i - \begin{bmatrix} -v_i\omega_i\sin(\theta_i) - L\omega_i^2\cos(\theta_i) \\ v_i\omega_i\cos(\theta_i) - L\omega_i^2\sin(\theta_i) \end{bmatrix} \right). \tag{7.35}$$

Following [156], the states of actual system (7.31) is obtained from the states of linear system (7.34) as

$$\begin{aligned} r_{x,i} &= x_{1,i} - L\cos(x_{5,i}), \qquad r_{y,i} = x_{2,i} - L\sin(x_{5,i}), \\ \theta_i &= x_{5,i}, \qquad v_i = \frac{1}{2}x_{3,i}\cos(x_{5,i}) + \frac{1}{2}x_{4,i}\sin(x_{5,i}), \\ \omega_i &= -\frac{1}{2L}x_{3,i}\sin(x_{5,i}) + \frac{1}{2L}x_{4,i}\cos(x_{5,i}), \end{aligned} \tag{7.36}$$

where $\dot{x}_{5,i} = -\frac{1}{2L}x_{3,i}\sin(x_{5,i}) + \frac{1}{2L}x_{4,i}\cos(x_{5,i})$. To solve formation for the nonlinear MAS (7.31), one can design a control protocol for linear system (7.34) with control input $\boldsymbol{u}_i$. Trajectories of system (7.31) then follows (7.36), if the feedback linearizing control (7.35) is applied.

Consensus-based formation: The robots are desired to form a predefined geometric shape. To this end, a given formation vector $\boldsymbol{h}_i$ is included in disagreement (5.47). Formation is achieved if $\lim_{t\to\infty}(\boldsymbol{x}_i(t) - \boldsymbol{x}_j(t)) = \boldsymbol{h}_i - \boldsymbol{h}_j$, $(1 \le i, j \le 5)$. Formation can be achieved in (7.31) using the ROCCET algorithm with the following disagreement

$$\mathbb{X}_i(t) = \sum_{j\in\mathcal{N}_i} a_{i,j}\Big((\boldsymbol{\Lambda}_i(t)\boldsymbol{x}_i(t_k^i) - \boldsymbol{h}_i) - (\boldsymbol{\Lambda}_j(t)\boldsymbol{x}_j(t_k^j) - \boldsymbol{h}_j) \Big). \tag{7.37}$$

To compute formation vector $\boldsymbol{h}_i$, the same procedure used in Section 7.7 is considered here. This gives way to expressions (7.25) and (7.26). We use $\boldsymbol{h}_1 = [0,0,0,0]^T$. For $N = 5$ and $d = 3$, the agents in this example form a regular pentagon with an edge of $d = 3$m.

Optimization: Let $\zeta = 0.4$. The desired level of resilience to DoS is selected as $\gamma = 0.3$. Using the SDPT3 solver, a solution for optimization (5.73) is computed as

$$\begin{aligned} &\boldsymbol{K} = -[\,0.3948,\ 0.7973\,] \otimes \boldsymbol{I}_2, \quad \boldsymbol{\Phi}_1 = \begin{bmatrix} 7.3433 & 4.3451 \\ 4.3451 & 11.4059 \end{bmatrix} \otimes \boldsymbol{I}_2, \\ &\phi_2 = 0.4676, \quad \phi_3 = 0.9628, \quad \phi_4 = 1.1635, \quad \phi_5 = 0.4676. \end{aligned}$$

The value of the objective function is $\mathbb{F} = 127.94$.

DoS attacks: Consider the same DoS given in (7.29) with $T_0 = 0$, $T_1 = a$, and $F_0 = F_1 = 1$, Assumption 5 is satisfied for (7.29), [32]. Let the period for transmission attempts during DoS be $g = 0.01$s. With $T_1 = a = 3.5$, it holds that $\frac{1}{T_1} + \frac{g}{F_1} = 0.2957 < \gamma = 0.3$.

Implementation: Similar to (5.65), define the formation disagreement as $\boldsymbol{z}(t) = (\tilde{\boldsymbol{W}} \otimes \boldsymbol{I}_n)(\boldsymbol{x}(t) - \boldsymbol{h})$, where $\boldsymbol{h} = [\boldsymbol{h}_1^T, \ldots, \boldsymbol{h}_5^T]^T$. Let $\boldsymbol{x}_1(0) = [0,0,0,0]^T$, $\boldsymbol{x}_2(0) = [3,0,0,0]^T$, $\boldsymbol{x}_3(0) = [1.5,2,0,0]^T$, $\boldsymbol{x}_4(0) = [3,3,0,0]^T$, $\boldsymbol{x}_5(0) = [-3,-3,0,0]^T$, and

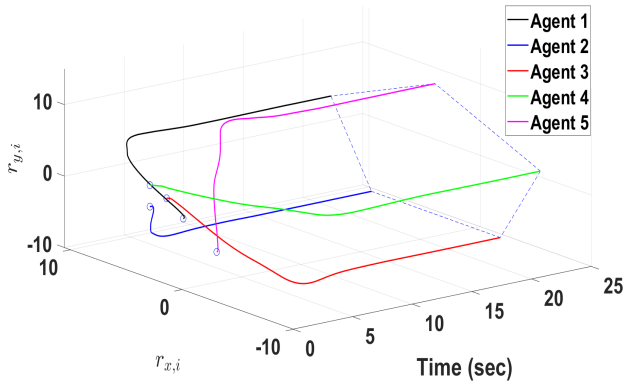

Figure 7.12: State evolution of the robots and forming a pentagon.

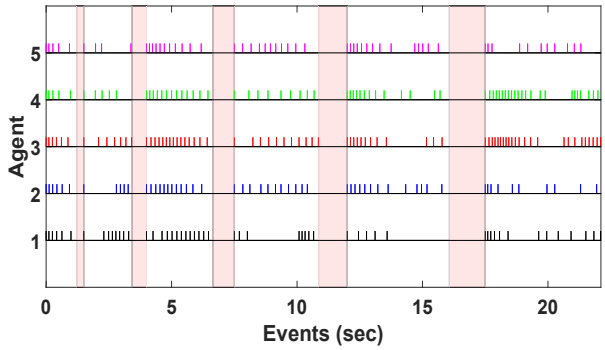

Figure 7.13: Event instants. The highlighted areas in pink color are the DoS intervals.

$\eta_i(0) = 1$, $(1 \leq i \leq 5)$. The consensus-based formation is run until time $t^\star$, where

$$t^\star = \inf\{\ t \mid \|\boldsymbol{z}(t)\| \leq 1 \times 10^{-4}\, \|\boldsymbol{z}(0)\|\ \}. \tag{7.38}$$

Time $t^\star$ is when formation is achieved within 0.01% of the initial disagreement. Parameter $t^\star$ is used as an index to compare the consensus (formation) convergence rate. A larger value for $t^\star$ corresponds to a smaller rate of convergence and vice versa. For this setting, $t^\star = 22.12$s. Trajectories of (7.31) is plotted in Fig. 7.12, where the agents reach a regular pentagon. The agents, respectively, trigger 52, 56, 74, 67, and 55 events which are shown in Fig. 7.13. The highlighted areas (in pink color) in Fig. 7.12 are the DoS attack intervals. The total average number of events per agent is AE $= 60.8$. Parameter AIET is also reported, which is computed by AIET$=(t^\star - |\mathcal{D}(0, t^\star)|)/$AE. In this example, AIET$= 0.3638$. The trajectories $\eta_i(t)$, $(1 \leq i \leq 5)$, are included in Fig. 7.14. As shown in Fig. 7.14, parameter $\eta_i(t)$, $(1 \leq i \leq 5)$, efficiently contributes in reducing the number of transmissions. Parameter $\eta_i(t)$ converges to zero and does not cause any steady-state error for formation.

Impact of given parameters ζ and γ: This section studies the impact of different values for convergence rate ζ and desired level of resilience γ on the formation features. To this end, optimization (5.73) is solved for given values of ζ and γ given in Table 7.12. The table is categorized into two sections. In the first section γ is fixed

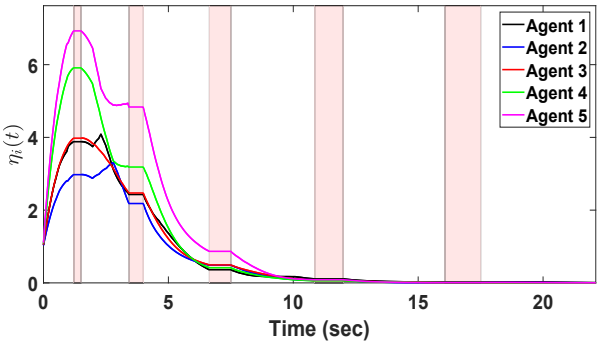

Figure 7.14: Trajectories of $\eta_i(t)$. The highlighted areas in pink color are the DoS intervals.

and ζ is incrementally increased. In the second part of the table, ζ is fixed and γ is increased. Formation for (7.31) is run using corresponding designed parameters. DoS sequence follows (7.29) with $a = 6$. According to Table 7.12, one observes:

- Higher values for ζ increase the rate of convergence. Therefore, convergence time $t^\star$ steadily gets reduced and formation achieves faster.
- Larger values for ζ lead to larger $\|\boldsymbol{K}\|$. In fact, increasing the desired convergence rate requires higher values for the control input $\boldsymbol{u}_i(t)$.
- As a result of larger values for ζ, the frequency of transmissions increases and parameter AIET becomes smaller (i.e., more frequent transmissions).

In the second half of the table, we set $\zeta = 0.4$ and observe the impact of different values for desired level of resilience to DoS γ. From Table 7.12, one observes that higher values for γ lead to smaller control gains. Therefore, formation is achieved with more conservation. As for the AIET no specific trend is found. It is worth noting that the largest resilience level that optimization (5.73) remains feasible is $\gamma = 0.47$ for this MAS setting.

These results verify the efficiency of ROCCET for a structured trade-off between the rate of convergence, frequency of transmission, and resilience to DoS.

Table 7.12: Impact of given parameters ζ and γ on ROCCET.

ζ	γ	$\|\boldsymbol{K}\|$	$\|\boldsymbol{\Phi}_1\|$	ϕ_2	ϕ_3	ϕ_4	ϕ_5	$t^\star$	AE	AIET
0.2	0.2	0.645	11.67	0.470	0.981	1.081	0.470	22.90	44.6	0.513
0.3	0.2	1.086	13.72	0.538	0.972	1.122	0.538	16.37	45.0	0.363
0.4	0.2	1.602	19.11	0.568	0.963	1.163	0.568	10.23	35.0	0.292
0.5	0.2	2.236	26.46	0.583	0.954	1.205	0.583	8.44	33.6	0.251
0.6	0.2	2.997	36.59	0.598	0.946	1.248	0.597	7.65	34.2	0.224
0.4	0.1	2.716	34.88	0.614	0.962	1.163	0.614	8.46	33.6	0.251
0.4	0.2	1.602	19.114	0.567	0.962	1.163	0.567	10.23	35.0	0.292
0.4	0.3	0.889	14.171	0.467	0.962	1.163	0.467	16.87	53.0	0.318
0.4	0.4	0.597	19.759	0.346	0.962	1.163	0.346	24.42	85.8	0.285

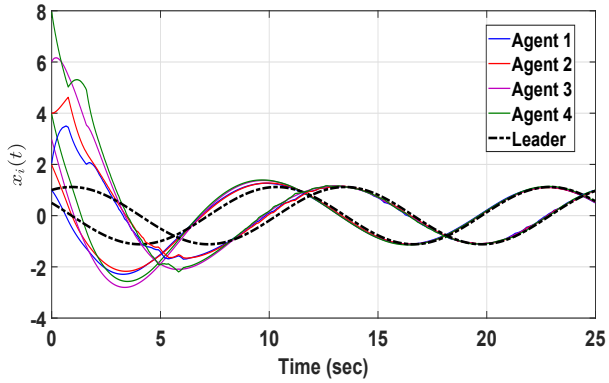

Figure 7.15: The states of MAS (7.39) following trajectories of the leader in a leader-following setup.

7.8.2 Comparison with Reference [1]

This section compares ROCCET with reference [1] in terms of transmission savings and the amount of guaranteed resilience to DoS. To this end, consider the leader-following application for a type of oscillatory MAS with the following parameters

$$\boldsymbol{A} = \begin{bmatrix} 0 & -0.5 \\ 0.5 & 0 \end{bmatrix}, \quad \boldsymbol{B} = \begin{bmatrix} 0 \\ 1 \end{bmatrix}. \tag{7.39}$$

A network with 5 agents is considered, where agent 5 is the leader and it has no neighbours. Agents 1 and 2 are connected to the leader and continuously receive state information from the leader. The information exchanges among the followers are event-triggered. The network configuration of the agents is modeled as

$$\boldsymbol{L} = \begin{bmatrix} 2 & 0 & 0 & -1 & -1 \\ 0 & 2 & -1 & 0 & -1 \\ 0 & -1 & 2 & -1 & 0 \\ -1 & 0 & -1 & 2 & 0 \\ 0 & 0 & 0 & 0 & 0 \end{bmatrix}. \tag{7.40}$$

Effectiveness of DET scheme: This part compares the effectiveness of DET scheme (5.49) with [1]. To focus only on the capability of transmissions schemes, consider the DoS free situation and solve optimization (5.68) with $\zeta = 0$ (i.e., asymptotic

Table 7.13: Comparison between Theorem 5.4 and [1, Theorem. 4].

Method	**Number of transmissions**				AE	AIET
	Agent 1	Agent 2	Agent 3	Agent 4		
Theorem 5.4	226	237	260	236	239.75	0.1043
Ref. [1]	493	533	526	540	523.00	0.0478

consensus). The following parameters are computed from (5.67)

$$\boldsymbol{K} = \begin{bmatrix} 0.8462 & -1.3384 \end{bmatrix}, \quad \boldsymbol{\Phi}_1 = \begin{bmatrix} 48.4832 & -9.1889 \\ -9.1889 & 15.1221 \end{bmatrix},$$
$$\phi_2 = 0.5672, \quad \phi_3 = 1, \quad \phi_4 = 1, \quad \phi_5 = 0.5672. \tag{7.41}$$

The transmission scheme used in [1, Eq. (24)] is a combination of an event-triggering scheme (in the form of $t^i_{k+1} = \inf\{\, t > t^i_k \mid \|\boldsymbol{e}_i(t)\| \geq \tilde{\beta}_i \|\mathbb{X}_i(t)\| \,\}$) and a periodic scheme with period $\tilde{b}_i$. The control protocol in [1] is similar to (5.48). To compute necessary consensus parameters using [1, Theorem 4], let $\tilde{\boldsymbol{R}} = 1$, $\tilde{\boldsymbol{Q}} = [1.6, 0; 0, 1]$, $\tilde{\tau} = 0.98$, $\tilde{s}_i = 1$, and $\tilde{\varrho} = 48$. These parameters are selected in such a way so as to compute the largest possible $\tilde{\beta}$ and almost the same control gain as in (7.41). Since the control gains are almost the same, the convergence rate for both simulations will be almost the same. This helps to have a fair comparison for the number of transmissions. The control gain for [1, Eq. (22)] and ET thresholds for [1, Eq. (24)] are computed as

$$\tilde{\boldsymbol{K}} = \begin{bmatrix} 0.8429 & -1.3366 \end{bmatrix}, \quad \tilde{\beta}_i = 0.0225, \quad \tilde{b}_i = 0.0345.$$

Let $\boldsymbol{x}_i(0) = i \times [1, 2]^T$, $(1 \leq i \leq 4)$, and $\boldsymbol{x}_5(0) = [0.5, 1]^T$. Using the two sets of parameters, the leader-following consensus problem is solved for (7.39) in a time horizon of 25s, i.e., $t \in [0, 25]$. Fig. 7.15 shows the trajectories of MAS (7.39) using parameters (7.41). Table 7.13 includes the number of transmissions for ROCCET (Theorem 5.4) and [1, Theorem 4]. It is observed that the number of transmissions triggered by ROCCET (Theorem 5.4) is lower as compared to [1]. This corroborates the superiority of the DET scheme compared to the so-called static scheme used in [1].

Guaranteed resilience level to DoS: Next, the theoretical resilience level guaranteed by ROCCET (Theorem 5.5) and that of [1] is compared. In [1], an algebraic Riccati equation (ARE) approach is used for stability analysis and control design. The guaranteed resilience level to DoS in [1, Eq. (27) and (28)] is obtained based on the norm and extremum eigenvalues of some associated matrices. With the ARE approach, the theoretical resilience guaranteed by [1] for MAS (7.39) is 0.1701. In other words, DoS attacks satisfying $\frac{1}{T_1} + \frac{g}{F_1} < 0.1701$ are theoretically guaranteed of maintaining a stable MAS (7.39). Theorem 5.5 is used to find the maximum guaranteed resilience to DoS for MAS (7.39). Let $\zeta = 0.3$. The maximum resilience to DoS is found by incrementally increasing γ in Theorem 5.5 until no feasible solution is computed. It is observed that optimization (5.73) remains feasible until $\gamma = 0.4802$, which implies that DoS attacks satisfying $\frac{1}{T_1} + \frac{g}{F_1} < 0.4802$ are theoretically admissible and do not destabilize MAS (7.39). Compared to [1], the theoretical DoS resilience guaranteed by ROCCET is higher and thus more realistic. The reason is that, unlike [1] where the DoS bound is computed from matrix norms and extremum eigenvalues, Theorem 5.5 uses the full information included in the system matrix $\boldsymbol{A}$ and decision matrices $\boldsymbol{P}$, $\boldsymbol{\Omega}$, and $\boldsymbol{S}_1$ in the LMI formulation.

7.9 FCC/DEME

Implementation FCC/DEME is evaluated for a MAS comprising of 4 leader and 6 follower robots with the same dynamics given in (7.31). The network topology shown in Fig. 6.1 is used, which is represented by the partitioned Laplacian matrices (6.3). It holds that

$$\tilde{\boldsymbol{J}}_1 = \text{diag}(2,2,4), \qquad \boldsymbol{J}_2 = \text{diag}(4.613, 3.808, 3.258, 0.387, 1.192, 1.742),$$
$$\tilde{\boldsymbol{W}} = \begin{bmatrix} 0.707 & 0 & -0.707 & 0 \\ 0 & 0.707 & 0 & -0.707 \\ -0.5 & 0.5 & -0.5 & 0.5 \end{bmatrix},$$
$$\boldsymbol{V}^{-1} = \begin{bmatrix} 0.354 & 0.261 & -0.300 & -0.381 & 0.524 & -0.544 \\ 0.216 & 0.355 & 0.064 & -0.707 & -0.472 & 0.317 \\ 0.425 & -0.413 & 0.565 & -0.046 & -0.299 & -0.488 \\ -0.381 & -0.544 & -0.524 & -0.354 & -0.300 & -0.261 \\ 0.707 & -0.317 & -0.472 & 0.216 & -0.064 & 0.355 \\ -0.046 & -0.488 & 0.299 & -0.425 & 0.565 & 0.413 \end{bmatrix}.$$

The formation-containment objective in this example is that the 4 leaders in (7.31) form a regular square and the 6 followers merge within the square form by the leaders. The same feedback linearization technique (7.33) is used here.

Formation vector and formation gain: As specified previously, the 4 leaders in (7.31) are supposed to form a regular square. To compute formation vector $\boldsymbol{h}_i$, the same procedure used in Section 7.7 is considered here. This gives way to expressions (7.25) and (7.26). We use $\boldsymbol{h}_1{=}[0,0,0,0]^T$. With $M=4$ and $d=3$, the leaders in this example will form a regular square with an edge of $d=3$m. It is straightforward to show that $\boldsymbol{A}\sum_{j\in\mathcal{N}^i_{\mathcal{L}\leftarrow\mathcal{L}}}(\boldsymbol{h}_i-\boldsymbol{h}_j)=\boldsymbol{0}$, $(1\leq i\leq 4)$, which implies that the formability condition (6.15) holds with $\boldsymbol{H}=\boldsymbol{0}$. Therefore, the formation gain in (7.43) is considered as $\boldsymbol{H}=\boldsymbol{0}$.

Parameter design for leaders: Let $\zeta_1=0.3$. Using the SDPT3 solver, optimization (6.28) is solved which leads to the following solution:

$$\boldsymbol{P} = \begin{bmatrix} 0.0675 & -0.0505 \\ * & 0.2057 \end{bmatrix} \otimes \boldsymbol{I}_2, \quad \tilde{\boldsymbol{\Phi}} = \begin{bmatrix} 1.1849 & -0.0437 \\ * & 1.4451 \end{bmatrix} \otimes \boldsymbol{I}_2,$$
$$\boldsymbol{\Omega} = [-0.0144 \quad -0.1971] \otimes \boldsymbol{I}_2, \quad \tilde{\alpha}=0.0178, \quad \tilde{\beta}=0.5980, \quad \tilde{\gamma}=1.3980, \quad \tilde{\rho}=0.0252,$$
$\tau_1=1.8783$, $\tau_2=0.0536$, $\theta_1=19.6111$, $\theta_2=2.1089$, $\theta_3=56.1314$, $\theta_4=1.6721$, $\theta_5=1.9545$, $\theta_6=39.6909$, $\theta_7=0.0391$.

Design parameters are calculated form (6.30) as follows

$$\boldsymbol{K}_1 = -[\,1.1414,\ 1.2390\,] \otimes \boldsymbol{I}_2,\ \boldsymbol{\Phi}_1 = \begin{bmatrix} 19.7233 & 4.8133 \\ * & 7.0278 \end{bmatrix} \otimes \boldsymbol{I}_2$$
$$\alpha_1=0.1335, \quad \beta_1=0.7733, \quad \gamma_1=1.3980, \quad \rho_1=0.1587.$$

The value of the objective function is $\mathbb{F}_1=121.20$.

Parameter design for followers: Next, design parameters for the followers are

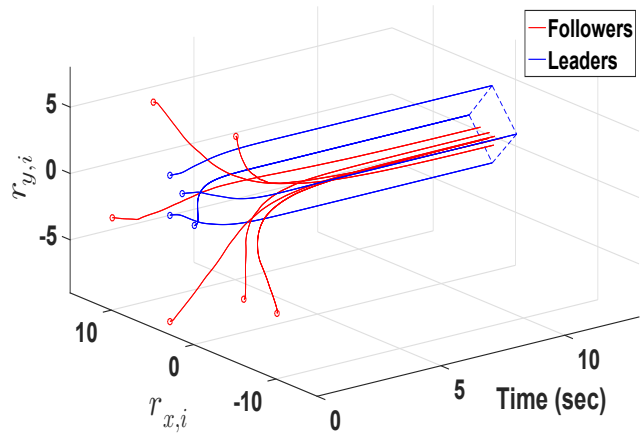

Figure 7.16: Formation-containment for MAS (7.31).

computed. Optimization (6.33) is solved with $\zeta_2 = 0.3$ which leads to the following solution

$$\boldsymbol{P} = \begin{bmatrix} 0.1844 & -0.0837 \\ * & 0.1605 \end{bmatrix} \otimes \boldsymbol{I}_2, \quad \tilde{\boldsymbol{\Phi}} = \begin{bmatrix} 1.6485 & -0.0651 \\ * & 1.7888 \end{bmatrix} \otimes \boldsymbol{I}_2,$$
$$\boldsymbol{\Omega} = [-0.0449 \quad -0.3973] \otimes \boldsymbol{I}_2, \quad \tilde{\alpha} = 0.0134, \quad \tilde{\beta} = 0.5980, \quad \tilde{\gamma} = 1.3980,$$
$$\tilde{\rho} = 0.0184, \quad \tau_1 = 1.9086, \quad \tau_2 = 0.0544, \quad \theta_1 = 11.3746, \quad \theta_2 = 3.2921, \quad \theta_3 = 74.6831,$$
$$\theta_4 = 1.6721, \quad \theta_5 = 1.9545, \quad \theta_6 = 52.8089, \quad \theta_7 = 0.1598.$$

The following design parameters are then computed

$$\boldsymbol{K}_2 = -[\,1.7906,\ 3.4091\,] \otimes \boldsymbol{I}_2, \quad \boldsymbol{\Phi}_2 = \left[\begin{smallmatrix} 9.0799 & 4.6743 \\ * & 10.7708 \end{smallmatrix}\right] \otimes \boldsymbol{I}_2$$
$$\alpha_2 = 0.1157, \quad \beta_2 = 0.7733, \quad \gamma_2 = 1.3980, \quad \rho_2 = 0.1376.$$

The objective function is computed as $\mathbb{F}_2 = 145.94$.

Formation-containment implementation: Let $\boldsymbol{x}_1(0) = [-10, -4, 0, 0]^T$, $\boldsymbol{x}_2(0) = [-6, -4, 0, 0]^T$, $\boldsymbol{x}_3(0) = [3, -8, 0, 0]^T$, $\boldsymbol{x}_4(0) = [10, -2, 0, 0]^T$, $\boldsymbol{x}_5(0) = [-5, 8, 0, 0]^T$, $\boldsymbol{x}_6(0) = [5, 8, 0, 0]^T$, $\boldsymbol{x}_7(0) = [0, 0, 0, 0]^T$, $\boldsymbol{x}_8(0) = [3, 0, 0, 0]^T$, $\boldsymbol{x}_9(0) = [1.5, 2, 0, 0]^T$, $\boldsymbol{x}_{10}(0) = [3, 3, 0, 0]^T$, and $\eta_i(0) = 1$, $(1 \leq i \leq 10)$. Time $t^\star$, which is the time when formation-containment is achieved, is determined as follows

$$t^\star = \inf\{\ t \mid \max\left\{\frac{\|\boldsymbol{\psi}_{\mathcal{L}}(t)\|}{\|\boldsymbol{\psi}_{\mathcal{L}}(0)\|}, \frac{\|\boldsymbol{\psi}_{\mathcal{F}}(t)\|}{\|\boldsymbol{\psi}_{\mathcal{F}}(0)\|}\right\} \leq \delta\ \}. \tag{7.42}$$

Conceptually speaking, time $t^\star$ is the smallest time when both the formation for leaders and containment for followers are achieved within at least δ factor of the initial disagreements specified by $\|\boldsymbol{\psi}_{\mathcal{L}}(0)\|$ and $\|\boldsymbol{\psi}_{\mathcal{F}}(0)\|$, respectively. This time, i.e., $t^\star$, is used as an index to compare the convergence rates for different examples. Let $\delta = 0.005$. This value provides a high accuracy for formation-containment achievement. For this

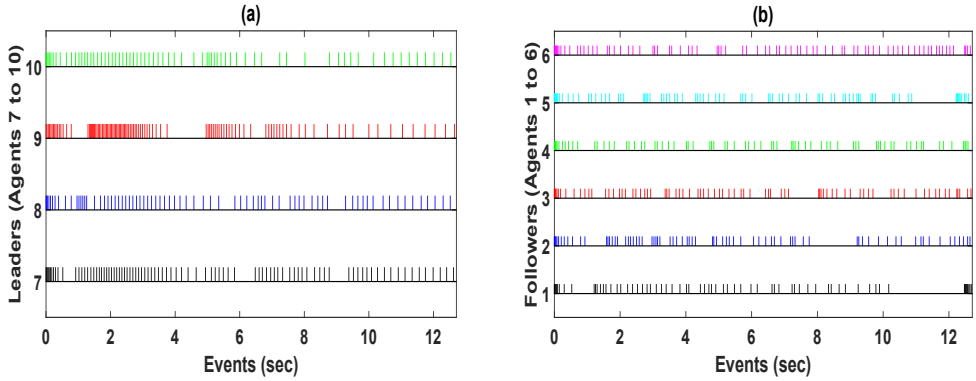

Figure 7.17: Event instants; (a): for Leaders, (b): for Followers.

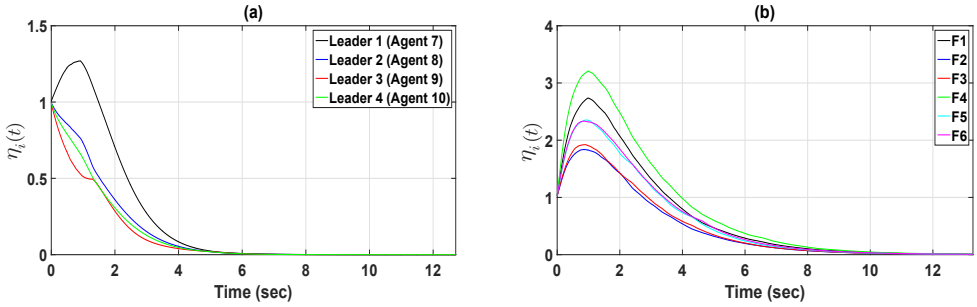

Figure 7.18: Trajectory of the dynamic threshold $\eta_i(t)$, (a): For Leaders; (b): For Followers.

setting, $t^\star = 12.72$s with $\delta = 0.005$. [2] In Fig. 7.16, the trajectory of (7.31) is plotted where the leaders (shown in blue color) reach a regular square and the followers (shown in red color) achieve containment inside the square. The leaders, respectively, trigger 89, 75, 104, and 69 events shown in Fig. 7.17(a). The number of events for the followers are, respectively, 69, 76, 79, 73, 83, and 80. The event instants for followers are shown in Fig. 7.17(b). The total average number of events (including both the leaders and followers) per agent is AE = 79.70. The average inter-event time is computed by AIET=$t^\star$/AE. In this example, AIET= 0.1596. The trajectories of $\eta_i(t)$, $(1 \leq i \leq 10)$, are included in Figs. 7.18(a) and (b). As shown in Figs. 7.18(a) and (b), parameter $\eta_i(t)$, $(1 \leq i \leq 10)$, provides a considerable threshold and efficiently contributes in reducing the number of events.

Impact of convergence rates ζ_1 and ζ_2: Optimizations (6.28) and (6.33) are solved for the given values of ζ_1 and ζ_2 listed in Table 7.14. Then, formation-containment is run using the designed parameters. According to Table 7.14, one observes that:

- With higher values for ζ_1 (or ζ_2) the rate of convergence increases and $t^\star$ steadily

[2] It should be noted that convergence within 1% of the initial disagreement(i.e., $\delta = 0.01$ in (7.42)) provides a satisfactory level of formation-containment convergence in MAS (7.31). With $\delta = 0.01$, formation-containment is achieved at $t^\star = 9.43$ in this example. Simulation is run using a higher accuracy of $\delta = 0.005$ to better observe the differences between different examples.

gets reduced. In return, the value AIET is also reduced which is translated to more dense event-triggerings.

- Larger values for ζ_1 (or ζ_2) lead to larger $\|\boldsymbol{K}_1\|$ (or $\|\boldsymbol{K}_2\|$). This is consistent with the fact that increasing the desired convergence rate requires higher values for the control input $\boldsymbol{u}_i(t)$.

- Larger values for ζ_1 (or ζ_2) lead to smaller values for $\{\alpha_1, \beta_1, \rho_1\}$ (or $\{\alpha_2, \beta_2, \rho_2\}$) and higher values for $\{\|\boldsymbol{\Phi}_1\|, \gamma_1\}$ (or $\{\|\boldsymbol{\Phi}_2\|, \gamma_2\}$) which together increase the frequency of the event-triggerings to cope with the higher given rate of convergence. The AIET, in return, becomes smaller (i.e., higher frequency for event-triggerings) as ζ_1 (or ζ_2) is increased.

These results verify the flexibility of FCC/DEME for formation-containment based on a structured trade-off between the rate of convergence and events frequency. FCC/DEME is tested for a variety of other multi-agent systems. The results corroborate the observations reported in the aforementioned simulation.

7.10 Summary

This chapter provides numerical examples to quantify the effectiveness of the proposed implementations. For average consensus, simulations are based on different networks of single-order MASs. For consensus in general linear agents and formation-containment, different dynamical agents, such as a class of second-order vehicles, spacecrafts, and non-holonimic mobile robots are selected for experiments. Simulations demonstrate the capability of the CEASE algorithm in achieving a guaranteed exponential rate for event-triggered average consensus using only sampled-data states. CEASE is based on an optimization which does not depend on the network size. The optimization attempts to increase the average inter-event time (AIET). It was observed that CEASE and Q-CEASE produce a bounded steady-state consensus error.

Due to involving a more advanced ET scheme, (dynamic event-triggering scheme), DEASE is more powerful than CEASE in terms of transmission savings. Additionally, it was observed that DEASE provides feasible solution for larger sampling periods than CEASE. DEASE guarantees asymptotic consensus with arbitrary small error.

Table 7.14: Impact of different desired convergence rates $\{\zeta_1, \zeta_2\}$ on computed parameters and FCC features.

Given Rates		Computed parameters from Opt. (6.28)						Computed parameters from Opt. (6.33)						Features		
ζ_1	ζ_2	$\|\boldsymbol{K}_1\|$	$\|\boldsymbol{\Phi}_1\|$	α_1	β_1	γ_1	ρ_1	$\|\boldsymbol{K}_2\|$	$\|\boldsymbol{\Phi}_2\|$	α_2	β_2	γ_2	ρ_2	$t^\star$	AE	AIET
0.00	0.00	0.8904	13.36	0.1339	0.8107	1.1573	0.1592	2.4696	9.66	0.1161	0.8107	1.1573	0.1381	19.76	86.3	0.2290
0.10	0.10	1.1307	15.59	0.1338	0.7975	1.2360	0.1591	2.9551	11.14	0.1160	0.7975	1.2360	0.1379	17.17	80.2	0.2141
0.20	0.20	1.3949	18.22	0.1336	0.7851	1.3163	0.1589	3.4106	12.81	0.1159	0.7851	1.3163	0.1378	14.93	74.5	0.2004
0.30	0.30	1.6846	21.28	0.1335	0.7733	1.3980	0.1587	3.8507	14.67	0.1157	0.7733	1.3980	0.1376	12.72	79.7	0.1596
0.40	0.40	2.0011	24.78	0.1333	0.7623	1.4811	0.1585	4.2849	16.75	0.1156	0.7623	1.4810	0.1374	11.81	88.5	0.1334
0.50	0.50	2.3465	28.75	0.1331	0.7518	1.5652	0.1583	4.7201	19.04	0.1154	0.7518	1.5652	0.1372	10.44	95.6	0.1092

RQ-CEASE considers the impact of DoS attacks. RQ-CEASE transmits more than CEASE, and Q-CEASE.

A second-order MAS is selected to study the ETC using PEC. It is shown that PEC provides an appropriate framework to cope with the uncertainties in the control protocol and preserves the desired exponential rate of consensus when the ET scheme is used. It is observed that PSEC outperforms PEC in terms of transmission savings. The reason lies within the fact that PSEC incorporates a sampler in its configuration. The sampling interval, inherently, reduces the transmission load. R-PSEC studies the impact of DoS attacks on PSEC. It is observed that R-PSEC considers a desired level of resilience to DoS in its parameter design. The resilience level has some trade-offs with the consensus performance. For example, higher DoS resilience leads to more frequent transmissions.

ROCCET benefits a dynamic event-triggering scheme and its parameter design includes an optimization in increase the MIET. Comparison with [1] shows that ROCCET provides more realistic (higher) resilience to DoS.

Finally, using FCC/DEME the problem of formation-containment in a class of non-holonimc agents is simulated. It is shown that FCC/DEME is capable of saving transmissions for follower-follower and leader-leader communication.

Chapter 8

Summary and Future Direction

This chapter summarizes the proposed event-triggered consensus (ETC) implementations based on their features. Some future research directions worthy of further investigations are included in this chapter.

8.1 Summary

In recent years, event-triggering (ET) transmission strategies have been widely studied to cope with the bandwidth constraints and save communication resources in networked control systems (NCSs) and cooperative multi-agent systems (MASs). Distributed consensus, which is an important algorithm required in many control and signal processing applications such as sensor networks, multi-robot systems, and unmanned aerial vehicles, is based on information exchanges between the neighbouring agents. Several ET strategies have been proposed for consensus to reduce the number of transmissions and prolong longevity of the agents. The literature review in Chapter 2 shows that existing ETC implementations have limitations especially in terms of their parameter design approach, resilience to Cyber-attacks, and transmission without quantization, to name a few. Based on the dynamics of the agents, proposed implementations are categorized to single-order and general linear agents.

Table 8.1 lists the proposed ETC implementations for first-order agents (average consensus) and compares them in terms of their different features. According to Table 8.1, each implementation offers some advantages and has some shortcomings. Based on the desired application, one can choose the suitable implementation. All proposed implementations for average consensus incorporate a sampler to reduce the burden of state measurement, event monitoring, and control update. Additionally, the receiver at each node awaits an update from the neighbouring nodes only at the sampling instants.

The parameter design in CEASE and DEASE include a parameter optimization to increase the inter-event time. The optimization in CEASE is independent of network

Table 8.1: Different proposed ETC implementations for first-order agents.

Characteristics	**CEASE** [77]	**Q-CEASE** [78]	**RQ-CEASE** [79]	**DEASE**
Transmitter scheme	Sampled-data Event-triggered	Sampled-data Event-triggered	Sampled-data Event-triggered	Sampled-data Event-triggered
Receiver scheme	Periodic	Periodic	Periodic	Periodic
State Measurement scheme	Periodic	Periodic	Periodic	Periodic
Control scheme	Sampled-data Event-triggered	Sampled-data Event-triggered	Sampled-data Event-triggered	Sampled-data Event-triggered
Event monitoring	Periodic	Periodic	Periodic	Periodic
Optimization for Design Parameters	Yes	No	No	Yes
Steady-state error	Yes	Yes	Yes	No
State Quantization	No	Yes	Yes	No
Control gain Design	Yes	No	No	No
Computation Complexity of Parameter Design	Medium	Low	Low	High
Relative expected number of transmissions	Medium	Medium	High	Low
Resilience to DoS attacks	No	No	Yes	No
Network Topology	Undirected	Undirected	Undirected	Undirected

size. Thus the computational complexity of optimization does not grow with the network size. In contrast, the computational complexity in DEASE grows with the network size. The benefits of DEASE compared to CEASE are threefold: (i) DEASE is more efficient in reducing the number of transmissions; (ii) DEASE does not produce steady-state error in consensus; (iii) Higher values of sampling period is applicable in DEASE.

Q-CEASE considers the information quantization in their configuration. Unlike CEASE and DEASE the parameter design in Q-CEASE and RQ-CEASE is analytical, which leads to some operating regions for the unknown parameters.

RQ-CEASE considers the impact of the unknown denial of service (DoS) attacks on the average consensus.

Three different implementations are proposed for ETC in general linear MAS. These implementations are listed in Table 8.2. The design approach for all implementations is co-design, i.e., all unknown parameters are designed simultaneously. In PEC, only the transmission is event-triggered and other processing are continuous-time. PEC includes an objective function to increase the AIET. The value of the objective function can be used as an index to predict and compare the expected AIET for different MASs. Unlike PEC, PSEC includes a sampler for each node. R-PSEC is the extended version of PSEC, where DoS attack is considered in the implementation.

Table 8.2: Comparison of different proposed ETC implementations.

Characteristics	**PEC** [80]	**PSEC** [81]	**R-PSEC**	**ROCCET** [82]
Transmitter scheme	Event-triggered	Sampled-data Event-triggered	Sampled-data Event-triggered	Event-triggered
Receiver scheme	Continuous-time	Periodic	Periodic	Continuous-time
State Measurement scheme	Continuous-time	Periodic	Periodic	Continuous-time
Control scheme	Continuous-time	Periodic	Periodic	Continuous-time
Event monitoring	Continuous-time	Periodic	Periodic	Continuous-time
Optimization for Design Parameters	Yes	No	No	Yes
Steady-state error	No	No	No	No
State Quantization	No	No	No	No
Control gain Design	Yes	Yes	Yes	Yes
Relative expected number of transmissions	Low	Low	Medium	Very Low
Resilience to DoS attacks	No	No	Yes	Yes
Network Topology	Undirected	Undirected	Undirected	Undirected

8.2 Future Direction

In what follows, some important and challenging research topics that are close to the subjects studied in the thesis are suggested. These research topics, which arise mainly from strict assumptions, bring potential space for improvement over the proposed implementations in the thesis.

1. **Asynchronous sampling period**: One common assumption considered in the thesis is that the sampling process, although performed locally, is synchronized in the MAS. When the network is large this might be a strict assumption. Therefore, it is important to consider asynchronous (different) sampling periods in the network. In [157] asynchronous sampled-data ET consensus is studied for first-order agents. Reference [158] extends the work in [157] to the second-order agents. For more general agents, however, the asynchronous sampled-data ET consensus is yet to be studied.

2. **Sampled-data dynamic event-triggering for more general agents**: Implementation DEASE is based on a sampled-data dynamic event-triggered transmission scheme. In Chapter 7, the capability of the dynamic event-triggering in saving transmissions is observed. How to extend the *sampled-data* dynamic event-triggering scheme to more general agent models, such as the general linear, is still yet to be discovered.

3. **Distributed DoS attacks**: As observed in RQ-CEASE, R-PSEC, and ROCCET, it was assumed that the DoS attacks target *all nodes* of the MAS at the same time. In practice, however, each node may experience a different pattern of attack. It is important to extend the synchronized attacks considered in Chapter 5 to a

distributed type of attack, where the adversary lunches different patterns of attack for each node. To date, it is an open problem to investigate distributed DoS attacks for cooperative control in general linear agents.

4. **Observer-based resilient strategies**: In this thesis two different control protocols are suggested during DoS attacks. In RQ-CEASE, the control input is constants and is based on the last available information before the DoS interval. In R-PSEC and ROCCET, on the other hand, the control input is kept zero in the presence of attack. A more advanced control protocol during DoS interval is to use an observer-based protocol. The main idea in the observed-based resilient strategies is to predict the local and neighbouring states during the attack intervals. The control input is then updated based on the predicted values. Using an observer-based control scheme in the presence of DoS leads to a *more smooth and faster consensus* as compared to the zero-input protocol. In other words, the DoS attack have less impact on the MAS when a state observer is used. There are still few works on the observed-based resilient strategies.

5. **Application to Smart-grids**: Microgrids are small-scale power systems consists of local generations, loads, and energy storage. The control of microgrids often follow a hierarchical structure with three levels, namely, primary, secondary, and tertiary control loops. The primary control loop maintains the voltage and frequency of the distributed generators (DGs) close to their nominal values as the power supply and demand change over time. However, even in the presence of the primary control loop, voltage and frequency can still deviate from their nominal values. To restore the voltage and frequency of DGs to their nominal values, the secondary control is also required. Tertiary loop is the highest level of the hierarchy and performs high-level tasks such as the optimization of economic performance and managing the main grids [10]. The problem of secondary voltage control in microgrids can be viewed as a distributed tracking control problem, also known as the leader-following consensus [11]. The ET communication and control approach for secondary voltage control in microgrids has been studied recently in [11]. There are still plenty of important topics to be investigated in this area. For example, with regards to the Cyber security, an important topic is to develop an optimized trade-off between the level of security and the amount of transmissions between the DGs.

6. **Application of learning algorithms:** The emergence and rapid development of different learning algorithms in recent years have opened new research areas in analysis of complex system. With no exception, the application of learning algorithms in ETC is currently a hot topic. In [159], an iterative approach is proposed for computing adaptive optimal controller gain for continuous-time linear systems where system matrices $\boldsymbol{A}$ and $\boldsymbol{B}$ are completely unknown. It is shown that the system can learn the optimal control gain using only a set of its own state measurements and control inputs. Therefore, this approach for finding the optimal control gain is also known as the 'model-free' method. The optimal model

free approach is extended to [160] where, unlike [159], the control updates are event-triggered. Recently, in [161] the model free approach has been extended to the ET containment control problem. The application of model-free learning approaches for ETC is still very open to study.

Appendix. Stabilization control under DoS attacks

Chapters 3 to 6 are focused on distributed MASs, where multiple agents (subsystems) are connected to each other and a cooperative behaviour is desired. In many control applications, only one plant is involved and stability or regulatory control is concerned. Stability is known as one of the most important subjects in design and analysis of various aspects of control systems [162]. Similar to MASs, in networked control systems (NCS), the limited on-board energy resources allocated to system necessitates strategies that reduce processings such as state measurement and control input update [123]. At the same time, with the emergence of Cyber-attacks, the resilience of NCS implementations to various types of attacks has been given considerable attention and is one of the hot topics in NCSs [32].

In NCSs some physical constraints such as energy and network bandwidth compelled the researchers to employ sampled-data schemes [163], in which state measurement and actuator updates are conducted periodically. To further reduce the burden of communication and control updates, there has been an increasing interest in event-triggered (ET) schemes in recent years. Recently, a dynamic event-triggering (DET) mechanism [75, 76, 164–167] is proposed in which an additional dynamic variable is included in the ET condition. It is shown in [123] that the number of transmissions in DETs is lower than the so-called static ET schemes. At the same time, DET schemes does not produce any steady-state error in the NCS. It should be noted that continuous-time state measurement and event monitoring is a common assumption in implementation of DET schemes [75, 76, 164–167]. Incorporation of a *sampled-data* measurement and monitoring method greatly enhances the applicability of DET schemes in practice.

In the same way as MASs, in the context of the ET control for NCSs, there are usually emulation [50, 63, 64, 168, 169] and co-design [37, 66, 144, 167, 170, 171] approaches to design unknown control and ET parameters. It should be reminded that one disadvantage of the emulation-based design is that the feasible regions obtained for the ET parameters are limited by the initial choice of the control gains [172]. This decreases the efficiency of the ET scheme in reducing the amount of transmissions. The applicability of the co-design technique is yet to be investigated for sampled-data dynamic event-triggered control.

Cyber-attacks can highly degrade the performance of NCSs by different ways

of malicious manipulation. If the impact of adversary is not properly taken into account in the stability analysis, the NCS may become unstable in the presence of attacks such as DoS. Resilience results for NCSs against DoS have been reported in [32,37,50,63,64,66,144,167,173–175] for different applications. Assuming that the DoS follows a periodic pattern, the resilience of different NCSs under DoS is investigated in [37, 63, 66, 144, 173–175]. Considering a periodic or stochastic pattern for DoS, as mentioned in Chapter 5, may not fully represent the unknown and malicious nature of the adversary. A more general model for DoS is considered in [32, 50, 64, 167], where DoS is assumed to occur with an unknown pattern. Such DoS models with unknown patterns can be characterized only by the energy constraints of the adversary (similar to Assumption 5 in Chapter 5). Implementations [32, 50, 52, 64] are based on emulation-based approaches to design control and ET parameters, and deriving the maximum amount of resilience to unknown DoS. As mentioned in R-PSEC and ROCCET in Chapter 5, one disadvantage of the emulation-based approaches for DoS analysis is that the theoretic resilience guaranteed for unknown DoS is conservative. The reason lies within the use of norms and extreme eigenvalues of the associated matrix to calculate the upped-bounds. An alternative approach is to include the desired resilience level within the co-design framework which excludes the use of such norms and eigenvalues.

Motivated by the above shortcomings and based on R-PSEC and ROCCET, this appendix focuses on a sampled-data dynamic event-triggering (S-DET) scheme for stabilization control in NCS with a designable level of resilience to unknown DoS attacks. The main features of the proposed framework are listed below:

- This is the first instance where a *co-design* sampled-data dynamic event-triggering (S-DET) scheme is developed for stabilization of networked control systems. Compared to existing results in the context of DET [75, 76, 164–167], the proposed S-DET scheme relaxes the continuous-time state measurement and monitoring.

- In the presence of DoS, the proposed co-design framework allows including *a priori* level of resilience to *unknown* DoS attacks. Therefore, the trade-offs between the stabilization convergence rate, average inter-event time, and the desired level of resilience to unknown DoS is formulated within LMI conditions. Compared to emulation-based approaches where the DoS resilience is based on matrix norms and eigenvalues [32, 50, 52, 64, 176], the proposed co-design framework results in less conservative (larger) upper-bounds for unknown DoS attacks.

A.1 Problem statement

Consider the following general linear plant

$$\dot{\boldsymbol{x}}(t) = \boldsymbol{A}\boldsymbol{x}(t) + \boldsymbol{B}\boldsymbol{u}(t), \tag{A.1}$$

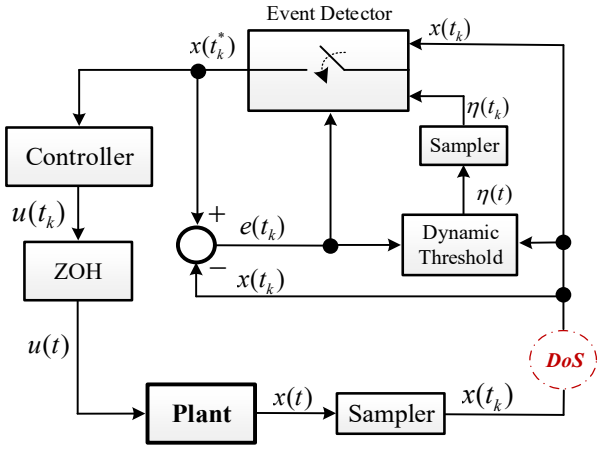

Figure A.1: Block diagram for the S-DET control against DoS attack.

where $\boldsymbol{x}(t) \in \mathbb{R}^n$ is the system state and $\boldsymbol{u}(t) \in \mathbb{R}^m$ is the control input. System matrices $\boldsymbol{A} \in \mathbb{R}^{n\times n}$ and $\boldsymbol{B} \in \mathbb{R}^{n\times m}$ are constant and known, and $(\boldsymbol{A}, \boldsymbol{B})$ is a controllable pair. In stabilization, and in particular exponential stabilization, the following objective is desired

Definition 5. *Exponential Stability* [137]: Given a convergence rate $\zeta > 0$, NCS (A.1) is said to be ζ-exponentially stable if there exists a positive scalar η such that

$$\|\boldsymbol{x}(t)\| \leq \eta\, e^{-\zeta t} \|\, \boldsymbol{x}(0)\, \|, \quad t \geq 0, \quad \forall \boldsymbol{x}(0) \in \mathbb{R}^n. \tag{A.2}$$

To guarantee (A.2), a control protocol for $\boldsymbol{u}(t)$ should be proposed which commands the NCS based on the state measurements of the system $\boldsymbol{x}(t)$. As shown in Fig. A.1, a sampler is incorporated with plant (A.1) to provide sampled states of the system, i.e., $\boldsymbol{x}(t_k)$, where $k \in \mathbb{N}_0$. In the ideal case where DoS does not occur the sampling period for measurement is h, i.e., $t_{k+1} - t_k = h$. To reduce the control input updates $\boldsymbol{u}(t)$, a sampled-data DET scheme (to be introduced) is also incorporated with the plant. The S-DET condition is monitored periodically at $t = t_k$, $(t_{k+1} - t_k = h)$, to determine whether or not to update the control input. Only if the DET condition is satisfied, an event is triggered and the controller is updated. In summary, the state measurement scheme is sampled-data (with period h). The scheme for control update is sampled-data event-triggered. The monitoring process of the DET condition is also periodic with period h.

A.1.1 Control and Dynamic Event-triggering protocols

Let $t_0^\star, t_1^\star, \ldots, t_k^\star$ denote the time sequence at which events are detected and control input $\boldsymbol{u}(t)$ is updated. Starting from $t_0^\star = 0$, the next event is triggered at $t_{k+1}^\star$ which satisfies the following S-DET condition

$$t_{k+1}^\star = \inf\{\, t_k \;\mid t_k > t_k^\star,\; \boldsymbol{e}^T(t_k)\boldsymbol{S}_1\boldsymbol{e}(t_k) \geq \boldsymbol{x}^T(t_k)\boldsymbol{S}_2\boldsymbol{x}(t_k) + \boldsymbol{\eta}^T(t_k)\boldsymbol{S}_3\boldsymbol{\eta}(t_k)\}, \tag{A.3}$$

where $\boldsymbol{e}(t_k) = \boldsymbol{x}(t_k^\star) - \boldsymbol{x}(t_k)$ is the measurement error. Symmetric matrices $\boldsymbol{S}_i \in \mathbb{R}^{n\times n}$, $(1 \leq i \leq 3)$ are S-DET gains to be designed. Parameter $\boldsymbol{\eta}(t)$ satisfies

$$\dot{\boldsymbol{\eta}}(t) = -\boldsymbol{\eta}(t) + \boldsymbol{S}_4\boldsymbol{x}(t_k) + \boldsymbol{S}_5\boldsymbol{e}(t_k), \tag{A.4}$$

where $\boldsymbol{S}_i \in \mathbb{R}^{n\times n}$, $(i = 4, 5)$, are other design parameters. From (A.3) it is clear that the S-DET scheme is monitored periodically on only samples of the system. The following sampled-data event-triggered state feedback protocol is proposed for stabilization of plant (A.1)

$$\boldsymbol{u}(t) = \boldsymbol{K}\boldsymbol{x}(t_k^\star), \quad t_k^\star \leq t < t_{k+1}^\star, \tag{A.5}$$

where $\boldsymbol{K} \in \mathbb{R}^{m\times n}$ is the control gain to be designed. Fig. A.1 is provided for visualization of the proposed S-DET scheme for stabilization of plant (A.1). The closed-loop system from (A.1) and (A.5) is given below for $t_k \leq t < t_{k+1}$

$$\dot{\boldsymbol{x}}(t) = \boldsymbol{A}\boldsymbol{x}(t) + \boldsymbol{B}\boldsymbol{K}(\boldsymbol{x}(t_k) + \boldsymbol{e}(t_k)). \tag{A.6}$$

Let $d(t) \triangleq t - t_k$ represent an artificial time-varying time-delay that satisfies $0 \leq d(t) < h$. Using $d(t)$, system (A.6) is given below for the interval $t_k \leq t < t_{k+1}$

$$\dot{\boldsymbol{x}}(t) = \boldsymbol{A}\boldsymbol{x}(t) + \boldsymbol{B}\boldsymbol{K}(\boldsymbol{x}(t-d(t)) + \boldsymbol{e}(t-d(t))), \tag{A.7}$$

with $\boldsymbol{x}(t) = \boldsymbol{x}(0)$ for $-h \leq t \leq 0$.

Remark A.1. Based on (A.4) parameter $\boldsymbol{\eta}(t)$ is time-varying and its dynamic updating protocol is related to state $\boldsymbol{x}(t)$, measurement error $\boldsymbol{e}(t)$, and a negative definite self-feedback. Intuitively speaking, $\boldsymbol{\eta}(t)$ can be regarded as a linear first-order filtered value of $\boldsymbol{x}(t)$ and $\boldsymbol{e}(t)$. Compared to the so-called static ET strategies (such as $\boldsymbol{e}^T(t_k)\boldsymbol{S}_1\boldsymbol{e}(t_k) \leq \boldsymbol{x}^T(t_k)\boldsymbol{S}_2\boldsymbol{x}(t_k)$ considered in [37,66,144]), the introduction of $\boldsymbol{\eta}(t)$ is a key element to regulate threshold (A.3) dynamically and in better connection with the plant dynamics. As shown in [123, Prop. 2.3], including parameter $\boldsymbol{\eta}(t_k)$ in (A.3) reduces the number of event-triggerings compared to the static ET schemes. As a final note, since $\boldsymbol{\eta}(t)$ follows a dynamic equation, it acts as an auxiliary *state* along with state $\boldsymbol{x}(t)$. As we will observe later in Theorems A.1 and A.2, $\boldsymbol{\eta}(t)$ can impact the stabilization convergence rate.

Remark A.2. Compared to most widely used ET schemes, S-DET scheme (A.3) is more general and many existing ET schemes used for NCSs are special cases of S-DET (A.3). For example, if $\boldsymbol{\eta}(t) = \boldsymbol{0}$, $(\forall t \geq 0)$, the S-DET condition reduces to $\boldsymbol{e}^T(t_k)\boldsymbol{S}_1\boldsymbol{e}(t_k) \leq \boldsymbol{x}^T(t_k)\boldsymbol{S}_2\boldsymbol{x}(t_k)$ which is considered in [2, 37, 66, 144]. In case that $\boldsymbol{S}_4 = \boldsymbol{S}_5 = \boldsymbol{0}$, then $\boldsymbol{\eta}(t)$ reduces to a mere exponentially decaying function [111]. In this case, $\boldsymbol{\eta}(t)$ is only dependent on time, not the state and error dynamics. If $\dot{\boldsymbol{\eta}}(t) = 0$, $(\forall t \geq 0)$, then parameter $\boldsymbol{\eta}(t)$ remains constant over time. The constant (set-valued) thresholds for ET schemes are considered in [170]. Including a constant value to the ET condition, however, leads to an unavoidable bounded error for stabilization, which is not desired. Note that the S-DET scheme (A.3) does not cause any steady-state error. Additionally, unlike DET schemes proposed in [75, 76, 164–167], S-DET (A.3)

is sampled and can be easily implemented in a digital platform with the desired sampling rate.

A.1.2 Denial of Service Attacks

As shown in Fig. A.1, the attacker in DoS attempts to jam the wireless communication link from the sampler to event-detector and destabilize the system. The model DoS attacks considered in this chapter is similar to the one considered in Chapter 5. In particular, expressions (5.4), (5.5), (5.6), and Assumption 5 are considered here.

A.1.3 Objectives

The design approach and objectives for the proposed S-DET scheme against DoS are discussed below.

Develop a co-design framework for S-DET control: We first consider an ideal scenario where DoS never happens. A co-design (unified) framework is proposed which simultaneously computes unknown parameters, i.e., the control gain $\boldsymbol{K}$ and S-DET parameters $\boldsymbol{S}_i$, $(1 \leq i \leq 5)$. The unified framework co-designs unknown parameters based on a desired sampling period h and a desired exponential rate for stabilization of plant (A.1).

Include a desired level of resilience against DoS with unknown pattern: In the presence of DoS, it is of great importance to include the *desired* level of tolerance to unknown DoS attacks within the co-design framework. It will be shown later in Theorem A.2 that the tolerable amount of DoS attack is closely related to (i): The desired convergence rate of stabilization in the ideal scenario, (ii): The sampling period, and (iii): The values of control gain $\boldsymbol{K}$ and S-DET gains $\boldsymbol{S}_i$, $(1 \leq i \leq 5)$. The co-design framework, as will be shown in simulations, allows obtaining less conservative upper-bounds for admissible DoS attacks.

A.2 Main results

A.2.1 DoS formulation

The formulation of DoS is similar to Section 5.2.4, where sampling period g is considered for attack intervals and expressions (5.38) and (5.39) are ultimately derived.

A.2.2 Closed-loop system

During DoS attacks the control input is kept zero, i.e., $\boldsymbol{u}(t) = \boldsymbol{0}$, if $t \in Z_m$. Therefore, the plant is open-loop when DoS is detected. Considering both the healthy (W_m) and

attack intervals (Z_m), the following system is obtained

$$\dot{\boldsymbol{x}}(t) = \begin{cases} \boldsymbol{A}\boldsymbol{x}(t) + \boldsymbol{B}\boldsymbol{K}(\boldsymbol{x}(t_k) + \boldsymbol{e}(t_k)), & t \in W_m, \\ \boldsymbol{A}\,\boldsymbol{x}(t), & t \in Z_m. \end{cases} \tag{A.8}$$

The dynamic variable $\boldsymbol{\eta}(t)$ is re-formulated as

$$\dot{\boldsymbol{\eta}}(t) = \begin{cases} -\boldsymbol{\eta}(t) + \boldsymbol{S}_4\boldsymbol{x}(t_k) + \boldsymbol{S}_5\boldsymbol{e}(t_k), & t \in W_m, \\ -\boldsymbol{\eta}(t), & t \in Z_m. \end{cases} \tag{A.9}$$

Note that switching between the two modes of (A.9) requires the knowledge of intervals W_m and Z_m. As observed in Section 5.2.4, the beginning of Z_m is the instant when DoS is detected by the system. Additionally, the end of Z_m is the first instant after DoS when a measurement is successfully transmitted. It is reminded that the event-detector sends an acknowledgment (to the sampler) when it successfully receives a new measurement. Thanks to these acknowledgments and the definition of Z_m, interval Z_m and its complement W_m are fully detectable in practice.

A.2.3 Parameter Design: General framework

This section develops a general co-design framework that simultaneously computes the control gain $\boldsymbol{K}$ and S-DET parameters $\boldsymbol{S}_i$, $(1 \leq i \leq 5)$. In this section, the attack-free (ideal) scenario is considered. Extension to DoS attack is given in Section A.2.4.

Theorem A.1. Given desired values for sampling period h and stabilization rate ζ_1, if there exist the following decision variables

- $m \times n$ dimensional matrix $\boldsymbol{V}$;
- $n \times n$ dimensional positive definite matrices $\boldsymbol{P}_1$, $\boldsymbol{Q}_1$, $\boldsymbol{Z}_1$, $\boldsymbol{P}_2$, $\boldsymbol{Q}_2$, $\boldsymbol{Z}_2$, $\boldsymbol{M}_i$, $(1 \leq i \leq 5)$;
- $n \times n$ dimensional matrices $\boldsymbol{N}$, $\boldsymbol{Y}_{11}$, $\boldsymbol{Y}_{12}$, $\boldsymbol{Y}_{22}$, $\boldsymbol{F}_1$, $\boldsymbol{F}_2$, $\boldsymbol{G}_1$, $\boldsymbol{G}_2$, $\boldsymbol{U}_{11}$, $\boldsymbol{U}_{12}$, $\boldsymbol{U}_{22}$, $\boldsymbol{W}_1$, $\boldsymbol{W}_2$, $\boldsymbol{E}_1$, $\boldsymbol{E}_2$,

satisfying the following LMIs

$$\boldsymbol{C}_1 = \begin{bmatrix} \boldsymbol{\Pi} & \boldsymbol{\Phi} \\ * & \boldsymbol{\Psi} \end{bmatrix} < 0, \tag{A.10}$$

$$\boldsymbol{C}_2 = \begin{bmatrix} \boldsymbol{Y} & \boldsymbol{F} \\ * & he^{-\zeta_1 h}\boldsymbol{Z}_1 \end{bmatrix} \geq 0, \quad \boldsymbol{C}_3 = \begin{bmatrix} \boldsymbol{Y} & \boldsymbol{G} \\ * & he^{-\zeta_1 h}\boldsymbol{Z}_1 \end{bmatrix} \geq 0, \tag{A.11}$$

$$\boldsymbol{C}_4 = \begin{bmatrix} \boldsymbol{U} & \boldsymbol{W} \\ * & he^{-\zeta_1 h}\boldsymbol{Z}_2 \end{bmatrix} \geq 0, \quad \boldsymbol{C}_5 = \begin{bmatrix} \boldsymbol{U} & \boldsymbol{E} \\ * & he^{-\zeta_1 h}\boldsymbol{Z}_2 \end{bmatrix} \geq 0, \tag{A.12}$$

then, control gain $\boldsymbol{K}$ and S-DET parameters $\boldsymbol{S}_i$, $(1 \leq i \leq 5)$, are computed from the following expressions

$$\boldsymbol{K} = \boldsymbol{V}(\boldsymbol{N}^{-1})^T, \qquad \boldsymbol{S}_1 = \boldsymbol{N}^{-1}\boldsymbol{M}_1(\boldsymbol{N}^{-1})^T, \qquad \boldsymbol{S}_2 = \boldsymbol{N}^{-1}\boldsymbol{M}_2(\boldsymbol{N}^{-1})^T,$$

$$\boldsymbol{S}_3=\boldsymbol{N}^{-1}\boldsymbol{M}_3(\boldsymbol{N}^{-1})^T,\qquad \boldsymbol{S}_4=\boldsymbol{M}_4(\boldsymbol{N}^{-1})^T,\quad \boldsymbol{S}_5=\boldsymbol{M}_5(\boldsymbol{N}^{-1})^T, \tag{A.13}$$

and closed-loop system (A.7) is ζ_1-exponentially stable with the following condition for the rate of convergence

$$\lambda_1\left\|\boldsymbol{x}(t)\right\|^2+\lambda_2\left\|\boldsymbol{\eta}(t)\right\|^2\leq e^{-\zeta_1 t}(\lambda_3\left\|\boldsymbol{x}(0)\right\|^2+\lambda_4\left\|\boldsymbol{\eta}(0)\right\|^2), \tag{A.14}$$

where $\lambda_1=\lambda_{\min}(\bar{\boldsymbol{P}}_1)$, $\lambda_2=\lambda_{\min}(\bar{\boldsymbol{P}}_2)$, $\lambda_3=\lambda_{\max}(\bar{\boldsymbol{P}}_1)+h\lambda_{\max}(\bar{\boldsymbol{Q}}_1)+h^2\lambda_{\max}(\bar{\boldsymbol{Z}}_1)$, and $\lambda_4=\lambda_{\max}(\bar{\boldsymbol{P}}_2)+h\lambda_{\max}(\bar{\boldsymbol{Q}}_2)+h^2\lambda_{\max}(\bar{\boldsymbol{Z}}_2)$, with $\bar{\boldsymbol{P}}_i=\boldsymbol{N}^{-1}\boldsymbol{P}_i(\boldsymbol{N}^{-1})^T$, $\bar{\boldsymbol{Q}}_i=\boldsymbol{N}^{-1}\boldsymbol{Q}_i(\boldsymbol{N}^{-1})^T$, and $\bar{\boldsymbol{Z}}_i=\boldsymbol{N}^{-1}\boldsymbol{Z}_i(\boldsymbol{N}^{-1})^T$, for $(i=1,2)$. Unknown block matrices in (A.10), (A.11), and (A.12) are defined below

$$\boldsymbol{\Pi}=\begin{bmatrix}\boldsymbol{\pi}_{11} & \boldsymbol{\pi}_{12} & -\boldsymbol{F}_1 & \boldsymbol{\pi}_{14} & \boldsymbol{BV}\\ * & \boldsymbol{\pi}_{22} & -\boldsymbol{F}_2 & \boldsymbol{\pi}_{24} & \boldsymbol{BV}\\ * & * & -e^{-\zeta_1 h}\boldsymbol{Q}_1 & \boldsymbol{0} & \boldsymbol{0}\\ * & * & * & \boldsymbol{\pi}_{44} & \boldsymbol{BV}\\ * & * & * & * & -\boldsymbol{M}_1\end{bmatrix}, \tag{A.15}$$

$$\boldsymbol{\Phi}=\begin{bmatrix}\boldsymbol{NA}^T & \boldsymbol{0} & \boldsymbol{0} & \boldsymbol{NA}^T\\ \boldsymbol{M}_4^T+\boldsymbol{V}^T\boldsymbol{B}^T & \boldsymbol{M}_4^T & \boldsymbol{0} & \boldsymbol{M}_4^T+\boldsymbol{V}^T\boldsymbol{B}^T\\ \boldsymbol{0} & \boldsymbol{0} & \boldsymbol{0} & \boldsymbol{0}\\ -\boldsymbol{N} & \boldsymbol{0} & \boldsymbol{0} & -\boldsymbol{N}\\ \boldsymbol{M}_5^T+\boldsymbol{V}^T\boldsymbol{B}^T & \boldsymbol{M}_5^T & \boldsymbol{0} & \boldsymbol{M}_5^T+\boldsymbol{V}^T\boldsymbol{B}^T\end{bmatrix}, \tag{A.16}$$

$$\boldsymbol{\Psi}=\begin{bmatrix}\boldsymbol{\psi}_{11} & \boldsymbol{\psi}_{12} & -\boldsymbol{W}_1 & \boldsymbol{P}_2-\boldsymbol{N}^T-\boldsymbol{N}\\ * & \boldsymbol{\psi}_{22} & -\boldsymbol{W}_2 & -\boldsymbol{N}^T\\ * & * & -e^{-\zeta_1 h}\boldsymbol{Q}_2 & \boldsymbol{0}\\ * & * & * & \boldsymbol{\psi}_{44}\end{bmatrix}, \tag{A.17}$$

$$\begin{aligned}
&\boldsymbol{\pi}_{11}=\boldsymbol{Q}_1+\boldsymbol{G}_1+\boldsymbol{G}_1^T+\boldsymbol{AN}+\boldsymbol{N}^T\boldsymbol{A}^T+h\boldsymbol{Y}_{11}+\zeta_1\boldsymbol{P}_1,\\
&\boldsymbol{\pi}_{12}=\boldsymbol{F}_1-\boldsymbol{G}_1+\boldsymbol{G}_2^T+h\boldsymbol{Y}_{12}+\boldsymbol{BV}+\boldsymbol{NA}^T,\\
&\boldsymbol{\pi}_{14}=\boldsymbol{P}_1-\boldsymbol{N}^T+\boldsymbol{NA}^T,\qquad \boldsymbol{\pi}_{22}=\boldsymbol{F}_2+\boldsymbol{F}_2^T-\boldsymbol{G}_2-\boldsymbol{G}_2^T+h\boldsymbol{Y}_{22}+\boldsymbol{BV}+\boldsymbol{V}^T\boldsymbol{B}^T+\boldsymbol{M}_2,\\
&\boldsymbol{\pi}_{24}=-\boldsymbol{N}^T+\boldsymbol{V}^T\boldsymbol{B}^T,\qquad \boldsymbol{\pi}_{44}=h^2\boldsymbol{Z}_1-\boldsymbol{N}-\boldsymbol{N}^T,\\
&\boldsymbol{\psi}_{11}=\boldsymbol{Q}_2+\boldsymbol{E}_1+\boldsymbol{E}_1^T+h\boldsymbol{U}_{11}-\boldsymbol{N}-\boldsymbol{N}^T+\zeta_1\boldsymbol{P}_2,\qquad \boldsymbol{\psi}_{12}=\boldsymbol{W}_1-\boldsymbol{E}_1+\boldsymbol{E}_2^T+h\boldsymbol{U}_{12}-\boldsymbol{N},\\
&\boldsymbol{\psi}_{22}=\boldsymbol{W}_2+\boldsymbol{W}_2^T-\boldsymbol{E}_2-\boldsymbol{E}_2^T+h\boldsymbol{U}_{22}+\boldsymbol{M}_3,\qquad \boldsymbol{\psi}_{44}=h^2\boldsymbol{Z}_2-\boldsymbol{N}-\boldsymbol{N}^T,\\
&\boldsymbol{Y}=\begin{bmatrix}\boldsymbol{Y}_{11} & \boldsymbol{Y}_{12}\\ * & \boldsymbol{Y}_{22}\end{bmatrix},\ \boldsymbol{U}=\begin{bmatrix}\boldsymbol{U}_{11} & \boldsymbol{U}_{12}\\ * & \boldsymbol{U}_{22}\end{bmatrix},\ \boldsymbol{F}=\begin{bmatrix}\boldsymbol{F}_1^T & \boldsymbol{F}_2^T\end{bmatrix}^T,\\
&\boldsymbol{G}=\begin{bmatrix}\boldsymbol{G}_1^T & \boldsymbol{G}_2^T\end{bmatrix}^T,\ \boldsymbol{W}=\begin{bmatrix}\boldsymbol{W}_1^T & \boldsymbol{W}_2^T\end{bmatrix}^T,\ \boldsymbol{E}=\begin{bmatrix}\boldsymbol{E}_1^T & \boldsymbol{E}_2^T\end{bmatrix}^T.
\end{aligned}$$

Proof. Consider the Lyapunov-Krasovskii functional (LKF) $V=\sum_{i=1}^{6}V_i$ where

$$\begin{aligned}
&V_1=\boldsymbol{x}^T(t)\bar{\boldsymbol{P}}_1\,\boldsymbol{x}(t),\qquad V_2=\int_{t-h}^{t}e^{\zeta_1(s-t)}\boldsymbol{x}^T(s)\bar{\boldsymbol{Q}}_1\,\boldsymbol{x}(s)ds,\\
&V_3=h\int_{-h}^{0}\int_{t+s}^{t}e^{\zeta_1(v-t)}\dot{\boldsymbol{x}}^T(v)\bar{\boldsymbol{Z}}_1\dot{\boldsymbol{x}}(v)dvds,
\end{aligned}$$

$$V_4 = \boldsymbol{\eta}^T(t)\bar{\boldsymbol{P}}_2\,\boldsymbol{\eta}(t), \qquad V_5 = \int_{t-h}^{t} e^{\zeta_1(s-t)}\boldsymbol{\eta}^T(s)\bar{\boldsymbol{Q}}_2\,\boldsymbol{\eta}(s)ds,$$
$$V_6 = h\int_{-h}^{0}\int_{t+s}^{t} e^{\zeta_1(v-t)}\dot{\boldsymbol{\eta}}^T(v)\bar{\boldsymbol{Z}}_2\dot{\boldsymbol{\eta}}(v)dvds, \tag{A.18}$$

where matrices $\bar{\boldsymbol{P}}_i$, $\bar{\boldsymbol{Q}}_i$, $\bar{\boldsymbol{Z}}_i$, $(i=1,2)$, are positive definite. We obtain time derivative of V as follows

$$\begin{aligned}
\dot{V}_1 &= 2\dot{\boldsymbol{x}}^T(t)\bar{\boldsymbol{P}}_1\boldsymbol{x}(t), \qquad \dot{V}_2 = \boldsymbol{x}^T(t)\bar{\boldsymbol{Q}}_1\boldsymbol{x}(t) - e^{-\zeta_1 h}\boldsymbol{x}^T(t-h)\bar{\boldsymbol{Q}}_1\boldsymbol{x}(t-h) - \zeta_1 V_2,\\
\dot{V}_3 &= h^2\dot{\boldsymbol{x}}^T(t)\bar{\boldsymbol{Z}}_1\dot{\boldsymbol{x}}(t) - h\int_{t-h}^{t} e^{\zeta_1(v-t)}\dot{\boldsymbol{x}}^T(v)\bar{\boldsymbol{Z}}_1\dot{\boldsymbol{x}}(v)dv - \zeta_1 V_3\\
&\le h^2\dot{\boldsymbol{x}}^T(t)\bar{\boldsymbol{Z}}_1\dot{\boldsymbol{x}}(t) - he^{-\zeta_1 h}\int_{t-h}^{t}\dot{\boldsymbol{x}}^T(v)\bar{\boldsymbol{Z}}_1\dot{\boldsymbol{x}}(v)dv - \zeta_1 V_3,\\
\dot{V}_4 &= 2\dot{\boldsymbol{\eta}}^T(t)\bar{\boldsymbol{P}}_2\boldsymbol{\eta}(t), \qquad \dot{V}_5 = \boldsymbol{\eta}^T(t)\bar{\boldsymbol{Q}}_2\boldsymbol{\eta}(t) - e^{-\zeta_1 h}\boldsymbol{\eta}^T(t-h)\bar{\boldsymbol{Q}}_2\boldsymbol{\eta}(t-h) - \zeta_1 V_5,\\
\dot{V}_6 &= h^2\dot{\boldsymbol{\eta}}^T(t)\bar{\boldsymbol{Z}}_2\dot{\boldsymbol{\eta}}(t) - h\int_{t-h}^{t} e^{\zeta_1(v-t)}\dot{\boldsymbol{\eta}}^T(v)\bar{\boldsymbol{Z}}_2\dot{\boldsymbol{\eta}}(v)dv - \zeta_1 V_6\\
&\le h^2\dot{\boldsymbol{\eta}}^T(t)\bar{\boldsymbol{Z}}_2\dot{\boldsymbol{\eta}}(t) - he^{-\zeta_1 h}\int_{t-h}^{t}\dot{\boldsymbol{\eta}}^T(v)\bar{\boldsymbol{Z}}_2\dot{\boldsymbol{\eta}}(v)dv - \zeta_1 V_6.
\end{aligned} \tag{A.19}$$

Considering $[t-h,t] = [t-h,t-d(t)]\cup[t-d(t),t]$, we obtain the following expressions

$$\int_{t-h}^{t}\dot{\boldsymbol{x}}^T(v)\bar{\boldsymbol{Z}}_1\dot{\boldsymbol{x}}(v)dv = \int_{t-h}^{t-d(t)}\dot{\boldsymbol{x}}^T(v)\bar{\boldsymbol{Z}}_1\dot{\boldsymbol{x}}(v)dv + \int_{t-d(t)}^{t}\dot{\boldsymbol{x}}^T(v)\bar{\boldsymbol{Z}}_1\dot{\boldsymbol{x}}(v)dv, \tag{A.20}$$
$$\int_{t-h}^{t}\dot{\boldsymbol{\eta}}^T(v)\bar{\boldsymbol{Z}}_2\dot{\boldsymbol{\eta}}(v)dv = \int_{t-h}^{t-d(t)}\dot{\boldsymbol{\eta}}^T(v)\bar{\boldsymbol{Z}}_2\dot{\boldsymbol{\eta}}(v)dv + \int_{t-d(t)}^{t}\dot{\boldsymbol{\eta}}^T(v)\bar{\boldsymbol{Z}}_2\dot{\boldsymbol{\eta}}(v)dv. \tag{A.21}$$

Let $\boldsymbol{a}_1 = [\boldsymbol{x}^T(t), \boldsymbol{x}^T(t-d(t))]^T$ and $\boldsymbol{b}_1 = [\boldsymbol{\eta}^T(t), \boldsymbol{\eta}^T(t-d(t))]^T$. For any matrices $\bar{\boldsymbol{F}} = [\bar{\boldsymbol{F}}_1^T\ \bar{\boldsymbol{F}}_2^T]^T$, $\bar{\boldsymbol{G}} = [\bar{\boldsymbol{G}}_1^T\ \bar{\boldsymbol{G}}_2^T]^T$, $\bar{\boldsymbol{W}} = [\bar{\boldsymbol{W}}_1^T\ \bar{\boldsymbol{W}}_2^T]^T$, and $\bar{\boldsymbol{E}} = [\bar{\boldsymbol{E}}_1^T\ \bar{\boldsymbol{E}}_2^T]^T$, the following null expressions hold

$$2\boldsymbol{a}_1^T\bar{\boldsymbol{F}}\Big[\boldsymbol{x}(t-d(t)) - \boldsymbol{x}(t-h) - \int_{t-h}^{t-d(t)}\dot{\boldsymbol{x}}(s)ds\Big] = 0, \tag{A.22}$$
$$2\boldsymbol{a}_1^T\bar{\boldsymbol{G}}\Big[\boldsymbol{x}(t) - \boldsymbol{x}(t-d(t)) - \int_{t-d(t)}^{t}\dot{\boldsymbol{x}}(s)ds\Big] = 0, \tag{A.23}$$
$$2\boldsymbol{b}_1^T\bar{\boldsymbol{W}}\Big[\boldsymbol{\eta}(t-d(t)) - \boldsymbol{\eta}(t-h) - \int_{t-h}^{t-d(t)}\dot{\boldsymbol{\eta}}(s)ds\Big] = 0, \tag{A.24}$$
$$2\boldsymbol{b}_1^T\bar{\boldsymbol{E}}\Big[\boldsymbol{\eta}(t) - \boldsymbol{\eta}(t-d(t)) - \int_{t-d(t)}^{t}\dot{\boldsymbol{\eta}}(s)ds\Big] = 0. \tag{A.25}$$

The following expressions hold for any matrices $\bar{\boldsymbol{Y}} = \begin{bmatrix}\bar{\boldsymbol{Y}}_{11} & \bar{\boldsymbol{Y}}_{12}\\ * & \bar{\boldsymbol{Y}}_{22}\end{bmatrix}$ and $\bar{\boldsymbol{U}} = \begin{bmatrix}\bar{\boldsymbol{U}}_{11} & \bar{\boldsymbol{U}}_{12}\\ * & \bar{\boldsymbol{U}}_{22}\end{bmatrix}$

$$\int_{t-h}^{t-d(t)}\boldsymbol{a}_1^T\bar{\boldsymbol{Y}}\boldsymbol{a}_1 ds + \int_{t-d(t)}^{t}\boldsymbol{a}_1^T\bar{\boldsymbol{Y}}\boldsymbol{a}_1 ds = h\boldsymbol{a}_1^T\bar{\boldsymbol{Y}}\boldsymbol{a}_1, \tag{A.26}$$
$$\int_{t-h}^{t-d(t)}\boldsymbol{b}_1^T\bar{\boldsymbol{U}}\boldsymbol{b}_1 ds + \int_{t-d(t)}^{t}\boldsymbol{b}_1^T\bar{\boldsymbol{U}}\boldsymbol{b}_1 ds = h\boldsymbol{b}_1^T\bar{\boldsymbol{U}}\boldsymbol{b}_1. \tag{A.27}$$

From (A.7), it holds that

$$2\Big(\boldsymbol{x}^T(t)+\dot{\boldsymbol{x}}^T(t)+\boldsymbol{x}^T(t-d(t))+\boldsymbol{\eta}^T(t)+\dot{\boldsymbol{\eta}}^T(t)\Big)\boldsymbol{N}^{-1} \\ \times\Big(\boldsymbol{A}\boldsymbol{x}(t)+\boldsymbol{B}\boldsymbol{K}\boldsymbol{x}(t-d(t))+\boldsymbol{B}\boldsymbol{K}\,\boldsymbol{e}(t-d(t))-\dot{\boldsymbol{x}}(t)\Big)=0. \tag{A.28}$$

Likewise, from (A.4) we obtain

$$2\Big(\boldsymbol{\eta}^T(t)+\dot{\boldsymbol{\eta}}^T(t)+\boldsymbol{\eta}^T(t-d(t))\Big)\boldsymbol{N}^{-1}\Big(-\boldsymbol{\eta}(t)+\boldsymbol{S}_4\boldsymbol{x}(t-d(t))+\boldsymbol{S}_5\boldsymbol{e}(t-d(t))-\dot{\boldsymbol{\eta}}(t)\Big)=0. \tag{A.29}$$

The event-triggering condition (A.3) ensures that

$$\boldsymbol{e}^T(t-d(t))\boldsymbol{S}_1\boldsymbol{e}(t-d(t))\leq\boldsymbol{x}^T(t-d(t))\boldsymbol{S}_2\boldsymbol{x}(t-d(t))+\boldsymbol{\eta}^T(t-d(t))\boldsymbol{S}_3\boldsymbol{\eta}(t-d(t)). \tag{A.30}$$

Let $\boldsymbol{a}_2=[\boldsymbol{a}_1^T,\ \dot{\boldsymbol{x}}^T(s)\,]^T$, $\boldsymbol{b}_2=[\boldsymbol{b}_1^T,\ \dot{\boldsymbol{\eta}}^T(s)\,]^T$, and $\boldsymbol{\nu}=[\boldsymbol{\nu}_1^T\ \ \boldsymbol{\nu}_2^T]^T$ where

$$\boldsymbol{\nu}_1=[\boldsymbol{x}^T(t),\,\boldsymbol{x}^T(t-d(t)),\,\boldsymbol{x}^T(t-h),\,\dot{\boldsymbol{x}}^T(t),\,\boldsymbol{e}^T(t-d(t))]^T,$$
$$\boldsymbol{\nu}_2=[\boldsymbol{\eta}^T(t),\,\boldsymbol{\eta}^T(t-d(t)),\,\boldsymbol{\eta}^T(t-h),\,\dot{\boldsymbol{\eta}}^T(t)]^T.$$

Considering all expressions from (A.19) to (A.30) the following upper bound holds

$$\dot{V}+\zeta_1 V\leq\boldsymbol{\nu}^T\bar{\boldsymbol{C}}_1\boldsymbol{\nu}-\int_{t-h}^{t-d(t)}\boldsymbol{a}_2^T\bar{\boldsymbol{C}}_2\boldsymbol{a}_2ds-\int_{t-d(t)}^{t}\boldsymbol{a}_2^T\bar{\boldsymbol{C}}_3\boldsymbol{a}_2ds \\ -\int_{t-h}^{t-d(t)}\boldsymbol{b}_2^T\bar{\boldsymbol{C}}_4\boldsymbol{b}_2ds-\int_{t-d(t)}^{t}\boldsymbol{b}_2^T\bar{\boldsymbol{C}}_5\boldsymbol{b}_2ds, \tag{A.31}$$

where

$$\bar{\boldsymbol{C}}_1=\begin{bmatrix}\bar{\boldsymbol{\Pi}} & \bar{\boldsymbol{\Phi}}\\ * & \bar{\boldsymbol{\Psi}}\end{bmatrix},\ \bar{\boldsymbol{C}}_2=\begin{bmatrix}\bar{\boldsymbol{Y}} & \bar{\boldsymbol{F}}\\ * & he^{-\zeta_1 h}\bar{\boldsymbol{Z}}_1\end{bmatrix},\ \bar{\boldsymbol{C}}_3=\begin{bmatrix}\bar{\boldsymbol{Y}} & \bar{\boldsymbol{G}}\\ * & he^{-\zeta_1 h}\bar{\boldsymbol{Z}}_1\end{bmatrix},$$
$$\bar{\boldsymbol{C}}_4=\begin{bmatrix}\bar{\boldsymbol{U}} & \bar{\boldsymbol{W}}\\ * & he^{-\zeta_1 h}\bar{\boldsymbol{Z}}_2\end{bmatrix},\quad \bar{\boldsymbol{C}}_5=\begin{bmatrix}\bar{\boldsymbol{U}} & \bar{\boldsymbol{E}}\\ * & he^{-\zeta_1 h}\bar{\boldsymbol{Z}}_2\end{bmatrix},$$
$$\bar{\boldsymbol{\Pi}}=\begin{bmatrix}\bar{\boldsymbol{\pi}}_{11} & \bar{\boldsymbol{\pi}}_{12} & -\bar{\boldsymbol{F}}_1 & \bar{\boldsymbol{\pi}}_{14} & \boldsymbol{N}^{-1}\boldsymbol{B}\boldsymbol{K}\\ * & \bar{\boldsymbol{\pi}}_{22} & -\bar{\boldsymbol{F}}_2 & \bar{\boldsymbol{\pi}}_{24} & \boldsymbol{N}^{-1}\boldsymbol{B}\boldsymbol{K}\\ * & * & -e^{-\zeta_1 h}\bar{\boldsymbol{Q}}_1 & \boldsymbol{0} & \boldsymbol{0}\\ * & * & * & \bar{\boldsymbol{\pi}}_{44} & \boldsymbol{N}^{-1}\boldsymbol{B}\boldsymbol{K}\\ * & * & * & * & -\boldsymbol{S}_1\end{bmatrix},\qquad \bar{\boldsymbol{\Phi}}=\begin{bmatrix}(\boldsymbol{N}^{-1}\boldsymbol{A})^T & \boldsymbol{0} & \boldsymbol{0} & (\boldsymbol{N}^{-1}\boldsymbol{A})^T\\ \bar{\boldsymbol{\phi}}_{21} & (\boldsymbol{N}^{-1}\boldsymbol{S}_4)^T & \boldsymbol{0} & \bar{\boldsymbol{\phi}}_{24}\\ \boldsymbol{0} & \boldsymbol{0} & \boldsymbol{0} & \boldsymbol{0}\\ -(\boldsymbol{N}^{-1})^T & \boldsymbol{0} & \boldsymbol{0} & -(\boldsymbol{N}^{-1})^T\\ \bar{\boldsymbol{\phi}}_{51} & (\boldsymbol{N}^{-1}\boldsymbol{S}_5)^T & \boldsymbol{0} & \bar{\boldsymbol{\phi}}_{54}\end{bmatrix},$$
$$\bar{\boldsymbol{\Psi}}=\begin{bmatrix}\bar{\boldsymbol{\psi}}_{11} & \bar{\boldsymbol{\psi}}_{12} & -\bar{\boldsymbol{W}}_1 & \bar{\boldsymbol{P}}_2-\boldsymbol{N}^{-1}-(\boldsymbol{N}^{-1})^T\\ * & \bar{\boldsymbol{\psi}}_{22} & -\bar{\boldsymbol{W}}_2 & -\boldsymbol{N}^{-1}\\ * & * & -e^{-\zeta_1 h}\bar{\boldsymbol{Q}}_2 & \boldsymbol{0}\\ * & * & * & \bar{\boldsymbol{\psi}}_{44}\end{bmatrix},$$
$$\bar{\boldsymbol{\pi}}_{11}=\bar{\boldsymbol{Q}}_1+\bar{\boldsymbol{G}}_1+\bar{\boldsymbol{G}}_1^T+\boldsymbol{N}^{-1}\boldsymbol{A}+(\boldsymbol{N}^{-1}\boldsymbol{A})^T+h\bar{\boldsymbol{Y}}_{11}+\zeta_1\bar{\boldsymbol{P}}_1,$$
$$\bar{\boldsymbol{\pi}}_{12}=\bar{\boldsymbol{F}}_1-\bar{\boldsymbol{G}}_1+\bar{\boldsymbol{G}}_2^T+h\bar{\boldsymbol{Y}}_{12}+\boldsymbol{N}^{-1}\boldsymbol{B}\boldsymbol{K}+(\boldsymbol{N}^{-1}\boldsymbol{A})^T,$$
$$\bar{\boldsymbol{\pi}}_{14}=\bar{\boldsymbol{P}}_1-\boldsymbol{N}^{-1}+(\boldsymbol{N}^{-1}\boldsymbol{A})^T,$$
$$\bar{\boldsymbol{\pi}}_{22}=\bar{\boldsymbol{F}}_2+\bar{\boldsymbol{F}}_2^T-\bar{\boldsymbol{G}}_2-\bar{\boldsymbol{G}}_2^T+h\bar{\boldsymbol{Y}}_{22}+\boldsymbol{N}^{-1}\boldsymbol{B}\boldsymbol{K}+(\boldsymbol{N}^{-1}\boldsymbol{B}\boldsymbol{K})^T+\boldsymbol{S}_2,$$
$$\bar{\boldsymbol{\pi}}_{24}=(\boldsymbol{N}^{-1}\boldsymbol{B}\boldsymbol{K})^T-\boldsymbol{N}^{-1},\qquad \bar{\boldsymbol{\pi}}_{44}=h^2\bar{\boldsymbol{Z}}_1-\boldsymbol{N}^{-1}-(\boldsymbol{N}^{-1})^T,$$
$$\bar{\boldsymbol{\phi}}_{21}=\bar{\boldsymbol{\phi}}_{24}=(\boldsymbol{N}^{-1}\boldsymbol{S}_4)^T+(\boldsymbol{N}^{-1}\boldsymbol{B}\boldsymbol{K})^T,\qquad \bar{\boldsymbol{\phi}}_{51}=\bar{\boldsymbol{\phi}}_{54}=(\boldsymbol{N}^{-1}\boldsymbol{S}_5)^T+(\boldsymbol{N}^{-1}\boldsymbol{B}\boldsymbol{K})^T,$$

$$\bar{\boldsymbol{\psi}}_{11} = \bar{\boldsymbol{Q}}_2 + \bar{\boldsymbol{E}}_1 + \bar{\boldsymbol{E}}_1^T + h\bar{\boldsymbol{U}}_{11} - \boldsymbol{N}^{-1} - (\boldsymbol{N}^{-1})^T + \zeta_1 \bar{\boldsymbol{P}}_2,$$
$$\bar{\boldsymbol{\psi}}_{12} = \bar{\boldsymbol{W}}_1 - \bar{\boldsymbol{E}}_1 + \bar{\boldsymbol{E}}_2^T + h\bar{\boldsymbol{U}}_{12} - (\boldsymbol{N}^{-1})^T,$$
$$\bar{\boldsymbol{\psi}}_{22} = \bar{\boldsymbol{W}}_2 + \bar{\boldsymbol{W}}_2^T - \bar{\boldsymbol{E}}_2 - \bar{\boldsymbol{E}}_2^T + h\bar{\boldsymbol{U}}_{22} + \boldsymbol{S}_3, \qquad \bar{\boldsymbol{\psi}}_{44} = h^2 \bar{\boldsymbol{Z}}_2 - \boldsymbol{N}^{-1} - (\boldsymbol{N}^{-1})^T.$$

Based on (A.31), if $\bar{\boldsymbol{C}}_1 < 0$, and $\bar{\boldsymbol{C}}_i \geq 0$, $(2 \leq i \leq 6)$, then it holds that $\dot{V} + \zeta_1 V < 0$. Now, consider $\boldsymbol{T}_1 = \boldsymbol{I}_9 \otimes \boldsymbol{N}$ and $\boldsymbol{T}_2 = \boldsymbol{I}_3 \otimes \boldsymbol{N}$. We pre- and post multiply $\bar{\boldsymbol{C}}_1$ by $\boldsymbol{T}_1$ and $\boldsymbol{T}_1^T$. In a similar fashion, block matrices $\bar{\boldsymbol{C}}_i$, $(2 \leq i \leq 6)$, are pre- and post multiplied by $\boldsymbol{T}_2$ and $\boldsymbol{T}_2^T$. For $i = 1, 2$ and $j = 1, 2$ the following alternative variables are considered $\boldsymbol{P}_i = \boldsymbol{N}\bar{\boldsymbol{P}}_i\boldsymbol{N}^T$, $\boldsymbol{Q}_i = \boldsymbol{N}\bar{\boldsymbol{Q}}_i\boldsymbol{N}^T$, $\boldsymbol{Z}_i = \boldsymbol{N}\bar{\boldsymbol{Z}}_i\boldsymbol{N}^T$, $\boldsymbol{F}_i = \boldsymbol{N}\bar{\boldsymbol{F}}_i\boldsymbol{N}^T$, $\boldsymbol{G}_i = \boldsymbol{N}\bar{\boldsymbol{G}}_i\boldsymbol{N}^T$, $\boldsymbol{W}_i = \boldsymbol{N}\bar{\boldsymbol{W}}_i\boldsymbol{N}^T$, $\boldsymbol{E}_i = \boldsymbol{N}\bar{\boldsymbol{E}}_i\boldsymbol{N}^T$, $\boldsymbol{Y}_{ij} = \boldsymbol{N}\bar{\boldsymbol{Y}}_{ij}\boldsymbol{N}^T$, and $\boldsymbol{U}_{ij} = \boldsymbol{N}\bar{\boldsymbol{U}}_{ij}\boldsymbol{N}^T$. Additionally, let $\boldsymbol{V} = \boldsymbol{K}\boldsymbol{N}^T$, $\boldsymbol{M}_i = \boldsymbol{N}\bar{\boldsymbol{S}}_i\boldsymbol{N}^T$, $(1 \leq i \leq 3)$, $\boldsymbol{M}_j = \boldsymbol{S}_j\boldsymbol{N}^T$, $(j = 4, 5)$. Using such transformations, LMIs (A.10), (A.11), and (A.12) are obtained. Parameters $\boldsymbol{K}$ and $\boldsymbol{S}_i$, $(1 \leq i \leq 5)$, are calculated from (A.13). □

Remark A.3. Based on Theorem A.1, the validity of (A.13) depends on the feasibility of LMIs (3.32), (A.11), and (A.12). The selected values for the sampling period h and stabilization rate ζ_1 impact the feasibility of the LMIs. Due to the dynamic constraints of the NCS (A.1), not all values for h and ζ_1 are guaranteed to have feasible solutions. The physical interpretation is that the desired sampling period h and stabilization rate ζ_1 should comply with the dynamics of the NCS (A.1). In general, to compute feasible solutions for the LMIs and design unknown parameters based on (A.13), smaller values for h and ζ_1 are first selected. Then, these parameters can be increased incrementally to find the maximum allowable sampling period and stabilization rate for NCS (A.1).

Remark A.4. In [168, 169], a periodic dynamic event-triggered implementation is proposed for stabilization in linear systems. The main differences between implementations [168], [169] and Theorem A.1 are as follows. The stability analysis in [168] is based on an impulsive system approach, where a time-dependent Lyapunov candidate with a simple quadratic function is used. Even though some sufficient conditions on the stability are derived, these conditions are closely dependent on the solution of a Riccati differential equation. As also mentioned in [177, Remark 2], the Riccati-based approach used in [168, 169] complicates the controller design, and the control gains should be known in advance. One approach to design the control gain in [168, 169] is through emulation. As mentioned previously, the initial choice of the control gain in emulation-based approaches limits the feasible regions for the event-triggering parameters [172] and reduces the efficiency of the event-triggering scheme. In contrast to [168], our proposed framework in Theorem A.1 co-designs all required control and DET parameters simultaneously. In fact, the control gain and DET parameters in Theorem A.1 are treated equally and this improves the feasibility regions for the unknown DET parameters.

A.2.4 Parameter Design: Extension to DoS Attacks

Similar to R-PSEC and ROCCET, a desired level of resilience to DoS is included within the proposed framework in Theorem A.1, which leads to the following theorem.

Theorem A.2. Select desired values for sampling periods h and g, ideal stabilization rate ζ_1, and DoS resilience level $\Omega<1$. Let $\zeta_2 = \frac{\zeta_1(1-\Omega)}{\Omega}$. If there exist

- $m\times n$ dimensional matrix $\boldsymbol{V}$;
- $n\times n$ dimensional positive definite matrices $\boldsymbol{P}_1$, $\boldsymbol{Q}_1$, $\boldsymbol{Z}_1$, $\boldsymbol{P}_2$, $\boldsymbol{Q}_2$, $\boldsymbol{Z}_2$, $\boldsymbol{M}_i$, $(1 \leq i \leq 5)$;
- $n\times n$ dimensional matrices $\boldsymbol{N}$, $\boldsymbol{Y}_{11}$, $\boldsymbol{Y}_{12}$, $\boldsymbol{Y}_{22}$, $\boldsymbol{F}_1$, $\boldsymbol{F}_2$, $\boldsymbol{G}_1$, $\boldsymbol{G}_2$, $\boldsymbol{U}_{11}$, $\boldsymbol{U}_{12}$, $\boldsymbol{U}_{22}$, $\boldsymbol{W}_1$, $\boldsymbol{W}_2$, $\boldsymbol{E}_1$, $\boldsymbol{E}_2$,

satisfying

$$\boldsymbol{C}_1 < 0, \quad \boldsymbol{C}_2 \geq 0, \quad \boldsymbol{C}_3 \geq 0, \quad \boldsymbol{C}_4 \geq 0, \quad \boldsymbol{C}_5 \geq 0, \tag{A.32}$$

$$\boldsymbol{C}_6 = \begin{bmatrix} \boldsymbol{A}\boldsymbol{N}^T + \boldsymbol{N}\boldsymbol{A}^T - \zeta_2 \boldsymbol{P}_1 + \boldsymbol{Q}_1 & \boldsymbol{P}_1 - \boldsymbol{N}^T + \boldsymbol{N}\boldsymbol{A}^T \\ * & h^2\boldsymbol{Z}_1 - \boldsymbol{N} - \boldsymbol{N}^T \end{bmatrix} < 0, \tag{A.33}$$

$$\boldsymbol{C}_7 = \begin{bmatrix} -(\boldsymbol{N}+\boldsymbol{N}^T) - \zeta_2 \boldsymbol{P}_2 + \boldsymbol{Q}_2 & \boldsymbol{P}_2 - \boldsymbol{N}^T - \boldsymbol{N} \\ * & h^2\boldsymbol{Z}_2 - \boldsymbol{N} - \boldsymbol{N}^T \end{bmatrix} < 0, \tag{A.34}$$

with $\boldsymbol{C}_i$, $(1 \leq i \leq 5)$, defined in Theorem A.1, then control gain $\boldsymbol{K}$ and S-DET parameters $\boldsymbol{S}_i$, $(1 \leq i \leq 5)$, are computed from the same equations given in (A.13). These parameters make system (A.1) resilient to DoS attacks satisfying

$$\frac{1}{T_1} + \frac{g}{F_1} < \Omega. \tag{A.35}$$

Additionally, trajectories of (A.7) satisfy

$$\lambda_1 \left\|\boldsymbol{x}(t)\right\|^2 + \lambda_2 \left\|\boldsymbol{\eta}(t)\right\|^2 \leq \rho e^{-\zeta t}(\lambda_3 \left\|\boldsymbol{x}(0)\right\|^2 + \lambda_4 \left\|\boldsymbol{\eta}(0)\right\|^2), \tag{A.36}$$

where

$$\rho = e^{(\zeta_1+\zeta_2)(T_0+gF_0)}, \quad \zeta = \zeta_1 - (\zeta_1+\zeta_2)\left(\frac{1}{T_1} + \frac{g}{F_1}\right). \tag{A.37}$$

Parameters λ_i, $(1 \leq i \leq 4)$, follow the same equations given below (A.14).

Proof. The proof is given in two steps.

Step I. Stability Analysis in the Presence of DoS: From Theorem A.1, with given ζ_1 and LMIs $\boldsymbol{C}_1 < 0$, $\boldsymbol{C}_2 \geq 0$, $\boldsymbol{C}_3 \geq 0$, $\boldsymbol{C}_4 \geq 0$, $\boldsymbol{C}_5 \geq 0$, it is guaranteed that $\dot{V}(t) < -\zeta_1 V(t)$ for healthy intervals $(t \in W_m)$. This leads to

$$V(t) \leq e^{-\zeta_1(t-\xi_m-\nu_m)} V(\xi_m + \nu_m), \quad t \in W_m. \tag{A.38}$$

In the presence of DoS $(t \in Z_m)$, system (A.1) is open loop and its states may diverge. Therefore, there exists a scalar ζ_2 such that $\dot{V}(t) < \zeta_2 V(t)$ for $t \in Z_m$. This inequality

is expanded as follows

$$V(t) \leq e^{\zeta_2(t-\xi_m)} V(\xi_m), \quad t \in Z_m. \tag{A.39}$$

Expressions (A.38) and (A.39) are combined to obtain the stability condition. If $t \in Z_m$, the following sequence of inequalities hold

$$\begin{aligned} V(t) \leq & e^{\zeta_2(t-\xi_m)} V(\xi_m) \\ \leq & e^{\zeta_2(t-\xi_m)} \left(e^{-\zeta_1(\xi_m - \xi_{m-1} - \nu_{m-1})} V(\xi_{m-1} + \nu_{m-1}) \right) \\ \leq & e^{\zeta_2(t-\xi_m)} e^{-\zeta_1(\xi_m - \xi_{m-1} - \nu_{m-1})} e^{\zeta_2(\xi_{m-1} + \nu_{m-1} - \xi_{m-2})} V(\xi_{m-2}) \\ \leq & \dots \\ \leq & e^{-\zeta_1 |\bar{\mathcal{H}}(0,t)|} e^{\zeta_2 |\bar{\mathcal{D}}(0,t)|} V(0). \end{aligned} \tag{A.40}$$

From (5.7), (5.8), (5.12), and (5.13), it holds that

$$e^{-\zeta_1 |\bar{\mathcal{H}}(0,t)|} e^{\zeta_2 |\bar{\mathcal{D}}(0,t)|} \leq \rho \, e^{-\zeta t}, \tag{A.41}$$

with ρ and ζ given in (A.37). Condition (A.41) gives way to

$$V(t) < \rho e^{-\zeta t} V(0), \quad t \geq 0, \tag{A.42}$$

which is equivalent to (A.36). Let $\Omega = \zeta_1/(\zeta_1 + \zeta_2)$. Based on (A.42), if DoS attacks satisfy $(\frac{1}{T_1} + \frac{g}{F_1}) < \Omega$, system (A.1) is exponentially stable.

Step II. Parameter Design with Given DoS resilience: For healthy intervals ($t \in W_m$), the parameter design based on LKF (A.18) leads to the LMIs given in (A.10), (A.11), and (A.12). Next, consider DoS intervals ($t \in Z_m$). Let $\Omega = \zeta_1/(\zeta_1 + \zeta_2)$ be a given DoS resilience level. Hence, $\zeta_2 = \frac{\zeta_1(1-\Omega)}{\Omega}$. We consider the following expressions for the derivatives of LKF (A.18) in $t \in Z_m$,

$$\begin{aligned} &\dot{V}_1 = 2\dot{\boldsymbol{x}}^T(t) \bar{\boldsymbol{P}}_1 \boldsymbol{x}(t), && \dot{V}_2 \leq \boldsymbol{x}^T(t) \bar{\boldsymbol{Q}}_1 \boldsymbol{x}(t), && \dot{V}_3 \leq h^2 \dot{\boldsymbol{x}}^T(t) \bar{\boldsymbol{Z}}_1 \dot{\boldsymbol{x}}(t) \\ &\dot{V}_4 = 2\dot{\boldsymbol{\eta}}^T(t) \bar{\boldsymbol{P}}_2 \boldsymbol{\eta}(t), && \dot{V}_5 \leq \boldsymbol{\eta}^T(t) \bar{\boldsymbol{Q}}_2 \boldsymbol{\eta}(t), && \dot{V}_6 \leq h^2 \dot{\boldsymbol{\eta}}^T(t) \bar{\boldsymbol{Z}}_2 \dot{\boldsymbol{\eta}}(t). \end{aligned} \tag{A.43}$$

The following null expressions hold based on (A.8) and (A.9)

$$\begin{aligned} &2\Big(\boldsymbol{x}^T(t) \boldsymbol{N}^{-1} + \dot{\boldsymbol{x}}^T(t) \boldsymbol{N}^{-1}\Big)\Big(\boldsymbol{A}\boldsymbol{x}(t) - \dot{\boldsymbol{x}}(t)\Big) = 0, \\ &2\Big(\boldsymbol{\eta}^T(t) \boldsymbol{N}^{-1} + \dot{\boldsymbol{\eta}}^T(t) \boldsymbol{N}^{-1}\Big)\Big(-\boldsymbol{\eta}(t) - \dot{\boldsymbol{\eta}}(t)\Big) = 0. \end{aligned} \tag{A.44}$$

Form (A.43), the following condition holds

$$\dot{V} - \zeta_2 V = \sum_{i=1}^{6} \dot{V}_i - \zeta_2 \sum_{i=1}^{6} V_i \leq \sum_{i=1}^{6} \dot{V}_i - \zeta_2 (V_1 + V_4). \tag{A.45}$$

Considering (A.43) and (A.44), we revise (A.45) as follows

$$\sum_{i=1}^{6} \dot{V}_i - \zeta_2 (V_1 + V_4) = \boldsymbol{\nu}_1^T \bar{\boldsymbol{C}}_6 \boldsymbol{\nu}_1 + \boldsymbol{\nu}_2^T \bar{\boldsymbol{C}}_7 \boldsymbol{\nu}_2, \tag{A.46}$$

where $\boldsymbol{\nu}_1 = [\boldsymbol{x}^T(t),\, \dot{\boldsymbol{x}}^T(t)]^T,\ \boldsymbol{\nu}_2 = [\boldsymbol{\eta}^T(t),\, \dot{\boldsymbol{\eta}}^T(t)]^T$, and

$$\bar{\boldsymbol{C}}_6 = \begin{bmatrix} \bar{\boldsymbol{c}}_1 & (\boldsymbol{N}^{-1}\boldsymbol{A})^T - \boldsymbol{N}^{-1} + \bar{\boldsymbol{P}}_1 \\ * & h^2\bar{\boldsymbol{Z}}_1 - \boldsymbol{N}^{-1} - (\boldsymbol{N}^{-1})^T \end{bmatrix}, \quad \bar{\boldsymbol{C}}_7 = \begin{bmatrix} \bar{\boldsymbol{c}}_2 & \bar{\boldsymbol{P}}_2 - \boldsymbol{N}^{-1} - (\boldsymbol{N}^{-1})^T \\ * & h^2\bar{\boldsymbol{Z}}_2 - \boldsymbol{N}^{-1} - (\boldsymbol{N}^{-1})^T \end{bmatrix},$$

with $\bar{\boldsymbol{c}}_1 = \boldsymbol{N}^{-1}\boldsymbol{A} + (\boldsymbol{N}^{-1}\boldsymbol{A})^T - \zeta_2\bar{\boldsymbol{P}}_1 + \bar{\boldsymbol{Q}}_1$, and $\bar{\boldsymbol{c}}_2 = -\boldsymbol{N}^{-1} - (\boldsymbol{N}^{-1})^T - \zeta_2\bar{\boldsymbol{P}}_2 + \bar{\boldsymbol{Q}}_2$. Considering (A.45) and (A.46), we conclude that if $\bar{\boldsymbol{C}}_6 < 0$ and $\bar{\boldsymbol{C}}_7 < 0$, then $\dot{V}(t) - \zeta_2 V(t) < 0$ is guaranteed for $t \in Z_m$. As shown previously, combining $\dot{V}(t) + \zeta_1 V(t) < 0$ for $t \in W_m$ and $\dot{V}(t) - \zeta_2 V(t) < 0$ for $t \in Z_m$ leads to (A.36). We pre- and post multiply $\bar{\boldsymbol{C}}_6$ and $\bar{\boldsymbol{C}}_7$ by $\boldsymbol{T}_3$ and $\boldsymbol{T}_3^T$, where $\boldsymbol{T}_3 = \boldsymbol{I}_2 \otimes \boldsymbol{N}$. Considering the same alternative variables used at the end of proof of Theorem A.1 leads to LMIs $\boldsymbol{C}_6 < 0$ and $\boldsymbol{C}_7 < 0$ given in (A.33) and (A.34). This completes the proof. □

Remark A.5. From Theorem A.2 it is possible to obtain the maximum resilience level, denoted by Ω_m, for given values of h and ζ_1. To this end, one can select desired values for h and ζ_1 and investigate the feasibility of Theorem A.2 by incrementally increasing the value of Ω until the LMIs become infeasible. The largest value of Ω which leads to a feasible solution is the maximum resilience level to DoS (Ω_m) guaranteed by Theorem A.2.

A.3 Numerical examples

To investigate the effectiveness of Theorems A.1 and A.2, this section conducts simulations over some widely-used NCSs used in the literature. The LMIs are solved using the Yalmip parser and SDPT3 solver in Matlab environment.

A.3.1 Batch reactor

Consider a batch reactor system with the dynamics given below [178, 179]

$$\boldsymbol{A} = \begin{bmatrix} 1.38 & -0.2077 & 6.715 & -5.676 \\ -0.5814 & -4.29 & 0 & 0.675 \\ 1.067 & 4.273 & -6.654 & 5.893 \\ 0.048 & 4.273 & 1.343 & -2.104 \end{bmatrix}, \ \boldsymbol{B} = \begin{bmatrix} 0 & 0 \\ 5.679 & 0 \\ 1.136 & -3.146 \\ 1.136 & 0 \end{bmatrix}. \tag{A.47}$$

The open-loop batch reactor system is unstable.

Case I. DoS-free: First, we evaluate the performance of our proposed attack-free framework (Theorem A.1). Let $h = 0.1$ and $\zeta_1 = 0.3$. The control gain $\boldsymbol{K}$ and S-DET parameters $\boldsymbol{S}_i$, $(1 \le i \le 5)$, are computed from Theorem A.1

$$\boldsymbol{K} = \begin{bmatrix} -0.1044 & -0.2509 & -0.0703 & -0.0322 \\ 1.3925 & 0.2116 & 1.0056 & -0.5246 \end{bmatrix}, \quad \boldsymbol{S}_1 = \begin{bmatrix} 26.1387 & 3.3468 & 22.2799 & -13.4629 \\ 3.3468 & 1.7992 & 2.0495 & -0.7013 \\ 22.2799 & 2.0495 & 21.9516 & -14.5033 \\ -13.4629 & -0.7013 & -14.5033 & 10.1517 \end{bmatrix},$$

$$\boldsymbol{S}_2 = \begin{bmatrix} 0.0980 & 0.0172 & 0.0417 & -0.0039 \\ 0.0172 & 0.1010 & -0.0184 & 0.0022 \\ 0.0417 & -0.0184 & 0.1331 & -0.0965 \\ -0.0039 & 0.0022 & -0.0965 & 0.0893 \end{bmatrix}, \quad \boldsymbol{S}_3 = \begin{bmatrix} 0.1049 & 0.0135 & 0.0558 & -0.0216 \\ 0.0135 & 0.0284 & 0.0068 & 0.0027 \\ 0.0558 & 0.0068 & 0.0495 & -0.0229 \\ -0.0216 & 0.0027 & -0.0229 & 0.0280 \end{bmatrix},$$

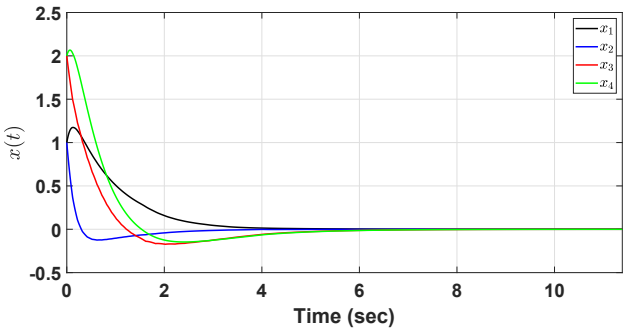

Figure A.2: States trajectories $\boldsymbol{x}(t)$.

$$\boldsymbol{S}_4 = \begin{bmatrix} -0.3231 & -0.0883 & -1.2185 & 1.0344 \\ 0.1745 & 1.1114 & 0.1081 & -0.0051 \\ 0.8943 & -0.1917 & 2.2328 & -1.7619 \\ -0.6044 & -0.2011 & -1.4848 & 1.3926 \end{bmatrix}, \qquad \boldsymbol{S}_5 = \begin{bmatrix} 1.3829 & -0.0365 & 1.0043 & -0.6815 \\ 0.3152 & 0.8205 & 0.2128 & 0.0437 \\ 0.8441 & 0.2810 & 0.9656 & -0.3317 \\ -0.0768 & 0.1609 & -0.1036 & 0.4349 \end{bmatrix}.$$

The stabilization time is computed by $T_s = \inf\{t \,|\, \frac{\|\boldsymbol{x}(t)\|}{\|\boldsymbol{x}(0)\|} \leq \delta\}$. In fact, T_s is the time when stabilization is achieved within at least δ factor of $\boldsymbol{x}(0)$. Let $\delta = 0.0001$, $\boldsymbol{x}(0) = [1, 1, 2, 2]^T$, and $\boldsymbol{\eta}(0) = 0.5[1, 1, 2, 2]^T$. For this setting, the settling time is computed as $T_s = 11.40$ sec. The state trajectories of system (A.47) are shown in Fig. A.2. The evolution of thresholds $\boldsymbol{x}^T(t)\boldsymbol{S}_2\boldsymbol{x}(t)$ and $\boldsymbol{\eta}^T(t)\boldsymbol{S}_3\boldsymbol{\eta}(t)$ are shown in Fig. A.3. It can be observed that the value of the dynamic threshold $\boldsymbol{\eta}^T(t)\boldsymbol{S}_3\boldsymbol{\eta}(t)$ can significantly increase the combined ET threshold (A.3). The control update instants are show in Fig. A.4. The total number of events is $N_e = 37$. This implies that only $37/114 \approx 32\%$ of the total packets are used to update the control input. We also report the average inter-event time (AIET) which is roughly the frequency of the event-triggerings and computed by AIET $= T_s/N_e$. In this case, AIET $= 0.3078$.

Impact of h and ζ_1: Next, two scenarios are considered to observe how the performance of the batch reactor system (in terms of T_s, N_e, and AIET) is influenced by different values of the sampling time h and decaying rate ζ_1. First in scenario (a), h is fixed at $h = 0.1$ and ζ_1 is varied. Next, in scenario (b), we set $\zeta_1 = 0.3$ and vary h. Table A.1 lists the corresponding results for each case. According to Table A.1, with fixed h, increasing the stabilization rate ζ_1 reduces the settling time T_s at the expense of lower AIET, which implies a more frequent control updates. When ζ_1 is fixed and h is varying, the settling time T_s does not significantly change. However, higher values of h help reducing the number of events and increasing AIET.

Table A.1: Impact of h and ζ_1 on batch reactor system.

Scenario (a): $h = 0.1$				**Scenario (b):** $\zeta_1 = 0.3$			
ζ_1	T_s	N_e	AIET	h	T_s	N_e	AIET
0.2	12.48	39	0.3200	0.01	11.05	38	0.2908
0.4	10.24	35	0.2926	0.05	10.69	34	0.3144
0.6	8.28	31	0.2671	0.15	12.34	37	0.3335

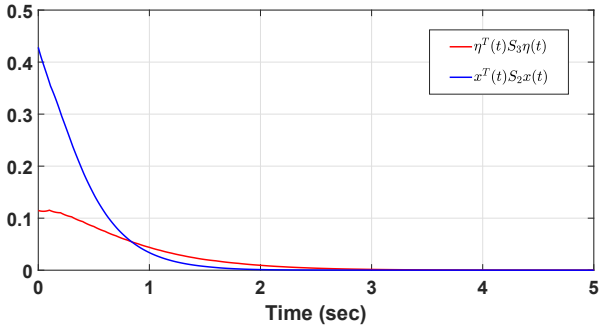

Figure A.3: Trajectories of the thresholds in S-DET (A.3).

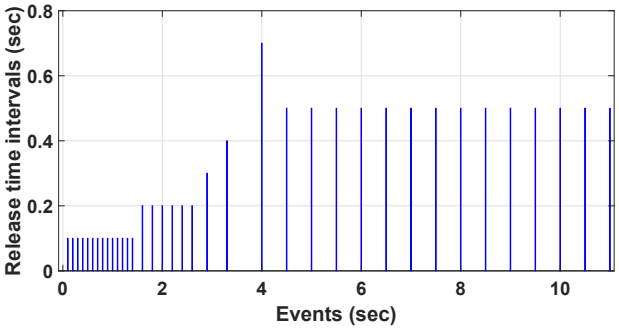

Figure A.4: Release time intervals.

Case II. In the presence of DoS: Next, stabilization for NCS (A.47) is studied against DoS attacks using Theorem A.2. Let $h=0.05$ and $\zeta_1=0.8$. The desired level of resilience to DoS is selected as $\Omega=0.15$. The control gain and S-DET parameters are computed from Theorem A.2 as follows

$$\boldsymbol{K}=\begin{bmatrix}-0.2970 & -0.3779 & -0.1621 & -0.0857\\ 1.5520 & 0.1952 & 1.2311 & -0.6972\end{bmatrix},\qquad \boldsymbol{S}_1=\begin{bmatrix}44.1827 & 7.0762 & 35.3298 & -19.7294\\ 7.0762 & 3.1661 & 4.7343 & -1.5658\\ 35.3298 & 4.7343 & 30.8121 & -18.6282\\ -19.7294 & -1.5658 & -18.6282 & 12.3279\end{bmatrix},$$
$$\boldsymbol{S}_2=\begin{bmatrix}0.1729 & 0.0423 & 0.0451 & 0.0358\\ 0.0423 & 0.0902 & -0.0015 & 0.0060\\ 0.0451 & -0.0015 & 0.0940 & -0.0564\\ 0.0358 & 0.0060 & -0.0564 & 0.0701\end{bmatrix},\qquad \boldsymbol{S}_3=\begin{bmatrix}0.0850 & 0.0134 & 0.0455 & -0.0161\\ 0.0134 & 0.0195 & 0.0087 & 0.0013\\ 0.0455 & 0.0087 & 0.0354 & -0.0123\\ -0.0161 & 0.0013 & -0.0123 & 0.0181\end{bmatrix},$$
$$\boldsymbol{S}_4=\begin{bmatrix}-0.1407 & 0.0929 & -1.5234 & 1.4449\\ 0.6006 & 1.3157 & 0.3534 & -0.0133\\ 1.0296 & -0.3216 & 2.6016 & -2.1145\\ -0.2407 & -0.2103 & -1.2832 & 1.3263\end{bmatrix},\qquad \boldsymbol{S}_5=\begin{bmatrix}1.4743 & -0.0048 & 0.9454 & -0.6158\\ 0.4734 & 0.9886 & 0.2454 & 0.2090\\ 1.0416 & 0.3636 & 1.0525 & -0.3043\\ -0.1099 & 0.2571 & -0.2465 & 0.6392\end{bmatrix}. \tag{A.48}$$

Consider the following DoS attack sequence for $c\in\mathbb{N}_0$

$$d_c=0.5+1.4c,\qquad \tau_c=0.12+0.08|\cos(d_c)|. \tag{A.49}$$

This DoS sequence satisfies Assumption 5 with $T_0=0.2$, $T_1=7$, $F_0=1$, and $F_1=1$. Let $g=0.005$. Condition (A.35) holds, i.e., $\frac{1}{7}+\frac{0.005}{1}<0.15$. The same initial conditions given in the previous section are used. The settling time in the presence of DoS (A.49) is computed as $T_s=10.08$ sec. The state trajectories $\boldsymbol{x}(t)$ and event-triggerings in the presence of DoS are depicted in Figs. A.5 and A.6. The total number of events is $N_e=55$. This implies that $55/202\approx 25\%$ of the total packets are used to update

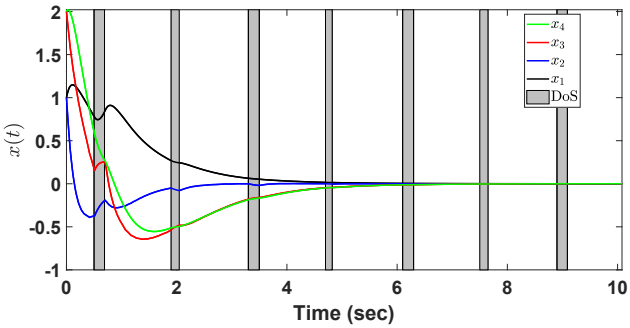

Figure A.5: States trajectories $\boldsymbol{x}(t)$ in the presence of (A.49).

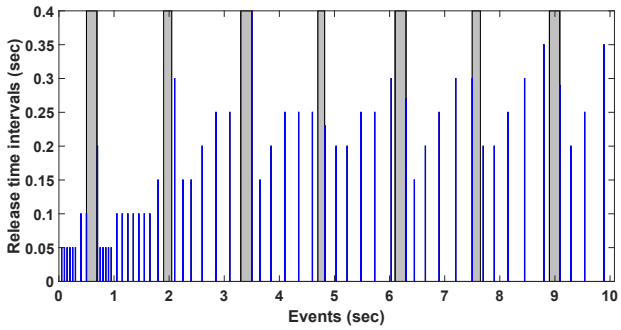

Figure A.6: Release time intervals in the presence of DoS (A.49).

the control input. Simulation is run using parameters (A.48) with no DoS attacks. The results are as follows: $T_s = 8.34$, $N_e = 31$, and AIET $= 0.2687$. Compared to the DoS-free case, the settling time T_s is higher in the presence of DoS. Additionally, the total number of events N_e is higher and AIET is lower. This observation shows that by considering the impact of DoS in Theorem A.2, computed control gain and S-DET parameters from Theorem A.2 are more conservative compared to Theorem A.1. This is consistent with the anticipated trade-off between the performance of the system (in terms of stabilization convergence rate and number of control updates) and the resilience to attacks.

A.3.2 Comparison

In this section, the proposed method in Theorems A.1 and A.2 is compared with existing methods in terms of the effectiveness of the S-DET scheme and also the amount of guaranteed resilience to DoS.

Effectiveness of S-DET (DoS-free situation): The ability of the proposed S-DET scheme in terms of reducing the amount of control updates is compared with [2], where a sampled-data *static* ET scheme is proposed considering an attack free scenario. In order to be consistent with [2], the following assumptions are considered here (i): There is no consideration for DoS in [2]. Therefore, Theorem A.1 (attack-free framework) is used for comparison. (ii): Asymptotic stability is investigated in [2].

To be consistent, we also set $\zeta_1 = 0$. Initial conditions for $\boldsymbol{x}(0)$ and $\boldsymbol{\eta}(0)$ are set as unity vectors. The following widely-used systems are selected from literature for comparison with [2].

- **System. I:** The batch reactor system given in (A.47).
- **System. II:** An inverted pendulum system [180] described by

$$\boldsymbol{A} = \begin{bmatrix} 0 & 1 & 0 & 0 \\ 0 & -0.1818 & 2.6727 & 0 \\ 0 & 0 & 0 & 1 \\ 0 & -0.4545 & 31.1818 & 0 \end{bmatrix}, \ \boldsymbol{B} = \begin{bmatrix} 0 \\ 1.18182 \\ 0 \\ 4.5455 \end{bmatrix}. \tag{A.50}$$

- **System. III:** A widely-used linear plant [181]

$$\boldsymbol{A} = \begin{bmatrix} 0 & 1 \\ 0 & -0.1 \end{bmatrix}, \ \boldsymbol{B} = \begin{bmatrix} 0 \\ 0.1 \end{bmatrix}. \tag{A.51}$$

- **Sys. IV:** An unstable linear plant [32]

$$\boldsymbol{A} = \begin{bmatrix} 1 & 1 \\ 0 & 1 \end{bmatrix}, \ \boldsymbol{B} = \begin{bmatrix} 1 & 0 \\ 0 & 1 \end{bmatrix}. \tag{A.52}$$

The simulation time horizon is set at $T_f = 25$ sec. Initial conditions for $\boldsymbol{x}(0)$ and $\boldsymbol{\eta}(0)$ are unity vectors. Table A.2 includes the number of control updates for different values of h. It is observed that the proposed S-DET scheme leads to fewer number of control updates compared to the static ET scheme used in [2].

The guaranteed DoS bounds: Finally, the resilience level guaranteed by the proposed approach in Theorem A.2 is compared with that of References [32, 50]. To this end, system (A.52) is considered, which is also studied in [32, 50]. The authors in [32,50] use the solutions of $\boldsymbol{\Phi}^T \boldsymbol{P} + \boldsymbol{P}\boldsymbol{\Phi} + \boldsymbol{Q} = \boldsymbol{0}$ where $\boldsymbol{\Phi} = (\boldsymbol{A} + \boldsymbol{B}\boldsymbol{K})$ to compute the control gain $\boldsymbol{K}$. The guaranteed upper-bound for DoS is then obtained from the largest and smallest eigenvalues of $\boldsymbol{P}$. With the LQR control gain, the tolerable amount of DoS guaranteed by [32] is 0.0321. In other words, only attacks satisfying $\frac{1}{T_1} + \frac{g}{F_1} < 0.0321$ are guaranteed to not destabilize system (A.52). Using some other

Table A.2: Number of control updates, Theorem A.1 and [2].

	System. I:			**System. II:**		
Method	h=0.01	h=0.05	h=0.10	h=0.01	h=0.05	h=0.10
Theorem A.1	56	56	59	108	90	79
Ref. [2]	87	91	89	136	106	91
	System. III:			**System. IV:**		
Method	h=0.01	h=0.05	h=0.10	h=0.01	h=0.05	h=0.10
Theorem A.1	48	45	44	38	36	37
Ref. [2]	50	54	51	137	129	113

values for $\boldsymbol{K}$ and $\boldsymbol{Q}$ an amount of 0.0971 for the admissible DoS is also reported in [32]. The authors in [32] suggest that the obtained bounds are conservative and the practical bounds are much larger.

The proposed method in Theorem A.2 is used to find the maximum resilience to DoS. For $h = 0.01$, a value for ζ_1 is selected and the maximum resilience to DoS (Ω_m) is found by incrementally increasing Ω in Theorem A.2 until no feasible solution is computed (see Remark A.5). Table A.3 lists the corresponding pairs ζ_1 and Ω_m. Based on Table A.3 the resilience level guaranteed by Theorem A.2 in much higher than that of [32, 50]. The reason is that, unlike [32, 50] where the DoS bound is computed from matrix norms and extreme eigenvalues, Theorem A.2 uses all the information included in the LKF matrices (i.e., $\boldsymbol{P}_i$, $\boldsymbol{Q}_i$, $\boldsymbol{Z}_i$, $(i = 1, 2)$). Therefore, the DoS resilience guaranteed by Theorem A.2 is higher and thus more practical than [32, 50]. As observed in Table A.3, the maximum resilience to DoS Ω_m is proportional to the ideal stabilization rate ζ_1. This is consistent with $\Omega = \frac{\zeta_1}{\zeta_1+\zeta_2}$ which implies a proportional relationship between Ω and ζ_1.

Table A.3: Maximum attack resilience (Ω_m) guaranteed by Theorem A.2 with varying ζ_1 and fixed $h = 0.01$.

ζ_1	Ω_m	ζ_1	Ω_m
0.5	0.192	1.0	0.331
0.6	0.231	1.1	0.355
0.7	0.259	1.2	0.374
0.8	0.283	1.3	0.392
0.9	0.307	1.4	0.411

Bibliography

[1] Z. Feng and G. Hu, "Secure cooperative event-triggered control of linear multiagent systems under DoS attacks," *IEEE Transactions on control systems technology*, 2019.

[2] X. Chen and F. Hao, "Periodic event-triggered state-feedback and output-feedback control for linear systems," *Int. J. Control Autom.*, vol. 13, no. 4, pp. 779–787, 2015.

[3] A. Dorri, S. S. Kanhere, and R. Jurdak, "Multi-agent systems: A survey," *IEEE Access*, vol. 6, pp. 28573–28593, 2018.

[4] R. Olfati-Saber, J. A. Fax, and R. M. Murray, "Consensus and cooperation in networked multi-agent systems," *Proceedings of the IEEE*, vol. 95, no. 1, pp. 215–233, 2007.

[5] F. Garin and L. Schenato, "A survey on distributed estimation and control applications using linear consensus algorithms," in *Networked control systems*, pp. 75–107, Springer, 2010.

[6] L. Ding, Q. Han, X. Ge, and X. Zhang, "An overview of recent advances in event-triggered consensus of multiagent systems," *IEEE Transactions on Cybernetics*, vol. 48, no. 4, pp. 1110–23, 2017.

[7] S. Rao and D. Ghose, "Sliding mode control-based autopilots for leaderless consensus of unmanned aerial vehicles," *IEEE Transactions on Control Systems Technology*, vol. 22, no. 5, pp. 1964–1972, 2014.

[8] Z.-Q. Liu, Y.-L. Wang, and T.-B. Wang, "Incremental predictive control-based output consensus of networked unmanned surface vehicle formation systems," *Information Sciences*, vol. 457, pp. 166–181, 2018.

[9] S. Chen and D. W. Ho, "Consensus control for multiple AUVs under imperfect information caused by communication faults," *Information Sciences*, vol. 370, pp. 565–577, 2016.

[10] A. Bidram, A. Davoudi, F. L. Lewis, and J. M. Guerrero, "Distributed cooperative secondary control of microgrids using feedback linearization," *IEEE Transactions on Power Systems*, vol. 28, no. 3, pp. 3462–3470, 2013.

[11] Y. Xie and Z. Lin, "Distributed event-triggered secondary voltage control for microgrids with time delay," *IEEE Transactions on Systems, Man, and Cybernetics: Systems*, 2019.

[12] Z. Li, W. Ren, X. Liu, and M. Fu, "Distributed containment control of multi-agent systems with general linear dynamics in the presence of multiple leaders," *International Journal of Robust and Nonlinear Control*, vol. 23, no. 5, pp. 534–547, 2013.

[13] L. Galbusera, G. Ferrari-Trecate, and R. Scattolini, "A hybrid model predictive control scheme for containment and distributed sensing in multi-agent systems," *Systems & Control Letters*, vol. 62, no. 5, pp. 413–419, 2013.

[14] A. Amini, A. Azarbahram, and M. Sojoodi, "h_∞ consensus of nonlinear multi-agent systems using dynamic output feedback controller: an LMI approach," *Nonlinear Dynamics*, vol. 85, no. 3, pp. 1865–1886, 2016.

[15] Z. Li, W. Ren, X. Liu, and M. Fu, "Consensus of multi-agent systems with general linear and lipschitz nonlinear dynamics using distributed adaptive protocols," *IEEE Transactions on Automatic Control*, vol. 58, no. 7, pp. 1786–1791, 2013.

[16] S. Zhu, C. Chen, X. Ma, B. Yang, and X. Guan, "Consensus based estimation over relay assisted sensor networks for situation monitoring," *IEEE Journal of Selected Topics in Signal Processing*, vol. 9, no. 2, pp. 278–291, 2015.

[17] G. Xie, H. Liu, L. Wang, and Y. Jia, "Consensus in networked multi-agent systems via sampled control: fixed topology case," in *American Control Conference*, pp. 3902–3907, IEEE, 2009.

[18] W. Ren and Y. Cao, "Convergence of sampled-data consensus algorithms for double-integrator dynamics," in *CDC 2008. 47th IEEE Conference on*, pp. 3965–3970, IEEE, 2008.

[19] W. Hu, L. Liu, and G. Feng, "Consensus of linear multi-agent systems by distributed event-triggered strategy," *IEEE Transactions on Cybernetics*, vol. 46, no. 1, pp. 148–157, 2016.

[20] A. Albert, "Comparison of event-triggered and time-triggered concepts with regard to distributed control systems," *Embedded world*, vol. 2004, pp. 235–252, 2004.

[21] G. S. Seyboth, D. V. Dimarogonas, and K. H. Johansson, "Event-based broadcasting for multi-agent average consensus," *Automatica*, vol. 49, no. 1, pp. 245–252, 2013.

[22] Z. Li, G. Wen, Z. Duan, and W. Ren, "Designing fully distributed consensus protocols for linear multi-agent systems with directed graphs," *IEEE Transactions on Automatic Control*, vol. 60, no. 4, pp. 1152–1157, 2015.

[23] J. Qin, Q. Ma, Y. Shi, and L. Wang, "Recent advances in consensus of multi-agent systems: A brief survey," *IEEE Transactions on Industrial Electronics*, vol. 64, no. 6, pp. 4972–4983, 2016.

[24] F. Wang, G. Wen, Z. Peng, T. Huang, and Y. Yu, "Event-triggered consensus of general linear multiagent systems with data sampling and random packet losses," *IEEE Transactions on Systems, Man, and Cybernetics: Systems*, 2019.

[25] Y. Liu and X. Hou, "Event-triggered consensus control of disturbed multi-agent systems using output feedback," *ISA transactions*, vol. 91, pp. 166–173, 2019.

[26] X. You, C. Hua, and X. Guan, "Event-triggered leader-following consensus for nonlinear multiagent systems subject to actuator saturation using dynamic output feedback method," *IEEE Transactions on Automatic Control*, vol. 63, no. 12, pp. 4391–4396, 2018.

[27] K. Patel and A. Mehta, "Discrete-time event-triggered higher order sliding mode control for consensus of 2-DOF robotic arms," *European Journal of Control*, 2020.

[28] J. Zhan, Y. Hu, and X. Li, "Adaptive event-triggered distributed model predictive control for multi-agent systems," *Systems & Control Letters*, vol. 134, p. 104531, 2019.

[29] G. Guo, L. Ding, and Q.-L. Han, "A distributed event-triggered transmission strategy for sampled-data consensus of multi-agent systems," *Automatica*, vol. 50, no. 5, pp. 1489–1496, 2014.

[30] L. Xing, C. Wen, F. Guo, Z. Liu, and H. Su, "Event-based consensus for linear multiagent systems without continuous communication," *IEEE Transactions on Cybernetics*, vol. 47, no. 8, pp. 2132–2142, 2016.

[31] Y. Cui, Y. Liu, W. Zhang, and F. E. Alsaadi, "Sampled-based consensus for nonlinear multiagent systems with deception attacks: The decoupled method," *IEEE Transactions on Systems, Man, and Cybernetics: Systems*, 2018.

[32] C. De Persis, P. Tesi, *et al.*, "Input-to-state stabilizing control under denial-of-service.," *IEEE Transactions on Automatic Control*, vol. 60, no. 11, pp. 2930–2944, 2015.

[33] B. Cheng and Z. Li, "Fully distributed event-triggered protocols for linear multiagent networks," *IEEE Transactions on Automatic Control*, vol. 64, no. 4, pp. 1655–1662, 2018.

[34] Z.-G. Wu, Y. Xu, R. Lu, Y. Wu, and T. Huang, "Event-triggered control for consensus of multiagent systems with fixed/switching topologies," *IEEE Transactions on Systems, Man, and Cybernetics: Systems*, vol. 48, no. 10, pp. 1736–1746, 2017.

[35] T.-H. Cheng, Z. Kan, J. R. Klotz, J. M. Shea, and W. E. Dixon, "Event-triggered control of multiagent systems for fixed and time-varying network topologies," *IEEE Transactions on Automatic Control*, vol. 62, no. 10, pp. 5365–5371, 2017.

[36] M. Abdelrahim, R. Postoyan, J. Daafouz, and D. Nešić, "Co-design of output feedback laws and event-triggering conditions for linear systems," in *53rd IEEE CDC*, pp. 3560–3565, 2014.

[37] S. Hu, D. Yue, X. Xie, X. Chen, and X. Yin, "Resilient event-triggered controller synthesis of networked control systems under periodic DoS jamming attacks," *IEEE Transactions on Cybernetics*, vol. 49, no. 12, pp. 4271–4281, 2018.

[38] C. Peng and Q.-L. Han, "A novel event-triggered transmission scheme and l_2 control co-design for sampled-data control systems," *IEEE Transactions on Automatic Control*, vol. 58, no. 10, pp. 2620–2626, 2013.

[39] C. Peng and T. C. Yang, "Event-triggered communication and H_∞ control co-design for networked control systems," *Automatica*, vol. 49, no. 5, pp. 1326–1332, 2013.

[40] M. Abdelrahim, R. Postoyan, J. Daafouz, D. Nevsi'c, and M. Heemels, "Co-design of output feedback laws and event-triggering conditions for the L_2-stabilization of linear systems," *Automatica*, vol. 87, pp. 337–344, 2018.

[41] X. Zhou, P. Shi, C.-C. Lim, C. Yang, and W. Gui, "Event based guaranteed cost consensus for distributed multi-agent systems," *Journal of The Franklin Institute*, vol. 352, no. 9, pp. 3546–3563, 2015.

[42] C. Wang, Z. Zuo, Z. Lin, and Z. Ding, "A truncated prediction approach to consensus control of lipschitz nonlinear multiagent systems with input delay," *IEEE Transactions on Control of Network Systems*, vol. 4, no. 4, pp. 716–724, 2016.

[43] H. Li, X. Jing, and H. R. Karimi, "Output-feedback-based control for vehicle suspension systems with control delay," *IEEE Transactions on Industrial Electronics*, vol. 61, no. 1, pp. 436–446, 2014.

[44] P. Badri, A. Amini, and M. Sojoodi, "Robust fixed-order dynamic output feedback controller design for nonlinear uncertain suspension system," *Mechanical Systems and Signal Processing*, vol. 80, pp. 137–151, 2016.

[45] C. Wang, Z. Zuo, Z. Lin, and Z. Ding, "A truncated prediction approach to consensus control of lipschitz nonlinear multi-agent systems with input delay," *IEEE Transactions on Control of Network Systems*, 2016.

[46] C. Peng and F. Li, "A survey on recent advances in event-triggered communication and control," *Information Sciences*, vol. 457, pp. 113–125, 2018.

[47] L. Ding, Q.-L. Han, L. Y. Wang, and E. Sindi, "Distributed cooperative optimal control of DC microgrids with communication delays," *IEEE Transactions on Industrial Informatics*, vol. 14, no. 9, pp. 3924–3935, 2018.

[48] B. Zhou, X. Liao, T. Huang, and G. Chen, "Leader-following exponential consensus of general linear multi-agent systems via event-triggered control with combinational measurements," *Applied Mathematics Letters*, vol. 40, pp. 35–39, 2015.

[49] H. Zhang, D. Yue, X. Yin, S. Hu, and C. xia Dou, "Finite-time distributed event-triggered consensus control for multi-agent systems," *Information Sciences*, vol. 339, pp. 132–142, 2016.

[50] S. Feng, P. Tesi, and C. De Persis, "Towards stabilization of distributed systems under denial-of-service," in *Decision and Control (CDC)*, pp. 5360–5365, IEEE, 2017.

[51] Z. Feng and G. Hu, "Distributed secure average consensus for linear multi-agent systems under DoS attacks," in *American Control Conference (ACC)*, pp. 2261–2266, IEEE, 2017.

[52] Y. Xu, M. Fang, Z.-G. Wu, Y.-J. Pan, M. Chadli, and T. Huang, "Input-based event-triggering consensus of multiagent systems under denial of service attacks," *IEEE Transactions on Systems, Man, and Cybernetics: Systems*, vol. 50, pp. 1455 – 1464, 2018.

[53] J. Lian, C. Li, and B. Xia, "Sampled-data control of switched linear systems with application to an F-18 aircraft," *IEEE Transactions on Industrial Electronics*, vol. 64, no. 2, pp. 1332–1340, 2017.

[54] L. Wu, Y. Gao, J. Liu, and H. Li, "Event-triggered sliding mode control of stochastic systems via output feedback," *Automatica*, vol. 82, pp. 79–92, 2017.

[55] F. Xiao and T. Chen, "Sampled-data consensus in multi-agent systems with asynchronous hybrid event-time driven interactions," *Systems & Control Letters*, vol. 89, pp. 24–34, 2016.

[56] M. Cao, F. Xiao, and L. Wang, "Second-order consensus in time-delayed networks based on periodic edge-event driven control," *Systems & Control Letters*, vol. 96, pp. 37–44, 2016.

[57] G. Duan, F. Xiao, and L. Wang, "Asynchronous periodic edge-event triggered control for double-integrator networks with communication time delays," *IEEE Transactions on Cybernetics*, vol. 48, no. 2, pp. 675–688, 2018.

[58] E. Garcia, Y. Cao, and D. W. Casbeer, "Periodic event-triggered synchronization of linear multi-agent systems with communication delays," *IEEE Transactions on Automatic Control*, vol. 62, no. 1, pp. 366–371, 2017.

[59] W. He, X. Gao, W. Zhong, and F. Qian, "Secure impulsive synchronization control of multi-agent systems under deception attacks," *Information Sciences*, vol. 459, pp. 354–368, 2018.

[60] D. Zhang, L. Liu, and G. Feng, "Consensus of heterogeneous linear multiagent systems subject to aperiodic sampled-data and DoS attack," *IEEE Transactions on Cybernetics*, no. 99, pp. 1–11, 2018.

[61] D. Zhang and G. Feng, "A new switched system approach to leader-follower consensus of heterogeneous linear multiagent systems with DoS attack," *IEEE Transactions on Systems, Man, and Cybernetics: Systems*, 2019.

[62] C. De Persis and P. Tesi, "Networked control of nonlinear systems under denial-of-service," *Systems & Control Letters*, vol. 96, pp. 124–131, 2016.

[63] H. S. Foroush and S. Martinez, "On event-triggered control of linear systems under periodic denial-of-service jamming attacks," in *Decision and Control (CDC)*, pp. 2551–2556, IEEE, 2012.

[64] Y.-C. Sun and G.-H. Yang, "Event-triggered resilient control for cyber-physical systems under asynchronous DoS attacks," *Information Sciences*, vol. 465, pp. 340–352, 2018.

[65] C. De Persis and P. Tesi, "Resilient control under denial-of-service," *IFAC Proceedings Volumes*, vol. 47, no. 3, pp. 134–139, 2014.

[66] X. Chen, Y. Wang, and S. Hu, "Event-based robust stabilization of uncertain networked control systems under quantization and denial-of-service attacks," *Information Sciences*, vol. 459, pp. 369–386, 2018.

[67] H. Yang, S. Ju, Y. Xia, and J. Zhang, "Predictive cloud control for networked multiagent systems with quantized signals under DoS attacks," *IEEE Transactions on Systems, Man, and Cybernetics: Systems*, 2019.

[68] S. Hu, D. Yue, X. Chen, Z. Cheng, and X. Xie, "Resilient H_∞ filtering for event-triggered networked systems under nonperiodic DoS jamming attacks," *IEEE Transactions on Systems, Man, and Cybernetics: Systems*, 2019.

[69] Y. Tang, D. Zhang, D. W. Ho, W. Yang, and B. Wang, "Event-based tracking control of mobile robot with denial-of-service attacks," *IEEE Transactions on Systems, Man, and Cybernetics: Systems*, 2018.

[70] D. Liu and G.-H. Yang, "Event-triggered non-fragile control for linear systems with actuator saturation and disturbances," *Information Sciences*, vol. 429, pp. 1–11, 2018.

[71] H. Shen, F. Li, Z.-G. Wu, J. H. Park, and V. Sreeram, "Fuzzy-model-based nonfragile control for nonlinear singularly perturbed systems with semi-markov jump parameters," *IEEE Transactions on Fuzzy systems*, vol. 26, no. 6, pp. 3428–3439, 2018.

[72] J. Ma, L. Liu, H. Ji, and G. Feng, "Quantized consensus of multiagent systems by event-triggered control," *IEEE Transactions on Systems, Man, and Cybernetics: Systems*, no. 99, pp. 1–12, 2018.

[73] T. C. Aysal, M. J. Coates, and M. G. Rabbat, "Distributed average consensus with dithered quantization," *IEEE Transactions on Signal Processing*, vol. 56, no. 10, pp. 4905–4918, 2008.

[74] W. Hu, C. Yang, T. Huang, and W. Gui, "A distributed dynamic event-triggered control approach to consensus of linear multiagent systems with directed networks," *IEEE Transactions on Cybernetics*, vol. 50, no. 2, pp. 869 – 874, 2018.

[75] X. Yi, K. Liu, D. V. Dimarogonas, and K. H. Johansson, "Dynamic event-triggered and self-triggered control for multi-agent systems," *IEEE Transactions on Automatic Control*, vol. 64, no. 8, pp. 3300–3307, 2018.

[76] W. He, B. Xu, Q.-L. Han, and F. Qian, "Adaptive consensus control of linear multiagent systems with dynamic event-triggered strategies," *IEEE Transactions on Cybernetics*, 2019.

[77] A. Amini, A. Asif, and A. Mohammadi, "CEASE: A collaborative event-triggered average-consensus sampled-data framework with performance guarantees for multi-agent systems," *IEEE Transactions on Signal Processing*, vol. 66, no. 23, pp. 6096–6109, 2018.

[78] A. Amini, A. Asif, and A. Mohammadi, "Quantized event-triggered sampled-data average consensus with guaranteed rate of convergence," in *ICASSP 2019-2019 IEEE International Conference on Acoustics, Speech and Signal Processing (ICASSP)*, pp. 4614–4618, IEEE, 2019.

[79] A. Amini, A. Asif, and A. Mohammadi, "RQ-CEASE: A resilient quantized collaborative event-triggered average-consensus sampled-data framework under denial of service attack," *IEEE Transactions on Systems, Man, and Cybernetics: Systems*, 2020.

[80] A. Amini, Z. Zeinaly, A. Mohammadi, and A. Asif, "Performance constrained distributed event-triggered consensus in multi-agent systems," in *2019 American Control Conference (ACC)*, pp. 1830–1835, IEEE, 2019.

[81] A. Amini, A. Asif, and A. Mohammadi, "A performance guaranteed sampled-data event-triggered consensus approach for linear multi-agent systems," *Information Sciences*, vol. 484, pp. 338–349, 2019.

[82] A. Amini, A. Asif, and A. Mohammadi, "A unified optimization for resilient dynamic event-triggering consensus under denial," *accepted in IEEE Trans. Cybern.*, 2020.

[83] L. Han, X. Dong, Q. Li, and Z. Ren, "Formation-containment control for second-order multi-agent systems with time-varying delays," *Neurocomputing*, vol. 218, pp. 439–447, 2016.

[84] X. Dong, Y. Hua, Y. Zhou, Z. Ren, and Y. Zhong, "Theory and experiment on formation-containment control of multiple multirotor unmanned aerial vehicle systems," *IEEE Transactions on Automation Science and Engineering*, vol. 16, no. 1, pp. 229–240, 2018.

[85] B. Zheng and X. Mu, "Formation-containment control of second-order multi-agent systems with only sampled position data," *International Journal of Systems Science*, vol. 47, no. 15, pp. 3609–3618, 2016.

[86] Y. Wang, Y. Song, and W. Ren, "Distributed adaptive finite-time approach for formation–containment control of networked nonlinear systems under directed topology," *IEEE Transactions on Neural Networks and Learning Systems*, vol. 29, no. 7, pp. 3164–3175, 2017.

[87] T. Han, M. Chi, Z.-H. Guan, B. Hu, J.-W. Xiao, and Y. Huang, "Distributed three-dimensional formation containment control of multiple unmanned aerial vehicle systems," *Asian Journal of Control*, vol. 19, no. 3, pp. 1103–1113, 2017.

[88] Y. Hua, X. Dong, L. Han, Q. Li, and Z. Ren, "Formation-containment tracking for general linear multi-agent systems with a tracking-leader of unknown control input," *Systems & Control Letters*, vol. 122, pp. 67–76, 2018.

[89] Y.-W. Wang, X.-K. Liu, J.-W. Xiao, and Y. Shen, "Output formation-containment of interacted heterogeneous linear systems by distributed hybrid active control," *Automatica*, vol. 93, pp. 26–32, 2018.

[90] W. Jiang, G. Wen, Z. Peng, T. Huang, and A. Rahmani, "Fully distributed formation-containment control of heterogeneous linear multiagent systems," *IEEE Transactions on Automatic Control*, vol. 64, no. 9, pp. 3889–3896, 2018.

[91] S. Zuo, Y. Song, F. L. Lewis, and A. Davoudi, "Time-varying output formation containment of general linear homogeneous and heterogeneous multiagent systems," *IEEE Transactions on Control of Network Systems*, vol. 6, no. 2, pp. 537–548, 2018.

[92] D. Li, W. Zhang, W. He, C. Li, and S. S. Ge, "Two-layer distributed formation-containment control of multiple euler–lagrange systems by output feedback," *IEEE Transactions on Cybernetics*, vol. 49, no. 2, pp. 675–687, 2018.

[93] C. Li, L. Chen, Y. Guo, and G. Ma, "Formation–containment control for networked euler–lagrange systems with input saturation," *Nonlinear Dynamics*, vol. 91, no. 2, pp. 1307–1320, 2018.

[94] L. Chen, C. Li, B. Xiao, and Y. Guo, "Formation-containment control of networked euler–lagrange systems: An event-triggered framework," *ISA Transactions*, vol. 86, pp. 87–97, 2019.

[95] W. Liu, C. Yang, Y. Sun, and J. Qin, "Observer-based event-triggered containment control of multi-agent systems with time delay," *International Journal of Systems Science*, vol. 48, no. 6, pp. 1217–1225, 2017.

[96] T.-H. Cheng, Z. Kan, J. R. Klotz, J. M. Shea, and W. E. Dixon, "Decentralized event-triggered control of networked systems-part 2: containment control," in *American Control Conference (ACC), 2015*, pp. 5444–5448, IEEE, 2015.

[97] H. Lü, W. He, Q.-L. Han, X. Ge, and C. Peng, "Finite-time containment control for nonlinear multi-agent systems with external disturbances," *Information Sciences*, 2019.

[98] L. Ma, H. Min, S. Wang, Y. Liu, and Z. Liu, "Distributed containment control of networked nonlinear second-order systems with unknown parameters," *IEEE/CAA Journal of Automatica Sinica*, vol. 5, no. 1, pp. 232–239, 2016.

[99] A. Mondal, L. Behera, S. R. Sahoo, and A. Shukla, "A novel multi-agent formation control law with collision avoidance," *IEEE/CAA Journal of Automatica Sinica*, vol. 4, no. 3, pp. 558–568, 2017.

[100] X. Ge and Q.-L. Han, "Distributed formation control of networked multi-agent systems using a dynamic event-triggered communication mechanism," *IEEE Transactions on Industrial Electronics*, vol. 64, no. 10, pp. 8118–8127, 2017.

[101] B. Cheng, Z. Wu, and Z. Li, "Distributed edge-based event-triggered formation control," *IEEE Transactions on Cybernetics*, 2019.

[102] A. Amini, A. Asif, and A. Mohammadi, "Formation-containment control using dynamic event-triggering mechanism for multi-agent systems," *IEEE/CAA Journal of Automatica Sinica*, vol. 7, no. 5, pp. 1235 – 1248, 2020.

[103] G. Battistelli, L. Chisci, and D. Selvi, "Distributed averaging of exponential-class densities with discrete-time event-triggered consensus," *IEEE Transactions on Control of Network Systems*, 2016.

[104] A. Mohammadi and A. Asif, "Distributed consensus innovation particle filtering for bearing/range tracking with communication constraints," *IEEE Transactions on Signal Processing*, vol. 63, no. 3, pp. 620–635, 2015.

[105] A. Amini, A. Mohammadi, and A. Asif, "Event-based consensus for a class of heterogeneous multi-agent systems: An LMI approach," in *ICASSP, 2017 IEEE International Conference on*, pp. 3306–3310, IEEE, 2017.

[106] A. Mohammadi and K. N. Plataniotis, "Event-based estimation with information-based triggering and adaptive update," *IEEE Transactions on Signal Processing*, vol. 65, no. 18, pp. 4924–4939, 2017.

[107] G. S. Seyboth, D. V. Dimarogonas, and K. H. Johansson, "Event-based broadcasting for multi-agent average consensus," *Automatica*, vol. 49, no. 1, pp. 245–252, 2013.

[108] P. Yu, L. Ding, Z.-W. Liu, and Z.-H. Guan, "A distributed event-triggered transmission strategy for exponential consensus of general linear multi-agent systems with directed topology," *Journal of the Franklin Institute*, vol. 352, no. 12, pp. 5866–5881, 2015.

[109] A. Sandryhaila, S. Kar, and J. M. Moura, "Finite-time distributed consensus through graph filters," in *ICASSP*, pp. 1080–1084, IEEE, 2014.

[110] G. Wen, Z. Duan, G. Chen, and W. Yu, "Consensus tracking of multi-agent systems with lipschitz-type node dynamics and switching topologies," *IEEE Transactions on Circuits and Systems I: Regular Papers*, vol. 61, no. 2, pp. 499–511, 2014.

[111] D. Yang, W. Ren, X. Liu, and W. Chen, "Decentralized event-triggered consensus for linear multi-agent systems under general directed graphs," *Automatica*, vol. 69, pp. 242–249, 2016.

[112] A. Gusrialdi and Z. Qu, "Distributed estimation of all the eigenvalues and eigenvectors of matrices associated with strongly connected digraphs," *IEEE Control Systems Letters*, vol. 1, no. 2, pp. 328–333, 2017.

[113] A. Bertrand and M. Moonen, "Topology-aware distributed adaptation of laplacian weights for in-network averaging," in *Proc. of the 21ste European Signal Processing Conference, 2013*, pp. 1–5, 2013.

[114] A. Bertrand and M. Moonen, "Distributed computation of the fiedler vector with application to topology inference in ad hoc networks," *Signal Processing*, vol. 93, no. 5, pp. 1106–1117, 2013.

[115] D. siljak and D. Stipanovic, "Robust stabilization of nonlinear systems: the LMI approach," *Mathematical problems in Engineering*, vol. 6, no. 5, pp. 461–493, 2000.

[116] G. Chiandussi, M. Codegone, S. Ferrero, and F. E. Varesio, "Comparison of multi-objective optimization methodologies for engineering applications," *Computers & Mathematics with Applications*, vol. 63, no. 5, pp. 912–942, 2012.

[117] F. Alizadeh, "Interior point methods in semidefinite programming with applications to combinatorial optimization," *SIAM journal on Optimization*, vol. 5, no. 1, pp. 13–51, 1995.

[118] M. Mesbahi and G. P. Papavassilopoulos, "LMIs, interior point methods, complexity theory, and robustness analysis," in *Decision and Control, 1996., Proceedings of the 35th IEEE Conference on*, vol. 4, pp. 4625–4630, IEEE, 1996.

[119] L. Vandenberghe and S. Boyd, "Semidefinite programming," *SIAM review*, vol. 38, no. 1, pp. 49–95, 1996.

[120] S. Boyd and L. Vandenberghe, *Convex optimization*. Cambridge university press, 2004.

[121] Z. Zhang, L. Zhang, F. Hao, and L. Wang, "Distributed event-triggered consensus for multi-agent systems with quantisation," *International Journal of Control*, vol. 88, no. 6, pp. 1112–1122, 2015.

[122] X. Meng and T. Chen, "Event based agreement protocols for multi-agent networks," *Automatica*, vol. 49, no. 7, pp. 2125–2132, 2013.

[123] A. Girard, "Dynamic triggering mechanisms for event-triggered control," *IEEE Transactions on Automatic Control*, vol. 60, no. 7, pp. 1992–1997, 2014.

[124] Y.-Y. Qian, L. Liu, and G. Feng, "Distributed event-triggered adaptive control for consensus of linear multi-agent systems with external disturbances," *IEEE transactions on cybernetics*, 2018.

[125] W. Hu, C. Yang, T. Huang, and W. Gui, "A distributed dynamic event-triggered control approach to consensus of linear multiagent systems with directed networks," *IEEE Transactions on Cybernetics*, no. 2, pp. 869 – 874, 50.

[126] M. Wu, Y. He, and J.-H. She, *Stability analysis and robust control of time-delay systems*, vol. 22. Springer, 2010.

[127] I. Shames, T. Charalambous, C. N. Hadjicostis, and M. Johansson, "Distributed network size estimation and average degree estimation and control in networks isomorphic to directed graphs," in *Communication, Control, and Computing (Allerton)*, pp. 1885–1892, IEEE, 2012.

[128] S. P. Boyd, L. El Ghaoui, E. Feron, and V. Balakrishnan, *Linear matrix inequalities in system and control theory*, vol. 15. SIAM, 1994.

[129] C.-H. Lien, "Non-fragile guaranteed cost control for uncertain neutral dynamic systems with time-varying delays in state and control input," *Chaos, Solitons & Fractals*, vol. 31, no. 4, pp. 889–899, 2007.

[130] L. Ding, Q.-L. Han, X. Ge, and X.-M. Zhang, "An overview of recent advances in event-triggered consensus of multiagent systems," *IEEE Transactions on Cybernetics*, vol. 48, no. 4, pp. 1110–1123, 2018.

[131] W. Xu, D. W. Ho, L. Li, and J. Cao, "Event-triggered schemes on leader-following consensus of general linear multiagent systems under different topologies," *IEEE Trans. Cybern.*, vol. 47, no. 1, pp. 212–223, 2015.

[132] E. Garcia, Y. Cao, and D. W. Casbeer, "Decentralised event-triggered consensus of double integrator multi-agent systems with packet losses and communication delays," *IET Control Theory A.*, vol. 10, no. 15, pp. 1835–1843, 2016.

[133] D. Liuzza, D. V. Dimarogonas, M. Di Bernardo, and K. H. Johansson, "Distributed model based event-triggered control for synchronization of multi-agent systems," *Automatica*, vol. 73, pp. 1–7, 2016.

[134] H. Li, X. Liao, T. Huang, and W. Zhu, "Event-triggering sampling based leader-following consensus in second-order multi-agent systems," *IEEE Transactions on Automatic Control*, vol. 60, no. 7, pp. 1998–2003, 2015.

[135] D. N. Borgers and W. M. Heemels, "Event-separation properties of event-triggered control systems," *IEEE Transactions on Automatic Control*, vol. 59, no. 10, pp. 2644–2656, 2014.

[136] Q. Wang, J.-L. Wang, H.-N. Wu, and T. Huang, "Consensus and h_∞ consensus of nonlinear second-order multi-agent systems," *IEEE Transactions on Network Science and Engineering*, 2019.

[137] V. Phat, Y. Khongtham, and K. Ratchagit, "LMI approach to exponential stability of linear systems with interval time-varying delays," *Linear Algebra and Its Applications*, vol. 436, no. 1, pp. 243–251, 2012.

[138] S. Boyd, L. El Ghaoui, E. Feron, and V. Balakrishnan, *Linear matrix inequalities in system and control theory*. SIAM, 1994.

[139] Z. A. Biron, S. Dey, and P. Pisu, "Real-time detection and estimation of denial of service attack in connected vehicle systems," *IEEE Trans. Intell. Transp. Syst.*, vol. 19, no. 12, pp. 3893–3902, 2018.

[140] A.-Y. Lu and G.-H. Yang, "Distributed consensus control for multi-agent systems under denial-of-service," *Information Sciences*, vol. 439, pp. 95–107, 2018.

[141] W. Xu, D. W. Ho, J. Zhong, and B. Chen, "Event/self-triggered control for leader-following consensus over unreliable network with dos attacks," *IEEE. T. Neur. Net. Lear.*, vol. 30, no. 10, pp. 3137–3149, 2019.

[142] C. Peng, J. Li, and M. Fei, "Resilient event-triggering h_∞ load frequency control for multi-area power systems with energy-limited dos attacks," *IEEE Trans. Power Syst.*, vol. 32, no. 5, pp. 4110–4118, 2016.

[143] M. Fu and L. Xie, "The sector bound approach to quantized feedback control," *IEEE Transactions on Automatic Control*, vol. 50, no. 11, pp. 1698–1711, 2005.

[144] S. Hu, D. Yue, Q.-L. Han, X. Xie, X. Chen, and C. Dou, "Observer-based event-triggered control for networked linear systems subject to denial-of-service attacks," *IEEE Trans. Cybern.*, vol. 50, no. 5, pp. 1952–1964, 2019.

[145] A. Cetinkaya, H. Ishii, and T. Hayakawa, "Networked control under random and malicious packet losses," *IEEE Transactions on Automatic Control*, vol. 62, no. 5, pp. 2434–2449, 2016.

[146] J. Wu and T. Chen, "Design of networked control systems with packet dropouts," *IEEE Transactions on Automatic control*, vol. 52, no. 7, pp. 1314–1319, 2007.

[147] W. Xu, G. Hu, D. W. Ho, and Z. Feng, "Distributed secure cooperative control under denial-of-service attacks from multiple adversaries," *IEEE Trans. Cybern.*, vol. 50, no. 8, pp. 3458 – 3467, 2019.

[148] W. Xu, D. W. Ho, L. Li, and J. Cao, "Event-triggered schemes on leader-following consensus of general linear multiagent systems under different topologies," *IEEE Transactions on Cybernetics*, vol. 47, no. 1, pp. 212–223, 2017.

[149] M. Yu, C. Yan, D. Xie, and G. Xie, "Event-triggered tracking consensus with packet losses and time-varying delays," *IEEE/CAA Journal of Automatica Sinica*, vol. 3, no. 2, pp. 165–173, 2016.

[150] H. Xia, W. X. Zheng, and J. Shao, "Event-triggered containment control for second-order multi-agent systems with sampled position data," *ISA transactions*, vol. 73, pp. 91–99, 2018.

[151] G. Miao, J. Cao, A. Alsaedi, and F. E. Alsaadi, "Event-triggered containment control for multi-agent systems with constant time delays," *Journal of the Franklin Institute*, vol. 354, no. 15, pp. 6956–6977, 2017.

[152] W. Zou and Z. Xiang, "Event-triggered containment control of second-order nonlinear multi-agent systems," *Journal of the Franklin Institute*, vol. 356, no. 17, pp. 10421–10438, 2019.

[153] W. Zou and Z. Xiang, "Event-triggered distributed containment control of heterogeneous linear multi-agent systems by an output regulation approach," *International Journal of Systems Science*, vol. 48, no. 10, pp. 2041–2054, 2017.

[154] J. Lofberg, "Yalmip: A toolbox for modeling and optimization in matlab," in *Computer Aided Control Systems Design, 2004 IEEE International Symposium on*, pp. 284–289, IEEE, 2004.

[155] K.-C. Toh, M. J. Todd, and R. H. Tütüncü, "SDPT3—a matlab software package for semidefinite programming, version 1.3," *Optimization Methods and Software*, vol. 11, no. 1-4, pp. 545–581, 1999.

[156] J. R. Lawton, R. W. Beard, and B. J. Young, "A decentralized approach to formation maneuvers," *IEEE Transactions on Robotics and Automation*, vol. 19, no. 6, pp. 933–941, 2003.

[157] X. Meng, L. Xie, and Y. C. Soh, "Asynchronous periodic event-triggered consensus for multi-agent systems," *Automatica*, vol. 84, pp. 214–220, 2017.

[158] Q.-Q. Yang, J. Li, X. Feng, S. Wu, and F. Gao, "Event-triggered consensus for second-order multi-agent systems via asynchronous periodic sampling control approach," *International Journal of Control, Automation and Systems*, pp. 1–13, 2020.

[159] Y. Jiang and Z.-P. Jiang, "Computational adaptive optimal control for continuous-time linear systems with completely unknown dynamics," *Automatica*, vol. 48, no. 10, pp. 2699–2704, 2012.

[160] K. G. Vamvoudakis and H. Ferraz, "Model-free event-triggered control algorithm for continuous-time linear systems with optimal performance," *Automatica*, vol. 87, pp. 412–420, 2018.

[161] Y. Yang, H. Modares, K. G. Vamvoudakis, Y. Yin, and D. C. Wunsch, "Model-free event-triggered containment control of multi-agent systems," in *2018 Annual American Control Conference (ACC)*, pp. 877–884, IEEE, 2018.

[162] H. Gao, T. Chen, and J. Lam, "A new delay system approach to network-based control," *Automatica*, vol. 44, no. 1, pp. 39–52, 2008.

[163] T. Chen and B. A. Francis, *Optimal sampled-data control systems*. Springer Science & Business Media, 2012.

[164] Z. Zuo, S. Guan, Y. Wang, and H. Li, "Dynamic event-triggered and self-triggered control for saturated systems with anti-windup compensation," *J. Franklin I.*, vol. 354, no. 17, pp. 7624–7642, 2017.

[165] Y.-Y. Qian, L. Liu, and G. Feng, "Distributed dynamic event-triggered control for cooperative output regulation of linear multiagent systems," *IEEE Trans. Cybern.*, vol. 50, no. 7, pp. 3023 – 3032, 2019.

[166] Y. Wang, W. X. Zheng, and H. Zhang, "Dynamic event-based control of nonlinear stochastic systems," *IEEE Trans. Automat. Contr.*, vol. 62, no. 12, pp. 6544–6551, 2017.

[167] Z.-H. Zhang, D. Liu, C. Deng, and Q.-Y. Fan, "A dynamic event-triggered resilient control approach to cyber-physical systems under asynchronous DoS attacks," *Information Sciences*, vol. 519, pp. 260–272, 2020.

[168] D. P. Borgers, V. S. Dolk, and M. W. Heemels, "Dynamic periodic event-triggered control for linear systems," in *International conference on hybrid systems: computation and control*, pp. 179–186, 2017.

[169] D. P. Borgers, V. S. Dolk, and W. Heemels, "Riccati-based design of event-triggered controllers for linear systems with delays," *IEEE Trans. Automat. Contr.*, vol. 63, no. 1, pp. 174–188, 2017.

[170] S. Li, D. Sauter, and B. Xu, "Co-design of event-triggered H_∞ control for discrete-time linear parameter-varying systems with network-induced delays," *J. Franklin I.*, vol. 352, no. 5, pp. 1867–1892, 2015.

[171] A. Seuret, C. Prieur, S. Tarbouriech, and L. Zaccarian, "LQ-based event-triggered controller co-design for saturated linear systems," *Automatica*, vol. 74, pp. 47–54, 2016.

[172] X. Meng and T. Chen, "Event detection and control co-design of sampled-data systems," *International Journal of Control*, vol. 87, no. 4, pp. 777–786, 2014.

[173] Y. Zhu and W. X. Zheng, "Observer-based control for cyber-physical systems with periodic dos attacks via a cyclic switching strategy," *IEEE Trans. Automat. Contr.*, vol. 65, no. 8, pp. 3714 – 3721, 2019.

[174] L. Su and D. Ye, "Observer-based output feedback H_∞ control for cyber-physical systems under randomly occurring packet dropout and periodic dos attacks," *ISA transactions*, vol. 95, pp. 58–67, 2019.

[175] M. Wang and B. Xu, "Observer-based guaranteed cost control of cyber-physical systems under dos jamming attacks," *Eur. J. Control*, vol. 48, pp. 21–29, 2019.

[176] Y. Xu, M. Fang, P. Shi, and Z.-G. Wu, "Event-based secure consensus of mutiagent systems against dos attacks," *IEEE Trans. Cybern.*, vol. 50, no. 8, pp. 3468 – 3476, 2019.

[177] D. Liu and G.-H. Yang, "Dynamic event-triggered control for linear time-invariant systems with L_2 gain performance," *Int. J. Robust Nonlin.*, vol. 29, no. 2, pp. 507–518, 2019.

[178] B. Luo, T. Huang, and D. Liu, "Periodic event-triggered suboptimal control with sampling period and performance analysis," *IEEE Trans. Cybern.*, 2019.

[179] Y.-C. Sun and G.-H. Yang, "Periodic event-triggered resilient control for cyber-physical systems under denial-of-service attacks," *Journal of the Franklin Institute*, vol. 355, no. 13, pp. 5613–5631, 2018.

[180] H. Yang, Y. Xu, and J. Zhang, "Event-driven control for networked control systems with quantization and markov packet losses," *IEEE transactions on cybernetics*, vol. 47, no. 8, pp. 2235–2243, 2016.

[181] E. Fridman, *Introduction to time-delay systems: Analysis and control*. Springer, 2014.